CXCR4 TARGETED PEPTIDE CARRIERS FOR THE INHIBITION OF HIV AND DELIVERY OF ANTI-VIRAL DRUGS

By

MATTHEW S. PALOMBO

A Dissertation submitted to the

Graduate School-New Brunswick

Rutgers, The State University of New Jersey

In partial fulfillment of the requirements

For the degree of

Doctor of Philosophy

Graduate Program in Pharmaceutical Science

written under the direction of

Patrick J. Sinko

and approved by

_____

_____

_____

_____

New Brunswick, New Jersey

May, 2013

ABSTRACT OF THE DISSERTATION

CXCR4 Targeted Peptide Carriers for the Inhibition of HIV and Delivery of Anti-viral Drugs

By MATTHEW S. PALOMBO

Dissertation Director:
Patrick J. Sinko

HIV-1 continues to be a major epidemic affecting the global population and responsible for millions of deaths annually. Despite the mortality of the virus, great improvement in the currently available retroviral pharmacotherapy has lead to a chronic treatment of infected individuals. However the current therapy is not a cure for HIV-1 infection and eventually drug resistant viral strains will deplete the infected individual of $CD4^+$ T cells.

The chemokine receptor CXCR4 plays an important role to HIV-1 infection of host cells. CXCR4 acts as a coreceptor to viral entry. CXCR4 is expressed several types of HIV-1 susceptible cells and therefore has been identified as a target for anti-viral intervention as well as a targeted drug delivery system. The thesis herein is focused developing peptide drug conjugates targeting CXC4.

Peptide carriers were synthesized to specifically interact with CXCR4 by the targeting sequence DV3. Multivalent DV3 peptide carriers containing 1, 2, or 4 copies of the CXCR4 targeting sequence DV3 were tested in vitro for the inhibition of HIV-1 entry and cellular uptake via confocal microscopy. Only the 4 copy DV3 peptide carriers

(4DV3) significantly inhibited HIV-1 from infecting the reporter cell line TZM-bl and were entrapped within cellular endosomes. 4DV3 inhibited the HIV-1 strain IIIB in vitro (IC_{50}=553nM). The small molecule, AMD3100 (47%), and a CXCR4 monoclonal antibody (IC_{50} = 398nM) inhibited the 4DV3/CXCR4 interaction. Molecular modeling of 4DV3 interacting with CXCR4 demonstrated the ability of 4DV3 to interact with a tetramer of the receptor.

4DV3 was further modified to carry drug cargoes with known anti-viral activity. Comparative analysis of the peptides carrier's ability to enhance the anti-HIV activity of the drug, the 4DV3, or act synergistically was investigated. 4DV3 conjugates of AZT (IC_{50}=32nM) and RTV (IC_{50}=598nM) improved the effectiveness of 4DV3 (IC_{50}=23μM) inhibition of HIV-1 replication. The stability of the ester drug conjugate was evaluated over time. Finally, third generation compounds were designed and synthesized to increase the drug loading. The studies that have been performed were designed to evaluate the potential of a targeted CXCR4 peptide carrier as a drug delivery system for HIV-1 therapy.

DEDICATION

To Joanne, Cecelia, Max

and the rest of my family

for their encouragement and support

to achieve my goals.

ACKNOWLEDGEMENTS

The PhRMA Foundation, the American Foundation for Pharmaceutical Education, and the Parke-Davis Endowed Chair are acknowledged for their financial fellowship support. The United States Department of Education is also acknowledged for their financial support through the Graduate Assistance in an Area of National Need (GAAN) Program. Additionally the National Institute of Health MERIT Award grant (R37 AI/DK-51214) on "Enhancing Intestinal & Brain Uptake of Anti-AIDS Drugs."

My dissertation advisor, Professor Patrick J. Sinko, and committee members; Professors Kathryn Uhrich and Aresh Hatefi, and Dr. Yaming Su are acknowledged for their support and guidance. Professors Xiaoping Zhang and Zoltan Szekely are recognized for their expertise and knowledge in the areas of biology and chemistry, respectively. Professor Yashveer Singh for his encouragement and efforts as coauthor as well as Steven Johnson for his efforts in chemistry. I would also like to acknowledge the other members of the Sinko laboratory past and present. They were all essential to the research put forth in this thesis. Additionally, I would like to thank Amy Grabowski, Christal Louison, Marianne Shen, and Sharana Taylor for all of their assistance over the years.

I would also like to thank my family: Joanne, Max and Cecelia; Rich and Sandi; Zach, Lori, Lucia and Rocco; Jerry, Audrey, Pat and Kelly for all of their support without them I would not have succeeded.

TABLE OF CONTENTS

LIST OF TABLES

LIST OF SCHEMES

LIST OF FIGURES

CHAPTER 1

INTRODUCTION

Human immunodeficiency virus (HIV-1) is the retrovirus responsible for the development of acquired immunodeficiency syndrome (AIDS). HIV-1/AIDS continues to be a major epidemic affecting the global population that causes millions of deaths each year (*1*). Despite the associated mortality of AIDS, the currently available pharmacotherapies have greatly improved the life expectancy of HIV-1 infected patients by delaying the onset of AIDS. These therapies have the ability to suppress circulating virus levels in the plasma below the limit of detection and have led to HIV-1 being chronically treated in some patients for >20 years (*2*). Unfortunately, chronic therapy is not a cure and patients will eventually suffer from viral rebound of drug resistant strains, depletion of $CD4^+$ T cells, and ultimately succumb to AIDS (*3*).

The chemokine receptor CXCR4 plays an important role in infection of host cells by HIV-1. Although CXCR4 is endogenously responsible for the chemotaxis of expressing cells via interaction with its natural ligand CXCL12, CXCR4 becomes hijacked by HIV-1 (*4, 5*). CXCR4 acts as a coreceptor to viral entry of many strains of HIV-1 after the virus binds to its primary receptor CD4. Several types of HIV-1 susceptible cells express CXCR4, including naïve CD4 T-cells, macrophages, and dendritic cells of the immune system (*6*). Blocking the interaction between HIV-1 and CXCR4 inhibits the virus' ability to infect immune cells. Therefore, CXCR4 is a strong

target for therapeutic intervention as well as a possible portal for drug delivery via receptor-mediated endocytosis.

The proposed thesis herein focuses on exploiting one of the receptors essential to HIV-1 entry, CXCR4. Peptide carriers were synthesized to specifically interact with CXCR4. These peptides were evaluated for their ability to competitively inhibit HIV-1 strains in vitro. Additionally, the peptides were modified to carry a drug cargo with known anti-viral activity. Comparative analysis of the peptide carriers' ability to enhance the anti-HIV activity of the drug, the peptide, or act synergistically was investigated. Furthermore, the efficiency of the drug cargo's release from its ester linkage was evaluated over time. Finally, the in vivo biodistribution of CXCR4 targeted peptides will be evaluated in a rodent model. The studies that have been performed were designed to evaluate the potential of a targeted CXCR4 peptide carrier as a drug delivery system for anti-HIV therapy.

Therefore, the overall objective was to complete the following specific aims: to design, synthesize, and characterize CXCR4 targeted peptide nanocarriers containing multiple copies of the targeting sequence (DV3) and evaluate their in vitro properties for uptake, cytotoxicity, and their inhibition of HIV-1 by competitive CXCR4 interaction in susceptible cells; to design, synthesize and characterize DV3 containing peptide carriers conjugated with antiviral drugs and evaluate their ability to synergistically inhibit HIV-1 activity in susceptible cells through inhibition of HIV-1 enzymes and the coreceptor for infection, CXCR4; To evaluate the capacity of DV3 peptide carriers to accommodate and delivery larger drug payloads through PEGylation and biodistribution of the DV3 peptide carriers through pharmacokinetic analysis.

CHAPTER 2

BACKGROUND AND SIGNIFICANCE

2.1 CXCR4 Endogenous Function

CXCR4 is a member of the chemokine family of receptors, which is a subset of the rhodopsin superfamily of seven transmembrane spanning, G protein coupled receptors that bind to small protein ligands (Figure 1) (*7-9*). These protein ligands are characterized by their ability to induce cell motility in a variety of cell types, thus the term 'chemokine' was derived from 'chemoattractant cytokine' as the acceptable nomenclature and classification during the Third International Symposium on Chemotactic Cytokines in 1992 (*8, 10-14*). Chemokines are classified by a highly conserved sequence of cystein residues in their sequence, and furthermore chemokine receptors are similarly classified by the chemokine ligand nomenclature (*10, 15*). For example, a chemokine with two cysteine residues that are separated by another amino acid are designated as CXC chemokines and act as a ligand for a CXC receptor (Figure 2) (*15, 16*). Currently, there are 18 chemokine receptors and over 50 chemokines endogenously expressed by humans that are recognized by the International Union of Basic and Clinical Pharmacology Committee on Receptor Nomenclature and Drug Classification (*17*).

Chemokines and their receptors serve an important role in the cell trafficking processes of immune cells. Chemokines affect the following activities of immune cells as the cells migrate from the vasculature to lymphoid tissue to organs; circulation, homing, adhesion, extravasation, and re-circulation (*10*). Specifically, CXCR4 is critical to numerous endogenous functions; T-cell activation and migration, embryogenisis, brain development, hematopoiesis, and vascularization (*18-27*). Besides the receptors importance to normal physiology and homeostasis, CXCR4 plays a significant role in several pathologies, including as a coreceptor to HIV-1 infection and in numerous types of metastatic tumors (*27-31*).

The chemokine, stromal cell-derived factor-1 (SDF-1) and more formally referred to as CXCL12, is the one known endogenous ligand of CXCR4 (*4, 5, 10, 32-36*). CXCL12 is a highly conserved chemokine among vertebrates with >99% homology between the human and murine amino acid sequences, similarly human and murine CXCR4 are >90% homologous (*37, 38*). Unlike other identified CXC chemokines that are located on chromosome 4, CXCL12's gene is located on human chromosome 10 (*18, 37, 39*). Strong conservation of the CXCL12 gene was also observed in lower vertebrate species demonstrating that the CXCR4-CXCL12 axis is essential to vertebrate physiology (*37*).

CXCL12 can exist as an 8kDa monomer under physiological ionic strength, but similar to many other chemokines CXCL12 has a propensity to dimerize in vivo (*32, 40, 41*). Additionally, CXCL12 is rich in basic amino acids with over 21% of its sequence consisting of arginine, histidine, or lysine residues with a predicted pI = 11.1 (*36, 42*). The residues generate a cluster of positively charged surfaces along the first and second β

strands of the protein (*32*). CXCL12's net positive charge contributes to the chemokine's high affinity for heparin and heparan sulfate in vitro, which would indicate an attraction toward the negatively charged cell surface glycosaminoglycans (*32, 36*). Although the actual physiologically function is not certain, the prevailing theory is that glycosaminoglycans can amplify local concentrations through interactions with the chemokine, facilitate dimerization, or enhance the display of the ligand to their cognate receptor (*41, 43, 44*).

Receptor-ligand interaction requires a two-site binding; an initial association of the motif RFFESH of CXCL12 with the N-terminal section of CXCR4, followed by several conformational changes that enhance interaction between the N-terminal residues of CXCL12 and the second extracellular loop of CXCR4 (*32, 40, 45*). The initial docking site is believed to be essential for receptor-ligand binding, while the second binding site is responsible for receptor activation (*32*). The N-terminus of the receptor may also displace CXCL12 that is bound to glycosaminoglycan for initiation of the receptor-ligand interaction (*46*). There are three sulfotyrosine residues in the receptor's sequence that are critical to CXCL12 CXCR4 binding. These posttranslational modified residues are located in the N-terminal domain of the receptor at the sequence positions 7, 12, and 21 (*46-48*). The sulfotyrosine residues 7 and 12 occupy the positively charged clefts of SDF-1α necessary for receptor ligand association (*46, 47*). The presence of the sulfotyrosine residues in the N-terminus is believed to enhance dimerization of CXCL12 on the receptor surface and that the positioning of the sulfotyrosine residues allow for the accommodation of the chemokine dimer (*46, 47*).

X-ray crystallography studies have supported the two-site binding model between CXCL12/CXCR4, where site one resides in the N-terminus of the receptor containing the sulfotyrosine residues and site two consists of an acidic rich binding pocket formed by transmembrane helices I, II, III, and VII containing the residues Asp^{187}, Glu^{288}, and Asp^{97} (*49-51*). It was also found that Lys^{1} was the critical residue of CXCL12 that reaches into the binding pocket described and activates the receptor (*49*).

CXCR4/CXCL12 binding activates the exchange of GDP to GTP initiating numerous downstream pathways that lead to Ca^{2+} mobilization, chemotaxis, and receptor internalization (*10, 32, 34, 35, 42, 46, 49*). Signaling cascades initiated by chemokine receptors remain an active area of research and evidence is mounting that the class of G protein coupled to the receptor can be cell specific, as well as the pathways downstream, even for the same receptor (*52*). Activation of chemokine receptors stimulates phospholipase C, which in turn generates diacylglyceride. The cascade then activates protein kinase C and ionositol 1,4,5 triphosphate, eventually inducing calcium release (*52-54*). In addition, several MAPK enzymes, like ERK, JNK, and/or p38 MAPKs, become activated upon receptor ligand interaction, but activation is variable and dependent upon the cell type (*34, 55*). The role of the MAPK proteins remains unclear in this instance, but they are believed to be important to the chemotaxis of cells (*56*). Several tyrosine kinase proteins are also reported to activate as a result of CXCL12/CXCR4 interaction including JAK2 and JAK3. The activation of JAK2 and JAK3 led to further downstream signaling via the STAT family transcription factors (*57*). CXCL12/CXCR4 interaction also activates the nuclear transcription factor, NF-κB, which can influence cell proliferation and the expression of additional chemokine genes

(*34*). Ultimately, CXCL12/CXCR4 binding leads to rapid receptor internalization, and has been shown that over 90% of radiolabled CXCL12 resides intracellularly over a 2 h period in vitro (*35*).

CXCR4 has been experimentally shown by several groups to form hetero/homodimers upon ligand binding (*57-61*). Although the physiological importance of CXCR4 dimerization is still not fully understood, a considerable homodimer interface area of 850Å^2 has been identified by crystallography (*49*). Homodimerization results from hydrophobic interactions of the extracellular portions of V and VI transmembrane helices with further dimerization occurring from conformational changes during ligand binding (*49*). Chemokines themselves also have a proclivity to dimerize, and specifically CXCL12 dimerization can induce alternative down stream activation processes compared to a CXCL12 monomer (*32, 46*). For example, the binding of dimeric CXCL12 has the ability to mobilize intracellular Ca^{2+} without inducing cell mobilization, whereas monomeric CXCL12 generates the release of intracellular Ca^{2+} and chemotaxis (*46*). Despite some ambiguity in the literature on oligomerization of the receptor or ligand, some indications point to the dimers' ability to adjust affinity through conformational changes in the receptor structure and thus modulate biological signaling through positive or negative cooperation (*49*).

2.2 CXCR4 Expression Profile

CXCR4 is differentially expressed in various tissues in the body as well as diverse populations of cell types. The most notable of these are T-cells and macrophages.

Chemokine receptor expression is often used to characterize subsets of T-cells and to distinguish their cellular functions (*62, 63*). CXCR4 expression is also commonly differentiated by another important chemokine receptor to HIV-1 pathology, CCR5. Subsets of HIV susceptible cells can be distinguished by the expression of one, the other, or both of these chemokine coreceptors along with the primary receptor CD4 (*64*).

CXCR4 is expressed on cord blood and adult naïve T-cells, whereas CCR5 is more commonly found on memory T-cells. The isoforms of CD45 are often used to distinguish between naïve ($CD45RA^+$) and memory T-cells ($CD45R0^+$) (*36, 63, 65*). Additionally, CXCR4 is expressed on polarized T helper cells (Th1 and Th2), in which Th1 cells produce IFN-γ and lymphotoxin and Th2 cells produce IL-4, IL-5, and IL-13 (*62, 63*). However, only Th1 express CCR5. Throughout the body, naïve T-cells expressing CXCR4 are found recirculating through the high endothelial venules (HEVs) found in the lymph nodes between the secondary lymphoid tissues and the blood, with small populations accessing non-lymphoid tissues (*66-70*). The CXCL12/CXCR4 axis is important to naïve cell recruitment into the secondary lymphoid tissues and encourages transendothelial migration of the T-cells into the HEVs (*69, 71*).

Besides naïve T-cell subsets, B-lymphocytes (CD20+) cells and B lymphocyte precursor cells express CXCR4. CXCR4 and CXCL12 are vital in the hematopoietic process directing the migration of B-cell precursor cells into the bone marrow so they may be further differentiated into mature B-cells (*18, 33*). Interestingly, CXCL12 only acts as a chemoattractant to B-cell precursors despite measurable CXCR4 expression on mature B-cells (*72, 73*). Furthermore, 75% of monocytes isolated from peripheral blood leukocytes and measured by flow cytometry expressed CXCR4 (*36, 74*). Additionally,

monocyte-derived macrophages were shown to upregulate CXCR4 expression when exposed to macrophage colony-stimulating factor (M-CSF), while receptor expression was suppressed by granulocyte-macrophage colony-stimulating factor (GM-CSF) (*6*). A large percentage of mature dendritic cells express CXCR4 at high levels, but immature peripheral dendritic cells express CXCR4 to a lesser extent (*6, 75*). The literature is conflicting on whether CXCR4 is expressed by the granulocyte cells such as neutrophils and eosinophils, but there is little to no expression of CXCR4 by natural killer cells (*36, 64, 74, 76, 77*). Regardless, CXCR4 is expressed on a wide variety of cells that make up the adaptive and innate immune systems. An outline of the percentages of peripheral blood leukocytes expression of CXCR4 and CCR5 can be found in Table 1, and the expression levels of CXCR4 on different cell lines with their affinity to CXCL12 can be seen in Table 2 and Figure 3 (*6, 35, 78*).

Cells outside the hematopoietic and lymphatic systems also express CXCR4 and CXCL12, indicating its importance to other tissue and cellular functions (*9, 32*). Knockout of either CXCL12 and/or CXCR4 results in perinatal death of mice, which occurs around the 17th embryonic day (*21*). The result is malformations of the cerebellum and the dentate gyrus (the afferent pathway into the hippocampus) (*21-23, 79*). Therefore, CXCR4/CXCL12 axis is important to the migration of neural cells and axons, as well as neuronal survival (*80, 81*). Expression of CXCR4 is found throughout the central nervous system in developing wild-type embryos (*21-23, 26, 81, 82*). Additional cell types of the CNS, including astrocytes, microglial, and glial cells also express CXCR4 (*83-86*).

Just as CXCR4 is critical to the formation of critical portions of the CNS, CXCR4 is also a major player in neo-angiogenesis and other parts of the cardiovascular system.

Western blot and confocal microscopy analysis of cardiomyocytes revealed that these muscle cells of the heart express CXCR4 in the plasma membrane while its ligand, CXCL12, was localized in the Z-line of the cardiac tissue from the ventricles of rat hearts (*24*). Mounting evidence suggests that the CXCR4/CXCL12 axis is a pathway by which the heart modulates calcium homeostasis and contraction (*24*). Furthermore, CXCR4 is expressed in the endothelial lining of the cardiovascular system and endocardium (*24, 87*). It is believed that CXCR4 and other chemokine receptors are expressed on the endothelial surface for two major functions, angiogenesis and leukocyte transmigration (*87*). In embryonic development, areas of vascularization are associated with high levels of CXCL12 expression (*82*). Similarly, areas of induced ischemia become homing sites for CXCR4 expressing endothelial progenitor cells by generating a CXCL12 gradient as part of the endogenous vascular and tissue remodeling processes (*20, 88-91*). This same mechanism of revascularization appears to be exploited in tumor angiogenesis and metastasis (*30, 92*).

CXCR4 expression by epithelial derived cells was found to be variable and tissue dependent. The type II alveolar epithelial cell line A549 expresses functional CXCR4 receptors that respond to CXL12 by calcium mobilization, but do not induce chemotaxis or cell proliferation (*18, 93*). In the same investigation, primary cell cultures of type II alveolar cells were shown to express the CXCR4 gene by RT-PCR, however protein expression was only evaluated in the A549 cells (*93*). However, the true protein expression of alveolar epithelial cells is unknown, since A549 cells are adenocarcinomal epithelial cells and numerous malignant cells are known to express CXCR4 (*16, 30, 94*). Other normal epithelial tissues have been shown to have little to no expression of CXCR4

including breast, ovarian, and prostate epithelia (*16, 95, 96*). However, the epithelial cells of the colon normally express CXCR4, as do the retinal pigment epithelial cells of the eye, and yet the endogenous function of CXCR4 in the epithelial tissues is not fully understood (*16, 18*).

Though CXCR4 is extensively expressed on a wide variety of cellular subsets and tissues, current research suggests that CXCR4 expression is heterogeneously represented by posttranslational modifications, splice variants, and dimerization (*49, 58, 61, 97*). This variation allows CXCR4 to discriminately mitigate the different processes under the receptors' control (*97*). Furthermore, despite its wide spectrum of cellular expression, CXCR4 remains a pharmacological target because its importance to many pathologies, in particular HIV-1 (*16, 52, 77, 98-112*).

2.3 CXCR4 and HIV-1 Infection

CXCR4 plays a critical role in the infection of cells by HIV-1 as a coreceptor to viral entry. A correlation exists between CXCR4 acting as an HIV-1 coreceptor, disease progression over time, and rapid depletion of $CD4^+$ T-cells (Figure 4) (*110, 113, 114*). HIV-1 strains isolated from female patients experiencing cognitive impairment due to AIDS preferentially used CXCR4 as the viral entry coreceptor (*115*). Extensive research has been dedicated to the use of CXCR4 as a potential drug target to combat the disease (*105-108, 110, 112, 114, 116-118*). HIV-1 entry into $CD4^+$ cells is generally regulated by the chemokine receptors CXCR4 and CCR5. Selection between the two major coreceptors is determined by the third variable loop (V3) of the viral glycoprotein gp120

(*119-121*). Genotype variation in the V3 loop causes a phenotypic shift from the virus using primarily CCR5 as its coreceptor for infection to CXCR4. The phenotype shift was originally identified by the virus' ability to form syncytia in T-cells (X4 viral strains using CXCR4) versus non-syncytia inducing (R5 viral strains using CCR5) (*122, 123*).

Prior to coreceptor/gp120 binding, gp120 interacts with CD4, which induces conformational changes in the glycoprotein and leads to colocalizaion of CD4 with the viral coreceptor (*124*). These conformational adjustments expose and enhance the affinity for the coreceptor (*121, 125, 126*). Once the coreceptor binding has occurred, the virus inserts another glycoprotein, gp41, into the cell membrane and induces the fusion between the viral particle and the cell membrane (*127, 128*). The conformational changes and the cryptic conformation of the gp120/chemokine receptor binding site protect gp120 from the development of neutralizing antibodies (*116, 129*). The defining residues for coreceptor selection are the 11^{th} or 25^{th} residues of the V3 loop. If either residue is positively charged the gp120 molecule will bind CXCR4; otherwise CCR5 will be used as the coreceptor (*121, 130*). Other small mutations to the V3 loop have the ability to convert R5 strains phenotypically to X4 strains. Generally those mutations involve negatively charged residues becoming neutral residues (i.e. D329Q), negatively charged residues becoming positively charged residues (i.e. D329R), or neutral residues becoming positively charged (i.e. S313R) (*120, 131, 132*).

The V3 loop, sometimes also referred to as the third hypervariable region, consists of 19-37 amino acids, which forms a β hairpin structure (*120*). The V3 loop is essential for binding to the coreceptor and mimics a β hairpin found in the endogenous chemokines for either CCR5 or CXCR4 (*120, 121*). Superposition of the β hairpin

structures from V3 loop of the HIV-1 III_B strain (X4 strain) with homologous structure from CXCL12 are featured in Figure 5 (*120*). The CXCL12 motifs IVARLKN and NRQVCI were matched with the HIV-1 III_B gp120 motifs KSIRIQR and RAFVTI and demonstrate strong structural homology in the β turn despite the HIV-1 III_B turn containing two additional residues (G319 and P320) (*120*). The amazing mimicry that HIV-1 displays in the V3 loop accentuates one of the major challenges to interfering with the gp120/coreceptor interaction during viral entry(*133*).

Site directed mutagenesis of CXCR4 demonstrated that the second and third extracellular loops of the receptor are of particular importance to the binding of gp120 (*134-137*). Acidic residues of CXCR4 in the N-terminus, the extracellular loops, and transmembrane helices were shown to be influential to gp120 binding and CXCR4 coreceptor activity, due in part to charge interactions between the negatively charged receptor residues with the positively charged residues of HIV-1 V3 loop (*50, 131, 135, 138-140*) (Figure 1). Of particular importance to HIV-1 binding are the extracellular regions of CXCR4 rich in tyrosine, glutamic acid, and aspartic acid residues (*138*).

The binding site for gp120 for the most part is discrete from the binding site of CXCL12, where the later requires interaction with the N-terminus of the receptor for binding and the former dependent on the extracellular loops (*40, 50*). Mutagenesis analysis of the receptor revealed that those residues in the receptor influential in gp120 interaction had little effect the receptors ability to bind CXCL12 or induce receptor mediated signaling (*50*). Despite these findings, the endogenous CXCR4 ligand, CXCL12, possesses a moderate to high level of anti-HIV activity depending on the splice variant of CXCL12 and the viral strain of HIV-1 (*4, 5, 107, 116, 141-144*).

The first x-ray crystallography structures of CXCR4 reported by Wu et al. allowed for receptor modeling and prediction of the gp120/CXCR4 interaction (Figure 6). The binding of gp120 to CXCR4 adheres to the two-site binding model proposed for CXCR4/CXL12 interaction, previously described. In this instance, the V3 loop of gp120 interacts with the sulfotyrosine residues of CXCR4 in the first site. This association induces conformational changes in the V3 loop allowing for binding to the second site of CXCR4 on the extracellular loops, particularly the 2nd and 3rd loops (*49*). The binding model places emphasis on the electrostatic interactions that occur between the acidic residues of CXCR4 with the basic residues of the V3 loop in X4 gp120, previously described.

Additionally, the glycosylation of both gp120 and CXCR4 influence the selection and affinity of the virus for the coreceptor (*126*). Glycosylation in gp120 can shield positively charged amino acids, particularly in the V3 loop, and thereby effect association with either CCR5 or CXCR4 (*126*). The dual tropic NL-952 virus strain demonstrated that one glycosylation site was essential to distinguish between CCR5/CXCR4 (*126*). The lack of glycosylation at this site allowed for CXCR4 selection, otherwise CCR5 would be used as the coreceptor (*126*). Furthermore, the overall glycosylation of gp120 makes the virus highly resistant to the development of neutralizing antibodies against a broad array of viral strains (*129, 145-149*). Similarly glycosylation of CXCR4 is imperative to shield positive residues in its extracellular regions, enhancing the electrostatic interaction of positively charged gp120 with negatively charged CXCR4 extracellular regions (*126*).

2.4 Current HIV/AIDS Therapy

HIV-1 continues to affect over 33 million people worldwide with nearly 2.6 million new infections and 2.1 million HIV/AIDS related deaths in 2009, according to the Joint United Nations Programme on HIV/AIDS (*1*). However, despite nearly 30 years of research and over 20 approved drugs, neither a cure nor a vaccine is available. Therefore current HIV/AIDS therapy is relegated to a chronic treatment strategy (*1, 150-153*). Additionally, there is a great need for less expensive and more tolerable drug therapies, while managing the constant propagation of drug resistant strains of the virus in treatment experienced patients (*154*).

Antiviral drug development strategies have been targeted towards either the viral proteins or host's cellular proteins (*102, 103, 155*). Targeting viral proteins has the potential of selecting drugs that are more specific and highly potent, but with the added possibility of selecting for viral resistance. Targeting drugs to host proteins can confer a broader spectrum of anti-viral activity, while limiting the development of viral resistance (*103*). The majority of the marketed drugs for highly active antiretroviral therapy (HAART), including those used as first line therapies, are small molecule drugs that act as viral enzyme inhibitors. Three different drug classes have been developed to inhibit the ability of HIV-1 reverse transcriptase to convert viral RNA to double stranded DNA; non-nucleoside reverse transcriptase inhibitors (NNRTIs) like efavirenze, nucleoside reverse transcriptase inhibitors (NRTIs) like zidovudine (AZT), and one nucleotide reverse transcriptase inhibitor (NtRTI) tenofovir disoproxil fumarate (*151*). Integrase inhibitors are a relatively new class of HAART drugs that restrict the viral double

stranded DNA from integrating into the host genome. This class of drugs is composed of one currently approved agent, raltegravir (*151*). Protease inhibitors like saquinavir are another class of drugs that interfere with HIV's ability to generate new viral particles (*151*). A comprehensive list of the currently marketed HIV drugs can be found in Table 3.

Although current HIV-1 therapy is much improved of late, there are numerous shortcomings associated with HAART. One of the greatest challenges in HIV therapy is patient compliance. Treatment adherence must be maintained at a rate of 95%, which correlates to missing two doses per month. Missing more than two doses dramatically increases the therapeutic failure rate to 50% (*153, 156, 157*). A major factor in patient compliance is drug-drug interactions because of the combined therapy, adverse effects, and access to medicine (*156, 158, 159*). Other deficiencies include less than optimum pharmacokinetics, including but not limited to the oral bioavailability, the first-pass metabolism, and/or the biodistribution of drugs into sanctuary sites like the brain, secondary lymphoid organs, and testes (*151, 159-161*).

HAART drugs also inherently will select for drug resistant strains due to the error prone transcription of HIV RNA by viral reverse transcriptase and host DNA polymerase to double stranded DNA (*162*). The lack of DNA proofreading, by either of the aforementioned enzymes, compounded with a viral replication cycle of approximately two days will eventually generate a large pool of virus variants (*162, 163*). The drug resistant variants will predominate the newly replicated virus pool and can lead to modification of the prescribed therapy or in the worst-case scenario lead to therapeutic failure (*151, 162, 164*).

Antiviral therapy can effectively diminish the circulating plasma virus levels below the limit of detection. Despite these low levels of viremia, the virus continues to be replicated in physiological reservoirs and latently infected cells, both of which contribute to the inability to "cure" patients of the virus (*151*). Latently infected T-cells and macrophages produce little to no virus until activated and can serve as a pool for viral rebound if HAART therapy is discontinued or harbor drug resistant strains (*3, 165*). Although, these cells are limited in number (1 out of 1,000,000 resting cells $CD4^+$ T-cells), they pose a major hurdle to complete viral eradication in infected patients (*3, 165*). Furthermore, macrophages have longer circulating half-lives (~2 weeks) than many other cell populations, and therefore can produce virus for an extended period (*151, 166, 167*). Additionally, macrophages have the added ability to produce new virus without cytopathy (>200 virus particles/day), which differs from T-cell viral production (*151, 166, 167*). Although macrophages are responsible for very little viral production (T-cells produce >99% of HIV-1 particles), over 50% of tissue macrophages are infected in patients and normally reside in close proximity to other HIV susceptible cells (*151, 165*). Predictive models of viral decay dynamics in treatment-experienced patients show that HAART is most effective at stopping on going infection of circulating T-cells, but is ineffective at treating the latently infected cell populations (*160, 161, 168-170*). Furthermore, models predict that the long-term (>7 years of treatment) half-life of the virus in the body reaches infinity due to those latently infected cells and persistent viremia that would likely lead to viral rebound if treatment was discontinued (Figure 7) (*3, 171*).

The virus level in the plasma is used clinically to determine a patients' viral load, however viral replication can be ongoing in physiological reservoirs and sanctuary sites outside plasma. Of particular interest are the gut associated lymphoid tissues (GALT), the brain, and the testes (*151*). The greatest numbers of CD4+ T-cells are located within the GALT and this reservoir of T-cells becomes rapidly depleted upon HIV-1 infection (*172-174*). Therefore, the GALT becomes susceptible to other opportunistic infections due to a lack of host immunity (*172-174*). The brain and central nervous system are historically difficult to deliver drugs to because of the presence of the blood brain barrier (BBB). Many of the current HAART drugs are lacking the physicochemical properties to passively transverse the BBB and many are substrates for efflux transporters located at the BBB (*151, 175-180*). With little to no HAART drug concentrations on the other side of the BBB, HIV-1 replicates uninhibited in microglial and other cells of the CNS contributing to the development of HIV-1 associated dementia (*115, 151, 181*). The testes are another sanctuary site with a physiological barrier (blood-testes barrier, BTB) that prohibits the distribution of certain drugs from the plasma to the tissue (*182*). The BTB is similar to the BBB with tight junctions that are formed between the barrier cells, while expressing efflux transports (*182*). The virus is able to translocate the BTB by still unconfirmed mechanisms and form a pool of virus for transmission (*182*). Because the circulating drugs in the plasma are unable to penetrate these sancutatry sites, viral replication can proceed with little pharmacological hindrance.

Therefore, current investigation of alternative drug targets have emerged, particularly those focused upon other portions of the viral replication cycle. Some of these new therapies are classified as entry inhibitors, which interfere with HIV-1's ability

to adsorb the cell surface (*104, 183*). Others prevent the cell from become infected by targeting host proteins like CD4 or the chemokine coreceptors and disrupt binding to either site (*104, 105, 110, 116, 117, 158*). Currently, only two entry inhibitors have made it to the market, enfuvirtide and maraviroc. Enfuvirtide is a synthetic peptide drug that interferes with HIV-1 gp41's ability to fuse the viral and cell membranes together, thereby protecting the cell from viral infection (*183, 184*). Maraviroc is a small molecule drug that acts as a CCR5 antagonist to prevent the interaction between HIV and the coreceptor (*108, 153, 158*). Maraviroc is only clinically effective against the R5 strains of the virus and is ineffective against dual, mixed or X4 tropic viruses (*108, 153, 158*). In addition to these two members of the entry inhibitor drug class, many others have entered preclinical and clinical investigation and continue to be evaluated.

2.5 CXCR4 Targeted Drug Delivery

Viral reservoirs continue to be an underserviced portion of the HIV susceptible cell population and since many collectively believe that HAART has reached its full potential, new methods/drugs are needed to combat HIV-1 (*160, 161, 168, 169*). Targeted drug delivery could be one strategy to overcoming the challenge of viral reservoirs by boosting intracellular concentrations of anti-viral drugs within HIV-1 susceptible cells prior to their initiation of latent behavior, in their latent state, or prior to entering physiological sanctuary sites. Targeted drug delivery systems are more common in other therapeutic areas like cancer and exist in a wide variety of constructs (liposome, polymerosomes, denderimers, nanoparticles, peptidic conjugates, antibody directed,

PEGylated proteins, etc.) (*185*). However like cancer, many of the physicochemical, pharmacokinetic, and pharmacodynamic shortcomings of HAART drugs have drawn research to the use of targeted drug delivery and nanotechnology strategies to improve therapy (For extensive reviews see references) (*186, 187*).

CXCR4 is an attractive portal for drug delivery that has garnered attention previously as a target for small molecule and peptide entry inhibitors (Table 4) (*105, 106*). Targeting to a specific host protein like CXCR4, which is expressed on a smaller cellular subset, prevents the general cell population from exposure to the antiviral drug (*102, 103, 155, 188*). Additionally by acting through the CXCR4 receptor, a drug delivery system could act on two fronts against the virus. The first front would be as a HIV-1 coreceptor inhibitor. By occupying surface expressed CXCR4 on HIV-1 susceptible cells, a drug delivery system acting as an entry inhibitor could block the gp120 interaction with CXCR4 and prevent the insertion of gp41 into the host cell. The second front would be the delivery of a small molecule drug cargo, such as an NRTI or protease inhibitor, thereby interfering with a viral enzyme necessary for replication. Therefore, enhancing the anti-viral drug concentration in the susceptible cell if it were to become infected while attempting to protect the cell from the virus.

2.6 Modified Endogenous and Exogenous Viral Chemokines as CXCR4 Ligands

The anti-HIV activity of chemokines is derived from some level of competitive binding for the coreceptor, though the binding sites for the CXCL12 and gp120 are distinct (*4, 5, 143*). Additionally, the agonistic behavior of CXCL12 induces CXCR4

internalization, sequestering the receptor intracellularly with a majority being directed for degradation via lysosomes (*189*). Because of its natural ability to inhibit HIV-1, extensive research was dedicated to elucidating peptide segments of CXCL12 or modifying CXCL12 to enhance its anti-viral properties. Heveker at al. have looked at the binding and anti-HIV activity of several segmented peptides derived from CXCL12, those peptides derived from the N-terminus of CXCL12 had the ability to retain receptor binding and the capacity to inhibit HIV-1 (*190*). The best candidate from their research is a disulfide linked homodimer derivative sequence from amino acids 5-14 of CXCL12 with nanomolar binding affinity and anti-HIV activity (Figure 8) (*191*).

Although significant attention was drawn toward modifying and enhancing the anti-HIV of the endogenous CXCR4 ligand, exogenous viral encoded chemokines have been identified with the ability to interact with host chemokine receptors. Large DNA viruses, such as herpesviruses, have chemokine homologues integrated into their genome (Figure 2). It is possible that the virus has seized and manipulated chemokine genes from their hosts through parallel evolution with the goal of overcoming the hosts defenses or modulating certain cellular activation or differentiation pathways (*141*). Viral macrophage inflammatory protein-II (vMIPII also referred to as vCCL2) is a human herpesvirus-8 (also referred to as Kaposi's sarcoma associated herpesvirus) encoded chemokine with the capability to bind with both of the major HIV-1 coreceptors CCR5 and CXCR4 (*192-194*). Both CXCL12 and vMIPII share structural and sequence similarities (Figure 9 and Figure 10). Evaluation of the different motifs of vMIPII revealed that the N-terminus region, similar to that of CXCL12, was important to receptor binding (*195, 196*). The N-terminus of vMIPII contains multiple basic residues

giving the sequence a net positive charge. The positively charged region of vMIPII draws further similarities between it and CXCL12 and even the V3 loop of gp120 in X4 viral strains.

Synthetic peptides derived from N-terminus vMIPII retain affinity for CXCR4, while also demonstrating anti-HIV activity (*195, 197, 198*). Synthetic derivatives of vMIPII have the capacity to act as competitive antagonists to CXCL12 and HIV-1 without activating the downstream processes of CXCR4 like calcium mobilization (*196*). Because of the importance of CXCR4/CXCL12 interaction to many endogenous functions, antagonistic interaction is desirable for an anti-HIV molecule. Potentially, agonistic reaction could result in over activation of CXCR4 and likewise recruitment of cells unnecessarily.

The peptide derivative, V3, consists of the 10 amino acids that make up the N-terminus (Leu-Gly-Ala-Ser-Trp-His-Pro-Asp-Lys) of vMIPII. The V3 peptide binds to CXCR4 albeit with a K_D 1400 times less than CXCL12 (*192, 195, 196*). However, the V3 peptide does have greater affinity than similar peptide fragments of CXCL12 (*192*). Interestingly, modification of the same sequence by synthesis with unnatural D amino acid stereoisomers dramatically increased the affinity of peptide toward the receptor to the nanomolar range (*199*). The resulting peptide, DV3, is unique because of its improved affinity upon stereoconversion (inverso) from natural L amino acids to D amino acids (Figure 11) (*199, 200*). The peptide forms a turn structure between residues 5 and 8 (*200*). Another beneficial properties of DV3 is the built in protection from proteolysis by enzymes, since the peptides side chains are mirror images of natural peptide substrates for the enzyme.

The high affinity of DV3 with the added protection from proteolysis makes DV3 an attractive element for a drug delivery system. The short sequence can be easily synthesized by solid peptide phase synthesis and incorporated into a larger drug delivery system. The peptide can be modified through conjugation techniques to attach drugs, fluorophores, etc. DV3 has been shown to possess the ability to target and deliver proapoptotic peptide cargoes to enhance to cell death in tumor cells (*92, 201*). Therefore, demonstrating the DV3 sequence's ability to select for CXCR4 expressing cells and elicit a desired pharmacological effect. In the following thesis, a DV3 based peptide drug delivery system with multiple DV3 sequences was designed. The increased valency of DV3 in the drug delivery system should enhance the affinity toward DV3 as well as improve anti-HIV activity. The DV3 peptide carrier with the greatest affinity and anti-HIV activity will be selected and further modified by conjugation of antiviral drugs. Evaluation of the drug conjugate will be pursued in terms of the enhanced anti-HIV activity and the release of free drug from peptide. Finally, biodistribution analysis will determine if DV3 affinity toward CXCR4 will increase the accumulation in tissues/cells expressing CXCR4.

CHAPTER 3

SPECIFIC AIMS

The chemokine receptor, CXCR4, is essential to numerous endogenous functions, particularly cellular migration of naïve T-cells through interaction with CXCL12. The receptor is also critical to the pathology of HIV-1 acting as a coreceptor for viral entry into susceptible cells. Because of its importance in the HIV-1 infection process, it has the potential to serve as a portal into target cells for drug delivery as well as binding to the surface and acting as an entry inhibitor. The added benefit to targeted delivery is enhanced intracellular concentrations in infected or susceptible cells and consequently improved efficacy. DV3 is a short inverso peptide (10 amino acid residues) derived from the N-terminus sequence of vMIP-II that binds to CXCR4, thus making it a candidate for incorporation into a targeted drug delivery system. Therefore, DV3 containing peptide carriers designed to interact with CXCR4 were investigated, their effectiveness as entry inhibitors to HIV-1 was determined, and their ability to deliver a HAART drug to HIV-1 susceptible cells in vitro and in vivo was evaluated.

Therefore the specific aims of the thesis are:

1. To design, synthesize, and characterize CXCR4 targeted DV3 peptide carriers and evaluate their in vitro properties for uptake, cytotoxicity, and their capacity as CXCR4 entry inhibitors.

Hypothesis: Increasing DV3 valency on peptide carriers will enhance cellular association on CXCR4 expressing cells and inhibit HIV-1 infection through a competitive interaction with the coreceptor.

2. To design, synthesize, and characterize DV3 containing peptide carriers conjugated to either a reverse transcriptase or protease inhibitor and evaluate their ability to use CXCR4 as a drug delivery portal.

   Hypothesis: Enhancing the anti-HIV activity of the DV3 peptide carriers by the conjugation of potent anti-viral drugs as cargoes to be released intracellularly thereby utilizing CXCR4 as a drug delivery portal.

3. To improve drug loading and to increase the plasma persistence of the 4 copy peptide carriers by PEGylation

   Hypothesis: Increasing the number of drug molecules per DV3 peptide carrier will further enhance the anti-HIV activity of the peptide carriers by increasing the amount of intracellular anti-viral compound in vitro. Furthermore, the solubility of ritonovir is a limiting factor in its effectiveness therapeutically and PEGylation will overcome that limitation. Additionally, PEGylation will affect the biodistribution of the DV3 peptide carriers by increasing PEG size the DV3 peptide carriers will demonstrate longer residence time in vivo. DV3 peptide carriers will also increase cellular association with $CXCR4^{+}$ cells in vivo by accumulating in organs where $CXCR4^{+}$ cells are known to reside i.e., lymph nodes, spleen, gut, and lungs compared to untargeted controls.

CHAPTER 4

THE SYNTHESIS, CHARACTERIZATION, AND IN VITRO PROPERTIES OF MULTIVALENT DV3 PEPTIDE CARRIERS

4.1 INTRODUCTION:

AIM 1: To design, synthesize, and characterize CXCR4 targeted DV3 peptide carriers and evaluate their in vitro properties for uptake, cytotoxicity, and their capacity as CXCR4 entry inhibitors.

The inverso peptide of the 10 N-terminal amino acids of vMIPII has been identified as DV3. DV3 has been shown to bind to CXCR4 at a nanomolar concentration with an IC_{50} value 439 nM against CXCL12 (*199*). However, its capacity to act as an entry inhibitor HIV-1 has yet to be reported. The purpose of the current study was to design, synthesize, and characterize CXCR4 targeted DV3 peptide carriers. The novel designed multivalent peptide carriers incorporate orthogonally linked DV3 peptides to investigate the effect of targeting moiety number (copy number) on HIV-1 entry and cellular association. The DV3 peptide carriers were studied using a reporter cell line (TZM-bl) that is responsive to early infection by HIV-1 particles, which induce the expression of the luciferase enzyme and ultimately light output from the enzyme is proportional to the number of cells that are infected. Additionally, the best peptide carrier candidate was further tested for its specificity for CXCR4 and observed its ability to induce receptor mediate endocytosis.

4.2 MATERIALS AND METHODS:

4.2.1 Materials: Diisopropylethylamine (DIEA), N-methylpyrrolidone (NMP), methanol (MeOH), dichloromethane (DCM), piperidine, triisopropylsilane (TIS), trifluoroacetic acid (TFA), 3,6-dioxa-1,8-octanedithiol (DODT), ethanedithiol (EDT), acetonitrile (ACN), acetic acid, α-cyanohydroxy-cinnamic acid (CHCA) and ethanol (EtOH) were purchased from Sigma-Aldrich, J.T. Baker, Thermo Fisher Scientific, or Burdick-Jackson to biotech or HPLC grade. 1-hydroxy-7-azabenzotriazole (HOAt), O-(7-Azabenzotriazole-1yl)-N,N,N'N'-tetramethyluronium hexafluorophosphate (HATU) were purchased from GenScript USA Inc. (Piscataway, NJ). Fluorescein isothiocyanate (FITC), Fmoc-D-Lys(Mtt)-OH, Fmoc-D-Lys(Boc)-OH, Fmoc-D-Asp(OtBu)-OH, Fmoc-D-Pro-OH, Fmoc-D-Arg(Pbf)-OH, Fmoc-D-His(Trt)-OH, Fmoc-D-Trp(Boc)-OH, Fmoc-D-Ser(tBu)-OH, Fmoc-D-Ala-OH, Fmoc-Gly-OH, Boc-Leu-OH, 5-Fmoc-3-oxapentanoic acid, Fmoc-Gly-HMP-TentaGel resin and DiBoc were purchased from AnaSpec, Inc. (Freemont, CA) or Chemp-Impex International Inc. (Wood Dale, IL). Fmoc-D-Asp(OMpe)-OH was purchase from Bachem Americas, Inc. (Torrance, CA). NovaSyn-TG Sieb*r* resin was purchase from EMD Millipore (Billerica, MA). 2-ethoxyacetic acid was purchase from Oakwood Products, Inc. (West Columbia, SC). All water used was deionized water (diH_2O) from a MilliQ system (EMD Millipore, Billerica, MA).

4.2.2 FITC-2-amino-ethoxy-acetic acid conjugation: 2-amino-ethoxy-acetic acid and FITC were combined in a glass vial in a 1:1 molar ratio in a mixture of 9.5% diH_2O/

28.5% ACN/ 62% EtOH (v/v/v). Three eq of DIEA were added drop wise to the mixture for 48 h in the dark with stirring (Scheme 1). The reaction was stopped with 3 eq of acetic acid. The product was dried on a rotating evaporator. The product was then reconstituted in a 1:1 ratio of diH_2O/ACN and purified by semiprepartive HPLC on an XBridge BEH300 Prep C18 column (Water, Milford, MA) and mobile phase gradient consisting of (A) diH_2O with 0.05% TFA (v/v) and (B) ACN with 0.05% TFA (v/v) at flow rate of 5 ml/min. UV absorbance (UV_{ABS}) was measured at 254 nm, while fluorescence due to FITC was measured at excitation wavelength (λ_{EX}) of 494 nm and emission wavelength (λ_{EM}) of 519 nm and collected using a fraction collector. Similar fractions were pooled, lyophilized, and the presence of the final compound was characterized by electrospray ionization mass spectrometry (ESI-MS) on a Finnegan LCQDuo (Thermo Finnegan, San Jose, CA) by dissolving lyophilized FITC-2-amino-ethoxy-acetic acid conjugate in 500 µl MeOH. Additionally, analytical HPLC was conducted on a Waters e2695 Alliance System (Milford, MA) equipped with a photodiode array detector measuring UV_{ABS} from 200-600 nm and a fluorescence detector set for λ_{EX} of 494 nm and λ_{EM} of 519 nm. The mobile phase gradient consisted of (A) diH_2O with 0.05% TFA (v/v) and (B) ACN with 0.05% TFA (v/v) and the stationary phase was a Waters Symmetry C18 column (Milford, MA).

4.2.3 Fmoc solid-phase synthesis of peptide carriers: All DV3 peptide carriers were synthesized using a Nautilus 2400 (Argonaut Technologies, Redwood City, CA) automated synthesizer. For all DV3 peptide carriers, the D stereoisomers (inverso) of amino acids were used to confer resistance to proteolysis.

4.2.4 Fluorescently labeled 1 copy DV3 peptide carrier (MP100): (Scheme 2) Fmoc-Gly-HMP-TentaGel resin was swollen with DCM and washed several times with NMP. The Fmoc group was removed using 20% piperidine in NMP (v/v) for successive cycles of 8 min followed by 12 min followed by extensive washing with NMP. Amino acids were coupled to the resin using 5 eq of the amino acid, 5 eq of HOAt and HATU, and 10 eq of DIEA. Reactions proceeded for 1.5 h followed by washing of the resin with NMP. Fmoc deprotection was followed by the coupling of the next amino acid in the sequence continued until the DV3 peptide carrier sequence was completed as stated from the N-terminus to C-terminus with side chain protecting groups (Scheme 3); Boc-Leu-Gly-Ala-Ser(tBu)-Trp(Boc)-His(Trt)-Arg(Pbf)-Pro-Asp(OtBu)-Lys(Boc)-Lys(Mtt)-Gly-HMP-TentaGel-Resin (*202*). The orthogonal protecting group Mtt, shielding the ε amino group (the Lys sidechain amino group) of the first Lys residue, was removed using 8 successive washes of 1% TFA in DCM (v/v) for 3 min per wash as described elsewhere (*203-206*). After Mtt deprotection of the ε amino group of Lys, the resin was washed extensively with DCM. The resin was then washed with NMP several times and 5-Fmoc-3-oxapentanoic acid (5 eq) was coupled to the free ε amino group of Lys for 1.5 h in the presence of 5 eq of HOAt and HATU and a 10 eq of DIEA followed by several washes with NMP. Fmoc deprotection as previously described was used to remove the Fmoc group from the oxapentanoic acid residue. FITC was coupled to the oxapentanoic acid by using 5 eq of FITC in the NMP in the presence of 10 eq of DIEA for 16 h in the dark followed by several washes with NMP then DCM (*207-209*). MP100 was cleaved from the resin using 95% TFA/2.5% diH_2O/2.5% TIS (v/v/v) for 1 h with stirring. Cleaved peptide was precipitated in ice-cold diethyl ether, centrifuged, washed twice with ice-cold

diethyl ether, decanted, dried under fume hood, and stored at -80^{o} C. MP100 was purified using an XBridge BEH300 Prep C18 column (Waters, Milford, MA) and mobile phase gradient consisting of (A) diH_2O with 0.1% TFA (v/v) and (B) ACN with 0.1% TFA (v/v). UV_{ABS} at 254 nm, while fluorescence due to FITC was measured at λ_{EX} of 494 nm and λ_{EM} of 519 nm and collected using a fraction collector. Similar fractions were pooled and lyophilized and the presence of the final compound was characterized by ESI-MS and analytical HPLC. ESI-MS and analytical HPLC was conducted as previously described, however the stationary phase was a ZORBAX Eclipse Plus C18 column (Agilent, Santa Clara, CA) for analytical HPLC.

4.2.5 Fluorescently labeled 2 copy DV3 peptide carrier (MP200): (Scheme 4) Fmoc-Gly-HMP-TentaGel resin was swelled with DCM and washed several times with NMP. The Fmoc group was removed using 20% piperidine in NMP (v/v) for successive cycles of 8 min followed by 12 min and then extensive washing with NMP. Fmoc-D-Lys(Mtt) was coupled to the resin using 5 eq of the amino acid to be coupled, 5 eq of HOAt and HATU, and 10 eq of DIEA. The reaction was allowed to proceed for 4 h followed by washing with NMP then DCM. Mtt deprotection of ε amino group of the Lys residue was done by washing the resin 12 times with 2% TFA in DCM (v/v) for 5 min per wash (Scheme 5). The deprotection mixture was collected via the fraction collection port of the synthesizer to monitor the removal of the Mtt cation (freed Mtt cation appears yellow in solution) (Figure 12). Following the deprotection, the resin was washed several times with DCM, MeOH, then NMP. Fmoc-D-Lys(Mtt)-OH was coupled to the ε amine of the first Lys residue by using 5 eq of the amino acid to be coupled, 5 eq of HOAt and HATU,

and 10 eq of DIEA. Mtt deprotection was repeated for the second Fmoc-D-Lys(Mtt)-OH residue. To the free ε amino group, 3 eq of FITC-2-amino-ethoxy-acetic acid (synthesis described earlier) was coupled with 3 eq of HOAt and HATU and 6 eq of DIEA for 4 h in the dark then washed with NMP four times. Uncoupled free ε amino groups were blocked with 6 eq DiBoc and 6 eq DIEA in NMP for 2 h followed by several washes with NMP. The Fmoc groups located on the α amino groups of the Lys residues were removed by 20% piperidine in NMP (v/v) as previously described. Amino acids were coupled to the resin using 8 eq of the amino acid to be coupled, 8 eq of HOAt and HATU, and 16 eq of DIEA. Reactions proceeded for 4-6 h followed by washing of the resin with NMP, Fmoc deprotection, then the coupling of the next amino acid in the sequence continued until the DV3 peptide carrier sequence was completed as stated from the N-terminus to C-terminus with side chain protecting groups; [Boc-Leu-Gly-Ala-Ser(tBu)-Trp(Boc)-His(Trt)-Arg(Pbf)-Pro-Asp(OMpe)-Lys(Boc)]$_2$-Lys(Lys(2-aminoethoxy-aceticd-FITC)-Gly-HMP-TentaGel-Resin (*202, 210-213*). MP200 was cleaved from the resin, purified by semiprepartive HPLC, lyophilized, then characterized by analytical HPLC as described earlier. The mass of MP200 was determined by MALDI-TOF mass spectrometry as follows; lyophilized MP200 was dissolved in diH_2O and combined in a 1:1 ratio with prepared CHCA matrix and measured on an ABI-MDS SCIEX 4800 MALDI-TOF/TOF (Foster City, CA).

4.2.6 <u>Fluorescently labeled 4 copy DV3 peptide carrier (MP400):</u> (Scheme 6) Synthesis of MP400 was conducted in parallel to MP200 with the following differences: 4 residues of Fmoc-D-Lys(Mtt)-OH were joined through the coupling of their ε amino groups to the

C terminal carboxyl group of the incoming Fmoc-D-Lys(Mtt)-OH residue. Mtt deprotection protocol was applied after each Fmoc-D-Lys(Mtt)-OH coupling then FITC-2-amino-ethoxy-acetic acid was coupled to the ε amino group of the 4th Fmoc-D-Lys(Mtt)-OH after Mtt deprotection. The amino acids of the DV3 sequence were coupled after Fmoc deprotection using 16 eq of amino acid, 16 eq of HOAt and HATU, and 32 eq of DIEA. The resulting DV3 peptide carrier had the following sequence from the N-terminus to C-terminus with side chain protecting groups; [Boc-Leu-Gly-Ala-Ser(tBu)-Trp(Boc)-His(Trt)-Arg(Pbf)-Pro-Asp(OMpe)-Lys(Boc)]$_4$-Lys(Lys(Lys(Lys(2-aminoethoxy-acetic acid-FITC)))-Gly-HMP-TentaGel-Resin. Peptide cleavage, semipreparative HPLC, analytical HPLC, and MALDI-TOF MS were performed as described previously.

4.2.7 NMR of fluorescently labeled multivalent DV3 peptide carriers: Stock solution of MP100, MP200, and MP400 were concentrated and dried on a speed vacuum. Each was reconstituted with an ampule of deuterium oxide and transferred to an NMR tube. Proton NMR was performed on a Bruker 400MHZ NMR spectrophotometer (Billerica, MA). Characterization was determined as the count of expected aromatic/cyclic side-chain hydrogens by integration of the spectra.

4.2.8 FITC standard curve: Lyophilized MP100, MP200, and MP400 were dissolved in autoclaved PBS and their concentrations were determined by the generation of a FITC standard curve. The standard curve was created by dissolving free FITC in PBS and over concentrations ranging from 12 nM-7.5 μM in three separate dilutions. The fluorescence

of the FITC/PBS solutions was measured using a Tecan GENios microplate reader (Durham, NC) with the supplied λ_{EX} (485 nm) and λ_{EM} (535 nm) filters. The three separate standard curves were fit globally using a first order polynomial function. From the global standard curve, the concentration of MP100, MP200, and MP400 dilutions were interpolated and subsequently the concentrations of the stock solutions were determined.

4.2.9 Biotinylated 4 copy DV3 peptide carrier (MP401): (Scheme 7) Synthesis of biotinylated 4 copy DV3 peptide carrier (MP401) was conducted in a similar manner to MP400. Following the addition of the 4th Lys residue to the Lys backbone, the Mtt group of the ε amino was deprotected as previously described. To the free ε amino group, biotin was coupled using 5 eq of biotin, HOAt, and HATU with 10 eq of DIEA in NMP for 4 h, followed by washing with NMP and DCM. Biotin coupling was conducted twice. Following biotin addition, the α amino groups were Fmoc deprotected as previously described and the DV3 sequence amino acids were coupled in succession. MP401 was cleaved from the resin using 94/2/2/2% TFA/H_2O/TIS/DODT (v/v/v/v) for 4 h at room temperature with stirring. The peptides were precipitated in ice-cold ether, centrifuged, and washed 2 additional times with ice-cold ether. MP401 was lyophilized. The peptide was then dissolved in H_2O and ACN, flash frozen with liquid nitrogen then lyophilized. MP401 was purified by semipreparative HPLC as previously described, then lyophilized. The purified MP401 was then characterized by analytical HPLC, ESI-MS, and MALDI-TOF-MS.

4.2.10 Synthesis of DV3 peptide (DV3): DV3 was synthesized to be used as a control (Scheme 8). DV3 was synthesized using NovaSynTG Sieber resin using Fmoc peptide synthesis. Each coupling was performed using 4 eq of amino acid, 4 eq HOAT, 4 eq HATU, and 8 eq of DIEA for 2 h. Synthesis proceeded until the following sequence was complete Boc-Leu-Gly-Ala-Ser(tBu)-Trp(Boc)-His(Trt)-Arg(Pbf)-Pro-Asp(OMpe)-Lys(Boc)-Resin. The peptide was cleaved from the solid support by using 92.5/2.5/2.5/2.5 TFA/H_2O/TIS/DODT for 3.5 h with stirring. DV3 was precipitated in ice-cold ether centrifuged, decanted the supernatant, and washed 2 additional times with ether. The peptide was dried in the fume hood, reconstituted in H_2O/ACN, and lyophilized. DV3 was purified in a similar manner as previously described by semipreparative HPLC, and characterized using analytical HPLC and MALDI-TOF.

4.2.11 Reagents: Tzm-bl cells from Dr. John C. Kappes, Dr. Xiaoyun Wu, and Tranzyme Inc., HTLV-III_B/H9 (referred to as HIV-1 IIIB from this point forward) from Dr. Robert Gallo, HIV-1_{Ba-L} (referred to as HIV-1 BaL from this point forward) from Dr. Suzanne Gartner, Dr. Mikulas Popovic, and Dr. Robert Gallo, MT2 cells from Dr. Douglas Richman, CXCR4 monoclonal antibody (Clone 44708), and bicyclam JM-2987 (hydrobromide salt of AMD-3100, referenced as AMD3100 from this point forward) were obtained through the NIH AIDS Research and Reference Reagent Program, Division of AIDS, NIAID, NIH (*132, 183, 184, 214-222*). Additionally, the following reagents were purchased from the identified suppliers: Steady Glo® Luciferase System (Promega, Madison, WI); Rhodamine labeled dextran molecular weight 10,000 Da (Rho-DEX), Hank's Balanced Salt Solutions (HBSS), Dulbecco's Modified Eagle Medium

(DMEM), heat inactivated fetal bovine serum (FBS), penicillin-streptomycin (PEN/STREP), and non-essential amino acids (NEAA), Rhodamine-Lysotracker (Invitrogen, Carlsbad, CA); SuperBlock Blocking Buffer (Thermo Fisher Scientific, Inc., Rockford, IL); 4',6-diamidino-2-phynylindole dihydrochloride (DAPI) (AnaSpec, Inc., Fremont, CA); Goat anti-mouse IgG conjugated with horseradish peroxidase (referred to as 2^o Ab) (Santa Cruz Biotechnology, Inc., Santa Cruz, CA); TMB substrate solution (eBioscience.com, San Diego, CA); and 3-(4,5,-dimethylthiazol-2-yl)-2,5-diphenyltetrazolium bromide (MTT) (Sigma-Aldrich, St. Louis, MO).

4.2.12 Inhibition of HIV-1 entry: The reporter cell line TZM-bl was used to measure HIV-1 entry by the replication dependent expression of luciferase under control of HIV-1 long terminal repeat (*183*). TZM-bl cells were maintained in growth medium consisting of DMEM supplemented with 10% FBS, 2% PEN/STREP, and 1% NEAA (v/v/v). Cells in 200 µl of DMEM were seeded to 96 well plates at a density of $1.25x10^4$ cells/ml and allowed to attach to the well surface overnight. The DMEM was removed from the adherent cells and replaced with 100 µl of 5, 2.5, or 0.5 µM each MP100, MP200, and MP400 to designated sets of 6 wells. Control cells were untreated with DV3 peptide carriers. To triplicate wells, the X4 HIV-1 strain HIV-1 IIIB was added in 100 µl of growth medium for a multiplicity of infection (MOI) of 0.038, while to the remaining triplicate wells 100 µl of growth medium was added to act as a control. Cells were then incubated at 37^o C with 5% CO_2 for 72 h. Cells were then lysed using the Steady Glo® Luciferase reagent and the HIV-1 replication-dependent luminescence measured on a Tecan GENios microplate reader.

4.2.13 Cytotoxicity of DV3 peptide carriers: Cell viability was determined using the MTT assay. TZM-bl cells were seeded to a 96 well plate at a density of $1.5x10^4$ cells/ml and allowed to attach to the well surface overnight. The growth medium was removed and replaced with 100 µl of 5, 2.5, or 0.5 µM of each MP100, MP200, and MP400 to designated triplicate wells. Control cells were untreated with DV3 peptide carriers. Cells were incubated for 24 h at 37^o C with 5% CO_2. The contents of the wells were discarded and replaced with 100 µl PBS and 25 µl MTT (5 mg/ml) and incubated overnight at 37^o C. The contents of the wells were removed and the generated formazan crystals were dissolved in 200 µl DMSO. The absorbance at 570 nm was measured on a Tecan GENios microplate reader.

4.2.14 Confocal microscopy of DV3 peptide carriers: TZM-bl cells were added to a chambered cover glass slide at a density of $1.0x10^5$ cells/ml and allowed to attach overnight. MP100, MP200, and MP400 were added to individual chambers at a concentration of 1 µM in HBSS warmed to 37^o C with the nuclear stain 1 ng/ml DAPI and the endosome marker of 250 ng/ml Rho-DEX. Cells with DV3 peptide carriers were incubated for 2 h at 37^o C with 5% CO_2. Cells were then washed twice with PBS. The cells were fixed with 500 µl 3% formalin in PBS for 15 min, then washed twice with PBS, and imaged in 600 µl PBS on a Leica TCS SP5 Confocal Microscope (Leica Microsystems, Inc., Buffalo Grove, IL) at the Analytical Cytometry/Image Analysis Core Facility (EOHSI, Rutgers, The State University of New Jersey, Piscataway, NJ. Image adjustment was done using Adobe PhotoShop software with all images being brightened to the same levels.

4.2.15 Determination of anti-HIV IC50 of MP400: Tzm-bl cells were added to a 96 well plate at a density of $2.5x10^4$ cells/ml to triplicate wells and allowed to attach to the cell surface overnight. The growth medium was replaced with serial dilutions of MP400 from 5 μM to 0 μM in DMEM. After 1 h incubation, HIV-1 IIIB or HIV-1 BaL at an MOI of 0.038 was added to the designated wells and to control wells additional media in place of virus. Cells were incubated with the virus for 72 h at 37^o C with 5% CO_2. HIV-1 replication dependent luminescence was measured after lysing the cells with Steady Glo® reagent. To calculate the IC_{50} of MP400 after normalizing the data to the untreated control wells that were incubated in the absence of virus (set as 0%) and to the untreated control wells incubated in the presence of virus (set as 100%). Nonlinear regression analysis was performed using a down hill dose response model (Equation 1) to determine IC_{50}.

Equation 1:

$$Y = Bottom + \left(\frac{Top - Bottom}{1 + 10^{(X - LogIC50)}} \right)$$

Where Top and Bottom are fitted parameters to the data sets maximum and minimum Y value; X is the Log of the MP400 concentration; $LogIC_{50}$ is the fitted parameter that corresponds to concentration at which 50% of the Y value of the difference between Top and Bottom; and Y is the HIV-1 induced luminescence measured. The bottom parameter was constrained to 0 simplifying Equation 1 as follows:

Equation 2:

$$Y = \left(\frac{Top}{1 + 10^{(X - LogIC50)}} \right)$$

Additionally, the nonlinear fit was weighted by 1/(standard deviation)^2 and the curves generated from 3 separate experiments were statistically compared by F test.

4.2.16 Determination of anti-HIV IC50 of AMD3100 and CXCR4 monoclonal antibody: Procedure similar to described in 4.2.15. Briefly, TZM-bl cells were seeded to 96 well plate at 2.5x10^4 cell/ml in triplicate wells. Serial dilutions of the CXCR4 mAb and AMD3100 were added to designated sets of triplicates. HIV-1 strain IIIB was added at MOI=0.038 and the plates were incubated for 72h. HIV-1 infection dependent luciferase expression was measured using Steady Glo® reagent following manufactures instructions. The luminescence measured was normalized to untreated infected cells (100%) and untreated uninfected cells (0%).

4.2.17 Biotinylated 4 copy DV3 peptide carrier (MP401) inhibition by AMD3100: TZM-bl cells were plated to a 24 well plate in 0.75 ml at a cellular density of 1.0x10^5 cells/ml to triplicate wells in DMEM. Cells were allowed to attach to the surface of the plate overnight at 37^o C with 5% CO_2. AMD3100 was added to the growth medium to two sets of triplicate wells so that the final concentration was either 20 μM or 200 μM, while control wells were untreated. The plate was incubated for 30 min, the growth medium in all wells was removed, and then washed once with HBSS. Cells were treated with HBSS

(control), 1 μM of MP401, 1 μM of MP401 with 20 μM AMD3100, or 1 μM of MP401 with 200 μM AMD3100. The cells were incubated for 1 h at 37^{o} C, and then washed twice with HBSS. Cells were incubated with 20 μg/ml of F-SA in HBSS for 30 min at room temperature protected from light. Cells were washed twice with HBSS. Cells were lysed with 2 N NaOH overnight. NaOH was neutralized with 2 N HCl and the lysate transferred to an opaque black 96 well plate. Fluorescence was measured on a Tecan GENios microplate reader at an λ_{EX} of 485 nm and λ_{EM} 535 nm.

4.2.18 Biotinylated 4 copy DV3 peptide carrier (MP401) inhibition by CXCR4 monoclonal antibody: TZM-bl cells were plated to triplicate wells of a 96 well plate at a cellular density of 2.0x10^{5} cells/ml in 100 μl of DMEM. Cells were then incubated at 37^{o} C for 48 h until cells reached confluence in the well. Cells were then fixed with 3.7% formalin in PBS (v/v) for approximately 1 h at room temperature. The wells were then washed 3x with PBS. Cells were then incubated with varying concentrations of MP401 or AMD3100 in the presence of the 1 μg/ml or 10 μg/ml CXCR4 mAb (Clone 44708) in SuperBlock buffer, while control cells were treated with SuperBlock buffer without CXCR4 mAb, for 40 min on ice. Cells were washed 3x with TBST (tris buffered saline with 0.1% Tween 20 v/v). Cells were incubated with the 2^{o} Ab diluted to 1:50000 for 1 h at room temperature. Cells were washed 3x with TBST then incubated wells with 100 μl HRP substrate (TMB solution). Enzymatic conversion of the substrate was stopped with 100 μl 0.1 N HCl and absorbance at 450 nm was measured. Wells were normalized to triplicates that were blocking buffer only (0%) and triplicates treated with CXCR4 mAb

and without MP401 (100%). IC_{50} was calculated from 3 separate experiments for 1 μg/ml.

4.2.19 Comparison of intracellular versus extracellular association of 4 copy DV3 peptide carriers: Tzm-bl cells were seeded to 6 wells of a 24 well plate at a density of $1.0x10^5$ cells/ml and allowed to attach overnight. One pair of wells were untreated with MP401, but subjected to staining by DAPI and Rhodamine-Lysotracker. To a 2nd set of wells, MP401 was added at a concentration of 1 μM in HBSS warmed to 37° C with DAPI and the Rhodamine-Lysotracker. The 3rd set of wells contained MP401, DAPI, Rhodamine-Lysotracker and 100 μM of DV3. The cells were incubated for 1 h at 37° C CO_2. Cells were then washed twice with PBS. The cells were fixed with 500 μl 3.7% formalin for 20 min, then washed twice with PBS. One well from each treatment was further treated with 0.2% Triton-X 100 in PBS and washed once with PBS. All treatment groups were incubated with 10 μg/ml of F-SA. Cells will then be washed 3x with PBS and imaged in 500 μl PBS on an Olympus IX71 Inverted Microscope (Melville, NY). The PBS was removed and cells were lysed with 2 N NaOH for 24 h. The lysate was neutralized with equal amount of 2 N HCl and the contents transferred to a black walled black bottomed 96 well plate and fluorescence measured. Ratios of intracellular/extracellular fluorescence were calculated from untreated controls (0%), cells treated with MP401 (100%), and cells treated with MP401 and DV3.

4.2.20 Molecular modeling of 4 copy DV3 peptide carrier CXCR4 interaction:

A structural hypothesis on the 4 copy DV3 peptide carrier – CXCR4 binding was established using Discovery Studio 3.5 software suite. (Accelrys Inc. San Diego, CA). Dimeric (consisting A and B chains) x-ray diffraction-based structure of CXCR4 (PDB entry ID: 3ODU) was used as a starting data set for molecular simulations (*49*). Two identical copies of CXCR4 were positioned to form a tetrameric cluster facilitating a binding interface for one 4 copy DV3 peptide carrier molecule. The 4 copy DV3 peptide carrier was docked the to the receptor cluster manually using a set of H-bond interactions published previously (Choi et al Biochemistry 2012) to describe the binding of a bivalent DV1 ligand (*223*). Residue interactions are listed in Table 5. For energy minimization and molecular dynamics calculations CHARMm force filed was used to provide a conformer for the 4 copy DV3 peptide carrier – CXR4 complex at -107566.2 kcal/mol energy level and with satisfactory gradient tolerance of 0.0001 kcal/mol Å. The molecular dynamics simulation was performed for 100 ps at the temperature of 300K.

4.2.21 Statistical Analysis: Results are represented as the mean $\pm$ standard deviation unless otherwise specified. Statistical analyses were performed using GraphPad Prism Software v4.0c (GraphPad Software, Inc., La Jolla, CA) by ANOVA analysis and Tukey's posthoc test. Statistical significance was determined by a value of $p<0.05$. Non-linear regression analysis was also performed using GraphPad Prism Software with statistical analysis between curves and curve parameters determined by F test at a value of $p<0.05$.

4.3 RESULTS:

4.3.1 FITC-2-amino-ethoxy-acetic acid conjugation: The final product was characterized using multiple methods. FITC-2-amino-ethoxy-acetic acid had an expected molecular weight of 508.5 Da (Scheme 1), which was demonstrated in the negative mode setting as the predominant peak (507.1 Da) on a spectrum from ESI-MS (Figure 13). FITC-2-amino-ethoxy-acetic acid had a retention time of 11.71 minutes by both UV_{ABS} and fluorescence emission by analytical HPLC (Figure 14). The purity after semipreparative HPLC of FITC-2-amino-ethoxy-acetic acid was determined to be greater than 90% by area under the curve processing conducted by the Empower 2 Software (Waters, Milford, MA).

4.3.2 1 copy DV3 peptide carrier (MP100): MP100 was characterized in a similar fashion to FITC-2-amino-ethoxy-acetic acid. Final product had an expected molecular weight of 1842 Da (Scheme 2). ESI-MS spectra demonstrated three peaks that all correlate to different ionization states of MP100; [M/z] = 1842 Da, $[M+2H^+]/2$ = 921 Da, and $[M+3H^+]/3$ = 614 Da (Figure 15). MP100 had a retention time of 2.9 minutes by analytical HPLC that was detected by both UV_{ABS} and fluorescence emission (Figure 16) with a purity of approximately 90% after semipreparative HPLC purification. Proton NMR was used to further characterize MP100 and peak integration of the chemical shifts corresponding to the aromatic hydrogen correlate with the expected hydrogen count (Figure 17).

4.3.3 2 copy DV3 peptide carrier (MP200): MP200 was characterized in a manner similar to the other compounds. Final product had an expected molecular weight of 3118.44 Da (Scheme 4), however an observed in the MALDI-TOF spectrum of 1580.9 Da corresponds to an ionization state of $[M+2Na^+]/2$. Another peak of significantly less intensity at 3154 Da corresponds to an ionization state of $[M+K^+]/1$ (Figure 18). Analytical HPLC, following semipreparative HPLC, demonstrated a cluster of peaks with a retention time of 2.9 minutes by both UV absorbance and fluorescence emission (Figure 19). The peak clustering observed in the 2 copy DV3 peptide carrier HPLC is believed to be due to conformational isomers resulting from amino acid side chain interactions of the branched structure, but do not indicate a difference in the overall peptide carrier sequence. Proton NMR was used to further characterize MP200 and peak integration of the chemical shifts corresponding to the aromatic hydrogen correlate with the expected hydrogen count (Figure 20).

4.3.4 4 copy DV3 peptide carrier (MP400): MP400 was characterized in a manner similar to the other compounds previously described. The final product of MP400 had an expected molecular weight of 5671.34 Da (Scheme 6). Because of ionization of the peptide, an observed peak of 1418 Da was found to correlate with $[M+4H^+]/4$ (Figure 21). A retention time of 2.8 min was observed for analytical HPLC following the purification of MP400 by semipreparative HPLC (Figure 22). The 4 copy DV3 peptide carriers also generated a broad peak due to conformational isomers similar to the 2 copy DV3 peptide carriers. Proton NMR was used to further characterize MP400 and peak

integration of the chemical shifts corresponding to the aromatic hydrogen correlate with the expected hydrogen count (Figure 23).

4.3.5 Standard curve of FITC fluorescence: FITC dissolved in PBS was found to generate a standard curve for concentrations ranging from around 12 nM to 7.5 μM on a log-log scale. Regression analysis was able to fit the three standard curves to a global first order polynomial equation of $y = 1.396x + 19.91$ with an R^2 value of 0.9737 (Figure 24). The three generated standard curves were determined to be statistically similar by F test and therefore the global non-linear regression was used for the determination of the concentration of DV3 peptide carriers. Dilutions of stock solutions for MP100, MP200, or MP400 were interpolated from the standard curve and the stock solutions were determined to have the following concentrations MP100 = 62.9 μM, MP200 = 57.2 μM, and MP400 = 15.3 μM.

4.3.6 Biotinylated 4 copy DV3 peptide carrier (MP401): MP401 (Scheme 7) was successfully synthesized, purified, and characterized as the other DV3 peptide carriers. MP401 was shown to have a retention time of 3.52 min by UV_{ABS} (Figure 25). MALDI-TOF mass spectrometry detected the expected molecular mass for MP401 of 5407 Da (Figure 26). Additionally, ESI-MS measured several different M/z values corresponding to MP401 (Figure 27). Stock solution was made from lyophilized MP401 in sterile PBS and divided into aliquots to avoid excessive freeze thawing.

4.3.7 Synthesis of DV3 peptide (DV3): DV3 (Scheme 8) was successfully synthesized, purified, and characterized. DV3 had a retention time of 2.360 min by analytical HPLC and a measured mass of 1165 Da by MALDI-TOF (Figure 28). Stock solution was prepared from lyophilized peptide in sterile PBS and separated into aliquots to avoid freeze thawing.

4.3.8 Inhibition of HIV-1 entry: The 1, 2, or 4 copy DV3 peptide carriers (MP100, MP200, and MP400) were assessed for their ability to inhibit HIV-1 entry by the TZM-bl assay. The X4 strain of HIV-1 IIIB induced a strong luminescence signal in the untreated +HIV-1 IIIB group by HIV-1 replication dependent luciferase expression in TZM-bl cells. Only the 4 copy DV3 peptide carrier (MP400) was shown to inhibit the production of HIV-1 induced luminescence compared to the untreated +HIV group ($p<0.001$) (Figure 29). Concentrations as low as 500 nM were able to significantly inhibit the induction of luciferase activity. The results indicate that the 4 copy DV3 peptide carriers alone were able to inhibit early HIV-1 entry/infection. The same was not observed for 1 and 2 copy DV3 peptide carriers, which were unable to significantly inhibit the luminescence induced by HIV-1 at any of the concentrations used. The results demonstrate that at least 4 copies of the DV3 sequence were necessary to inhibit HIV-1 entry.

4.3.9 Cytotoxicity of DV3 peptide carriers: The MTT cell viability assay was used to determine if 1, 2, and 4 copy DV3 peptide carriers (MP100, MP200, and MP400) were cytotoxic at the concentrations used to inhibit HIV-1 entry. Three separate experiments

confirmed that 1, 2, and 4 copy DV3 peptide carriers did not significantly affect the enzymatic conversion of MTT to formazan crystals and therefore the cell viability when compared to an untreated control group (Figure 30). The results from the MTT assays demonstrate that the anti-HIV activity observed was due to HIV-1 entry inhibition and not a reduction of cell viability.

4.3.10 Confocal microscopy of DV3 peptide carriers: 1, 2, and 4 copy DV3 peptide carriers (MP100, MP200, and MP400) all demonstrated some appreciable uptake in TZM-bl cells during the 2 hour incubation period. Fluorescent signal was markedly stronger in the MP400 treated cells versus MP100 and MP200. Additionally, the images for the MP400 showed strong colocalization with the endosomal marker rhodamine dextran (Figure 31).

4.3.11 Determination of anti-HIV IC50 of MP400: The 4 copy DV3 peptide carrier (MP400) was shown to significantly inhibit HIV-1 entry over several arbitrarily chosen concentrations, and therefore the concentration dependent response was investigated. The IC_{50} due to HIV-1 entry inhibition for MP400 was 553 nM with a 95% confidence interval of 246 nM to 1.24 μM for the X4 strain HIV-1 IIIB (Figure 32). However, when MP400 was used for its anti-HIV activity for the R5 strain, HIV-1 BaL, MP400 was found to be less potent. The calculated IC_{50} from two separate experiments was found to be in the micromolar range (4.32 μM) and a 95% confidence interval of 2.85 to 6.55 μM (Figure 33). The difference between the entry inhibition of the X4 and R5 viral strains demonstrates the specificity of the DV3 peptide carriers for CXCR4 versus CCR5.

4.3.12 Determination of anti-HIV IC50 of AMD3100 and CXCR4 monoclonal antibody: Comparison of 4 copy DV3 peptide carrier to that of the small molecule AMD3100 and CXCR4 mAb inhibition of HIV-1 IIIB demonstrated that AMD3100 was significantly more potent of HIV-1 entry inhibitor (1000-fold) with IC_{50} = 0.415nM (95% CI = 0.219-0.785nM) (Figure 34). However, the inhibition (IC_{50}) of HIV-1 entry by a CXCR4 mAb was approximately 5-fold better than 4DV3 at 106nM (95% CI = 60-187nM) (Figure 35).

4.3.13 CXCR4 specificity of 4 copy DV3 peptide carriers: Competitive inhibition of the biotinylated 4 copy DV3 peptide carrier (MP401) by both the small molecule CXCR4 inhibitor AMD3100 and a CXCR4 monoclonal antibody demonstrated that the 4 copy DV3 peptide carriers maintained their specificity to CXCR4 expressed by TZM-bl cells. No significant change in streptavidin bound fluorescence was observed for those cells treated with 20 μM AMD3100 despite a 31% reduction in the fluorescence intensity. However when TZM-bl cells were treated with 200 μM of AMD3100, a significant reduction (47%) in cell-associated fluorescence was measured ($p<0.001$) (Figure 36).

MP401 was also shown to inhibit mAb binding to CXCR4 in a concentration dependent manner with similar IC_{50} values to HIV-1 entry inhibition. The IC_{50} of MP401 against 1 μg/ml IC50 was 398 nM with a 95% confidence interval of 101 nM to 1.57 μM (Figure 37). Comparison of MP401 to AMD3100 showed that MP401 was an effective inhibitor to CXCR4 mAb whereas AMD3100 showed little ability to inhibit mAb binding to CXCR4.

4.3.14 Comparison of intracellular versus extracellular associated 4 copy DV3 peptide carriers: Fluorescent microscope images demonstrated an observable difference between the extracellular and intracellular amount of fluorescence, however there was little difference between treatment groups (Figures 38 and 39). Additionally, the ratio of intracellular to extracellular fluorescence was not statistically different between the treatment groups, however there was a reduction of 65% in the ratio when free DV3 peptide was coincubated with 4 copy DV3 peptide carriers (Figure 40).

4.3.15 Molecular modeling of 4 copy DV3 peptide carrier CXCR4 interaction: Molecular modeling of the 4 copy DV3 peptide carrier interacting with four CXCR4 receptors demonstrates (Figure 41). The Lys residues of the 4 copy DV3 peptide carrier backbone provide rotational freedom for each of the DV3 sequences to orient within the CXCR4 binding pockets. Based on the modeling of a bivalent vMIPII derivative and the reduction in CXCR4 binding of DV3 by point mutations of CXCR4, molecular modeling of 4 copy DV3 peptide carriers and CXCR4 tetramer interactions were simulated (*224, 225*). The DV3 chains of 4 copy DV3 peptide carrier were identified as chains 1, 2, 3, and 4 respectively and the CXCR4 as chains A, B, C, and D respectively (Figure 41). Interactions between 4 copy DV3 peptide carrier chains 1 and 3 and receptor chains A and C were modeled as follows: Leu^{1} of 4DV3 formed a hydrogen bond with Asp^{171} of CXCR4; Ser^{4} with Arg^{188}, His^{6} with Asp^{193}, Arg^{7} with Glu^{32}, Asp^{9} with Cys^{28} (Table 5). For 4 copy DV3 peptide carrier chains 2 and 4 interaction with CXCR4 chains B and D, the binding residues were as follows: Leu^{1} of 4 copy DV3 peptide carrier formed a hydrogen bond with Glu^{288} of CXCR4, His^{6} with Asp^{193}, and Trp^{5} with Arg^{188} (Table 5).

The simulations demonstrate the ability of 4 copy DV3 peptide carrier to reach into the binding pocket of multiple receptors simultaneously. The binding conformation forms a cap of the receptor cluster and gives insight into the inhibition of HIV-1 gp120, mAb, and AMD3100 binding to CXCR4 by 4 copy DV3 peptide carrier.

4.4 DISCUSSION:

In the following studies, novel branched peptide carriers containing multiple copies of the CXCR4 targeting peptide DV3 were designed and synthesized. Multivalent DV3 peptide carriers were shown to have more significant anti-HIV activity and cellular association, than the DV3 peptide alone. The results further confirm previous work by our lab and others that multivalency improves cellular affinity of targeted nanocarriers (*226, 227*). Furthermore CXCR4, like the formyl peptide receptor, is a 7 transmembrane G coupled protein that is expressed on several types of HIV-1 susceptible cells, drawing additional parallels between the current DV3 peptide carriers and those previous systems. The results demonstrated that the 4 copy DV3 peptide carrier was the most effective DV3 peptide carrier at HIV-1 entry inhibition through CXCR4 interaction. The affinity and anti-HIV activity of the 4 copy DV3 peptide carriers were investigated and in both cases, the 4 copy DV3 peptide carriers displayed nanomolar level inhibition toward CXCR4 mAbs and an X4 HIV-1 strain.

However, the same level of anti-HIV-1 activity (~10 fold increase in IC_{50}) was not observed when an R5 HIV-1 strain was used. For R5 strains, a reduction in entry inhibition demonstrates the specificity of 4 copy DV3 peptide carriers for CXCR4. However, the inhibition of the R5 strain at micromolar concentrations may be attributed

to several interactions between the 4 DV3 peptide carriers and the cell surface. The charge repulsion between the positively charged 4 copy DV3 peptide carrier bound to CXCR4 and the overall positive charge of HIV-1 gp120 may inhibit R5 entry. Additionally, CXCR4 and CCR5 are known to colocalize within the lipid rafts of the plasma membrane, the CXCR4 bound 4 copy DV3 peptide carriers, could sterically interfere with the HIV-1/CCR5 interaction (*228*). The 4 copy DV3 peptide carriers could also be attracted and concentrated on the cell surface by the negatively charged cell surface GAGs, in a similar manner to CXCL12, thus inhibiting the HIV-1 gp120/CCR5 interaction (*43, 228*).

Receptor specificity of 4 copy DV3 peptide carriers was evaluated by competitive inhibition experiments using two different classes of CXCR4 inhibitors: the small molecule drug AMD3100 and a monoclonal antibody for CXCR4. AMD3100, a small molecule CXCR4 inhibitor, was unable to significantly reduce 4 copy DV3 peptide carrier binding CXCR4 except at high concentrations (200 μM). In addition, the difference between the inhibition of 4 copy DV3 peptide carrier binding by mAb and AMD3100 maybe attributed to two factors (i) the size of the molecule (AMD3100 MW = 502 Da, 4DV3-Biot = 5407 Da and mAb = 150,000 Da respectively) and (ii) binding sites of each molecule. Peptides with containing DV3 sequences have been shown to interact with the following CXCR4 residues Tyr^{45}, Phe^{87}. Asp^{97}, Tyr^{121}, Asp^{171}, Trp^{252}, Tyr^{255}, Glu^{288} and the N-terminus for binding (Table 6) (*224*). AMD3100 binding to CXCR4 requires Asp^{171}, Asp^{262}, and Glu^{288} and overlaps several of the binding residues for 4 copy DV3 peptide carrier (Table 6) (*13, 14, 229*). Mutations of Asp^{171}, Glu^{179}, Asp^{181}, Tyr^{184}, Tyr^{190} and Asp^{193} of CXCR4 reduced the binding capacity of the CXCR4 mAb

(Clone 44708) (Table 6) (*230, 231*). Insights derived from the molecular modeling showed the capacity of 4 copy DV3 peptide carrier to interact with multiple CXCR4 molecules at one time resulting in capping effect of the receptor tetramer. This binding conformation would explain the inhibition of mAb despite a lack of overlap in the binding sites. In addition, 4 copy DV3 peptide carrier requires interaction with the N-terminus for binding while AMD3100 interacts with the charged residues within the binding pocket.

The extended binding surface of 4 copy DV3 peptide carrier could explain the different inhibitory effects observed for mAb and AMD3100 and anti-viral activity. The steric hindrance from the size and binding proximities of the 4 copy DV3 peptide carrier and the CXCR4 mAb may account for the inhibition of binding observed based on concentration of 4 copy DV3 peptide carrier. Whereas, the small size of AMD3100 and its lack of binding to the N-terminus weakly inhibited 4 copy DV3 peptide carrier - CXCR4 interaction.

The 4 copy DV3 peptides were not only the most effective HIV-1 entry inhibitor but also the DV3 peptide carrier with the greatest cellular association. It was observed that 4 copy DV3 peptides carriers became entrapped in the endosomal space during confocal imaging. However, there was little visible cellular association for either FITC labeled 1 or 2 copy DV3 peptide carriers. The lack of cellular association for the 1 and 2 copy DV3 peptide carriers could explain the lack of entry inhibition of HIV-1 by both peptide carriers. Endosomal entrapment of the 4 copy DV3 peptide carriers may be advantageous to the antiviral activity. 4 copy DV3 peptide carriers bound to CXCR4 inhibit HIV-1 gp120 interaction with CXCR4. Additionally, induction of endocytosis by

the 4 copy DV3 peptide carriers will sequester CXCR4 intracellularly and limit the extracellular viral particles from interacting with CXCR4 at the cellular membrane surface. CXCL12 induced CXCR4 internalization acts in a similar manner to inhibit HIV-1 infection (*232*).

Furthermore, localization of the 4 copy DV3 peptide carriers within the endosome could be advantageous in future manifestations of the DV3 peptide carriers. CXCR4 mediated endocytosis induced by 4 copy DV3 peptide carriers could exploit the receptor as a drug delivery portal. Potent antiviral drugs can be conjugated to the 4 copy DV3 peptide carrier through enzymatic labile bonds. Drugs that are membrane permeable are strong candidates for conjugation, since they would not require disruption of the endosome to enter the cytosol. Therefore, 4 copy DV3 peptide carriers could utilize CXCR4 as a drug delivery portal and as an entry inhibitor to HIV-1.

CHAPTER 5

THE SYNTHESIS, CHARACTERIZATION, AND IN VITRO PROPERTIES OF MULTIVALENT DV3 PEPTIDE DRUG CONJUGATES

5.1 INTRODUCTION

AIM 2: To design, synthesize and characterize DV3 containing peptide carriers conjugated to either a reverse transcriptase or protease inhibitor and evaluate the drug loaded DV3 peptide carriers' capacity to use CXCR4 as a drug delivery portal.

In the previous chapter, 4 copy DV3 peptide carriers were shown to have a strong affinity for the chemokine receptor CXCR4. Their ability to associate and accumulate within the CXCR4 expressing cell line, TZM-bl, indicates the potential to utilize receptor mediated endocytosis of CXCR4 as a drug delivery portal. DV3 peptides have been shown by other groups to specifically delivery proapototic peptides when incorporated into a fusion peptide along with a cell penetrating peptide sequence (*92, 201*). However, it has yet to be shown if DV3 can deliver other types of cargo molecules. In the current studies, 4 copy DV3 peptide carriers conjugated with small molecule HAART drugs were designed synthesized and characterized. The 4 copy DV3 peptide drug conjugates were tested for their ability to inhibit replication of HIV-1 in $CD4^+$ T-cell lines. The antiviral drug cargos were selected based on their physicochemical properties. AZT is a water-soluble nuceloside reverse transcriptase inhibitor that is normally transported intracellularly by

nucleoside transporters at the cell membrane. Ritonavir is a poorly soluble and highly permeable protease inhibitor. Each drug is currently marketed as oral tablets, but each drug would benefit from targeted drug delivery approach because of their lack of specificity for HIV-1 susceptible/infected cells. The drug conjugation was designed so the enzymes of the late endosome could release the drug from the 4 copy DV3 peptide carrier. The novel 4 copy DV3 peptide drug conjugates were designed to utilize multiple antiviral mechanisms; one as an entry inhibitor and the other as a drug delivery portal for potent small molecule drugs.

5.2 MATERIALS AND METHODS:

5.2.1 Materials: The majority of the materials are the same as previously described in Chapter 4 including the amino acids, resins, and solvents. Additional materials include: the nucleoside reverse transcriptase inhibitor 1-[(2*R*,4*S*,5*S*)-4-azido-5-(hydroxymethyl)oxolan-2-yl]-5-methylpyrimidine-2,4-dione (AZT) was purchased from OChem, Inc. (Des Plaines, IL), succinic anhydride was purchased from Chemp-Impex International Inc. (Wood Dale, IL), 4-dimethylaminopyridine (DMAP), N-(3-dimethyylaminopropyl)-N'-ethycarbodimide hydrochloride (EDCI), and 4M HCl in dioxane were purchased from Sigma-Aldrich (St. Louis, MO). Norvir (ritonavir oral solution) was obtained from Abbott Laboratories (North Chicago, IL). N-methylimidazole (NMI) and 1-(2-mesitylenesulfonyl)-3-nitro-1,2,4-triazole (MSNT) were purchased from Oakwood Products, Inc. (West Columbia, SC).

5.2.2 Synthesis of Ala-AZT ester: (Scheme 9) Equivalent molar amounts of Boc-Ala-OH and AZT were dissolved in NMP coupled in the presence of 1.25 eq of EDCI and 10 mg of DMAP. AZT and Boc-Ala-OH were reacted for 24 h at room temperature with stirring. The Boc group was removed from the Ala residue using 1:1 TFA:DCM (v/v) solution for 30 min. The Ala-AZT ester was purified before and after Boc removal using a silica gel column on an Isco CombiFlash System (Teldyne Isco, Inc., Lincoln, NE) with mobile phases of (A) hexane and (B) ethyl acetate. Additional batches of Ala-AZT were prepared in the same manner as the Ala-RTV ester (see below).

5.2.3 Synthesis of Ala-RTV ester: (Scheme 9) Synthesis was modified from J.Nielsan Tetrahedron Letters 1996 (*233*). Boc-Ala-OH (2 eq) was combined with 1 eq of RTV in DCM with 3 eq MSNT and 9 eq of NMI with stirring under an argon blanket. The reaction mixture was washed twice with H_2O in a seperation funnel. The aqueous layer was back extracted with DCM and washed the combined organic layers twice with 5% AcCOOH and once with concentrated NaCl. The Boc group was removed using 4 M HCl in dioxane, concentrated under vacuum, washed with MeOH, then DCM, and dried to an amorphous solid.

5.2.4 4 copy DV3 peptide carrier (MP402): (Scheme 10) Synthesis of MP402 was similar to the solid phase peptide synthesis for MP400 and MP401. Fmoc-Gly-HMP-TentaGel resin was Fmoc deprotected with 20% piperidine in NMP for 10 min then for 20 min then extensively washed with NMP. Fmoc-D-Lys(Mtt)-OH was coupled to deprotected Gly residues using 5 eq of Fmoc-D-Lys(Mtt)-OH in the presence of 5 eq of

both HOAt and HATU and 10 eq of DIEA. Coupling of the Lys residue proceeded for 4 h followed by NMP washing and DCM washing. The Mtt group of the Lys residue was removed with 12 cycles of 2% TFA in DCM for 5 min per cycle. Following Mtt deprotection, the resin was washed 4 times with DCM, 3 times with MeOH, and 3 times with NMP. To the free ε amine group, another Fmoc-D-Lys(Mtt)-OH was coupled. The process was repeated until a Lys backbone consisting of 4 Lys residues was synthesized. The Fmoc groups from the Lys residues were removed by 20% piperidine in NMP and the amino acids necessary for the DV3 sequences were coupled in succession as previously described.

5.2.5 AZT conjugated 4 copy DV3 peptide carrier (MP403): (Scheme 11) Synthesis of MP403 was conducted in parallel to MP402. The 4th Lys residue was Mtt deprotected as previously described. The resin was washed following deprotection using DCM, MeOH, and then DCM. Five equivalents of succinic anhydride were added to the resin in the presence of 10 eq of DIEA in anhydrous DCM for 4 h to form a succinyl derivative on the ε amine of the Lys residue (Scheme 12). The resin was then washed with NMP and DCM. Succinic anhydride addition was conducted as described twice. To the free carboxyl group of the succinyl derivative, the Ala-AZT ester was conjugated to peptide as follows: 10 eq of EDC and HOAt in NMP were added to the resin for 1 h with shaking then removed; 3 eq of Ala-AZT ester and 6 eq of DIEA in NMP were added to the resin for 12 h with shaking; then the resin was washed with NMP. Ala-AZT coupling was conducted as described twice. Following conjugation of the Ala-AZT ester, the α amino

groups of the Lys residues were Fmoc deprotected with 20% piperidine in NMP and the amino acids of the DV3 sequence were coupled in succession as previously described.

5.2.6 RTV conjugated 4 copy DV3 peptide carrier (MP404): (Scheme 13) The RTV-Ala ester was synthesized in a similar manner to that of the AZT-Ala ester, described previously. The Ala-RTV ester was conjugated (Scheme 14) to the 4th Lys residue after Mtt deprotection. The free ε amino group of the Lys residue was reacted with succinic anhydride (3.4 eq of succinic anhydride and 7.8 eq of DIEA for 4 h in anhydrous DCM). The Ala-RTV ester was coupled to the free carboxyl group as follows: 10 eq of EDC and HOAt in NMP were added to the resin for 1 h with shaking then removed; 2.26 eq of Ala-RTV ester with 5 eq of DIEA in NMP were added to the resin for 4 h with shaking; and the resin was washed with NMP. The completed Lys backbone coupled with RTV underwent successive rounds of Fmoc deprotection and coupling of the amino acids that make up the DV3 sequence, as previously described.

5.2.7 Purification and characterization of MP402, MP403, and MP404: MP402 and MP403 were cleaved from the resin using 94/2/2/2% TFA/H_2O/TIS/DODT for 4 h at room temperature with stirring. For MP404, peptides were cleaved using 92.5/2.5/2.5/2.5% TFA/H_2O/TIS/DDT for 3 h at room temperature. Each of the peptides were precipitated in ice-cold ether, centrifuged, and washed 2 twice with ice-cold ether. Peptides were dried under vacuum on a lyophilizer. Peptides were dissolved in H_2O and ACN and flash frozen with liquid nitrogen then lyophilized. The peptides were purified by semipreparative HPLC as previously described, then lyophilized. Characterization of

MP402, MP403, and MP404 was done by analytical HPLC and MALDI-TOF mass spectrometry, both described earlier.

5.2.8 Reagents: Many of the same reagents were used were described previously. Rat and human plasma with sodium citrate were purchased from Valley Biomedical (Winchester, VA). Additionally MT2 cells from Dr. Douglas Richman, ritonavir (RTV), and 3'-azido-3'-deoxythymidine (AZT) were obtained through the NIH AIDS Research and Reference Reagent Program, Division of AIDS, NIAID, NIH. Fluor-4-Direct™ Calcium Assay Kit was purchased from Life Technologies (Grand Isle, NY) and SDF-1α from ProSpec (East Brunswick, NJ).

5.2.9 Calcium mobilization due to CXCR4 activation: Activation of CXCR4 by compounds designed to bind to the receptor were analyzed by intracellular calcium mobilization. Utilizing the Fluor-4-Direct™ Calcium Assay Kit and following the manufacturers directions intracellular calcium release was measured. MT2 cells at a density of $2.5x10^6$ cells/ml were suspended in the calcium assay buffer provided. The cells were then added to triplicate wells of a microplate ($1.25x10^5$ cells/well) and incubated at 37^o C for 1 h. Prepared the Fluo-4 direct assay reagent with probenecid (250 mM) in the calcium assay buffer and added 50 µl/well and incubated at 37^o C for another 1 h. The following compounds were prepared in the calcium assay buffer: 200 nM SDF-1α; 200 µM 4 copy DV3 peptide carrier (4DV3); 200 µM of DV3; and PBS, then added to the designated triplicate wells. Fluorescence from three separate experiments was

measured on a microplate reader at λ_{EX} 485 nm and λ_{EM} 535 nm. Fluorescence measured was normalized to SDF-1α (100%) and PBS (0%) treatment groups.

5.2.10 Stability of AZT-DV3 (MP403) and RTV-DV3 (MP404) peptide carriers in plasma: Li et al. report that no carboxyesterases exist in human plasma, but butyrylcholinesterase, paraoxonase, and albumin esterase are present in the plasma and therefore could lead to premature degradation of the amide ester bond prior to cellular internalization (*234*). The stability of the drug conjugation was tested in human and rat plasma using modified procedures from (*235-238*). MP403 and MP404 peptide carriers at a concentration of 150 and 55.5 μM respectively (equivalent of 40 μg/ml of parent drug) were added to pre-warmed human or rat plasma, aliquoted into 75 μl volumes, and incubated at 37^{o} C. At the following predetermined time points (0, 1, 2, 4, 8, and 24 h), the plasma proteins were precipitated with 350 μl ACN + 50 μl of H_2O followed by 15 min incubation at room temperature, mixing by vortex, and 15 min of centrifugation at 10000 g and 4^{o} C. The supernatants were transferred to new tubes and stored at -80^{o} C until frozen. Frozen supernatants were dried on a speed vacuum at 40^{o} C. The dried supernatants were then reconstituted using 75 μl of H_2O/ACN (1:1 v/v), centrifgued at 10000 g and 4^{o} C for 30 min, and the supernatant transferred to an HPLC vial. Release of AZT or RTV from the DV3 peptide carriers was determined by HPLC (10 μl injection of sample) via a standard curve of AZT or RTV for MP403 and MP404, respectively. Detected amounts of free drug were normalized to the theoretical dose equivalent and plotted. The one phase exponential association model was applied to determine the drug release half-life ($t_{1/2}$) by non-linear regression.

5.2.11 Prevention of HIV-1 infection and replication by 4 copy DV3 peptide carriers: MT2 cells were prepared in RMPI at a cellular density of $5.0x10^4$ cells/ml and divided into two treatment groups. The first group were untreated cells (-DV3) and to the second group 2 μM of 4 copy DV3 peptide carriers (MP402) (+DV3). The treatment groups were plated to three sets of triplicate wells (100 μl/well) HIV-I strain IIIB was added in 100 μl of RMPI at an MOI = 0.03 to each well. The plate was incubated for 0.5, 1, or 2 h then centrifuged. The supernatant was removed and replaced with 200 μl of RPMI to the – DV3 groups and 200 μl of 1 μM MP402 to the +DV3 groups. The plate with cells was incubated for an additional 5 d and p24 amount measured by ELISA following the manufacturers instructions (Advanced BioScience Laboratories, Inc., Kensington, MD).

5.2.12 Determination of anti-HIV IC50 of 4 copy DV3 peptide carriers: Serial dilutions of 4 copy DV3 peptide carriers (MP402) were prepared in RPMI and added to triplicate wells of a 96 well plate. MT2 cells were prepared in RPMI at a cellular density of $5.0x10^4$ cell/ml. Untreated cells were used at negative controls. The HIV-1 strain IIIB (X4 strain) was added to the cells at an MOI = 0.03. Cells were incubated for 5 days, then the extracellular p24 protein content was measured using an ELISA based kit following the manufacture's instructions. HIV-1 induced syncytia (multinucleated cells) were counted by observation under a light microscope. The IC_{50} of HIV-1 p24 amount and syncytia count was determined by non-linear analysis from three separate experiments.

5.2.13 Determination of anti-HIV IC50 of AZT-DV3 (MP403) and RTV-DV3 (MP404) peptide carriers: Serial dilutions of the following treatments: free drug (AZT or RTV), 4

copy DV3 peptide carriers (MP402), MP402 + free drug (AZT or RTV), and drug conjugate 4 copy DV3 peptide carriers (MP403 or MP404) were prepared in RPMI and added to triplicate wells of a 96 well plate. MT2 cells were prepared in RPMI at a cellular density of $5.0x10^4$ cells/ml. Untreated cells served as a negative control. The HIV-1 strain IIIB (X4 strain) was added to the cells at an MOI = 0.03. Cells were incubated for 5 d, then the extracellular p24 protein content was measured using an ELISA based kit following the manufacture's instructions. HIV-1 induced syncytia were counted by observation under a light microscope. The IC_{50} of HIV-1 p24 amount and syncytia was determined by non-linear analysis from three separate experiments.

5.2.14 Statistical Analysis: Results are represented as the mean ± standard deviation unless otherwise specified. Statistical analyses were performed using GraphPad Prism Software v4.0c (GraphPad Software, Inc., La Jolla, CA) by ANOVA analysis and Tukey's posthoc test. Statistical significance was determined by a value of $p<0.05$. Non-linear regression analysis was also performed using GraphPad Prism Software for statistical analysis between curves and curve parameters determined by F test at a value of $p<0.05$ as previously described.

5.3 RESULTS:

5.3.1 Synthesis of Ala-AZT and Ala-RTV esters: Syntheses of AZT and RTV amino acid esters were characterized by analytical HPLC and ESI-MS (Figure 42 and 43 respectively). Ala-AZT ester had a retention time of 4.224 minutes and measured mass of

437 Da by ESI-MS in negative mode. The Ala-RTV ester had a retention time of 5.895 minutes and measured mass of 892 Da by ESI-MS in positive mode an additional peak of corresponding to $[M+Na^+] = 914$ Da.

5.3.2 Synthesis of MP402, MP403, and MP404: Synthesis of the 4 copy DV3 peptide carriers and 4 copy DV3 peptide carriers conjugated with AZT or RTV were characterized using analytical HPLC and MALDI-TOF mass spectrometry. MP402 had a retention time of 3.501 min and an expected molecular mass of 5180.85 Da (Figure 44). The final product of the 4 copy DV3 peptide carrier conjugated with the Ala-AZT ester via the succinyl linkage (MP403) had a retention time of 3.731 min and an expected molecular mass of 5601.23 Da (Figure 45). The final product of the 4 copy DV3 peptide carrier conjugated with the Ala-RTV ester via the succinyl linkage (MP404) had a retention time of 3.186 min and an expected molecular mass of 6055 Da (Figure 46).

5.3.3 Calcium mobilization due to CXCR4 activation: The activation of CXCR4 was measured by calcium mobilization (intracellular calcium release) in MT2 cells as a result of exposure to known and experimental receptor ligands (Figure 47). The endogenous agonist SDF-1α was shown to induce the greatest amount of fluorescence compared to the other compounds tested. 4 copy DV3 peptide carriers and free DV3 peptide were calcium mobilization was reduced by 90% and 83% respectively. The lack of activation of CXCR4 by DV3 and 4 copy DV3 was anticipated and confirms observations by others (*196, 199*). However, there was no statistical difference that was found between any of the treatment groups by ANOVA from the three separate experiments.

5.3.4 Stability of 4DV3-AZT (MP403) and 4DV3-RTV (MP404) peptide carriers in plasma: The stability of the ester linkage between the drug and the 4 copy DV3 peptide carrier was examined in human and rat plasma. Detection was based on the release of free drug into the plasma, which was then extracted and analyzed by HPLC. Representative calibration curves can be seen in (Figures 48 and 49). For human plasma, free AZT was detected by HPLC during 24 h period with a calculated half-life of 4.43 h. Indicating a hydrolysis of the ester bond from the 4 copy DV3 peptide AZT conjugate (MP403). However for the 4 copy DV3 peptide RTV conjugate (MP404), release of RTV was below the limit of detection over the course of the study period indicating a resistance conjugate degradation (Figure 50). A similar trend for RTV release from MP404 was observed in rat plasma, where the free RTV amount was predominantly outside of the detection limit and the determined calculated half-life was 117 h (Figure 51). For MP403, free AZT was detected in samples incubated for greater than 2 h at 37^{o} C and the calculated half-life was 2.78 h.

5.3.5 Prevention of HIV-1 infection and replication by 4 copy DV3 peptide carriers: The prevention of HIV-1 infection and replication was measured by p24 production in the T-cell line (MT2) by pre-incubation with 4 copy DV3 peptide carrier (MP402). Inhibition of viral replication was observed for each of the HIV-1 exposure times that were investigated 93% and 35% for 0.5 and 1h incubation times respectively (Figure 52). However, statistically significant ($p<0.05$) reduction (>80% reduction) in p24 production was found for MT2 cells that were incubated with 1 μM MP402 and exposed to HIV-1 for a 2 h period versus those cells exposed to HIV-1 alone. The results confirm the

observations made by the TZM-bl assay earlier, that 4 copy DV3 peptide carriers are effective at inhibiting the entry of viral particles to susceptible cells. This study further demonstrates that inhibiting viral entry is effective at inhibiting the replication of new viral particles and prevents the formation of syncytia a phenomenon observed with X4 strains of HIV-1.

5.3.6 Determination of anti-HIV IC50 of 4 copy DV3 peptide carriers (MP402): Previously it was demonstrated that 4 copy DV3 peptide carriers were able to inhibit viral entry by the reporter assay utilizing TZM-bl cells. These studies were conducted to measure viral replication via the extracellular p24 protein amount. p24 is a matrix protein of HIV-1 and its production is the result of the packaging of new viral particles during replication. Similarly, the formation of syncytia (aggregates of cells) by X4 strains of HIV-1 demonstrates the active replication of HIV-1. The 4 copy DV3 peptide carriers were 2 orders of magnitude less effective at inhibiting viral replication than inhibiting viral entry (Figure 53). The IC_{50} value from the p24 assay was 16.98 μM (95% confidence interval 7.08 μM to 40.74 μM) and from syncytia formation experiments were 23.60 μM (95% confidence interval 21.38 μM to 26.12 μM) (Table 7).

5.3.7 Determination of anti-HIV IC50 of AZT-DV3 (MP403) and RTV-DV3 (MP404) peptide carriers: The anti-HIV-1 effect of the 4 copy DV3 peptide drug conjugates were evaluated by p24 ELISA and the formation of syncytia. The calculated inhibitory concentrations (IC_{50}) for each of the treatment groups are outlined Table 7. For the 4 copy DV3 peptide carrier conjugated with the reverse transcriptase inhibitor AZT

(MP403), the IC_{50} was 31.9 nM (95% CI 21.7-53 nM) by the p24 ELISA and 80.2 nM (95% CI 75.3-83.0 nM) by the syncytia count. The IC_{50} for MP403 was a significant improvement in the anti-viral activity of the 4 copy DV3 peptide carrier (MP402), however MP403 was not as potent as AZT alone (IC_{50} = 8.51 nM 95% CI 4.25-12.9 nM for p24 and IC_{50} = 33.1 nM 95% CI 30.2-34.7 nM for syncytia count) or the mixture of MP402 with AZT (IC_{50} = 11.4 nM 95% CI 6.30-20.4 nM for p24 and IC_{50} = 25.9 nM 95% CI 23.6-27.2 nM) (Figure 54).

A similar trend of diminished potency was observed for the RTV conjugated 4 copy DV3 peptide carrier (MP404) (Figure 55). The anti-viral activity of MP404 was 598 nM (95% CI 301 nM-1.03 μM) by the p24 ELISA and 713 nM (95% CI 664-774 nM) by syncytia formation. The inhibitory concentrations were similar in magnitude to those for the 4 copy DV3 peptide carriers assessed as entry inhibitors. A more dramatic difference in the anti-viral activity compared to MP404 was calculated for the parent drug RTV (11.9 nM 95% CI 3.05-21.7nM) by p24 ELISA and (26.7 nM CI 95% 22.6-32.8 nM) by syncytia formation. For the treatment group of 4 copy DV3 peptide carriers combined with RTV, there was a slight improvement in the IC_{50} values recorded for both assays. IC_{50} was 10.0 nM (95% CI 1.49-32.3 nM) by p24 ELISA and 23.6 nM (95% CI 20.4-28.3 nM).

5.4 DISCUSSION

Inhibition of viral entry was previously demonstrated in AIM 1 by the reporter cell line TZM-bl. However, TZM-bl cells do not replicate new viral particles. Therefore, the inhibition of viral replication was investigated with the 4 copy DV3 peptide carriers

(MP402). The 4 copy DV3 peptide carrier was dramatically less effective (by 2 orders of magnitude) in the inhibition of viral replication as compared to its ability to inhibit viral entry. The discrepancy between the inhibition of viral entry and the inhibition of viral replication may be due to several factors. The first is that during the incubation period for the p24 and syncytia assays the concentration of viral particles increases each time a new viral particle is produced. Therefore, the inhibitory effect of the 4 copy DV3 peptide carriers decreases as the each new generation of viral particles are produced. To account for the creation of new viral progeny, experiments were designed to initially protect against HIV-1 cell entry and limit new virus production. In these experiments, there was a significant reduction in new virus production in cells that were treated with 1 μM of 4 copy DV3 peptide carriers during a two-hour incubation period with HIV-1. The results confirm that the 4 copy DV3 peptide carrier acts as an entry inhibitor, but also indicate that its potential as a therapy on its own maybe limited.

Second generation 4 copy DV3 peptide carries were synthesized with a drug cargo to make multi-targeted anti-HIV compound (i) the 4 copy DV3 peptides acts as an entry inhibitor and (ii) the conjugated anti-viral drug acts as a viral enzyme inhibitor. Therefore novel 4 copy DV3 peptide drug conjugates were designed to construct a multi-target multi-mechanistic HIV-1 inhibitor. The results demonstrated several interesting trends. The drug conjugates were not as effective as the parent drug alone. The combination of the 4 copy DV3 peptide carrier and the parent drug were the most effective treatment group at preventing the formation of syncytia.

However, each of the 4 copy DV3 peptide drug conjugates was markedly more effective at inhibiting the production of new viral particles than 4 copy DV3 peptide

carriers alone with effective concentrations in the nanomolar range. Therefore, the added benefit of drug conjugation are realized when comparing a purely entry inhibition system that the 4 copy DV3 peptide carrier represents compared to the 4 copy DV3 peptide drug conjugates. Furthermore, the results confirm our hypothesis by inhibiting HIV-1 infection and replication by multiple mechanisms is a more effective therapy than inhibiting one stage of the HIV-1 lifecycle. The observations are also aligned with the clinical success of HAART, where patients' initial therapy generally includes multiple drugs of different drug classes that are inhibitors for different viral enzymes (*2, 239*).

Additionally, the AZT conjugated 4 copy DV3 peptide carriers were better HIV-1 inhibitors than the RTV conjugated 4 copy DV3 peptide carriers. The reason for the difference may be due to the rate of release of the parent drug from the ester bond linking the drug to the peptide carrier. In the plasma studies, freed AZT was detected after two hours of incubation, while virtually no freed RTV was detected over the 24 hour period. Indicating that AZT is more readily released from the ester bond than RTV, and therefore the increased drug release translated into greater antiviral activity. The difference in release could be due to the steric hindrance (RTV is approximately 3 times the size of AZT) limiting the accessibility for esterases to hydrolyze the ester bond.

However, one of the benefits of the conjugation for RTV was improved water solubility. The shift if in retention time by analytical HPLC was dramatic going from 5 minutes for the parent to 3.1 min for the 4 copy DV3 peptide drug conjugate. During in vitro evaluation, RTV was dissolved in DMSO then diluted to lower concentrations in PBS while the lyophilized peptide drug conjugate was readily soluble in PBS.

Regardless of the peptide drug conjugates being less effective than their parent drug, the added benefit of specificity toward HIV-1 susceptible cells could not be evaluated in the in vitro studies. The loss of potency could be equated to the loss of potency observed after the PEGylation of a protein. While the loss of the potency is significant, the benefit of increased residence time and the reduction of clearance greatly improve the overall therapy compared to the unpegylated counterpart (*240, 241*). Similarly, the effectiveness of the 4 copy DV3 peptide drug conjugates remains to be fully determined until in vivo evaluation.

CHAPTER 6

THE SYNTHESIS, CHARACTERIZATION, AND IN VIVO PROPERTIES OF MULTIVALENT DV3 PEPTIDE DRUG CONJUGATES

6.1 INTRODUCTION

AIM 3: To improve drug loading and to increase the plasma persistence of the 4 copy peptide carriers by conjugation of branched PEG molecules.

The previous chapter demonstrated that the anti-HIV-1 activity of the 4 copy DV3 peptide carriers were enhanced when conjugated with potent small molecule drugs that inhibit viral enzymes. However, the ratio of the conjugates' size to the drug loading was less than ideal because of the overall size of the 4 copy DV3 drug conjugate (for AZT drug wt % = 4.77% and for RTV the ratio = 11.9%). Therefore the current studies are designed to demonstrate an increased drug loading through the synthesis of PEGylated peptide backbones that are functionalized to carrier multiple drug molecules per backbone. Furthermore, PEGylation is a strategy often used to enhance the circulating half-life of protein molecule or enhance the water solubility of poorly soluble constructs (*241, 242*). Therefore, the effect of PEGylation on the in vitro and in vivo properties of 4 copy DV3 peptide carriers was investigated with the intent to optimize the carrier size for residence time in vivo.

The studies are designed to enhance the drug payload of the 4 copy DV3 peptide carriers by attaching drug molecules to 3 of the 4 arms of a branched PEG molecule or to

PEGylated peptide carrier and to add 4 copy DV3 peptides to the carrier through 'click' chemistry. The same design platform will be used to synthesize 4 copy DV3 peptide carriers labeled with a near infrared dye. The near infrared dye allows for non-invasive in vivo imaging of the biodistribution of the 4 copy DV3 peptide carriers. The molecular weights of the compounds to be investigated were selected strategically above and below size for renal filtration.

6.2 MATERIALS AND METHODS

6.2.1 Materials: Many of the solvents used have been previously identified. Additional materials include the following: Fmoc-Ala-NovaSyn-TGA resin (EMD Millipore, Billerica, MA), 2-chlorotritylchloride resin (AnaSpec, Inc. Freemont, CA), and DBCO-PEG_4-DBCO (Click Chemistry Tools, Scottsdale, AZ). Four arm branched PEG amines (molecular weights 2, 10, 20, and 40kDa) were purchased from JenKem Technology USA, Inc. (Allen, TX) and are referred to as 2, 10, 20, and 40kDa PEG, respectively, from this point forward. Discreet PEGs were purchased from Quanta Biodesign, Ltd. (Powell, OH) as follows: Fmoc-N-amido-$dPEG_3$-acid, Azido-$dPEG_{24}$-acid, Azido-$dPEG_{12}$-acid, Fmoc-N-amido-$dPEG_6$-acid, and m-$dPEG_{37}$-acid.

6.2.2 Synthesis of 4 copy DV3 PEG azide peptide carriers (MP410): MP410 (Scheme 15) was synthesized in a similar manner to the other functionalized 4 copy DV3 peptide carriers. Briefly, 4 Lys residues will be linked via their ε amino groups through subsequent deprotection of the Mtt groups and coupling Fmoc-Lys(Mtt)-OH residues.

The 4th Lys residue after Mtt deprotection was coupled with azido-dPEG$_{12}$ acid (3.7 eq), 3.7 eq HOAt, 3.7 eq HATU, and 7.4 eq DIEA for 4 h. The resultant compound was Fmoc deprotected and the amino acids of the DV3 sequence were added through repeated Fmoc deprotections and amino acid coupling as previously described. MP410 was cleaved from the resin using 92.5/2.5/2.5/2.5% TFA/H_2O/TIS/DDT for 3 h at room temperature, purified by preparative HPLC using an Atlantis Prep dC18 OBD 19x100 mm, 5 μM column (Waters, Milford, MA), and characterized by analytical HPLC and MALDI-TOF MS as previously described.

6.2.2 Copper free 'click' addition of DBCO-PEG$_4$-DBCO to MP410: The general mechanism of the copper free 'click' addition (also referred to as azido cycloaddition) is outlined in Scheme 16. MP410 (1 eq) was dissolved in H_2O/MeOH (1:1 v/v) to a concentration of 10 mg/ml. DBCO-PEG$_4$-DBCO (4 eq) was dissolved in neat MeOH to a concentration of 1 mg/ml. The MP410 solution was added drop wise to the DBCO-PEG$_4$-DBCO solution with gentle stirring. Reaction was allowed to proceed to completion (approximately 3 h). The resultant MP411 (Scheme 17) was purified using preparative HPLC on an Atlantis Prep dC18 OBD 19x100 mm, 5 μM column and mobile phase consisting of H_2O and ACN with 1% acetic acid. Purified MP411 was characterized using previously described analytical HPLC and MALDI-TOF methods.

6.2.3 Synthesis of PEGylated carriers for 'click' addition (Strategy I): Strategy I is a solid phase method for selective substitution at 3 of the 4 arms of the branched PEG amine. 2-chlorotritylchloride resin (0.007mmol) was swelled in DMF. To couple one arm

of the 40 kDa PEG to the solid support, 1 eq of 40 kDa PEG was combined with 8 eq of DIEA and added to the resin. The reaction was allowed to precede overnight at room temperature with shaking. Reaction was drained and washed several times with DMF. Kaiser test was performed on the resin post reaction for the detection of free amine (*243*). To test the availability of the other free amines, 9 eq of Fmoc-Arg(Pbf)-OH were combined with 9 eq of HOAt and HATU and 13.5eq of DIEA. Reaction time was 4 h, followed by washing with NMP. Kaiser test was performed to detect free amine after coupling. Resin was washed twice with MeOH and dried. Resin was reswelled with DMF, the Fmoc group removed from the Arg residue using 20% piperidine in DMF for 1 h. Resin was washed 3x with NMP and subjected to Kaiser test.

6.2.4 Synthesis of PEGylated carriers for 'click' addition (Strategy II): Strategy II is a solution phase synthesis method for selective substitution of 1 of the 4 arms of the branched PEG amine.

For monosubstituted with amino acid ester drug, 20kDa PEG (0.0005 mmol) was dissolved with 200 µl of DCM. Succinic anhydride was prepared in DCM at a concentration 5 µg/ml with 8.9 µl of DIEA, 2.5 µl of the solution was added to the 4 arm branched PEG solution (0.25 eq compared to PEG). The reaction proceeded at room temp for 1.5 h. To the reaction 0.25 eq of HOAt and HATU were added with 2 eq of Ala-RTV ester (synthesis previously described). Reaction proceeded at room temp for overnight. Sampled reaction mixture for MALDI-TOF. The MALDI matrix CHCA was prepared by

dissolving 10 mg in 1 ml THF based on the method reported Yu et al Marcomolecules 1999 (*244*).

For monosubstituted 4 arm branched PEG with MP410 'clicked' to the macromolecule, 0.0005 mmole of 20 kDa PEG was dissolved in DCM with 5 eq of DIEA. To the PEG solution, DBCO-NHS (0.25 eq) was added and the reaction proceeded for 3 h. For 'click' reaction, MP410 (0.25 eq) was added to the reaction mixture. The reaction mixture was sampled for MALDI-TOF analysis as previously described.

6.2.5 Synthesis of PEGylated peptide carriers for 'click' addition (Strategy III): For synthesis strategy IV, solid phase peptide synthesis was used to form three unit types. The first designated the end unit (EU), the second the mass building unit (MBU), and the third the drug loaded unit (DU) and are represented in Schemes 18, 19, and 20, respectively. The EU, MBU, and DU were synthesized using Fmoc-Ala-NovaSyn-TGA resin. Resin was swelled in NMP, Fmoc deprotected with 20% piperidine in NMP for 40 min, washed several times with NMP. Fmoc-D-Lys(Mtt)-OH (3 eq) was coupled with HOAt (3 eq), HATU (3 eq) and DIEA (6 eq) to the free amine of Ala. The Lys residue was Fmoc deprotected as previously described and Fmoc-N-amido-dPEG$_3$-acid (3 eq) was coupled with HOAt (3 eq), HATU (3 eq) and DIEA (6 eq). Repeated couplings of Lys(Mtt) and amido-dPEG$_3$ (PEG$_3$) were repeated until the following sequence was produced: Fmoc-Lys(Mtt)-PEG$_3$-Lys(Mtt)-PEG$_3$-Lys(Mtt)-Ala.

For the EU (Scheme 18), Fmoc-Lys(Mtt)-PEG_3-Lys(Mtt)-PEG_3-Lys(Mtt)-Ala was Fmoc deprotected, Fmoc-N-amido-$dPEG_3$-acid coupled as previously described, and Fmoc deprotected. The EU was coupled with Fmoc-Lys(FITC)-OH (2 eq) with HOAt (2 eq), HATU (2 eq), and DIEA (4.5 eq) for 1 h in the dark. The Fmoc group was removed from the Lys residue and Fmoc-N-amido-$dPEG_{16}$-acid (2 eq) was coupled to the α amine of the Lys residue with HOAt (2 eq), HATU (2 eq), and DIEA (4.5 eq) for 1.5 h. The Fmoc on the $dPEG_{16}$ was deprotected and Azido-$dPEG_{24}$-acid (2 eq) was coupled with HOAt (2 eq), HATU (2 eq), and DIEA (4.5 eq). for 1.5 h. The orthogonal Mtt groups on the ε amines of the Lys residues were removed using 96/2/2 % of DCM/TFA/DTT (v/v/w) in a series of 12 washes with each was lasting 5 min. The resin was then washed several times with NMP. To the free ε amines of the Lys residues m-$dPEG_{37}$-acid (6 eq) was coupled in the presence of HOAt (6 eq), HATU (6 eq), and DIEA (12 eq) overnight. The resin was washed with NMP, MeOH, and dried under vacuum. The EU was help until fragment condensation was conducted.

For the MBU (Scheme 19), Fmoc-Lys(Mtt)-PEG_3-Lys(Mtt)-PEG_3-Lys(Mtt)-Ala was continued by repeated Fmoc deprotections, Lys(Mtt) couplings, and Fmoc-N-amido-$dPEG_3$-acid couplings until the sequence was Fmoc-Lys(Mtt)-PEG_3-Lys(Mtt)-PEG_3-Lys(Mtt)-PEG_3-Lys(Mtt)-Ala. The Fmoc was removed and Fmoc-N-amido-$dPEG_6$-acid (2eq) coupled to the MBU with HOAt (2 eq), HATU (2 eq), and DIEA (9 eq) for 1.5 h. The resin was washed with NMP and DCM three times each. The orthogonal Mtt groups on the ε amines of the Lys residues were removed using 11 washes each 5 min of 2% TFA in DCM. The resin was then washed with twice with DCM, 10% DIEA in DCM,

DCM, and NMP. To the ε amines of the Lys residues m-dPEG$_{37}$-acid (8 eq) was coupled in the presence of HOAt (8 eq), HATU (8 eq), and DIEA (18 eq) overnight. The resin was washed with NMP, MeOH, and dried under vacuum. MBU was held until fragment condensation.

For the DU (Scheme 20), Fmoc-Lys(Mtt)-PEG$_3$-Lys(Mtt)-PEG$_3$-Lys(Mtt)-Ala was Fmoc deprotected, and Fmoc-N-amido-dPEG$_6$-acid (3 eq) was coupled with HOAt (3 eq), HATU (3 eq) and DIEA (6 eq). The DU was washed with NMP, MeOH, and dried under vacuum until fragment condensation and drug loading.

For fragment condensation, the DU will be Fmoc deprotected to allow the coupling of the MBU to the amine group of the PEG$_6$. After addition of the MBU(s), the MBU Fmoc deprotection will be followed by the coupling of the EU and 'click' of MP411. After, the 'click' reaction the Mtt groups of the DU will be deprotected as previously described and succinylated Ala-RTV will be coupled to the DU resulting in 3 drug molecules attached to the PEGylated peptide carrier.

6.3 RESULTS

6.3.1 Synthesis of 4 copy DV3 PEG Azide peptide carriers (MP410):

4 copy DV3 PEG$_{12}$ azide (MP410) was successfully synthesized and characterized (Scheme 15). The peptide had a retention time of 2.025 min by analytical HPLC (Figure 55). Additionally,

the expected molecular weight of $[M+1H^+]$ = 5806 Da, as well as $[M+2H^+]/2$ = 2903, was observed from MALDI-TOF mass spectrometry (Figure 56).

6.3.2 Copper free click addition of DBCO-PEG_4-DBCO to MP410: MP410-DBCO-PEG_4-DBCO was successfully synthesized and purified. MP410-DBCO-PEG_4-DBCO had a retention time of 3.282 min by analytical HPLC (Figure 57). A major peak of the expected molecular mass equal to 6616.7 Da was observed by MALDI-TOF MS as well as a peak correlating to $[m+2H^+]/2$ = 3308.3 Da (Figure 57).

6.3.3 Synthesis of PEGylated carriers for 'click' addition (Strategy I): Strategy I was unsuccessful in an attempt to couple cargo to 3 of the 4 arms of the 40kDa branched PEG molecules. Kaiser tests were negative for free amines after coupling to the resin, after coupling Fmoc-Arg(Pbf)-OH, and after Fmoc deprotection. The results indicate two possible results: (i) that the 4 arm PEG never loaded onto the resin as intended or (ii) that the 4 arm PEG amine groups were taken up through crosslinking and therefore uanavailable for the addition of the Arg residue. Observation of the expansion of the resin bed after the addition of the 4 armed branch PEG amine to the resin. Therefore, Strategy II was employed utilizing a solution phase synthesis.

6.2.4 Synthesis of PEGylated carriers for 'click' addition (Strategy II): Confirmation of monosubstitution of the 4 arm branched PEG amine proved difficult. MALDI-TOF spectra in general demonstrated either a lack of modification the PEG molecule or the polydispersity of the PEG molecules from the commercial source. The polydispersity

would have limited the ability to distinguish between unreacted PEGs and those properly monosubstituted. Observed within the MALDI-TOF of the reaction mixture was the 'click' of MP410 with DBCO-NHS, but no indication of the desired compound. This strategy was repeated several times using DMF in place of DCM and after aziotropic distillation of the 20kDa PEG in toluene. In addition, different activators and catalysts were used to attempt to drive the reaction to the desired products, however confirmation of the desired compounds by MALDI-TOF. Therefore a discreet PEGylated peptide carrier method (Strategy III) was attempted.

6.3.5 Synthesis of PEGylated peptide carriers for 'click' addition (Strategy III): The EU, MBU, and DU have been synthesized and await characterization prior to fragment condensation to the desired molecular weight. Following additions of MBU to the DU, the EU will be added and MP411 'clicked'. Following 'click' addition, drug loading to the DU will be conducted via succinlyated Ala-RTV.

6.4 DISCUSSION

Synthesis of the PEGylated 4 copy DV3 peptide carriers has proven challenging. The lack of commercially available heterobifunctional 4 arm branched PEGs with a ratio of 1:3 of the functional groups. Therefore, we attempted to monosubstitute amino 4 arm branched PEGs (Strategy I and II). Both Strategy I and II were unsuccessful for differing reasons. Strategy I was a solid phase synthesis method that attempted to couple 1 of the 4 arms of the branched PEGs to the solid support and theoretically allowing the other 3 arms available for conjugation. However, Kaiser test after the initial coupling of the PEG

to the solid support indicated that there were no longer free amines available. Strategy II was a solution phase method for substitution of 1 of the 4 arms using stochiometry. Attempts to produce the monosubstituted 4 arm branch PEG may have been successful from synthesis standpoint, however characterization was difficult. For Strategy II, the changes in the molecular mass of the 4 arm branched PEG after reaction were small in magnitude compared to the 4 arm branched PEGs themselves and indistinguishable because of the PEGs polydispersity.

Strategy III is a PEGylated peptide carrier method similar to one that was previously utilized in our lab (*226, 245-247*). Strategy III does differ in several ways from those previously done. The use of discreet PEG molecules in both the backbone and side chains of the PEGylated peptide carrier constructs (DU, EU, and MBU). These PEGs reduces the polydispersity that is normally associated with PEGylation. Polydispersity can make characterization and purification difficult (*240, 248*). In addition, incorporation of PEG_3 residues between the Lys residues of the DU, EU, MBU, will provide flexibility and hyrdophilicity to the overall structure compared to PEGylated peptide carriers consisting of β-Ala and Lys residues (*226, 245-247, 249*). The PEG_3 also serve as spacers between the Lys residues to avoid steric hindrances during later functionalization of the Lys side chains. The modular design of the EU, MBU, and DU provides a flexible platform for the modification of the following parameters; size, number of drug conjugation sites, targeting moiety clicked, and labeling (fluorescence or otherwise).

While not all of the proposed experiments were achieved prior to the composition of this thesis, construction of the modular units is on going and upon completion will be purified. The current chemical design is for in vitro evaluation of the 4 copy DV3

PEGylated peptide carriers for uptake (confocal microscopy) and anit-HIV-1 acitivity (p24 assay). Modification of the fluorescent dye (FITC) to a near infrared dye will be necessary for in vivo biodistribution and basic pharmacokinetic analysis.

Future directions of the project include further evaluation of the 4 copy DV3 peptide carriers as a targeting moiety for CXCR4. Since, CXCR4 plays in important role in both HIV-1 and cancer the platforms and designs from Chapters 5 and 6 can be modified to different drug cargos dependent upon the disease or drug target. In addition, the synthesis of the 4 copy DV3 PEG azide (MP410) generated a compound that is easily incorporated through “click’ chemistry into other drug delivery systems for example nanoparticles or dendrimers. These other drug delivery systems have the capacity for even higher drug loading than the conjugate system utilized within this thesis.

Table 1: CXCR4 expression on various peripheral blood leukocytes. The percentage of cells expressing CXCR4 was determined from specific peripheral blood leukocyte subsets, then the number of antigen binding sites (ABS) were measured on those cells positive for the specific receptor. All measurements made using QFACS with fluorophore conjugated CXCR4 mAb (12G5). Table was modified from (*6*).

Cell	Mean CXCR4 positive % (range)	Median 12G5 ABS (range)
Total lymph Gated for CXCR4+ cells only	69.6 (51.7-80.1)	1,572 (834-1,961) 3,387 (2,498-3759)
Monocytes	70.9 (55.0-95.5)	2,491 (2,015-5,113)
CD4+/CD45RO+/CD26L- (True Memory)	36.8 (26.0-51.5)	505 (348-655)
CD4+/CD45RO+/CD26L+	63.9 (50.1-73.2)	1,013 (653-1,377)
CD4+/CD45RA+/CD26L-	40.8 (16.6-70.8)	902 (554-1,762)
CD4+/CD45RA+/CD26L+ (True Naïve)	91.3 (82.9-96.6)	3,386 (2,233-4,644)
CD8+ (Total Lymph) Gated for CXCR4+ cells only	54.9 (24.3-84.1)	1,030 (344-3,272) 4,033 (2,915-5,680)
NK cells (CD56+)	21.0 (2.6-58.9)	229 (152-1,189)
B cells (CD19+)	91.0 (80.9-98.2)	7,402 (4,227-10,941)
CD26-	54.7 (36.7-67.6)	546 (289-791)
CD26+	94.9 (92.3-96.6)	2,130 (1,508-2,784)
HLADR-	77.9 (62.2-87.3)	1,035 (545-1,668)
HLADR+	88.6 (79.1-96.3)	4,089 (1,915-6,734)
Immature DC/CD11c+	17.1 (7.92-47.2)	800 (681-1,962)
Immature DC/CD11c-	47.3 (36.7-60.3)	1,511 (1,031-2,259)
Mature DC	96.9 (93.1-100)	35,175 (16,598-62,375)

DC = dendritic cells, NK = natural killer cells

Table 2: Affinity of CXCL12 for CXCR4 in various cell lines. Jurkat CEM and HUT78 cells are all T-cell lines, while hNT cells are differentiated human neuron cells from the NTera 2 cell line.

Cell Type	Number of CXCL12 Binding Sites per Cell (CXCR4)	Affinity for CXCL12, Kd (nM)	Reference
Jurkat	163,521 ± 35,875	7.5 ± 2.6	(*35*)
CEM	120,968 ± 38,946	7.1 ± 3.5	(*35*)
HUT78	101,733 ± 28,209	18 ± 5.1	(*35*)
hNT	8000	54 ± 8.3	(*78*)

Table 3: Currently approved HAART drugs segregated by drug classes and target proteins. Updated from Palombo, Singh, and Sinko JDDST 2009 (*151*).

Drug	Brand Name	Manufacturer
Nucleoside reverse transcriptase inhibitors (NRTIs)		
Zidovudine (AZT)	Retrovir	GlaxoSmithKline
Didanosine (ddI)	Videx	Bristol Myers-Squibb
Zalcitabine (ddC)	Hivid	Roche
Stavudine (d4T)	Zerit	Bristol Myers-Squibb
Lamivudine (3TC)	Epivir and Zeffix	GlaxoSmithKline
Abacavir sulfate (ABC)	Ziagen	GlaxoSmithKline
Emtricitabine (FTC)	Emtriva	Gilead Sciences, Inc.
Nucleotide reverse transcriptase inhibitors (NtRTIs)		
Tenofovir diisoproxil fumarate	Viread	Gilead Sciences, Inc.
Non-nucleoside reverse transcriptase inhibitors (NNRTIs)		
Nevirapine (NVP)	Viramune	Boehringer Ingelheim
Delavirdine (DLV)	Rescriptor	Pfizer
Efavirenz (EFV)	Sustiva and Stocrin	Bristol Myers-Squibb
Entavirine (TMC125)	Intelence	Tibotec, Inc.
Rilpivirine	Edurant	Tibotec, Inc.
Protease Inhibitors (PIs)		
Saquinavir mesylate (SQV)	Invirase and Fortovase	Roche
Ritonavir (RTV)	Norvir	Abbot Laboratories
Indinavir (IND)	Crixivan	Merck & Co.
Nelfinavir mesylate (NFV)	Viracept	Pfizer
Amprenavir (AMP)	Agenrase and Prozei	GlaxoSmithKline
Fosamprenavire calcium (Prodrug of Amprenavir)	Lexiva and Telzir	GlaxoSmithKline
Atazanavir sulfate	Reyataz	Bristol Myers-Squibb
Lopinavir and ritonavir	Kaletra	Abbott Laboratories
Tipranavir	Aptivus	Boehringer Ingelheim
Darunavir	Prezista	Tibotec, Inc.
Entry and Fusion Inhibitors		
Maraviroc	Salzentry	Pfizer
Enfuvirtide	Fuzeon	Roche and Trimeris
Integrase inhibitors		
Raltegravir	Isentress	Merck & Co.

Table 4: Table recreated and modified from Zaitseva et al. 2003 (*139*). Summary of various chemokine receptor ligands investigated for anti-HIV activity and their affinity for their targets. The active concentration is dependent upon the assay used to evaluate the anti-HIV-1 activity as well as the viral strain. Chemical classification based upon protein, peptide, and small molecule drug additional classification is provided within parentheses.

Inhibitor	Coreceptor	Ligand activity	Chemical	Active Concentration
SDF-1α (CXCL12)	CXCR4	Ligand	Protein (Chemokine)	0.2-5 μg/ml (30 nM)
Met-SDF-1α (Met-CXCL12)	CXCR4	Agonist	Protein (Modified chemokine)	1.0-2.8 μg/ml
AMD-3100	CXCR4	Antagonist	Small molecule drug (Bicyclam)	2-7 ng/ml (20 nM)
KRH-1636	CXCR4	Antagonist	Small molecule drug (Peptidomimetic)	18-152 nM
ALX40-4C (Polyarginine)	CXCR4	Antagonist	Peptide (9 amino acids)	3-20 nM
T22	CXCR4	Antagonist	Peptide (18 amino acids)	5-290 nM
T140	CXCR4	Antagonist	Peptide (14 amino acids)	0.18-12 nM
T20	N/A	Binds to gp41 of HIV-1	Peptide (36 amino acids)	0.07 μg/ml (2-40 nM)

Table 5:
Hydrogen bonding simulated during molecular modeling. The matrix identifies the residues of 4 copy DV3 peptide carriers that interact with each of the CXCR4 receptors in the tertramer used for simulations. Interactions are identified with the DV3 sequence residues followed by the CXCR4 residue (*223*).

	CXCR4 Chain	A	B	C	D
4 copy DV3 chain	1	Leu^{1}-Asp^{171} Ser^{4}-Arg^{188} His^{6}-Asp^{193} Arg^{7}-Glu^{32} Asp^{9}-Cys^{28}			
	2		Leu^{1}-Glu^{288} Trp^{5}-Arg^{188} His^{6}-Asp^{193}		
	3			Leu^{1}-Asp^{171} Ser^{4}-Arg^{188} His^{6}-Asp^{193} Arg^{7}-Glu^{32} Asp^{9}-Cys^{28}	
	4				Leu^{1}-Glu^{288} Trp^{5}-Arg^{188} His^{6}-Asp^{193}

Table 6: Residues indentified as critical to binding of CXCR4 ligands by mutations of CXCR4. TM = transmembrane helix and ECL2 = second extracellular loop 2. DNX4 = deletion of the first 22 residues of CXCR4 N-terminus.(*13, 223, 225, 230, 250, 251*).

CXCR4 Domain	4DV3	SDF-1α	HIV-1 gp120	AMD3100	CXCR4 mAb (Clone 44708)
N-terminus	DNX4	DNX4	DNX4		
TM1	Tyr^{45}	-	Tyr^{45}		
TM2	Phe^{87}	Phe^{87}	-		
TM3	Tyr^{121}	-	-		
TM4	Asp^{171}	Asp^{171}	Asp^{171}	Asp^{171}	
ECL2					Glu^{179} Asp^{181} Tyr^{184} Tyr^{190}
TM5	-	-	-		
TM6	Trp^{252} Tyr^{255}	-	Trp^{252} Tyr^{255}	Glu^{288}	
TM7	Glu^{288} Phe^{292}	Phe^{292}	Glu^{288}	Glu^{288}	

Table 7: 4DV3 peptide and peptide drug conjugates inhibition of viral production as measured by p24 protein extracellular amount and by counting the formation of syncytia induced by replicating the X4 strain HIV-1 IIIB.

Treatment Group	p24 logIC50	p24 IC50	Syncytia logIC50	Syncytia IC50
4DV3	-4.638	23 μM	-4.708	19.6 μM
AZT	-8.070	8.5 nM	-7.48	33 nM
4DV3 + AZT	-7.943	11 nM	-7.586	26 nM
4DV3-Ala-AZT	-7.496	32 nM	-7.096	80 nM
RTV	-7.923	12 nM	-7.573	27 nM
4DV3 + RTV	-7.998	10 nM	-7.628	24 nM
4DV3-Ala-RTV	-6.223	598 nM	-6.147	713 nM

Scheme 1: Reaction scheme for the coupling of FITC to 2-amino-ethoxy-acetic acid

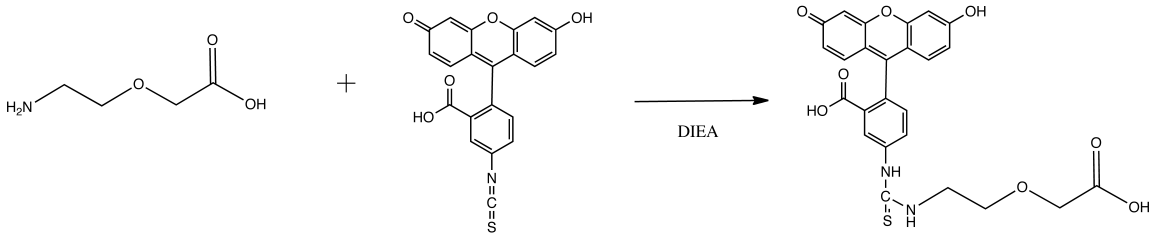

2-amino-ethoxy-acedtic acid

FITC

FITC-2-amino-ethoxy-acetic acid
Molecular Weight: 508.50

Scheme 2: Structure of 1 copy DV3 peptide carrier (MP100).

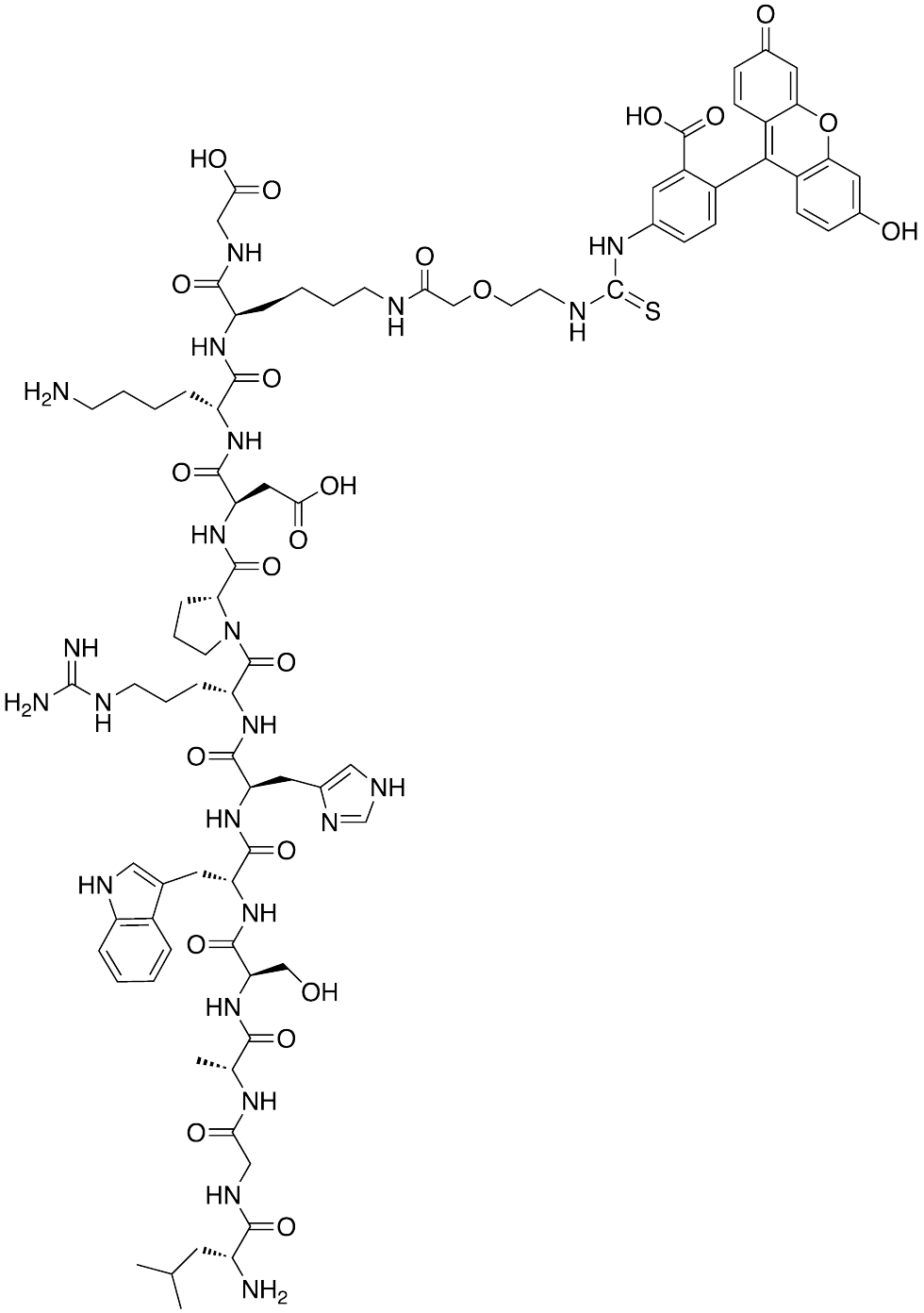

MP100
Molecular Weight: 1842.00

Scheme 3: MP100 sequence on the resin with protecting groups. In later syntheses the protecting group on Asp was changed from OtBu to OMpe to protect from aspartamide formation due to repeated Fmoc deprotection steps with piperidine.

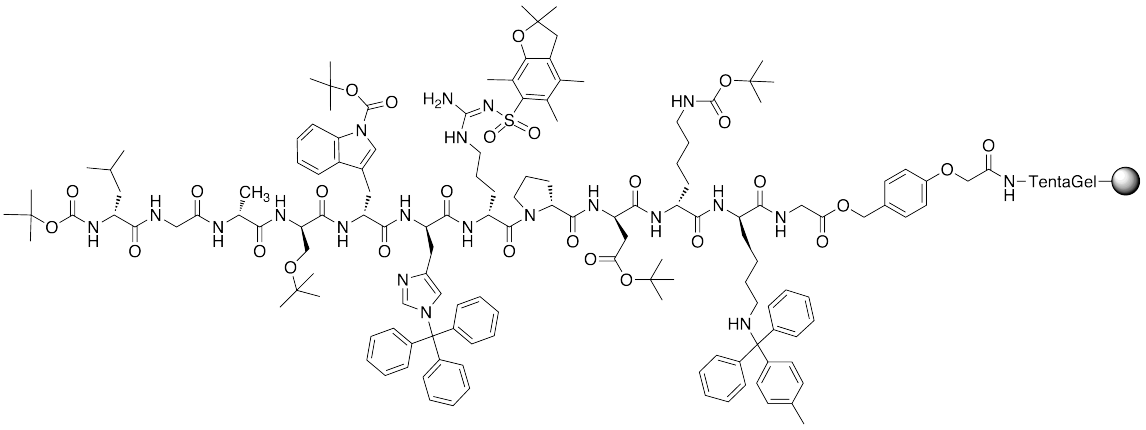

BOC—Leu—Gly—Ala—Ser(Trt)—Trp(Boc)—His(Trt)—Arg(Pbf)—Pro—Asp(OtBu)—Lys (Boc)—Lys(Mtt)—Gly—Wang - TentaGel Resin

Scheme 4: Structure of the FITC labeled 2 copy DV3 peptide carrier (MP200).

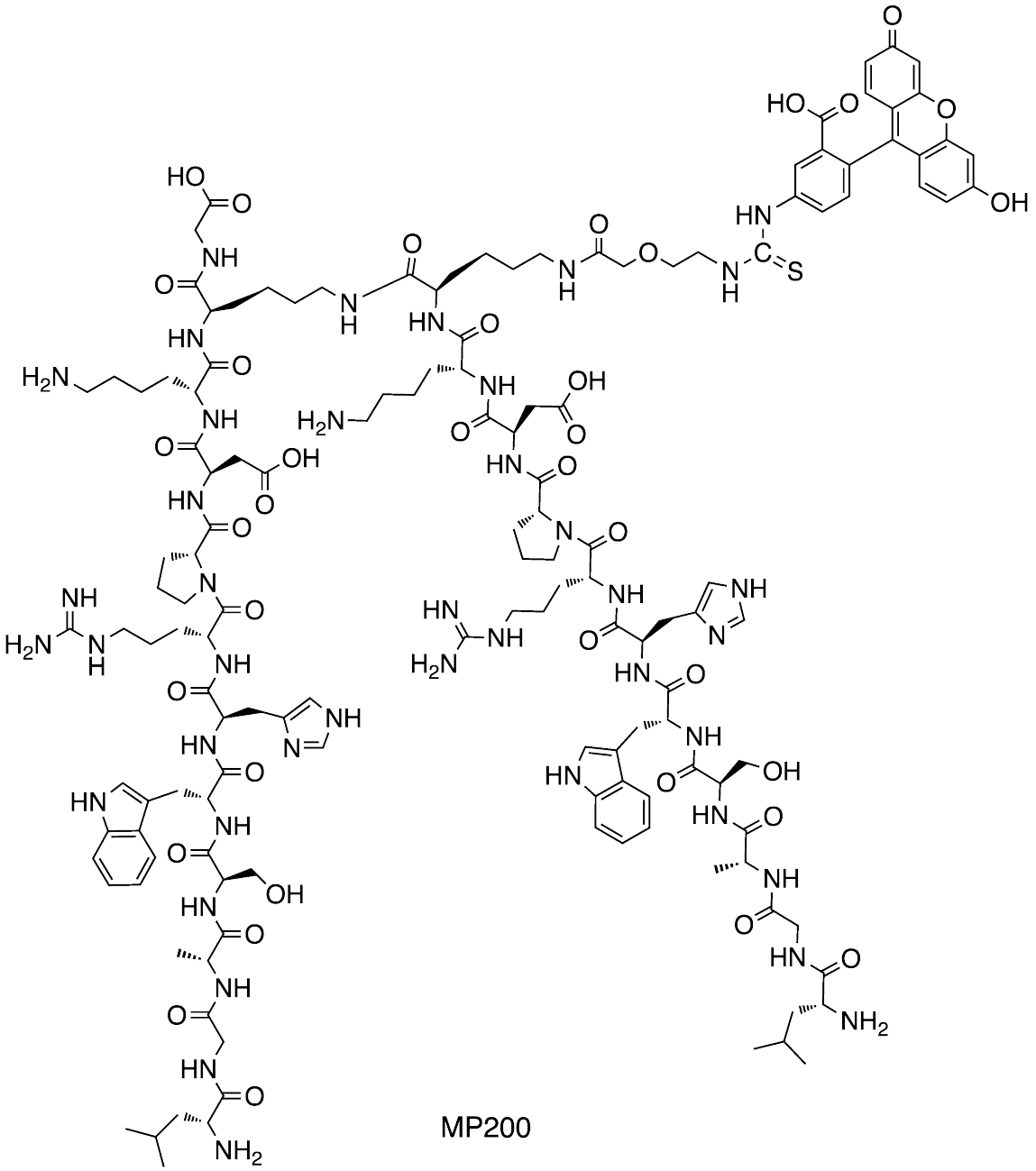

MP200

Exact Mass: 3116.48
Molecular Weight: 3118.44

Scheme 5: Mtt deprotection scheme for the synthesis of orthogonally linked copies of the DV3 peptide. For MP100 synthesis a similar scheme was used except 1% TFA in DCM was instead of 2% in all other syntheses. Mtt deprotection was also used for the conjugation of the FITC-2-amino-ethoxyacetic acid conjugate for MP200 and MP400 as well as biotinylation of MP401 and prior to drug conjugation for MP403.

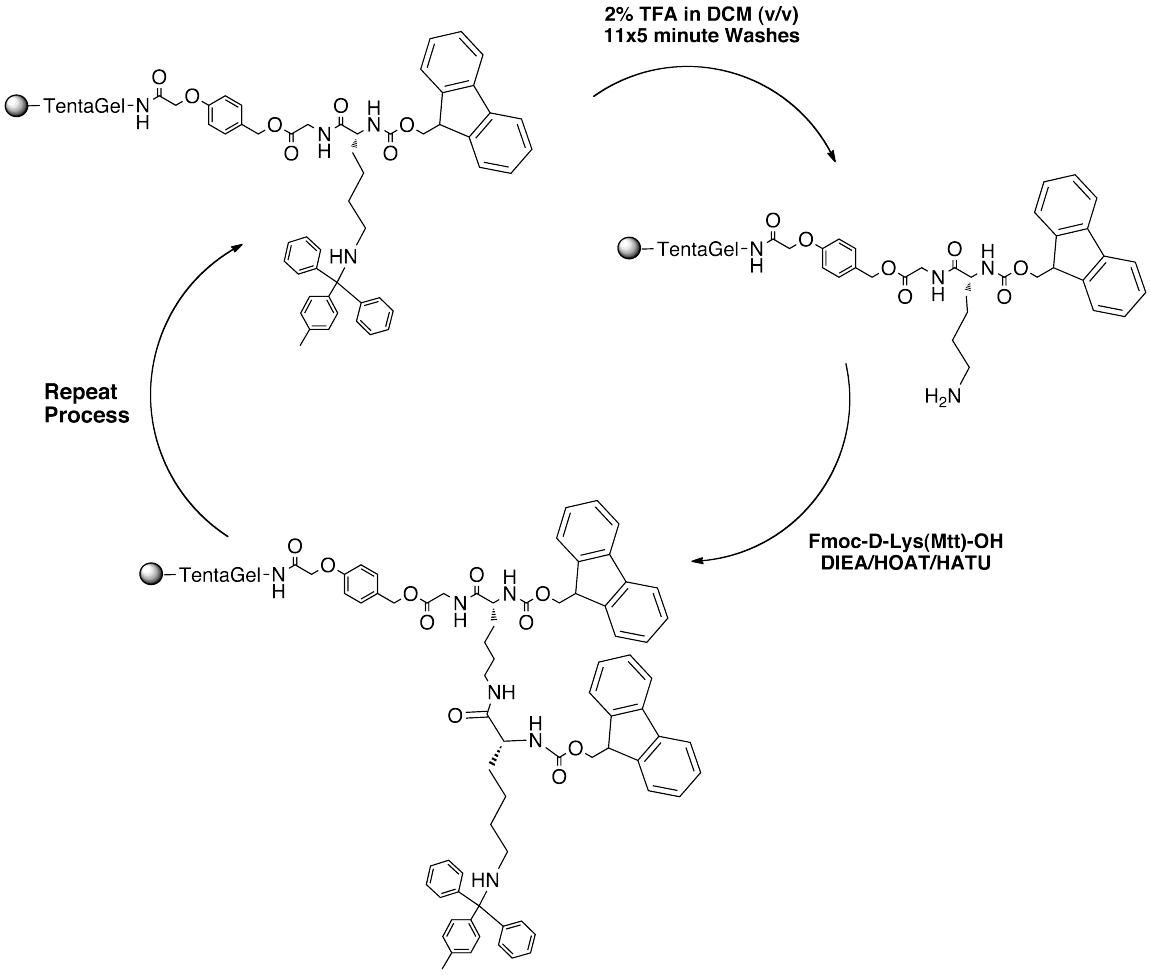

Scheme 6: Structure of the FITC labeled 4 copy DV3 peptide carrier (MP400).

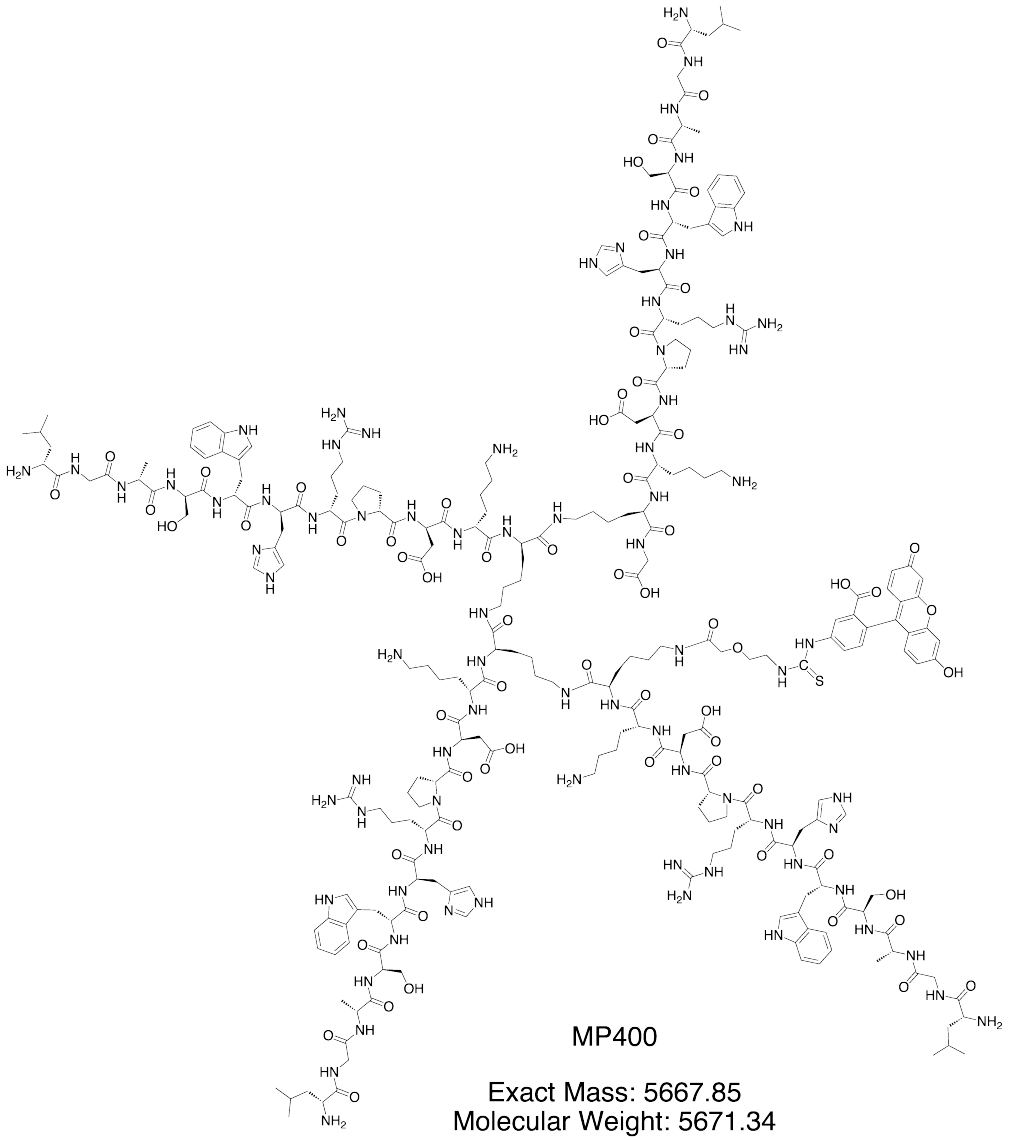

Scheme 7: Structure of biotinylated 4 copy DV3 peptide carrier (MP401).

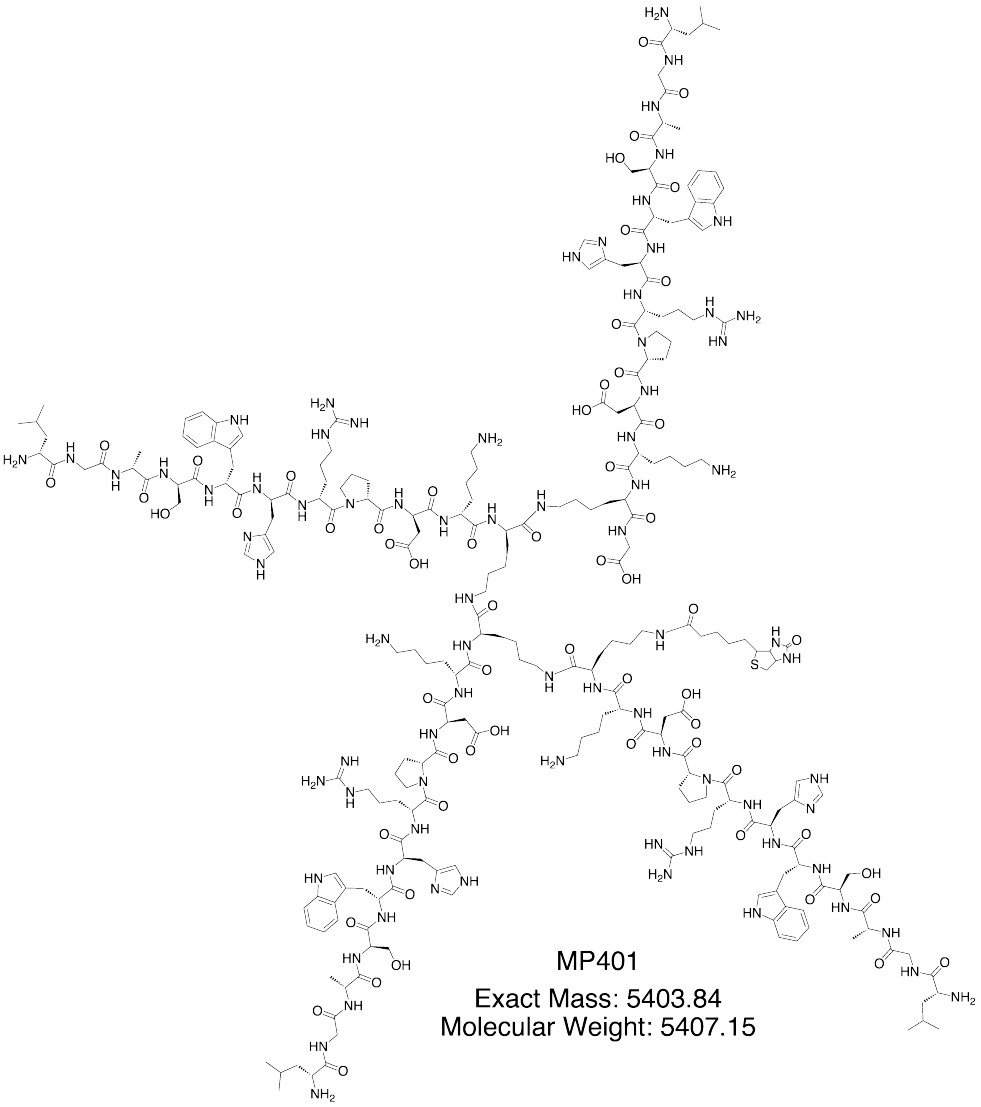

Scheme 8: DV3 Peptide was synthesized for use as an experimental control.

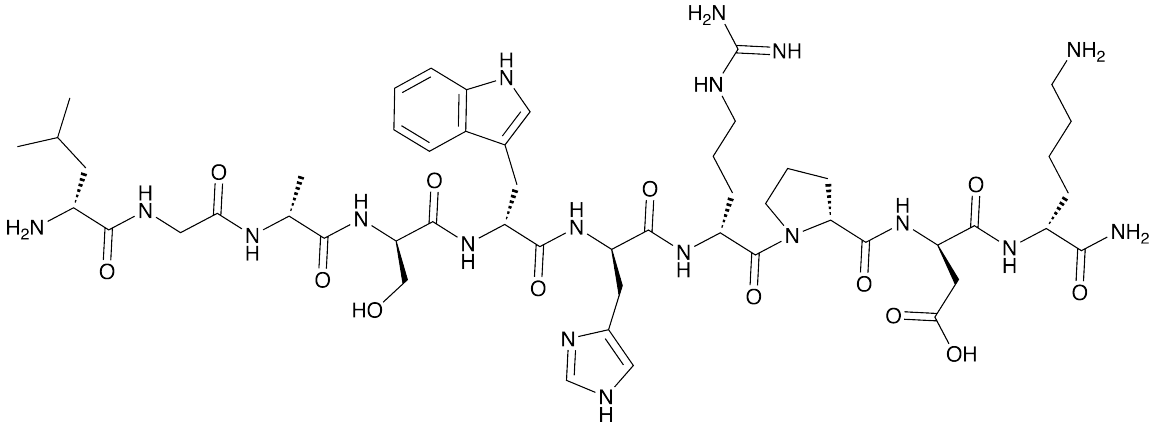

DV3 Peptide
Exact Mass: 1164.62
Molecular Weight: 1165.30

Scheme 9: Synthesis of Ala-AZT ester (TOP) and Ala-RTV ester (BOTTOM).

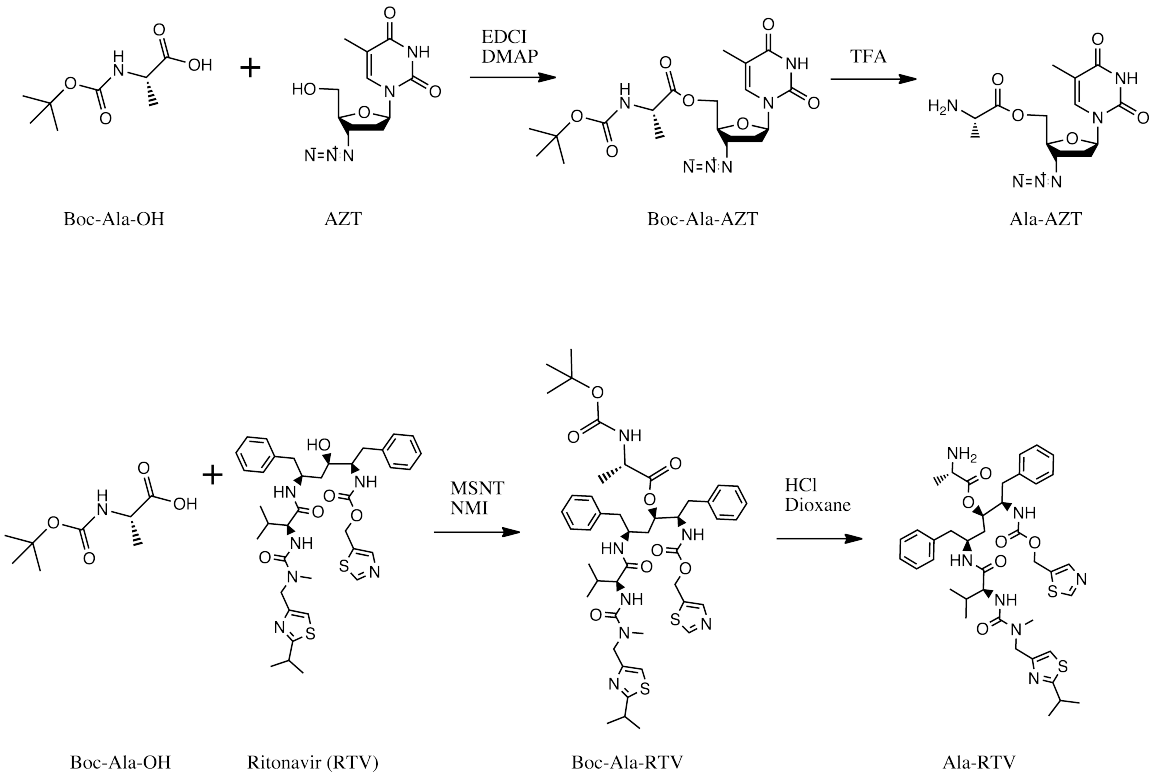

Scheme 10: Structure of unlabeled 4 copy DV3 peptide carrier (MP402).

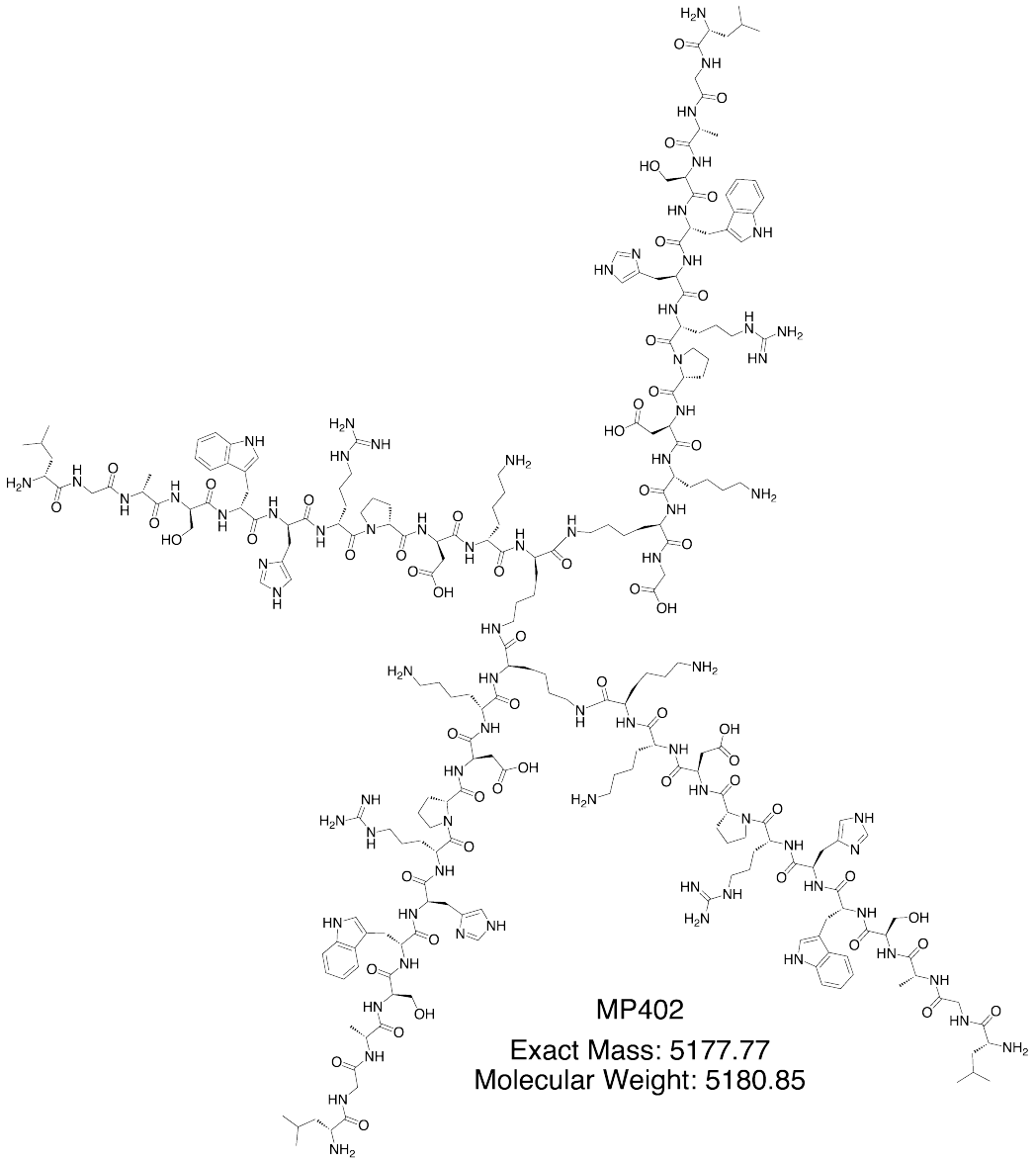

Scheme 11: Structure of 4 copy DV3 peptide carrier conjugated with alanine-AZT ester (MP403).

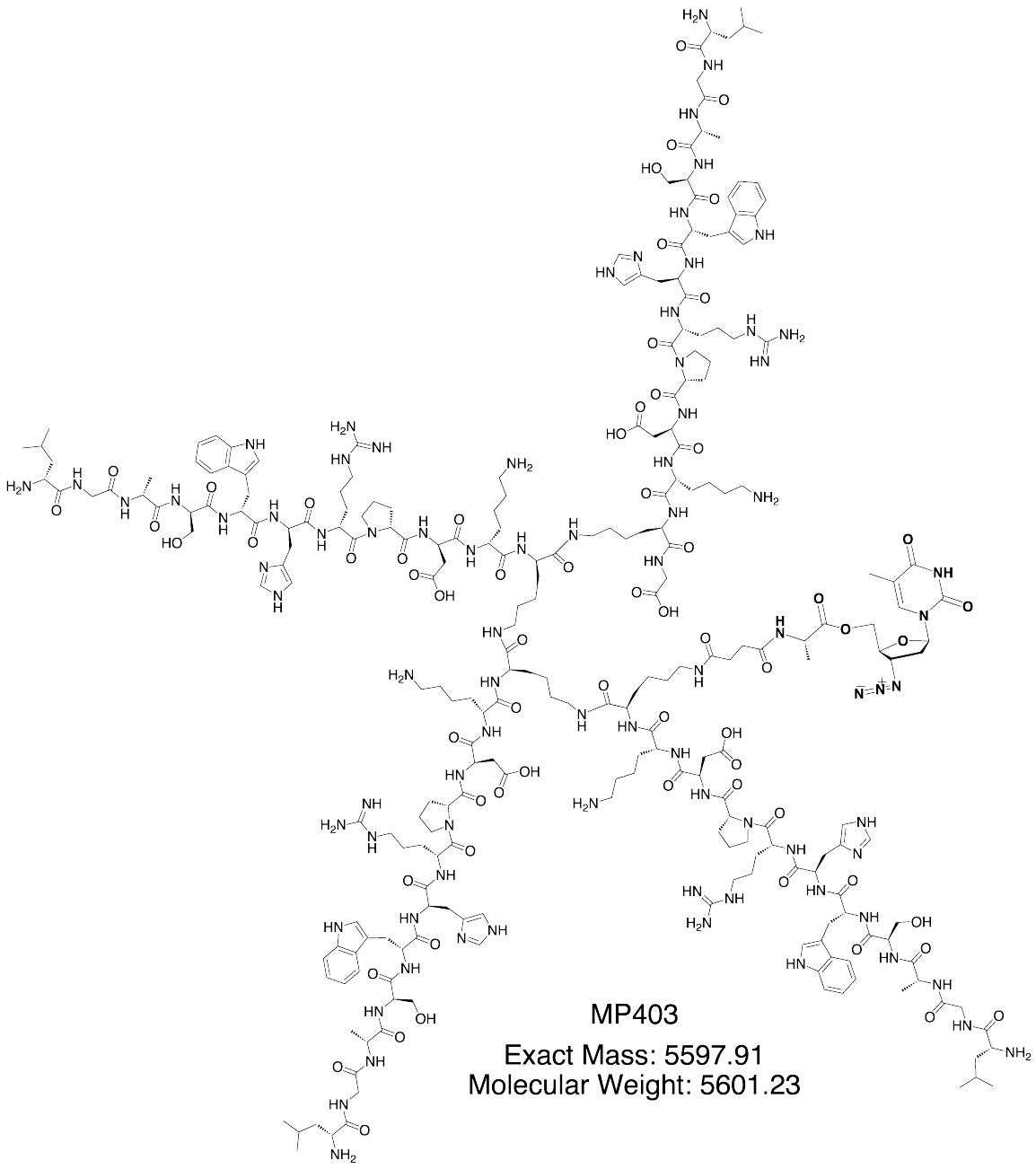

Scheme 12: Reaction sequence for the conjugation of Ala-AZT ester to 4 copy DV3 peptide carrier. The ε amino group was reacted with succinic anhydride in the presence of DIEA. The succinyl derivative was preactivated with EDC in the presence of HOAT for 1 h. The Ala-AZT ester was then coupled to the carboxyl group of the succinyl derivative in the presence of DIEA for 12 h.

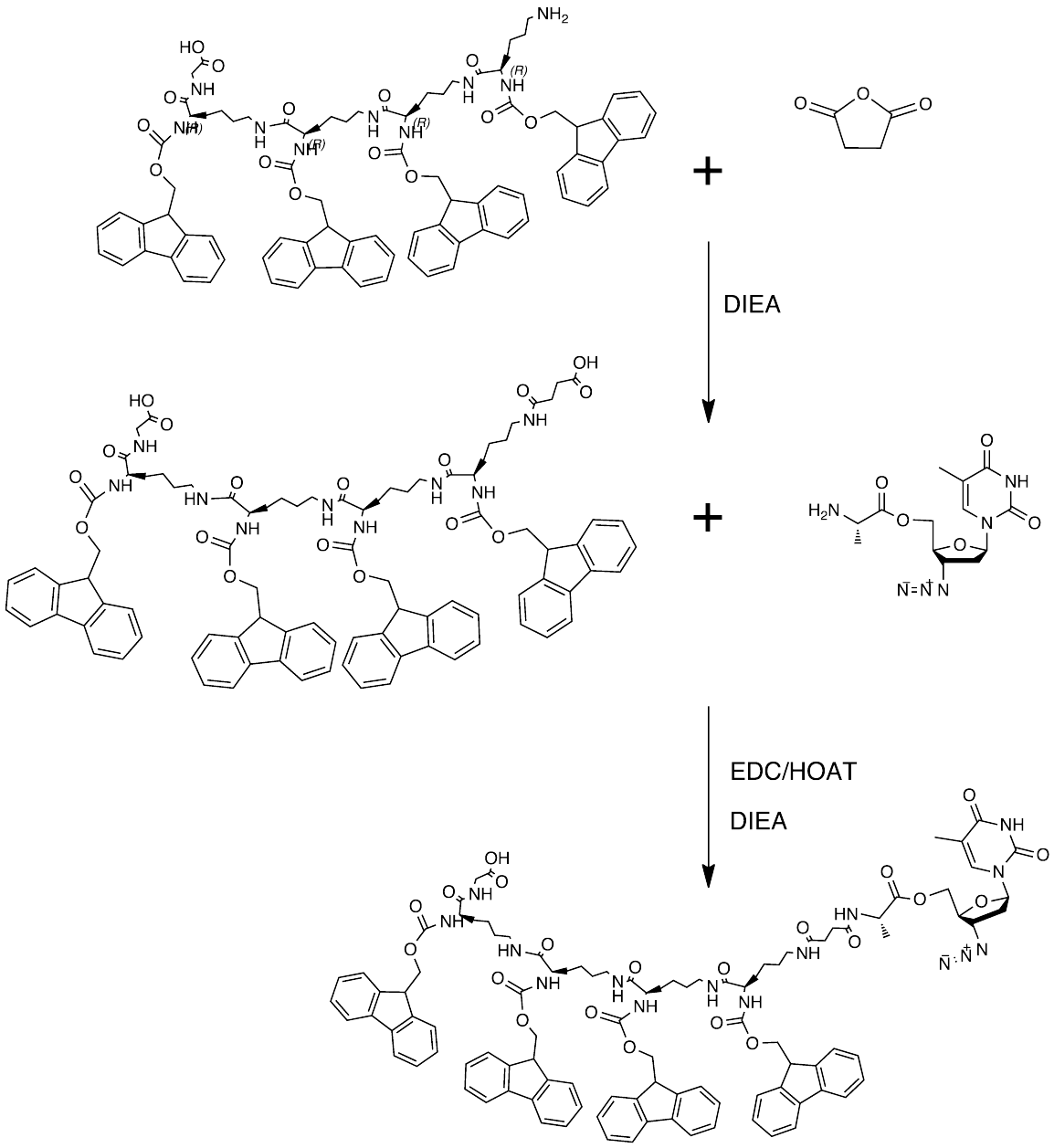

Scheme 13: Structure of 4 copy DV3 peptide carrier conjugated with alanine-RTV ester (MP404).

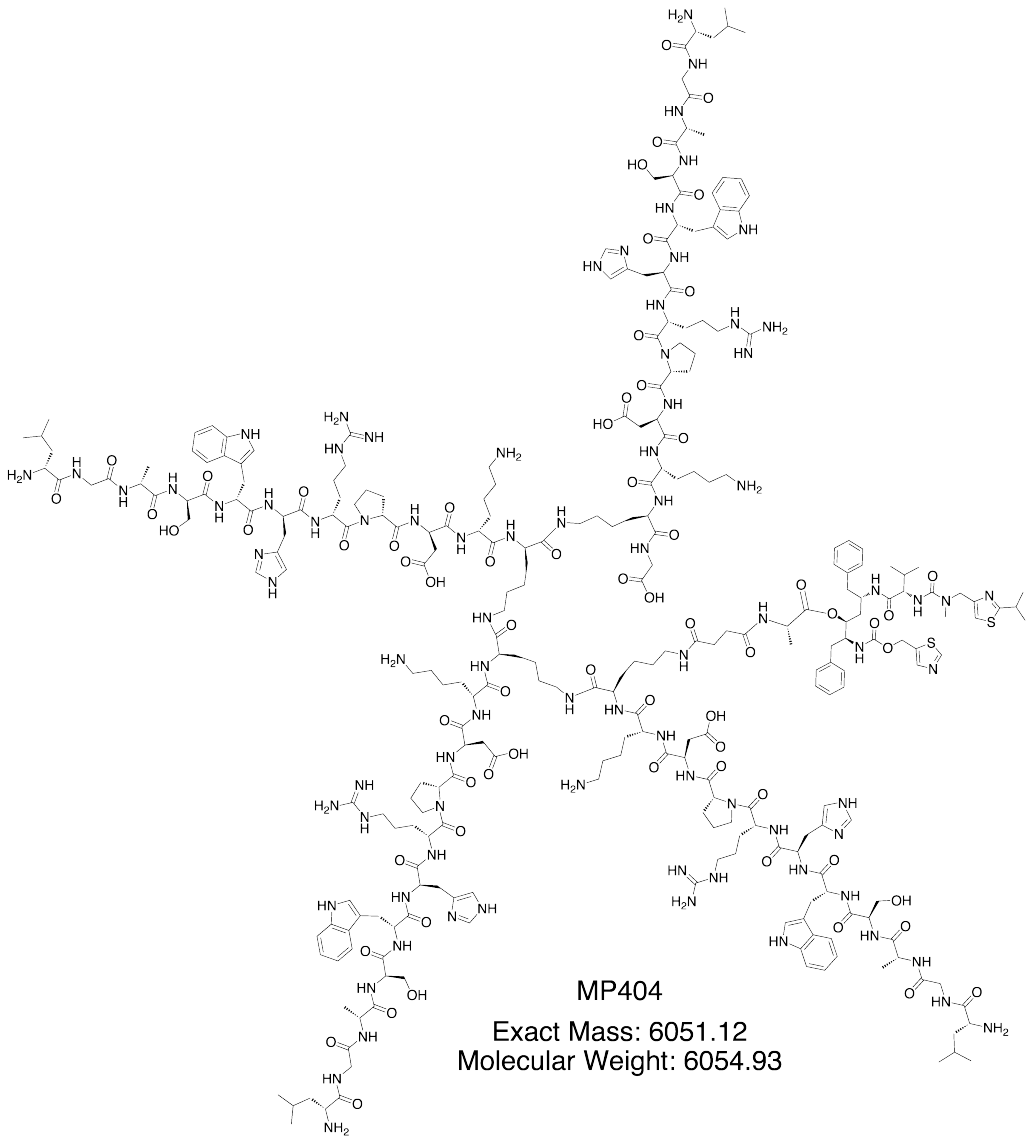

Scheme 14: Reaction sequence for the conjugation of Ala-RTV ester to 4 copy DV3 peptide carrier. The ε amino group was reacted with succinic anhydride in the presence of DIEA. The succinyl derivative was preactivated with EDC in the presence of HOAT for 1 h. The Ala-RTV ester was then coupled to the carboxyl group of the succinyl derivative in the presence of DIEA for 4 h.

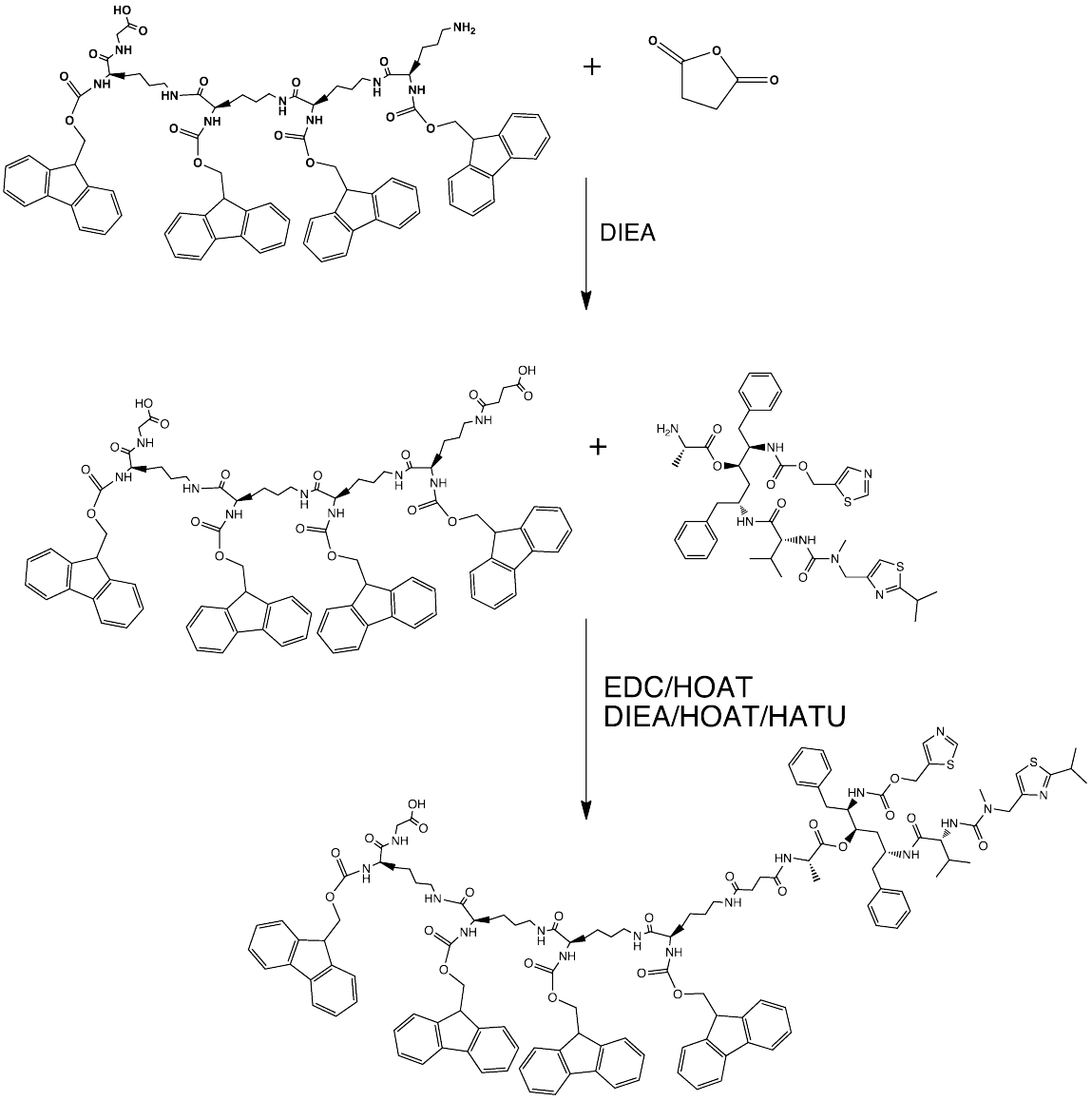

Scheme 15: Structure of 4 copy DV3 PEG_{12} azide peptide carrier (MP410).

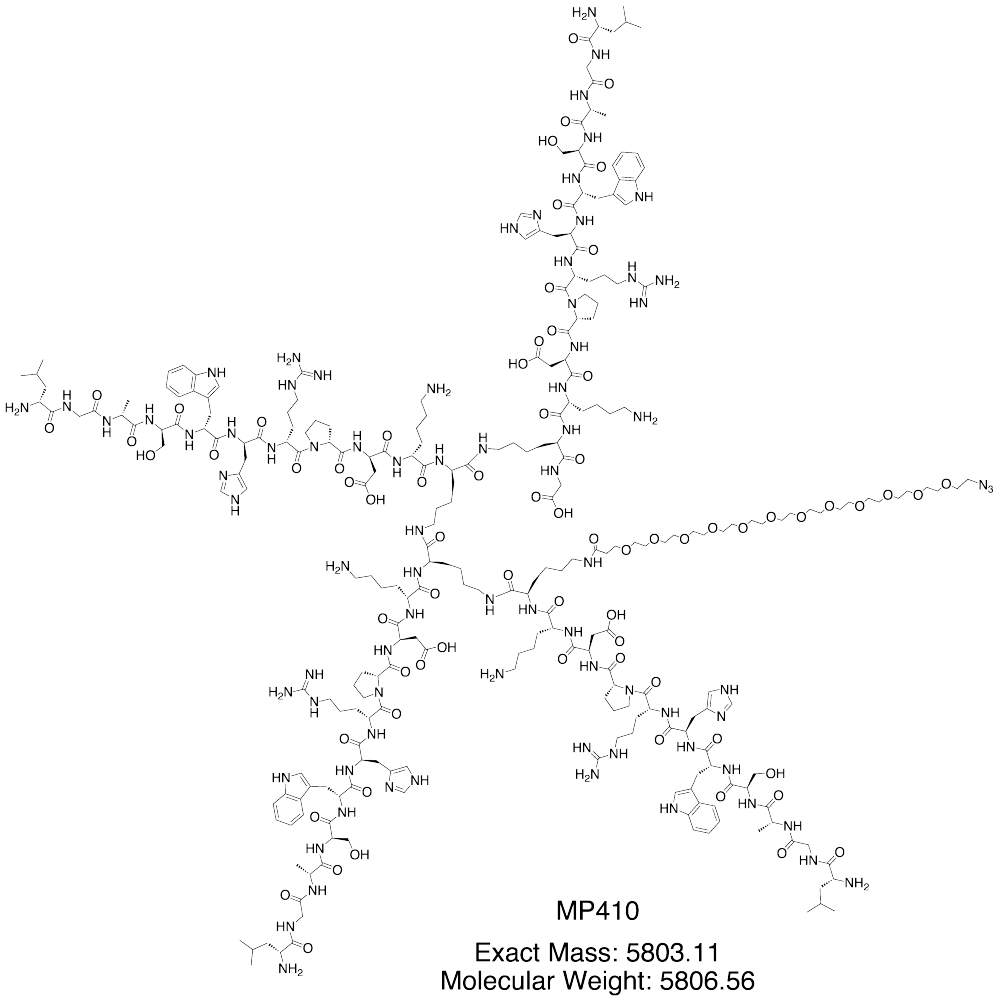

Scheme 16: Reaction scheme for azido cycloaddition commonly referred to as copper free click reaction.

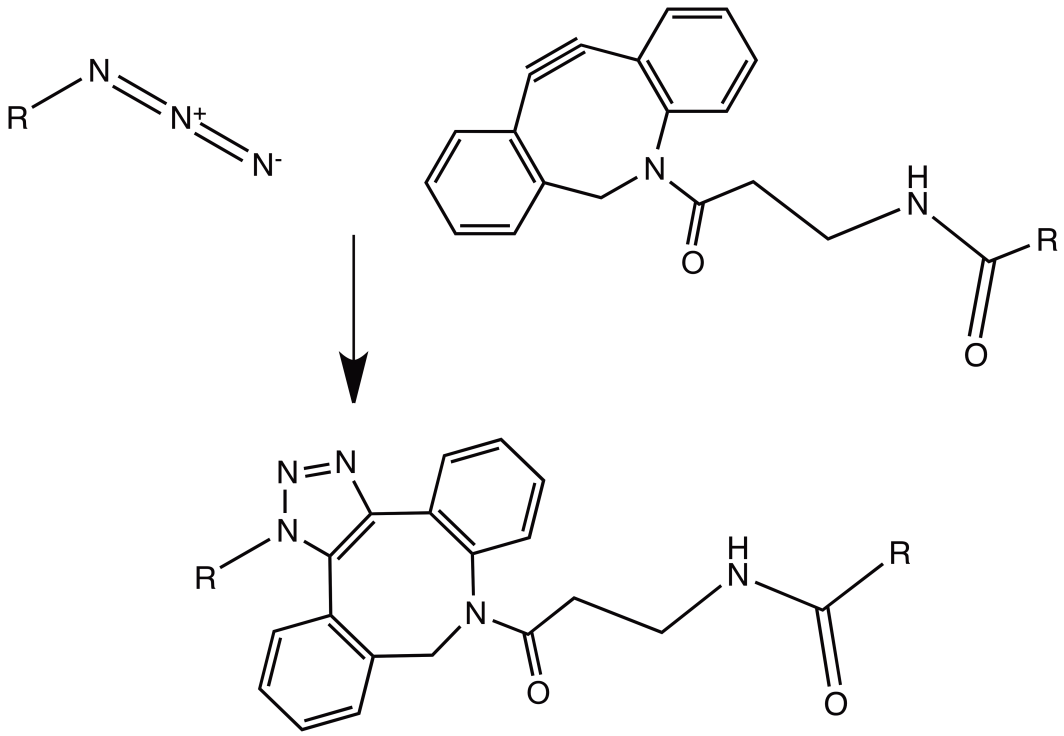

Scheme 17: Structure of 4 copy DV3 PEG_{12} azide after copper free click reaction with DBCO-PEG_4-DBCO (MP411).

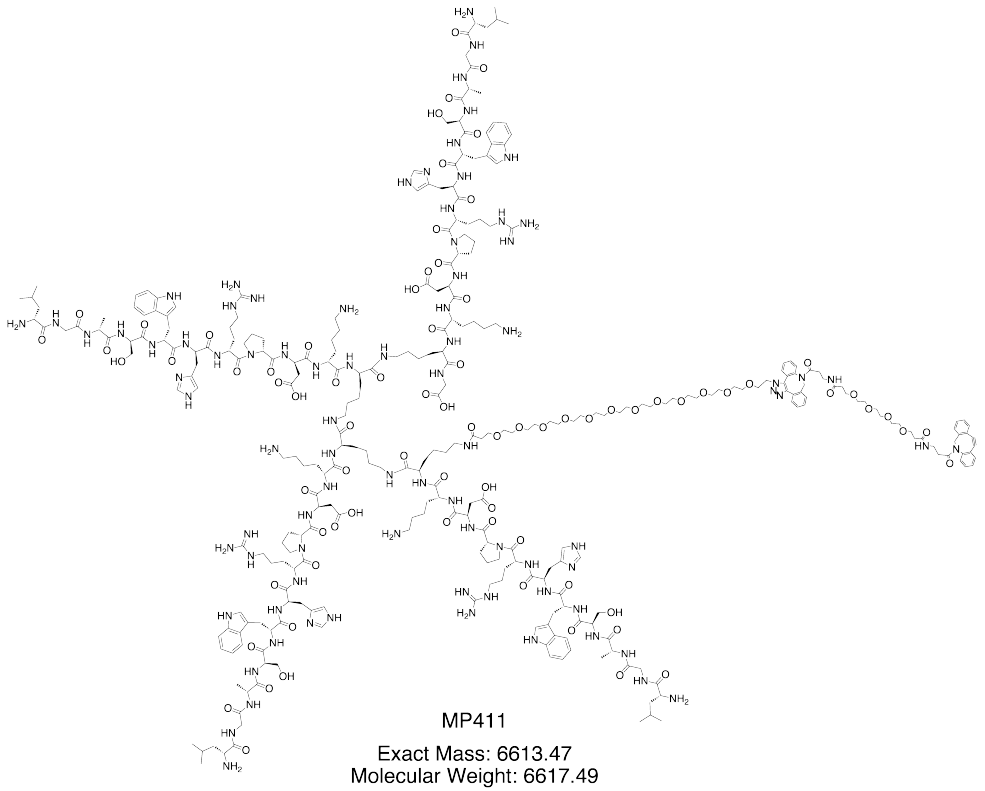

MP411

Exact Mass: 6613.47

Molecular Weight: 6617.49

Scheme 18: End Unit (EU) of PEGylated peptide carrier for Strategy III. The N-terminus of the EU has an azido-PEG_{16} for 'click' addition of MP411. The N-terminus Lys residue is also conjugated at the ε amine with a FITC molecule for fluorescent labeling. The EU was added to the DU and MBU after fragment condensation to the desired molecular weight.

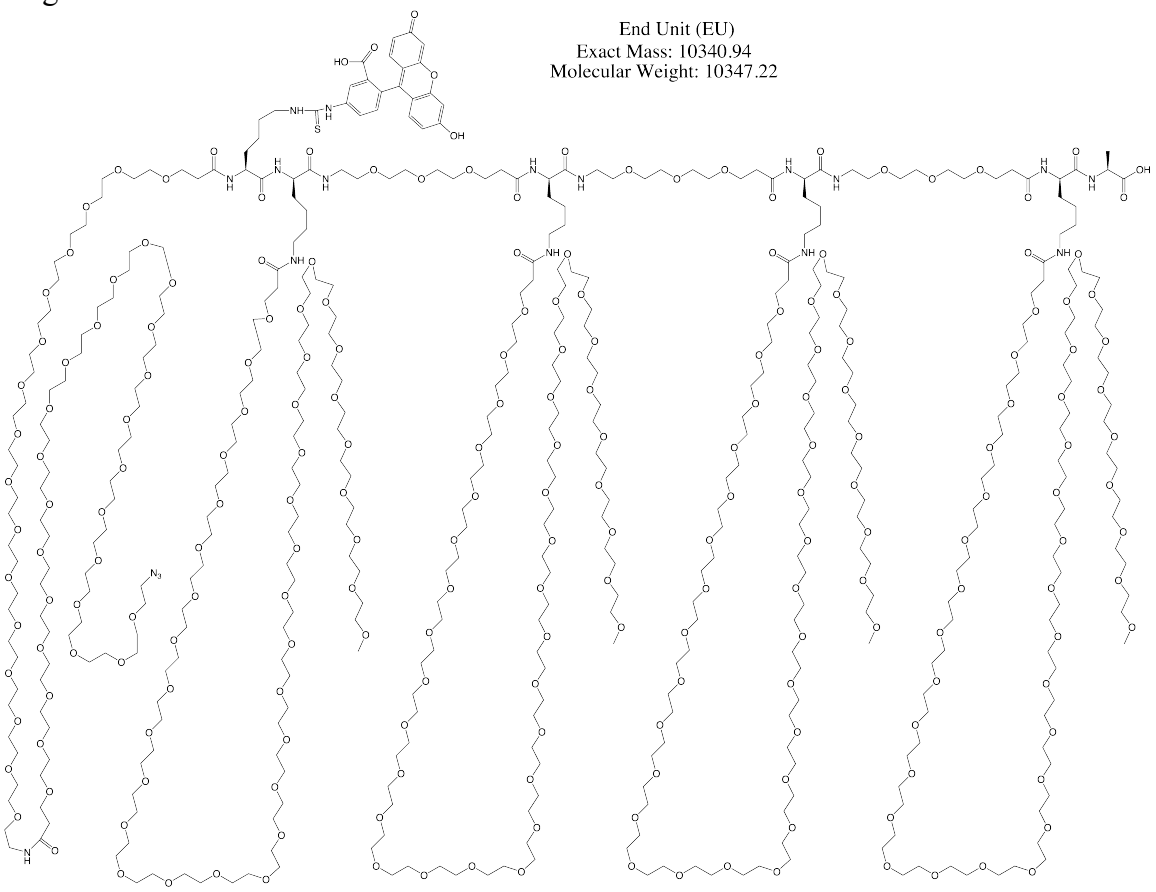

Scheme 19: Mass Building Unit (MBU) of PEGylated peptide carrier for Strategy III. The N-terminus of the MBU has an Fmoc-amido-PEG_6 for fragment condensation. The MBU was added to the DU during fragment condensation to build up the desired molecular weight prior to addition of the EU.

MBU

Exact Mass: 8451.96
Molecular Weight: 8457.05

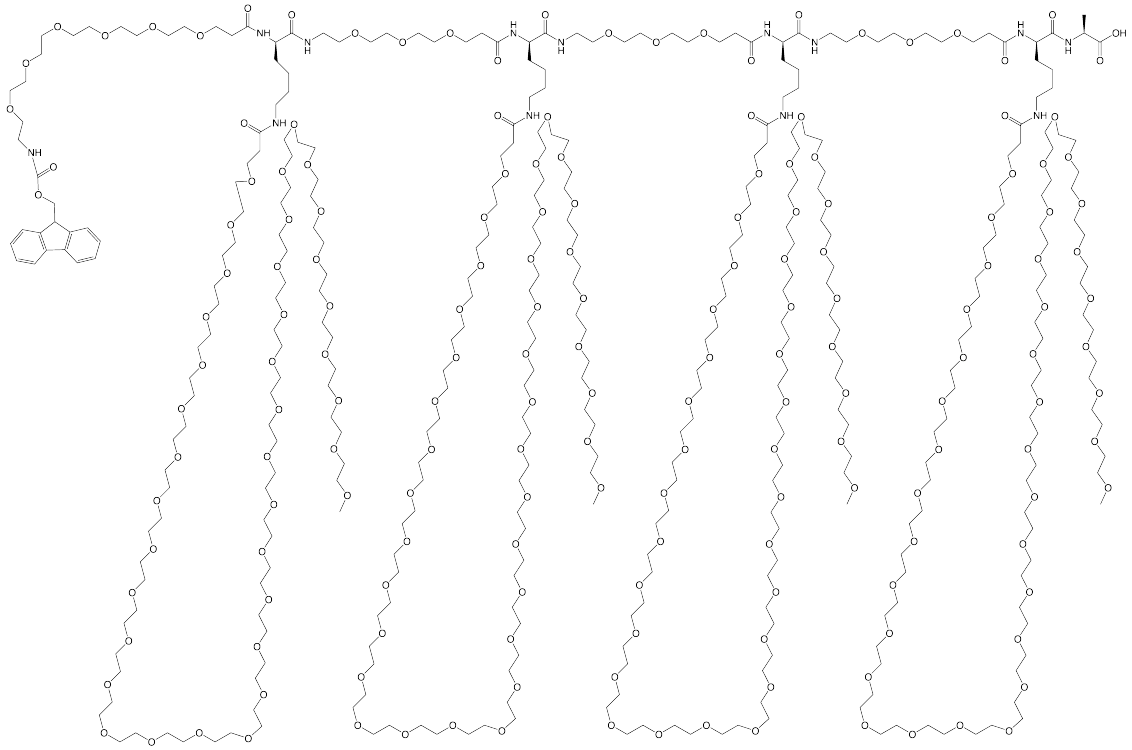

Scheme 20: Drug Loading Unite (DU) of PEGylated peptide carrier for Strategy III. The N-terminus of the DU has an Fmoc-amido-PEG_6 for fragment condensation. The DU will be Fmoc deprotected during fragment condensation to build up the desired molecular weight with MBUs prior to addition of the EU. Following addition of MBU and EU, the DU will be Mtt deprotected and Fmoc-amido-PEG_{16}-acid coupled to the ε amine. The Fmoc groups deprotected and recoupled with Fmoc-amido-PEG_{16}-acid. The Fmoc groups will again be removed and succinylated Ala-RTV will be coupled to the PEG_{16} residues (Scheme 22).

DU

Exact Mass: 2205.20
Molecular Weight: 2206.74

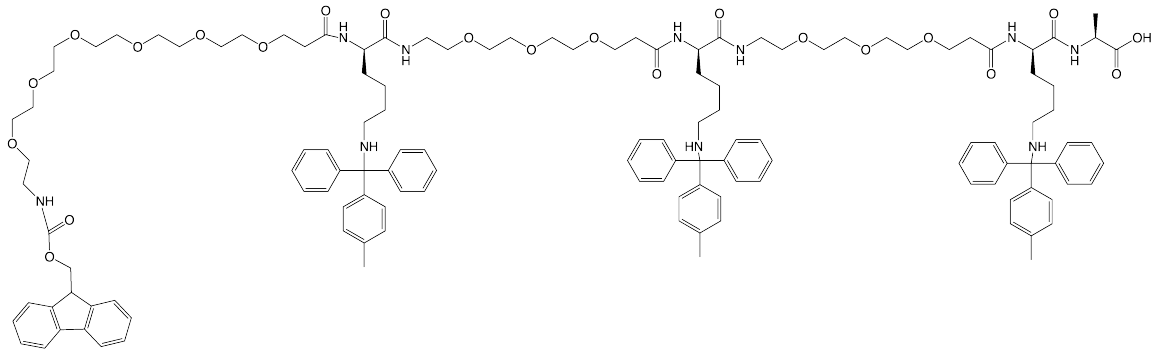

FIGURE 1**:** (A) Helical and (B) serpentine model of CXCR4 arranged to distinguish the amino acids that form the extracellular, transmembrane, and intracellular components. Like other chemokine receptors, CXCR4 features seven transmembrane regions similar to rhodopsin. Of particular importance to the endogenous and pathological functions are the N-terminus and the second extracellular loop (*14*). (C) Additional serpentine model of CXCR4 highlighting the charged and glycosylated residues of the extracellular portions of CXCR4 (*126*). The glycosylated and negatively charged residues are important to HIV-1 gp120 binding as well as other exogenous ligands like vMIPII and its derivatives for example DV3.

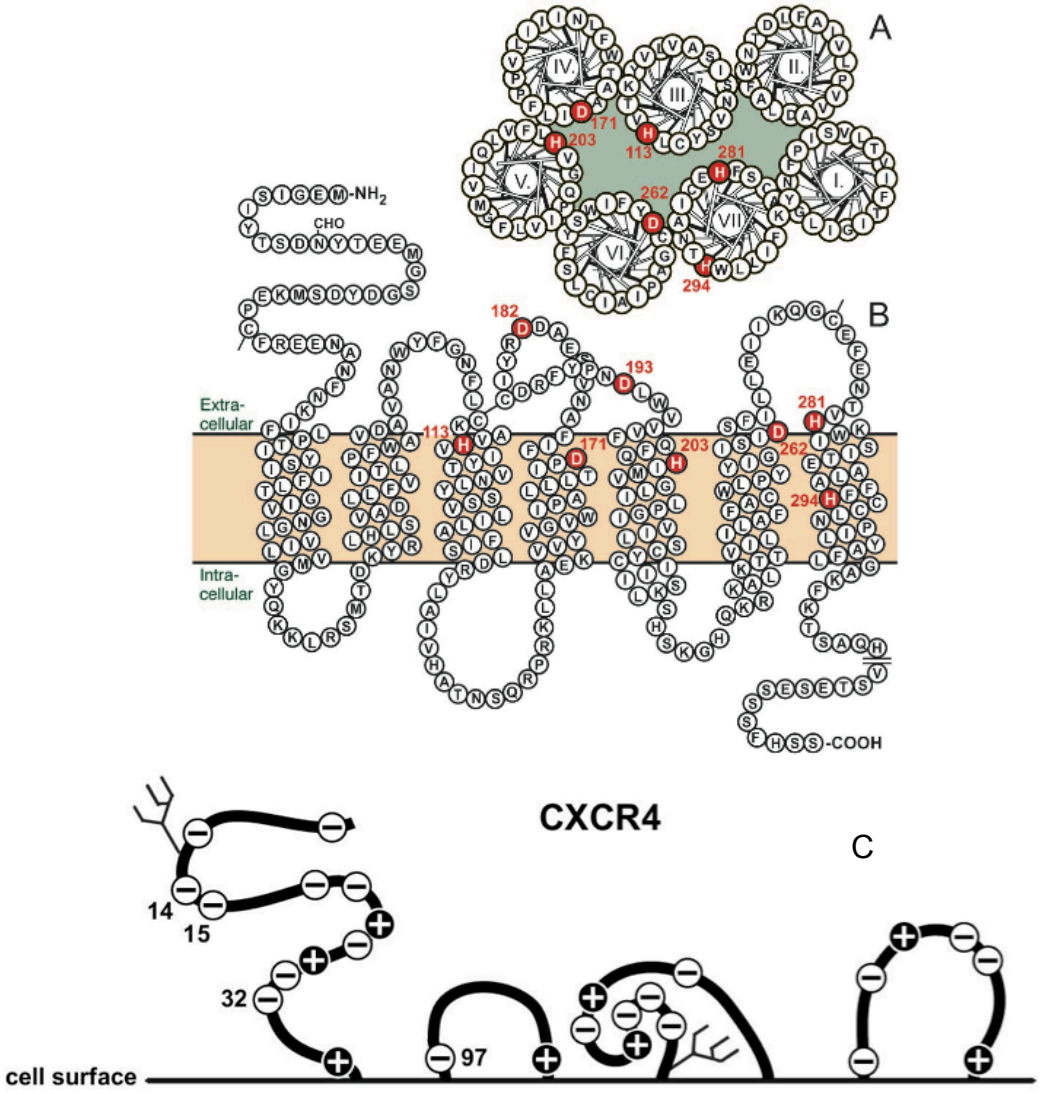

FIGURE 2: Classification of chemokines by their specificity, expression, or function. The specific receptors bind only one chemokine, while members of the shared group have the ability to bind several different chemokines. Additionally, those chemokines and receptors that are non-signaling serve as feedback mechanisms for other chemokines. Those chemokines and their receptors that are generated by viruses are denoted in red. CXCR4 is a member of the specific chemokine receptor class as it only binds CXCL12 (*16*). CXCR4 has also been shown to bind the viral chemokine vMIPII, represented here formally as CCL2.

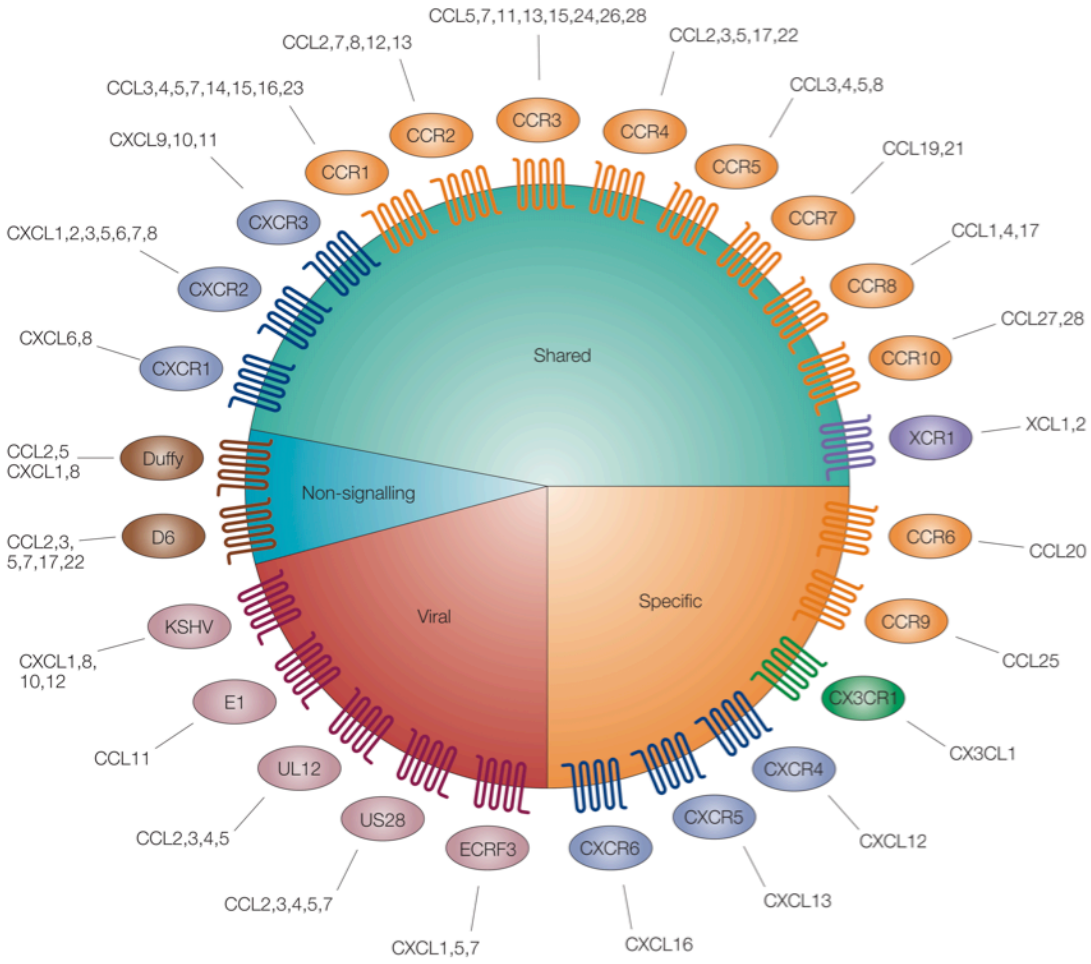

FIGURE 3: Antigen binding sites (ABS) measured by quantitative fluorescence-activated cell sorting (QFACS) on numerous T-cell lines used for HIV-1 experiments. Detection of ABS was achieved by using a fluorescently labeled monoclonal antibody for CXCR4 (12G5) and CD4 (Q4120). Jurkat-D and Jurkat-M groups are two batches of Jurkat cells acquired from different labs (*6*). Ghost X4 and Ghost R5 were transfected to express high levels of the HIV-1 coreceptors CXCR4 and CCR5 respectively, while its parent cell line GHOST-par only significantly expresses CD4. CD4 and a coreceptor (CXCR4 or CCR5) are necessary for HIV-1 entry.

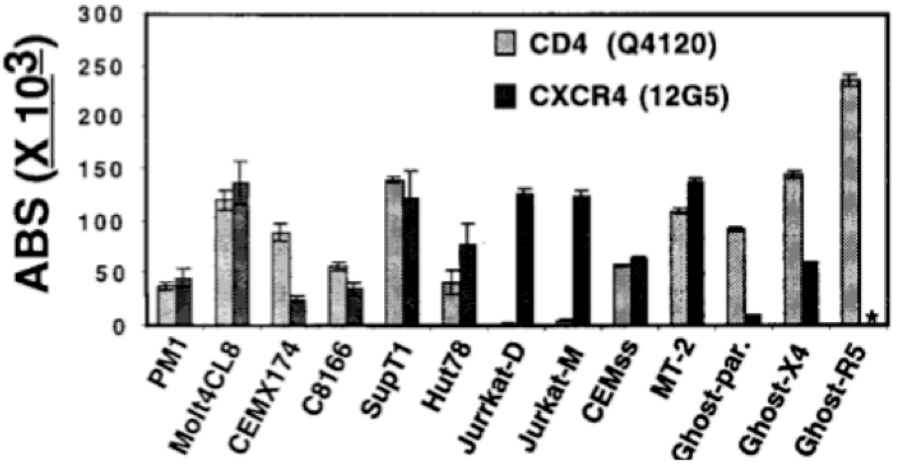

FIGURE 4: Schematic of HIV-1 disease progression highlighting the shift in tropism from HIV-1 chronic infection to the development of AIDS. A high level of viremia develops over the course of several weeks from infection with a R5 strain of HIV. Adapted immunity against the virus is able to stabilize circulating virus for several years. Eventually, a shift in viral tropism (to X4 and dual tropic virus) occurs in conjunction with viral load rebound and a decline in $CD4^+$ T cells leads to rapid deterioration of the infected person. Adapted from (*110, 114*)

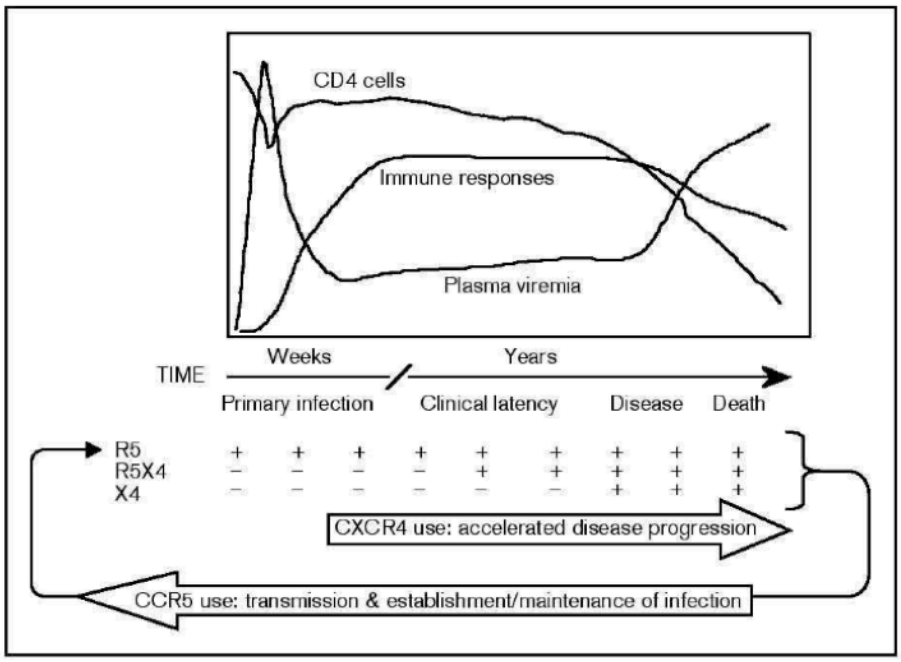

FIGURE 5: Superposition of the β hairpin structure from the CXCR4 endogenous ligand CXCL12 (purple) and the β hairpin structure form the X4 tropic HIV-1 strain HIV-1 IIIB (blue). Isoleucine residues 314 and 316 from HIV-1 IIIB were aligned with Ala^{40} and Leu^{42} residues from CXCL12 (*120*).

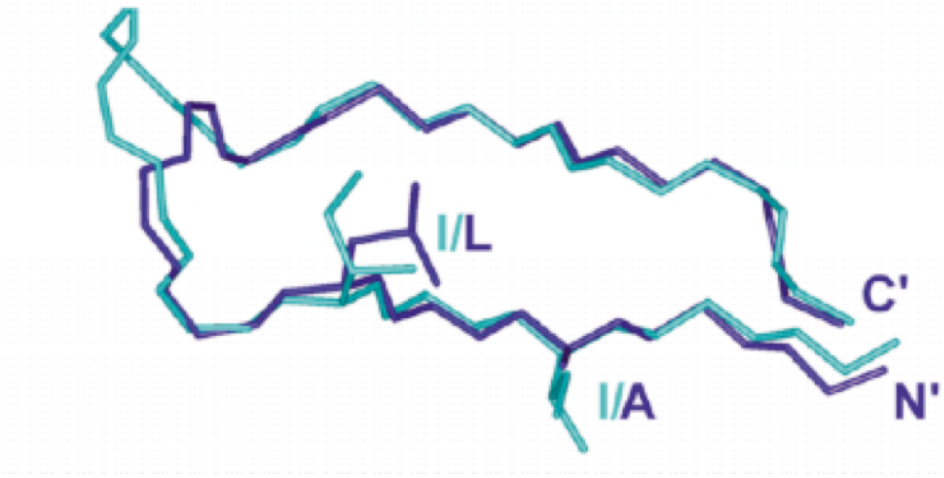

$V3_{IIIB}$ $-^{312}$KSIRIQRGPGRAFVTI^{327}
SDF-1 $-^{38}$IVARLKN--NNRQVCI^{51}

FIGURE 6: Model of the interaction between HIV-1 gp120, CD4, and the viral coreceptor CXCR4 from Wu et al. Science 2010 (*49*). (A) HIV-1 gp120 is represented as a heterotrimer with gp41 in a wire mesh format (PDB 3DNO). The core structure of gp120 is further accentuated by the color cyan (PDB 2QAD). Three CD4 receptors (tan in color, PDB 1WIP and 2KLU) are bound to gp120. The subsequent conformational changes from gp120/CD4 interaction result in CXCR4 recruitment and interaction. The V3 loops of the gp120 molecules (magenta) are shown to bind to three CXCR4 (blue) imbedded into the cell membrane. (B) A close up model of gp120/CXCR4 interaction through the V3 loop demonstrating the two-site binding model. Site 1 contains sulfotyrosine residues of CXCR4 binding initially to the V3 loop of gp120. Conformational changes in the V3 loop lead to further binding of gp120 to the negatively charged residues of the 2nd and 3rd extracellular loops that makeup Site 2.

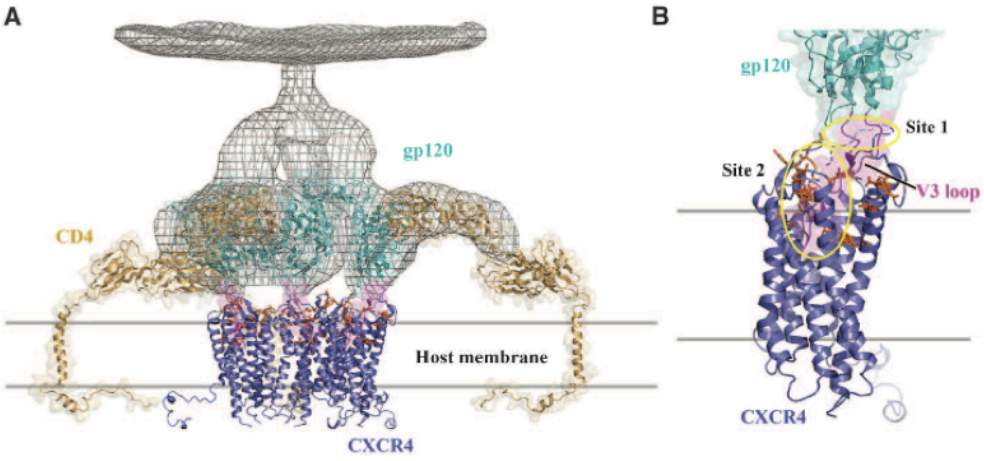

FIGURE 7: HIV-1 persistence in treatment experienced patient over a 7-year period. (A) Two-phase decay model of viral load after the initiation of HAART, the first phase has a $t_{1/2}$ = 1.5 days, possibly correlating to the response of $CD4^+$ activated T-cells. The second phase, $t_{1/2}$ = 2-3 weeks may be attributed to the viremia of macrophages. (B) The long-term half-life in treatment experienced patients after 1 year of treatment projects the viral load decay in the second phase as infinite. The horizontal line corresponds to the limit of detection (50 copies/ml) for the PCR based assay used to determine a patient's HIV-1 plasma concentration (*171*). The analysis demonstrates the ability to chronically treat HIV-1 infected patients, but the current therapies are ineffective in actually curing HIV-1 infection.

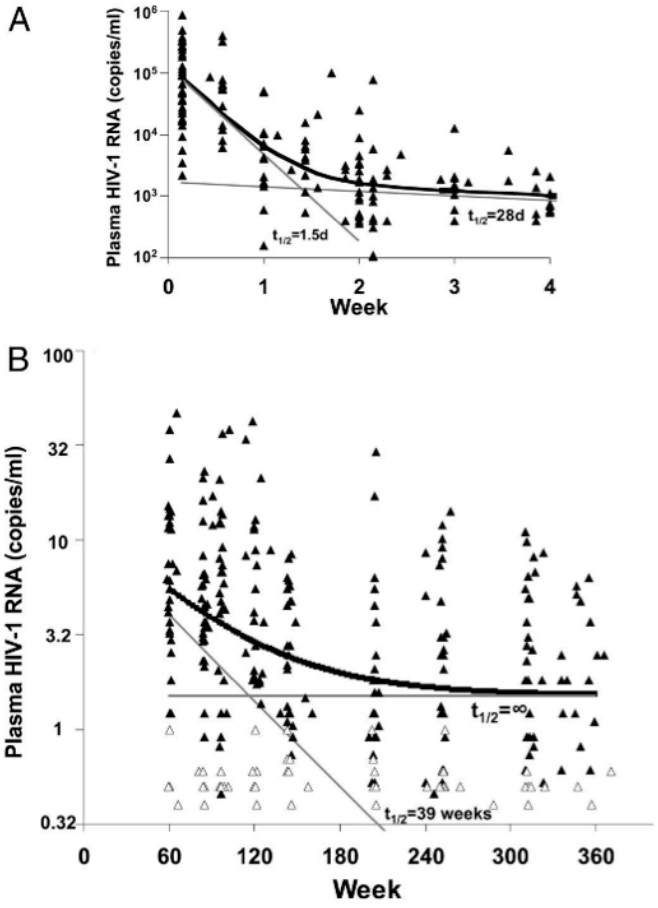

FIGURE 8: CXCL12 derived homodimer peptide with binding affinity (K_i = 290nM) and anti-HIV activity (130nM) (*191*).

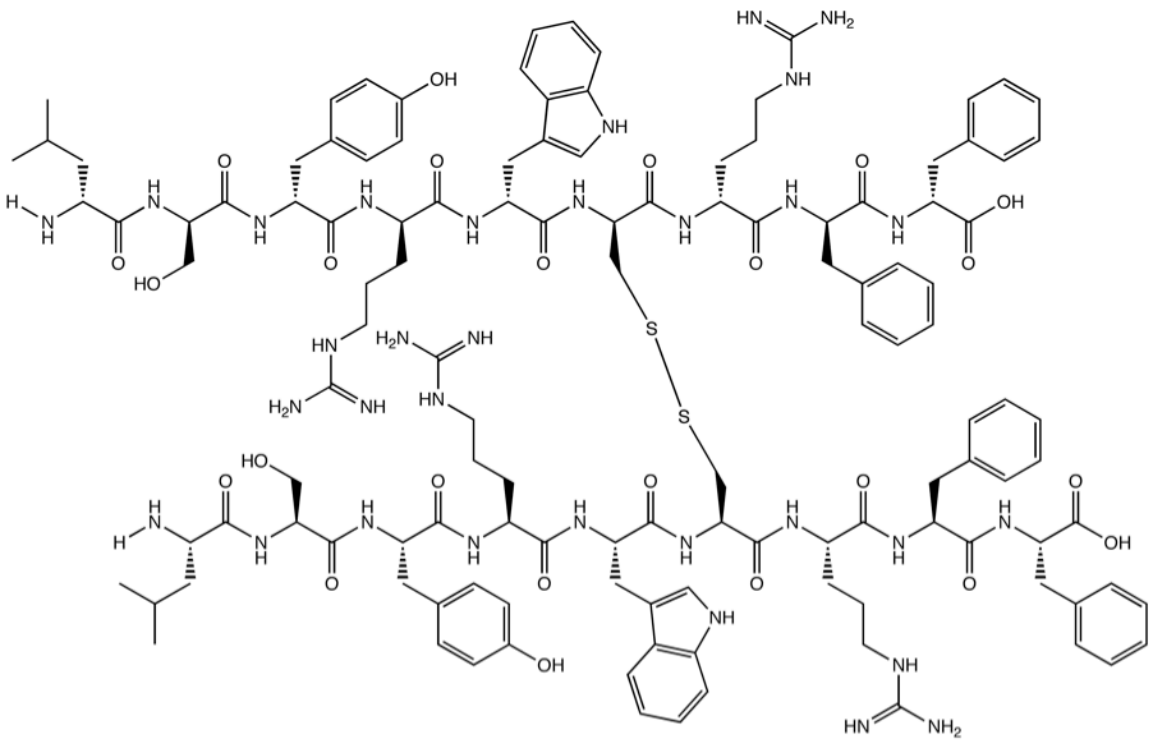

SDF-1 derived dimer of amino acids 5-14

FIGURE 9: Model structure of CXCL12 (SDF-1α) the endogenous ligand for CXCR4 (PDB 1SDF) (*32*).

FIGURE 10: Model structure of vMIPII (1-71) from the herpes simplex virus (PDB 1HFG). vMIPII has been found to bind many classes of chemokine receptors including the two important HIV-1 coreceptors CCR5 and CXCR4 (*32, 192*).

FIGURE 11: Structure of the N-terminal amino acids of vMIPII (aa 1-10) (*192*). The peptide consists of N-Leu-Gly-Ala-Ser-Trp-His-Arg-Pro-Asp-Lys-COOH and is listed as PDB 1HFF. This peptide fragment in the D stereoisomer form is described in the literature as DV3, a peptide with the ability to bind to CXCR4 (*199, 200*).

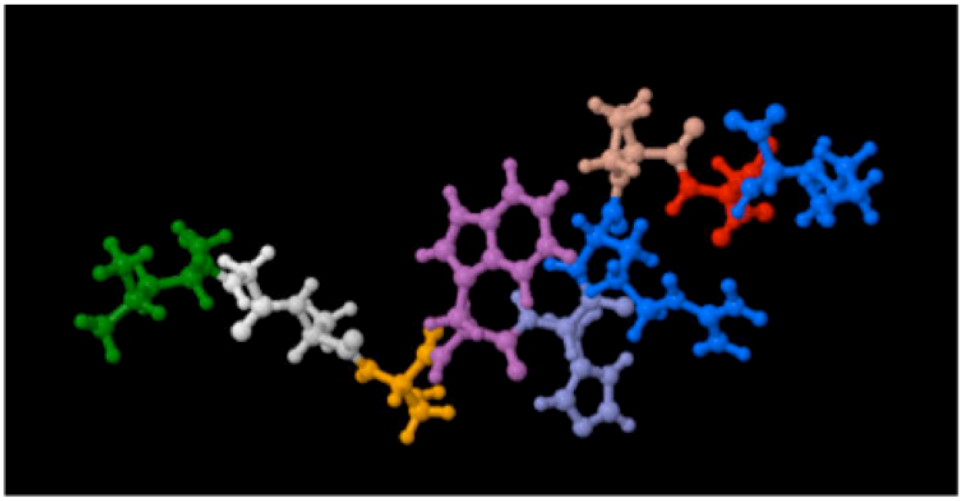

FIGURE 12: Representative image of MTT deprotection with 2% TFA in DCM. Yellow color is due to the presence of the MTT cation in the eluent collected by the fraction collector of the peptide synthesizer. Successive washing of the resin with 2% TFA in DCM resulted in deprotection of the ε amino group of the lysine residues.

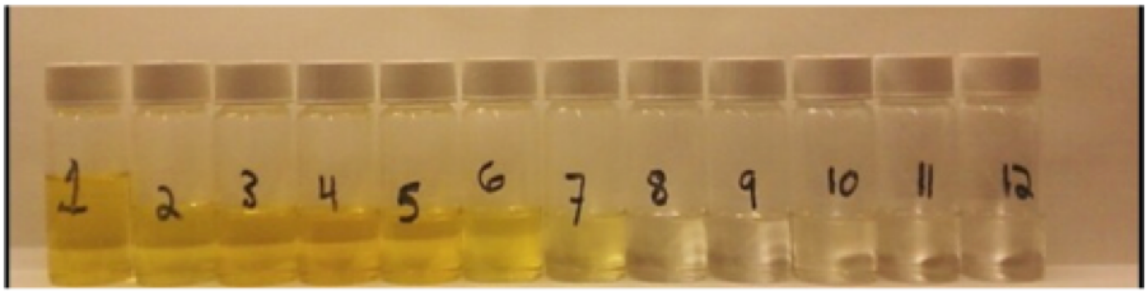

FIGURE 13: ESI-MS Spectrum of FITC-2-amino-ethoxy-acetic acid (507 Da). The spectrum represents an average of 20 spectra taken in the negative ion mode of a Finnegan LCQDuo.

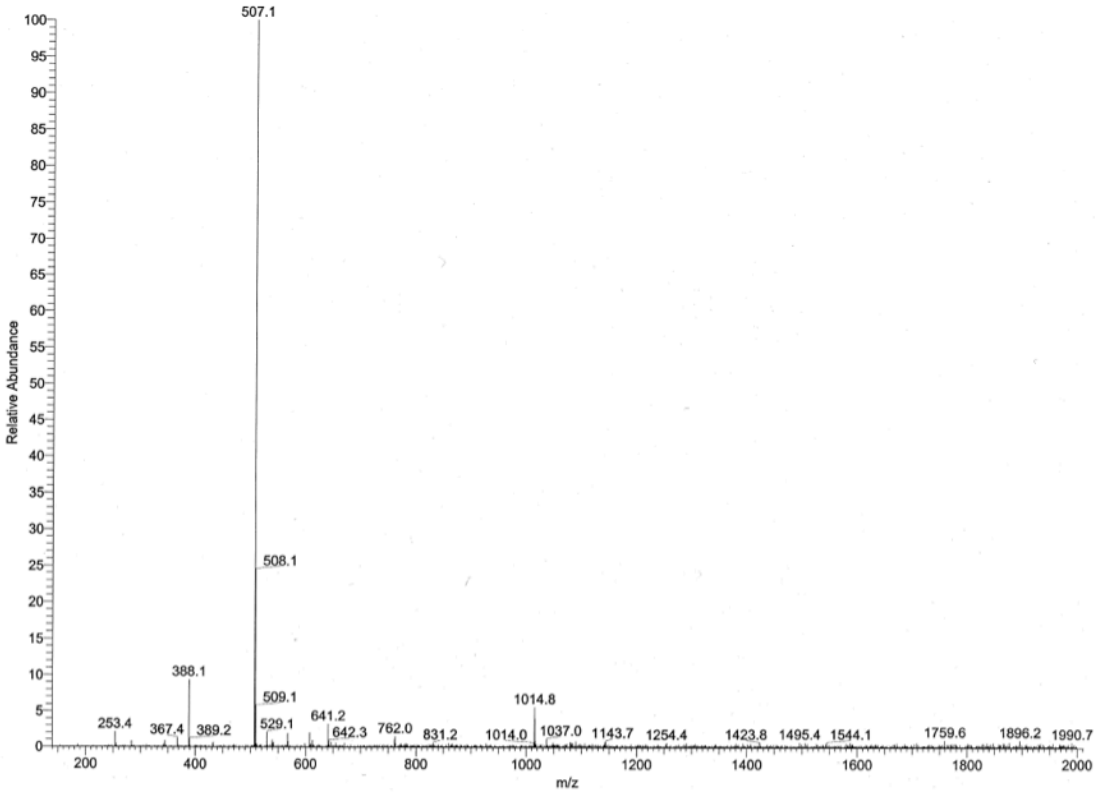

FIGURE 14: Representative HPLC chromatograms of FITC-2-amino-ethoxy-acetic acid. (TOP) UV_{ABS} at 254 nm and (BOTTOM) Fluorescence emission due to λ_{EX} of 494 nm and λ_{EM} of 519 nm. Retention time for FITC-2-amino-ethoxy-acetic acid is 11.71 minutes.

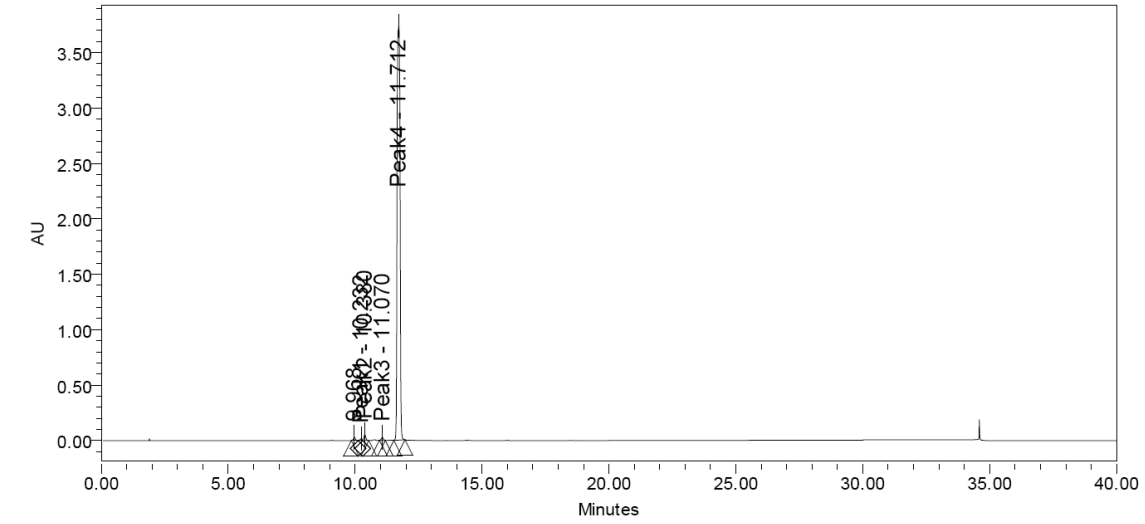

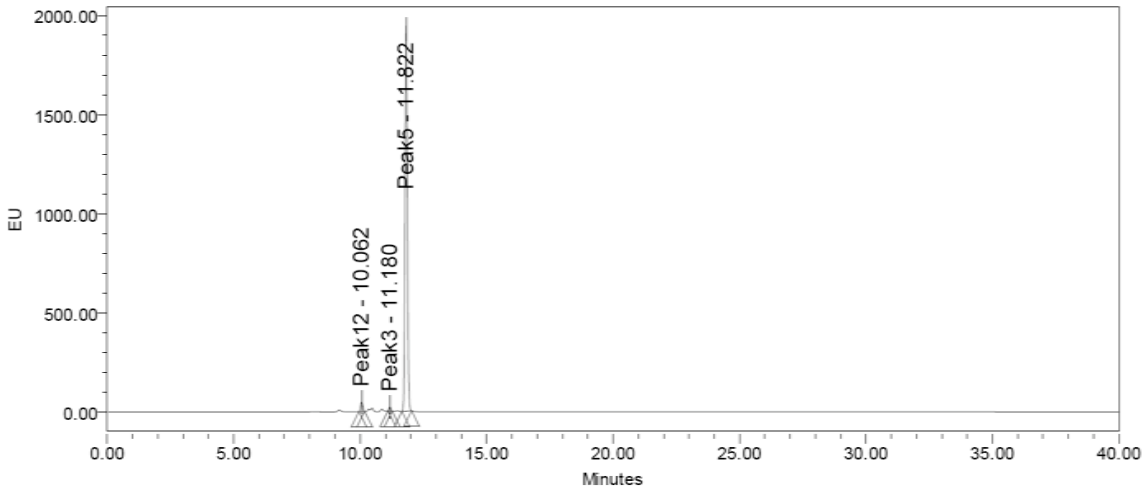

FIGURE 15: Representative ESI-MS Spectrum of MP100. Instrument was set to the positive ion mode. Spectrum represents an average of 20 spectra take on a Finnegan LCQDuo. Desired mass for MP100 = 1842 Da. The following peaks correspond to different ionization states of MP100: [m+2H]/2 = 921.3 and [m+3H]/3 = 614.9.

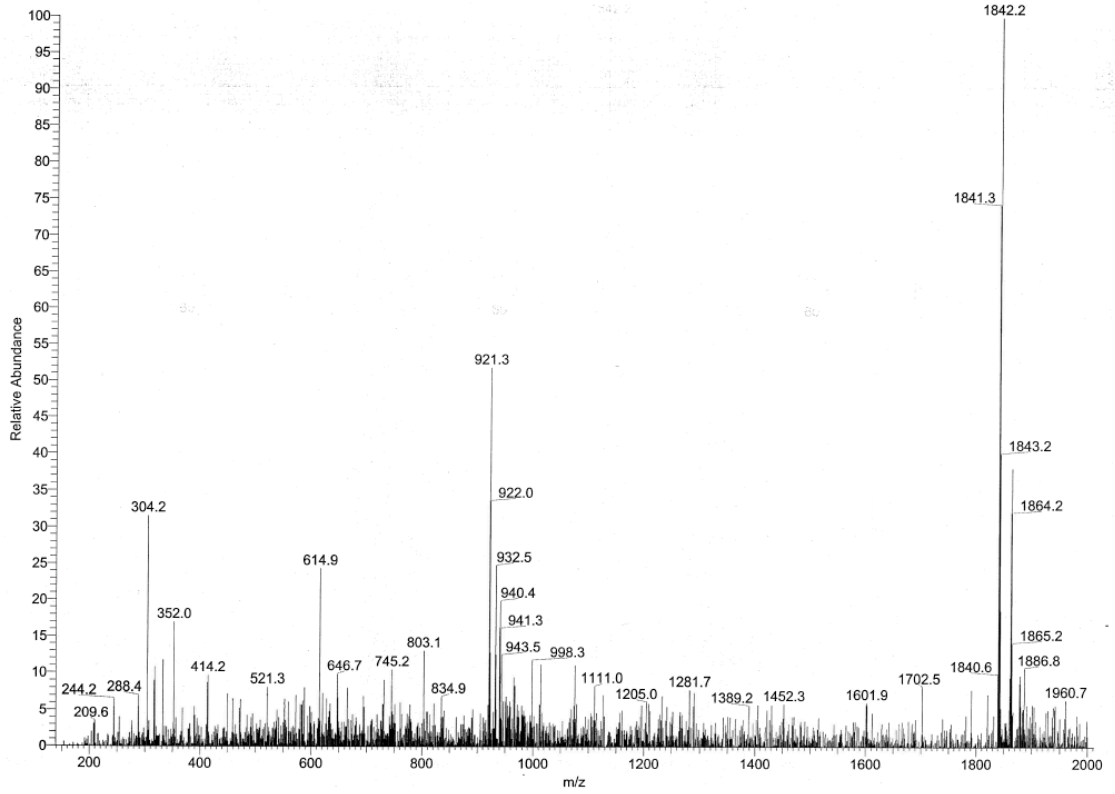

FIGURE 16: Representative HPLC chromatograms of MP100. (TOP) UV_{ABS} at 254nm and (BOTTOM) Fluorescence emission due to λ_{EX} of 494nm and λ_{EM} of 519nm. Retention time for MP100 is 2.9 minutes.

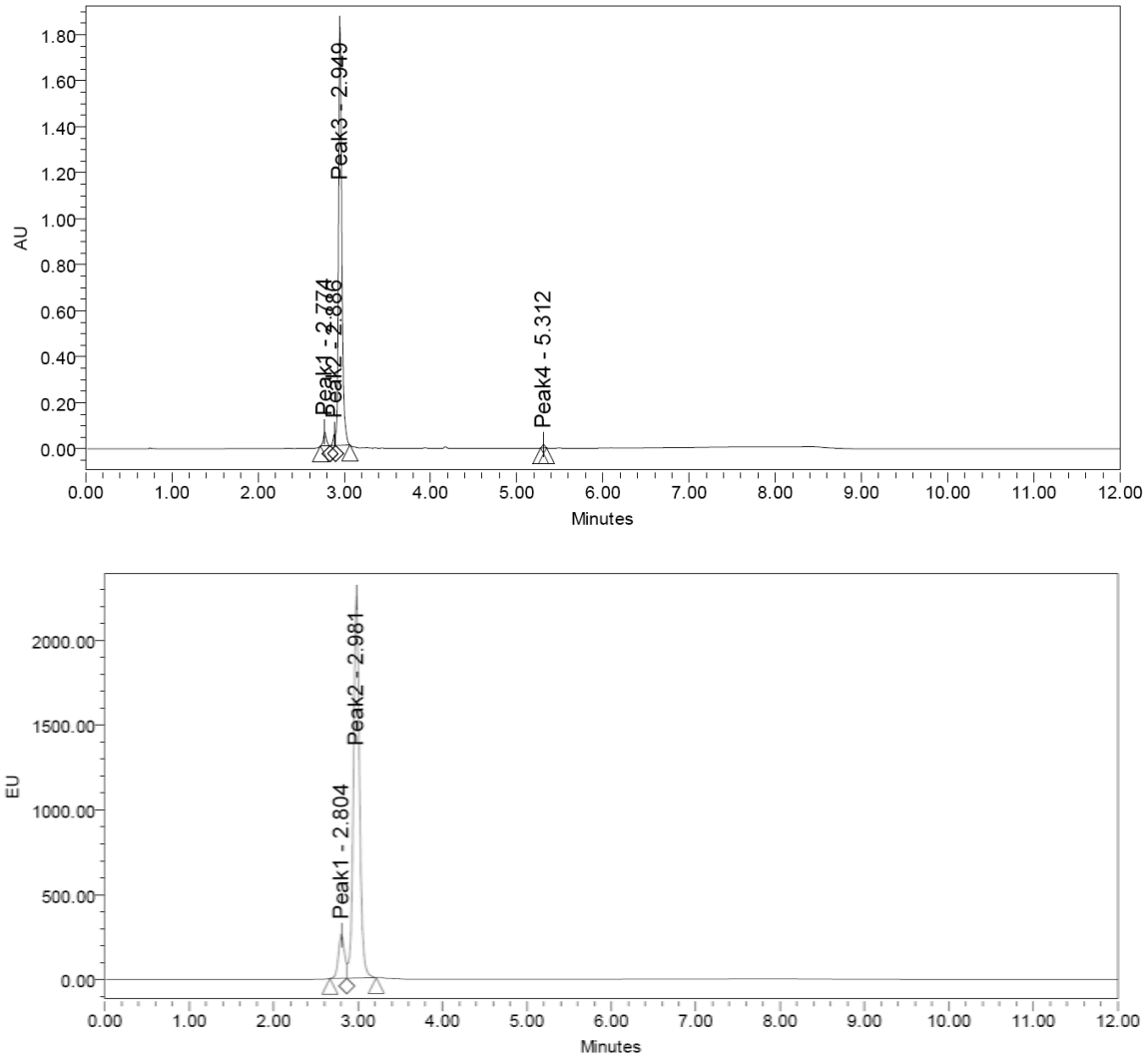

FIGURE 17: Proton NMR of MP100. Stock MP100 was dried using speed vacuum and reconstituted with deuterium oxide. NMR spectroscopy was conducted on a Bruker 400MHz NMR spectrophotemeter. The inset portion corresponds to the protons that are associated with the aromatic residues of the peptide and the FITC label. The sum of the integrated peaks is equal to the expected proton count of the aromatic hydrogen atoms of the desired structure.

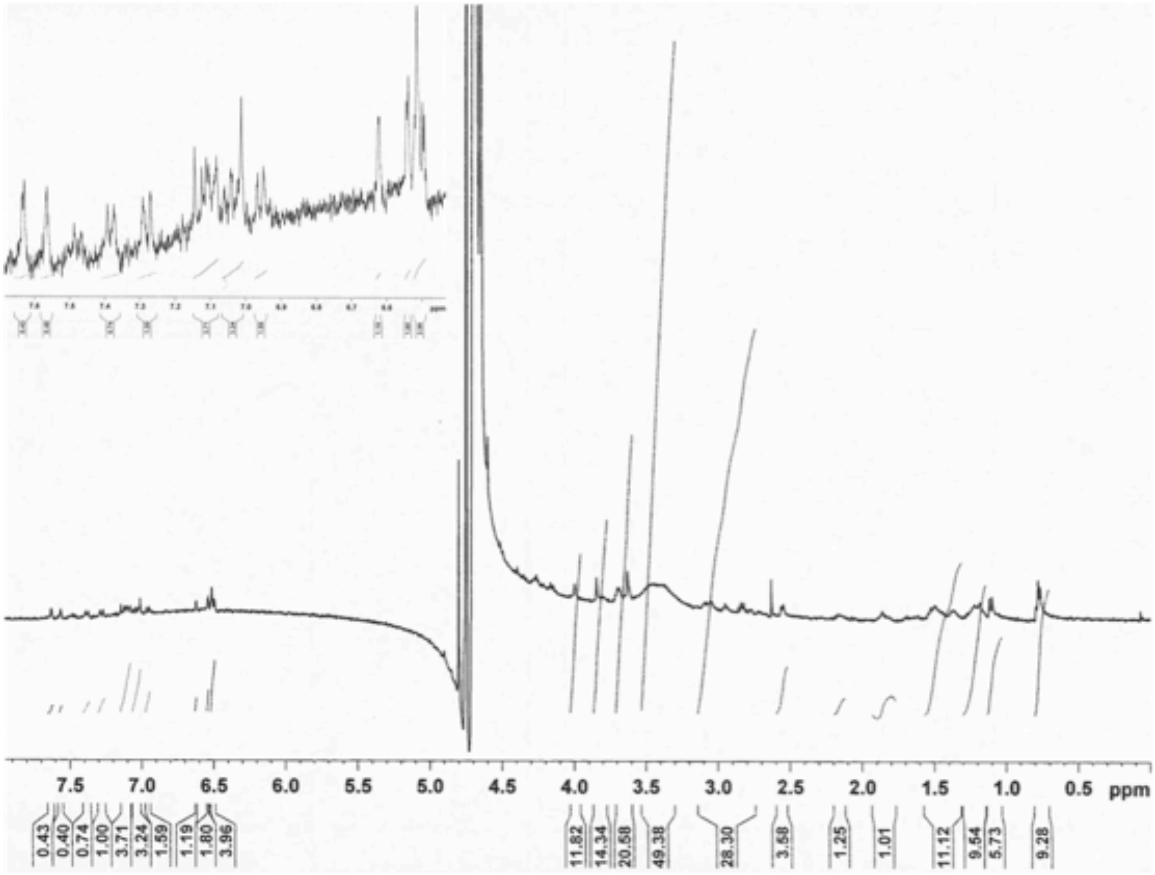

FIGURE 18: Representative MALDI-TOF MS spectrum of MP200. 1580.9 Da corresponds to an ionization state of $[m+2Na^+]/2$. Another peak of significantly less intensity at 3154 Da corresponds to an ionization state of $[m+K^+]/1$.

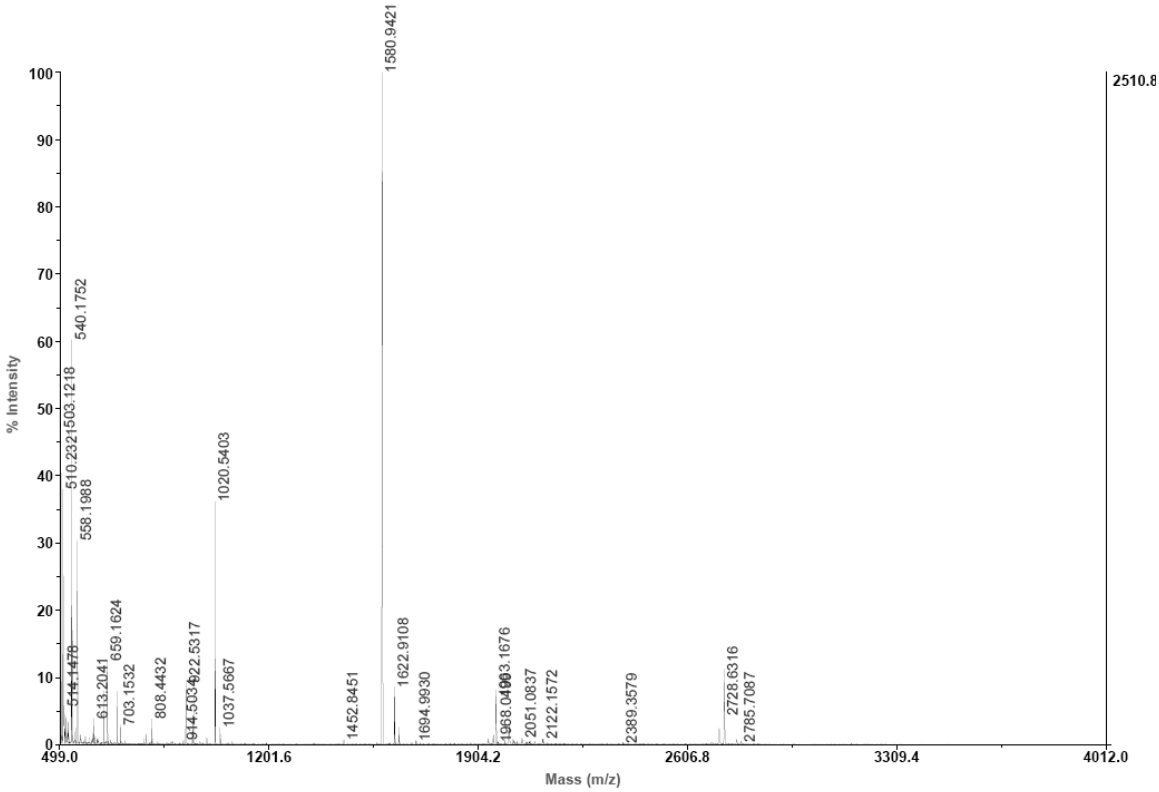

FIGURE 19: Representative HPLC chromatograms of MP200. (TOP) UV_{ABS} measured at 254nm. (BOTTOM) Fluorescence emission measured at λ_{EX} of 494nm and λ_{EM} of 519nm. Retention time for MP100 is 2.9 min. The broad peak is likely attributed to confomers of the 2 copy DV3 peptide carrier.

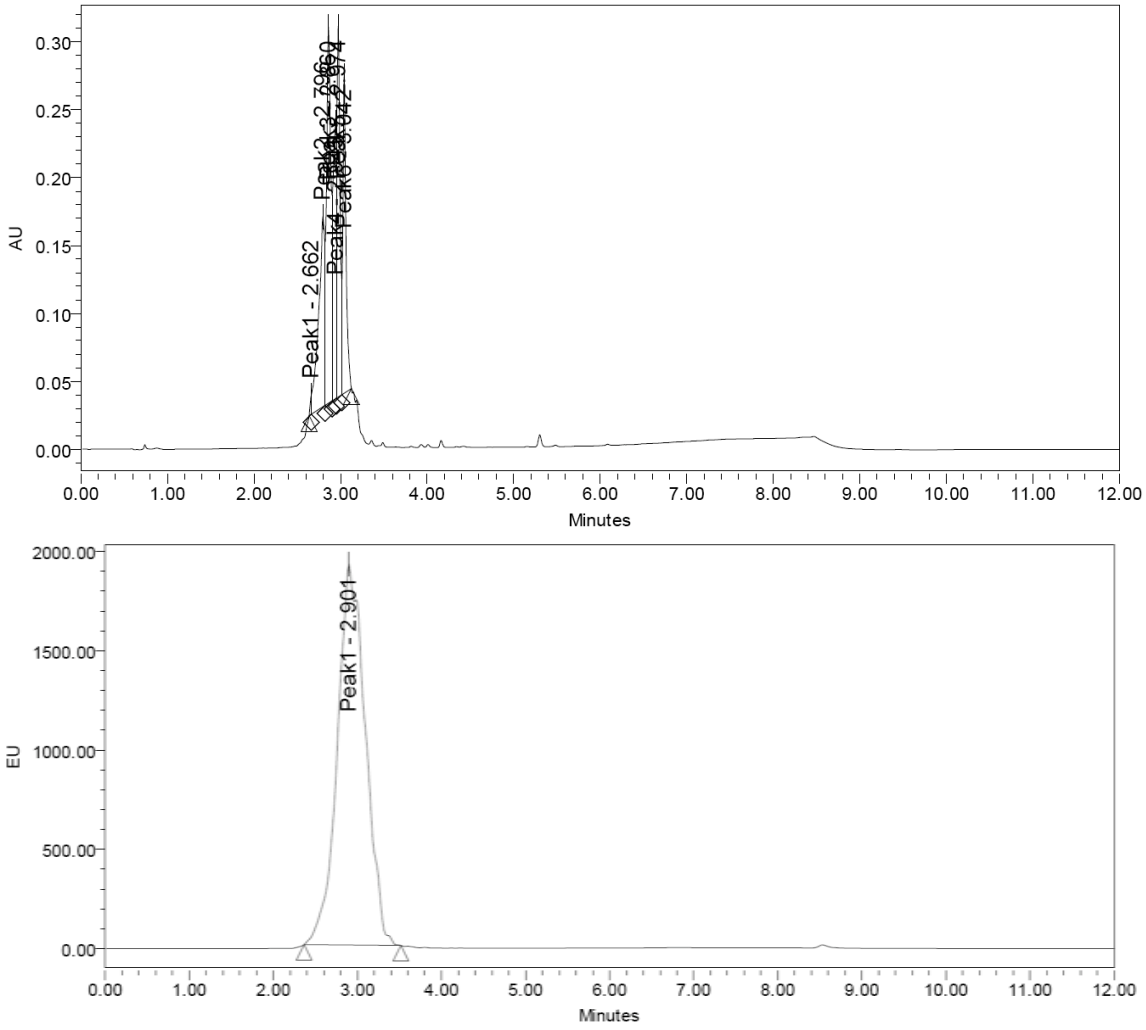

FIGURE 20: Proton NMR of MP200. Stock MP200 was dried using speed vacuum and reconstituted with deuterium oxide (Sigma-Aldrich, St. Louis, MO). NMR spectroscopy was conducted on a Bruker 400MHz NMR spectrophotemeter. The blown up portion corresponds to the protons that are associated with the aromatic residues of the peptide and the FITC label. The sum of the integrated peaks is equal to the expected proton count of the aromatic hydrogen atoms of the desired structure.

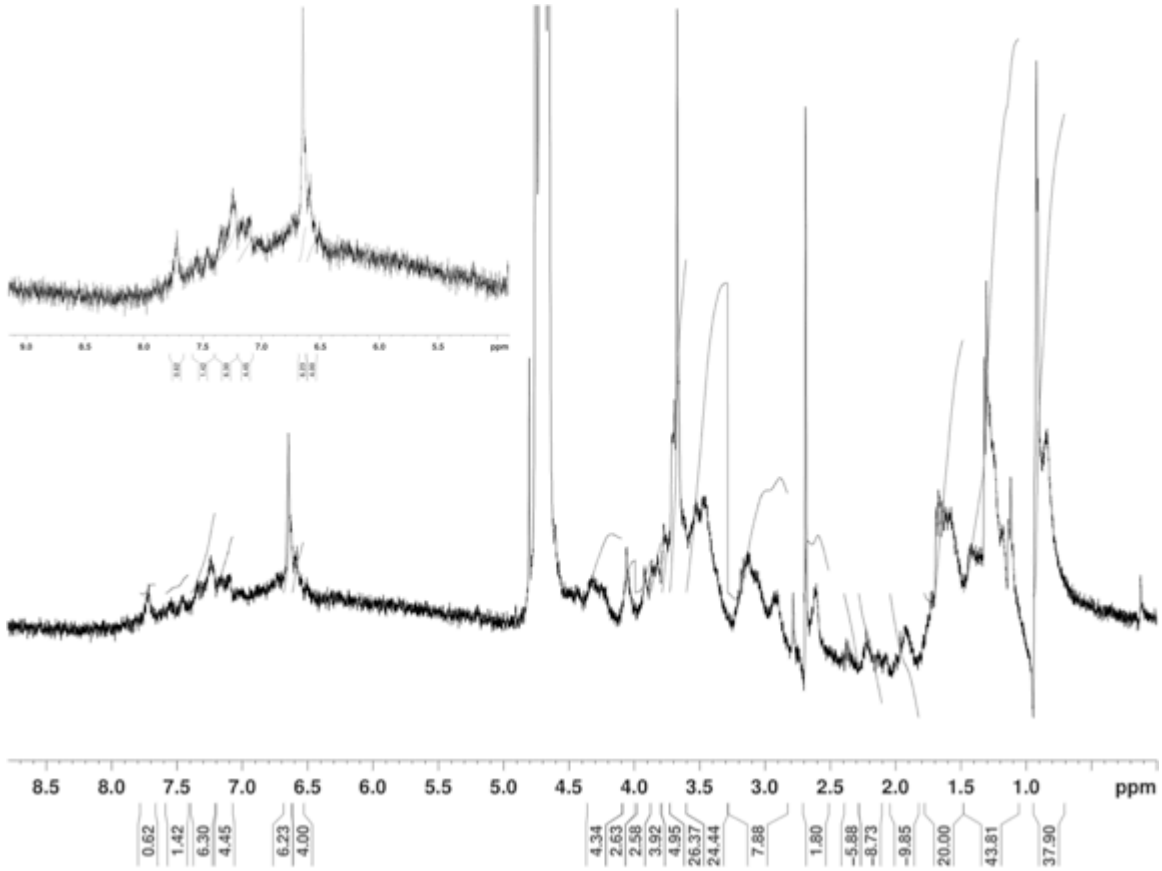

FIGURE 21: Representative MALDI-TOF spectrum for MP400. The major peak of 1418 correlates to the m/z state of [MP400+4H$^+$]/4.

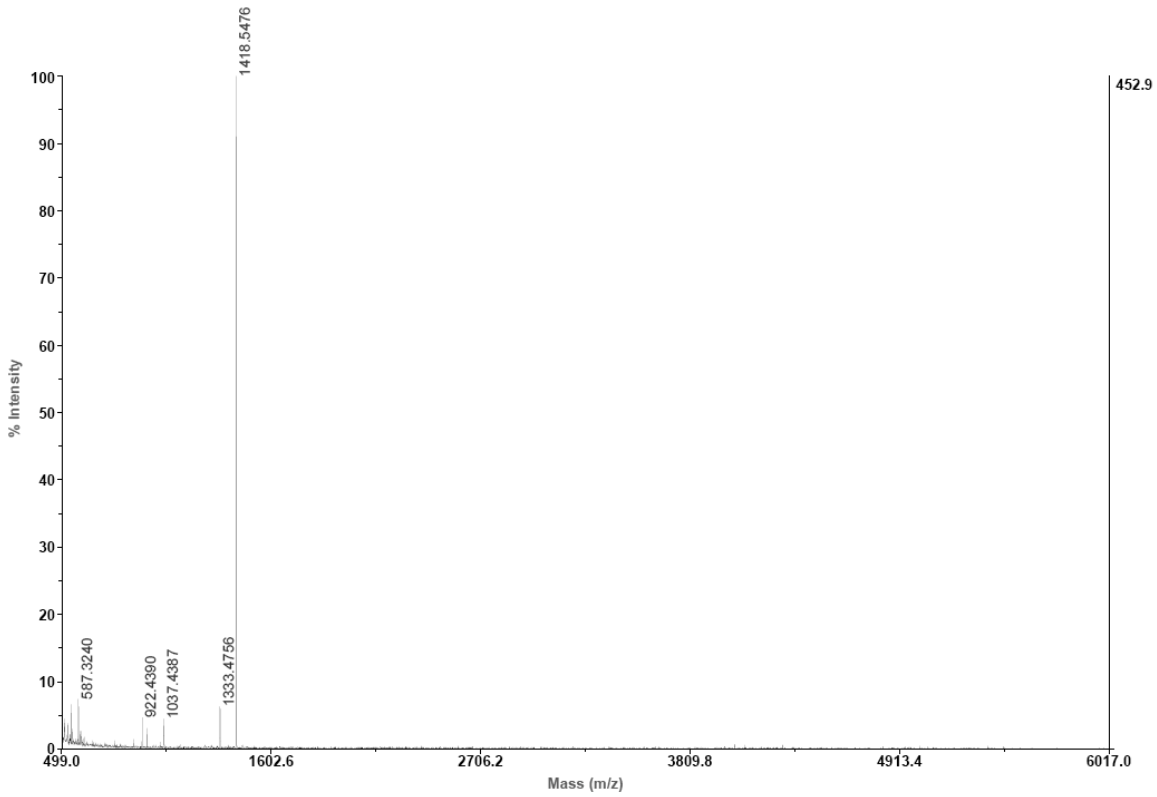

FIGURE 22: Representative HPLC chromatograms of MP400; (TOP) UV_{ABS} at 254nm and (BOTTOM) Fluorescence emission due to λ_{EX} of 494nm and λ_{EM} of 519nm. Retention time for MP100 is 2.8 minutes.

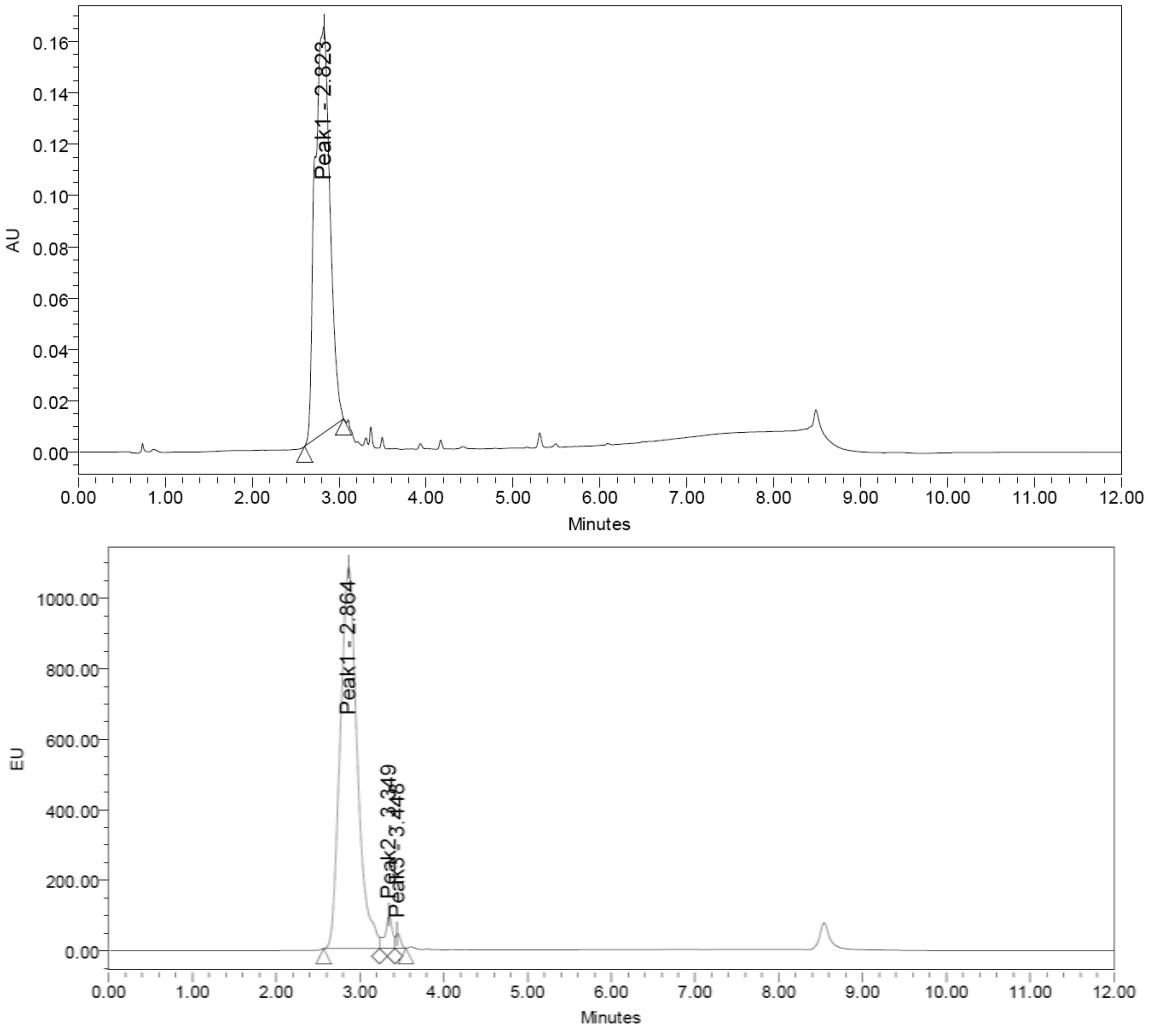

FIGURE 23: Proton NMR of MP400. Stock MP400 was dried using speed vacuum and reconstituted with deuterium oxide (Sigma-Aldrich, St. Louis, MO). NMR spectroscopy was conducted on a Bruker 400MHz NMR spectrophotemeter. The inset corresponds to the protons that are associated with the aromatic residues of the peptide and the FITC label. The sum of the integrated peaks is equal to the expected proton count of the aromatic hydrogen atoms of the desired structure.

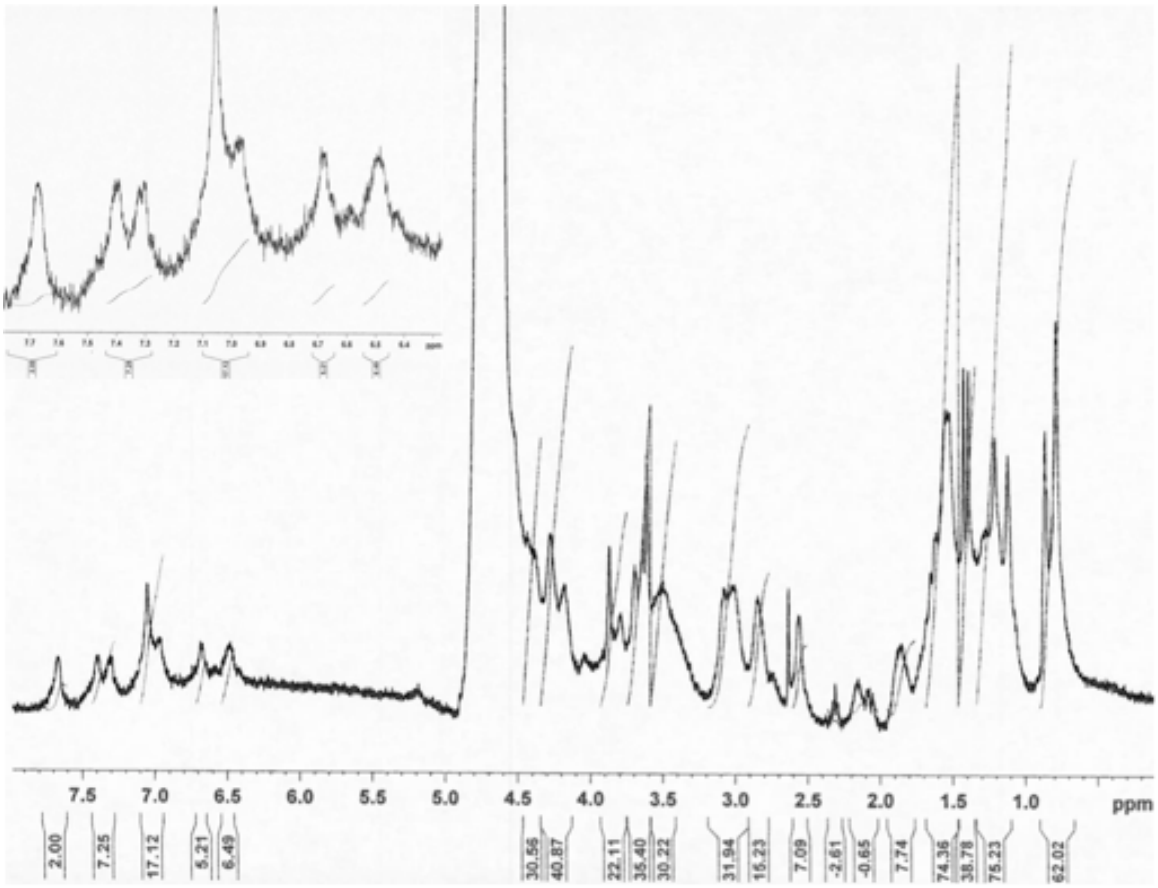

FIGURE 24: Fluorescence standard curve of FITC in PBS over the range from 12 nM to 7.5 μM from three separate experiments. Data was fit by nonlinear regression analysis to a first order polynomial equation. F test determined that all three experiments were statistically similar and a globally fit regression line was used to determine the concentrations of stock solutions of FITC labeled DV3 peptide carriers. The globally fit regression line has a calculated slope of 1.396, y-intercept of 19.91, and R^2 value of 0.9737.

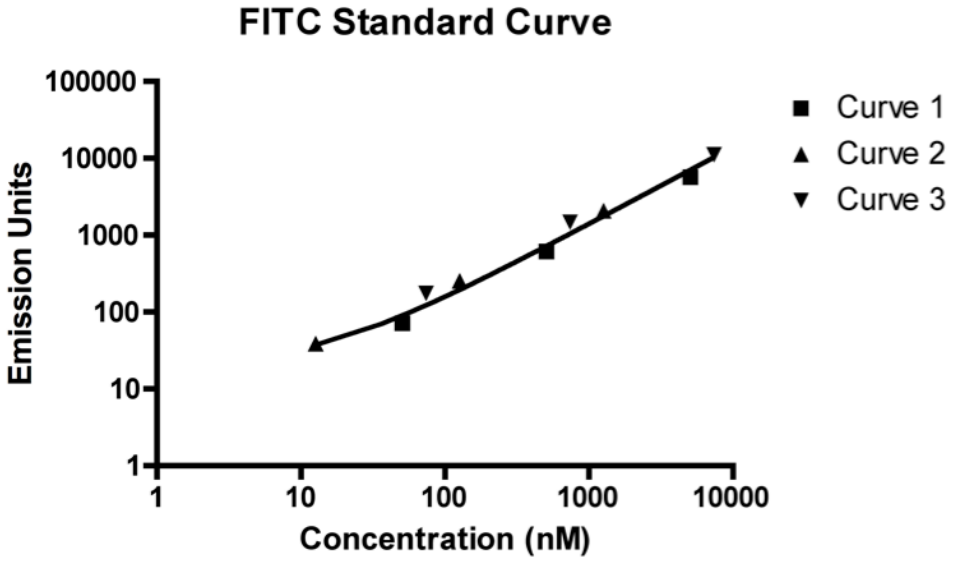

FIGURE 25: Representative analytical HPLC chromatogram of biotinylated 4 copy DV3 peptide carrier (MP401). UV_{ABS} was measured at 220nm. Retention time for MP401 was 3.521 minutes.

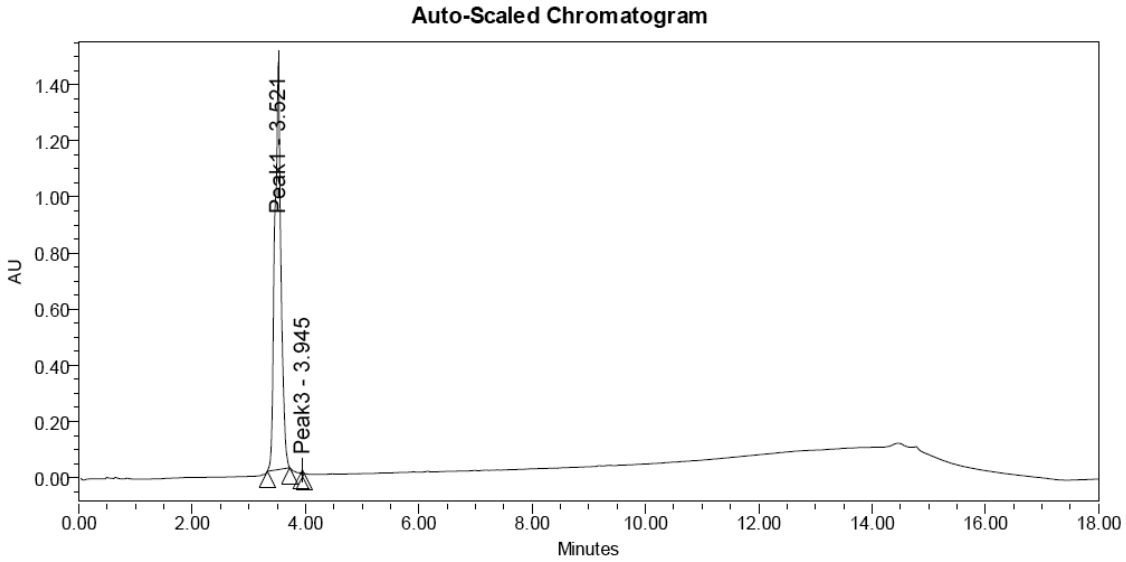

FIGURE 26: Representative MALDI-TOF spectrum of biotinylated 4 copy DV3 peptide carrier (MP401). The molecular mass is 5407 Da corresponding for the peak observed in the spectrum. MALDI-TOF was performed on an Applied Biosystems 4800 MALDI-TOF/TOF set to the linear mid mass mode.

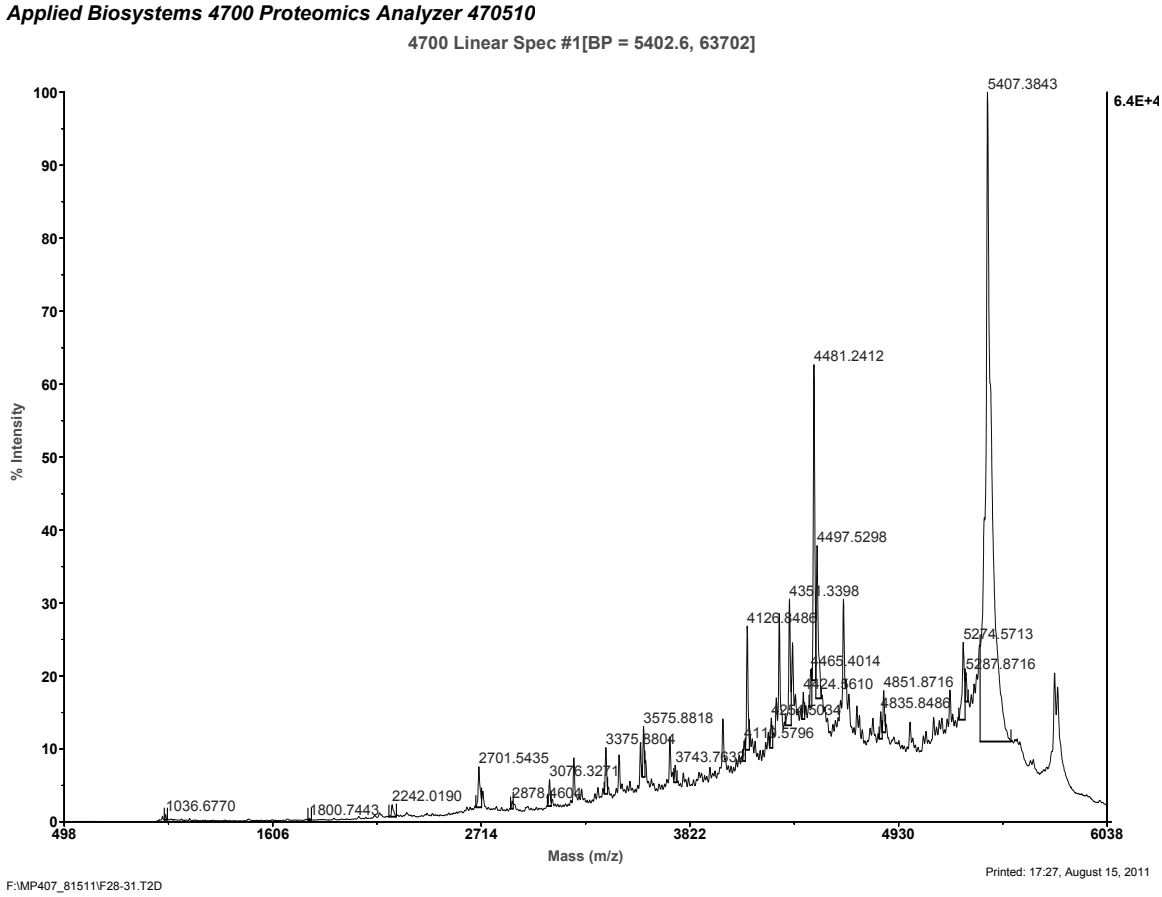

FIGURE 27: Representative ESI-MS Spectrum of MP401. Instrument was set to the positive ion mode. Spectrum represents an average of 20 spectra taken on a Finnegan LCQDuo. Observed peaks correlate to different ionization states of MP401 are annotated on the spectrum.

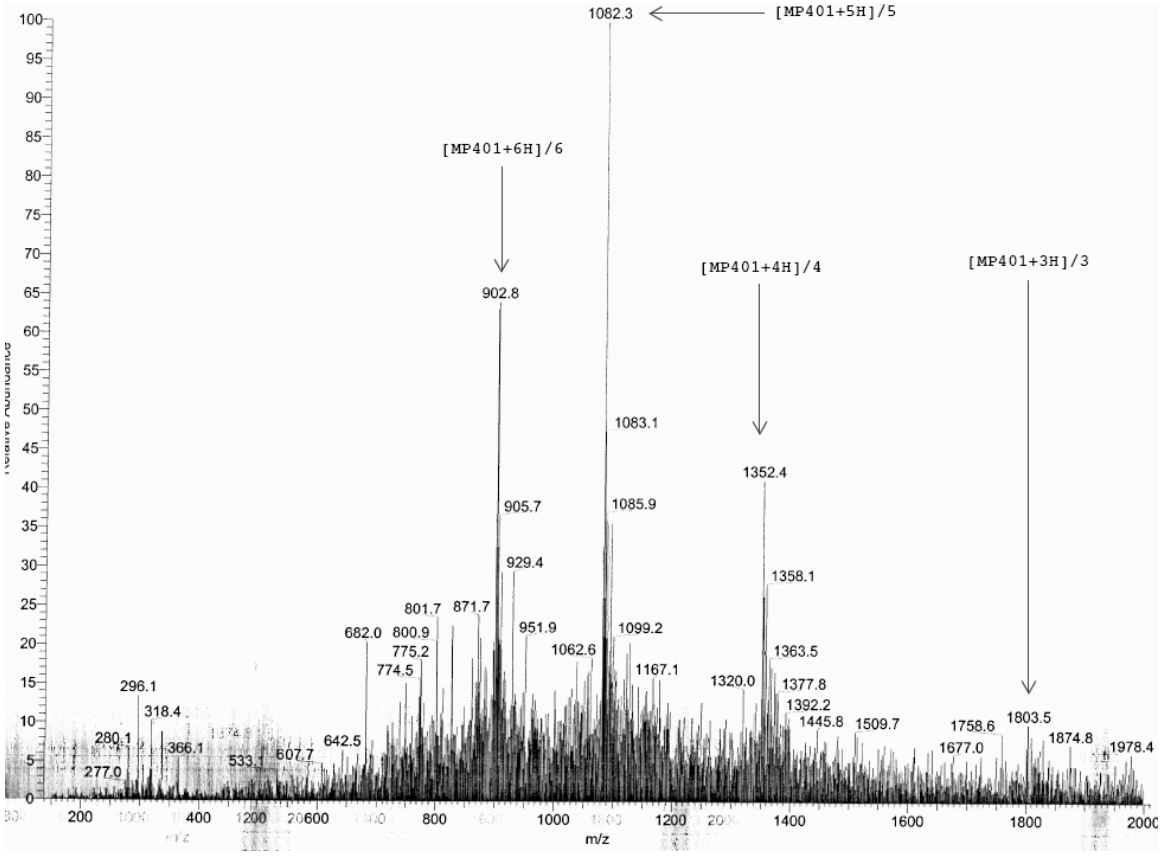

FIGURE 28: HPLC (Top) and MALDI-TOF of purified free DV3. DV3 has a rention time = 2.337 minutes. MALDI-TOF demonstrated 1 major peak of importance. 1165 corresponds to free DV3 desired molecular weight.

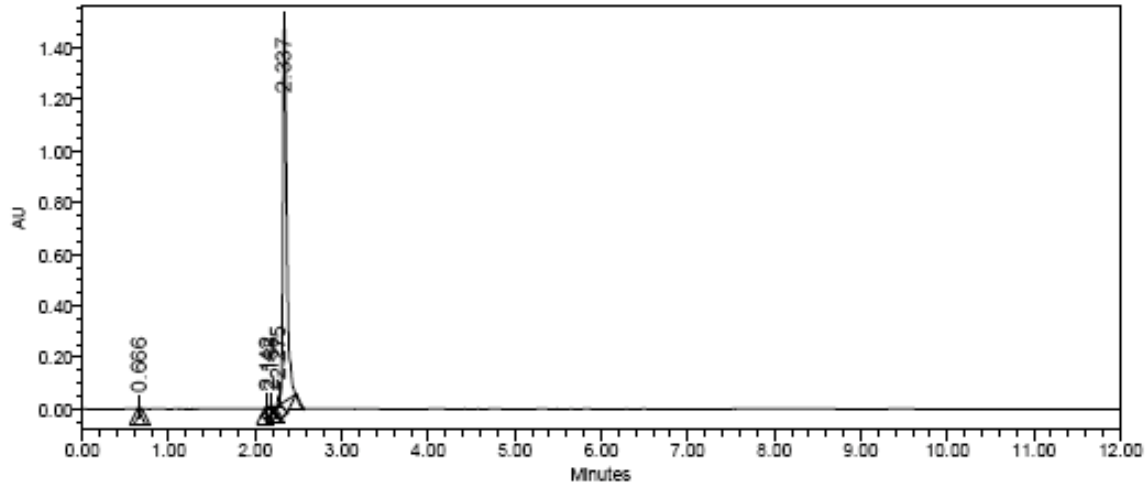

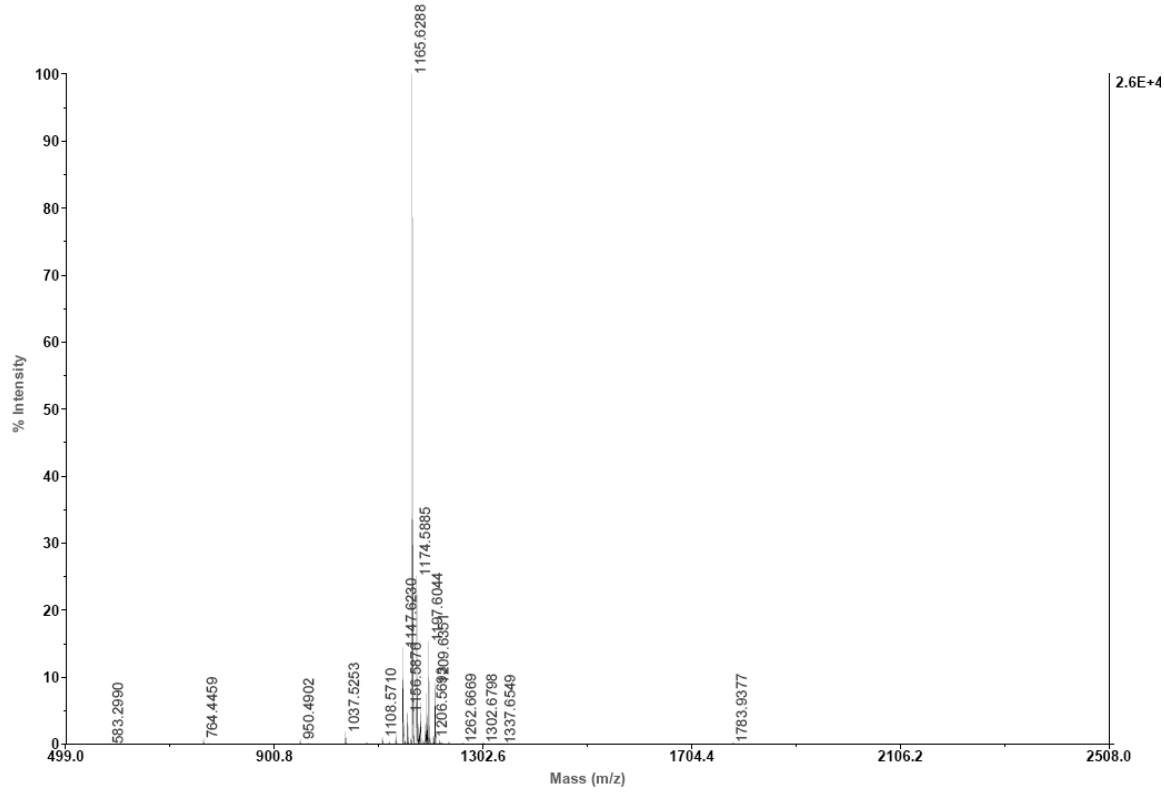

FIGURE 29: Tzm-bl Assay of DV3 peptides with 1, 2, and 4 copy DV3 (MP100, MP200, and MP400, respectively). Cells were plated at $1.25x10^4$ cells/ml in a black-walled 96 well plate. DV3 peptides and HIV-1 IIIB (X4 strain at MOI = 0.038) in DMEM were added to the wells and incubated 72 h. Controls for the experiment were Tzm-bl cells that were untreated with HIV-1 and DV3 peptide carriers (- HIV-1 IIIB) and Tzm-bl cells untreated with DV3 peptide carriers but exposed to HIV-1 IIIB (+ HIV-1 IIIB). Promega Steady-Glo Reagent was added to the wells and luminescence measured on Tecan GENios microplate reader. Mean $\pm$ standard deviation of triplicate wells were reported and * indicates those groups that were statistically different from the + HIV-1 IIIB group ($p<0.001$) and not statistically different from the – HIV-1 IIIB group by ANOVA. Each bar in a grouping corresponds to the DV3 peptide carrier concentration of 0.5 µM, 2.5 µM, and 5 µM from left to right. The results demonstrate that 4 copy DV3 is by the far the most active peptide against HIV-1 entry at each of the concentrations investigated.

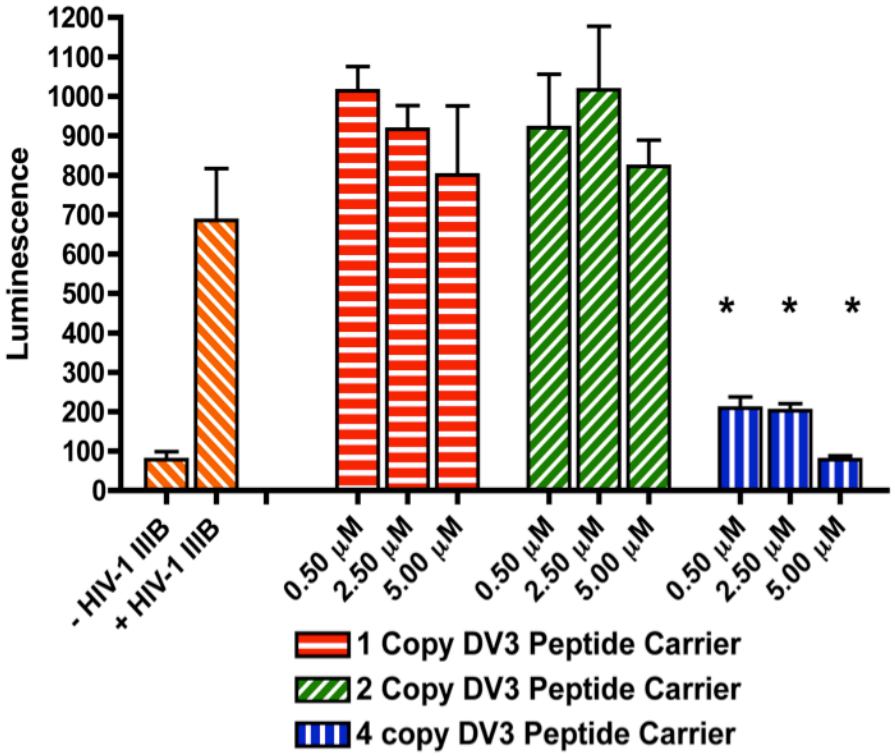

FIGURE 30: MTT assay of 1, 2, and 4 copy DV3 peptides (MP100, MP200, and MP400, respectively). TZM-bl cells were incubated with the drug for 24 h at 37°C with 5% CO_2 in DMEM with the following DV3 peptide carrier concentrations 0.5, 2.5, and 5 µM. Untreated cells were used as a control. Contents of the wells were replaced with PBS + MTT and incubated until crystals developed. Crystals were dissolved with 200 µl DMSO. Absorbance was measured at 570 nm and the mean ± standard deviation reported from 2 experiments. The groups of bars for each DV3 peptide carrier investigated represent the following concentration from left to right: 0.5, 2.5, and 5 µM. Data was normalized to Control = 100% and DMSO = 0%. One-way ANOVA analysis determined no statistical difference existed between the control group, the DV3 peptide carriers, and the concentration of DV3 peptide carrier investigated, indicating that the DV3 peptide carriers did not affect cell viability.

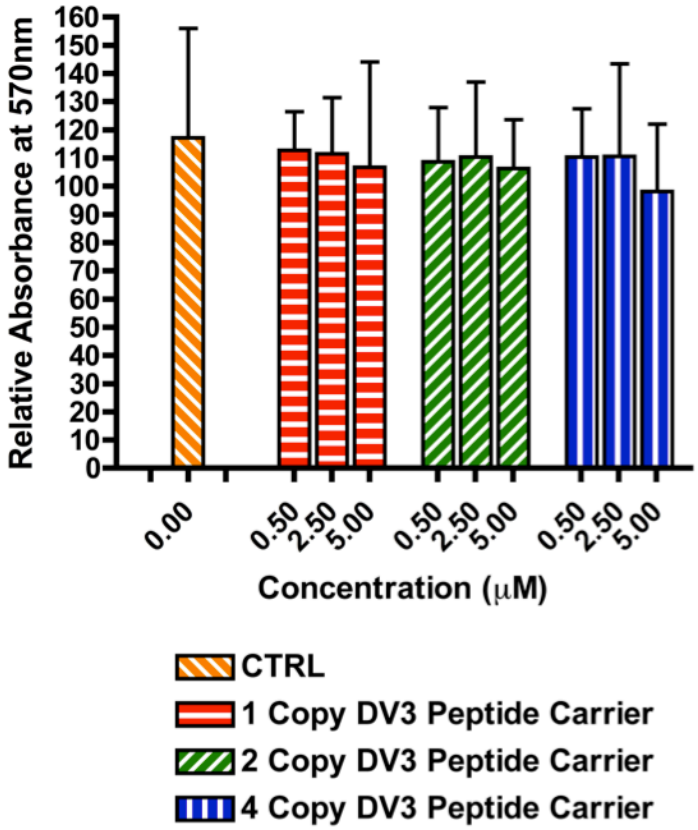

FIGURE 31: Confocal microscope images of TZM-bl cells incubated with DV3 peptide carriers. $5.0x10^4$ cells were plated in DMEM to chambered cover glass slides 24 h prior to microscope imaging. Cells were washed once with HBSS prewarmed to 37°C. Cells were then incubated with 1 μM of FITC labeled 1, 2, or 4 copy DV3 peptide carriers in HBSS with DAPI and Rho-Dex for 2 h. Cells were washed once with PBS, and then 500 μl of 3% formalin in PBS was added to the cells for fixation. Chambers were washed twice with PBS and imaged with 600 μl PBS. TOP, MIDDLE, and BOTTOM rows represent 1, 2, or 4 copy peptide carriers, respectively. Colocalization of peptide carriers with the endosome marker Rho-Dex is observed as yellow-orange color in the merged images.

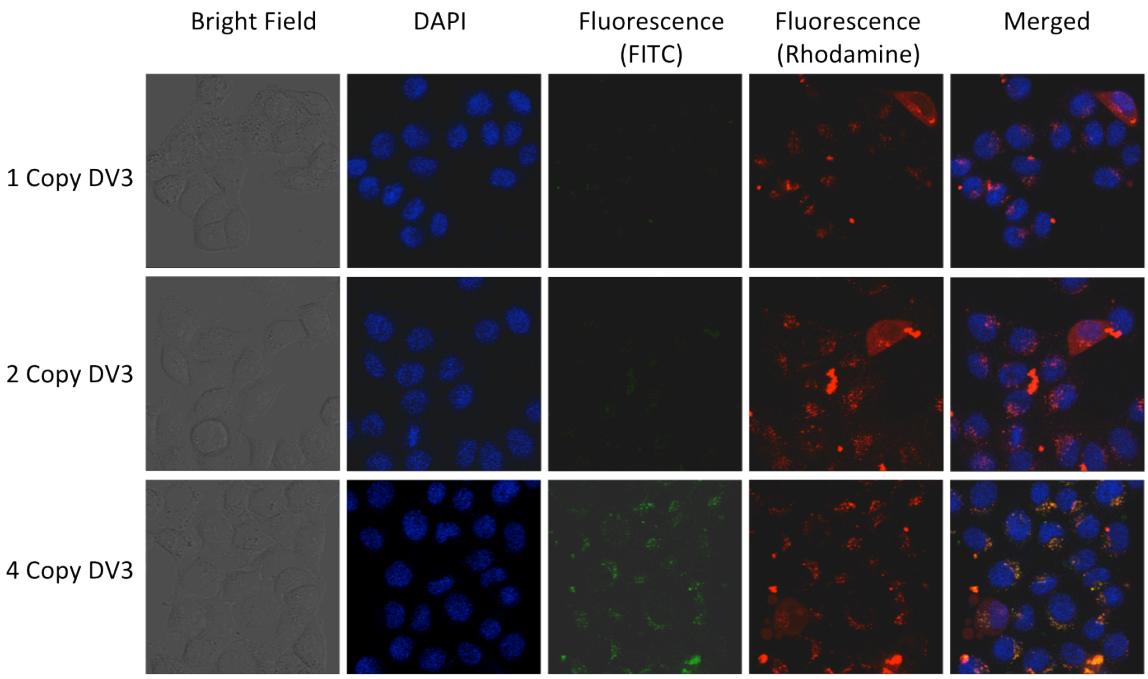

FIGURE 32: Tzm-bl assay of HIV-1 inhibition by 4 copy DV3 peptide carrier. Each point represents the mean ± standard deviation of 3 experiments. Tzm-bl cells were seeded to a 96 well plate at a density of $5x10^3$ cell/well. Serial dilutions of the 4 copy DV3 peptide carrier (MP400) were added in 100 µl of DMEM. HIV-I III_B (X4 strain) at an MOI = 0.03 was added to the wells in 100 µl of DMEM. Cells and virus were incubated for 72 h, lysed using Promega Steady-Glo reagent. HIV-1 replication dependent luciferase generated luminescence was measure using Tecan GENios Microplate reader. The IC_{50} of 4 copy DV3 peptide against HIV-1 X4 strain was 553 nM with a 95% confidence range of 246 nM to 1.24 µM.

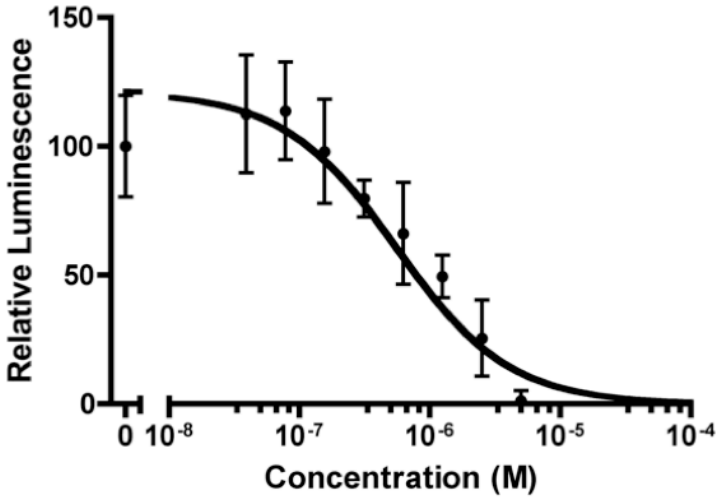

FIGURE 33: Tzm-bl assay of HIV inhibition by 4 copy DV3 peptide carriers. Each point represents the mean ± standard deviation of 2 experiments. Tzm-bl cells were seeded to a 96 well plate at a density of $5x10^3$ cell/well. Serial dilutions of the 4 copy DV3 peptide carrier (MP400) were added in 100 µl of DMEM. HIV-1_{BaL} (R5 strain) at an MOI = 0.03 was added to the wells in 100 µl of DMEM. Cells and virus were incubated for 72 h, lysed using Promega Steady-Glo reagent. HIV-1 replication dependent luciferase generated luminescence was measure using Tecan GENios Microplate reader. The IC_{50} of 4 copy DV3 peptide against HIV-1 R5 strain was 4.32 µM with a 95% confidence range of 2.85 µM to 6.55 µM.

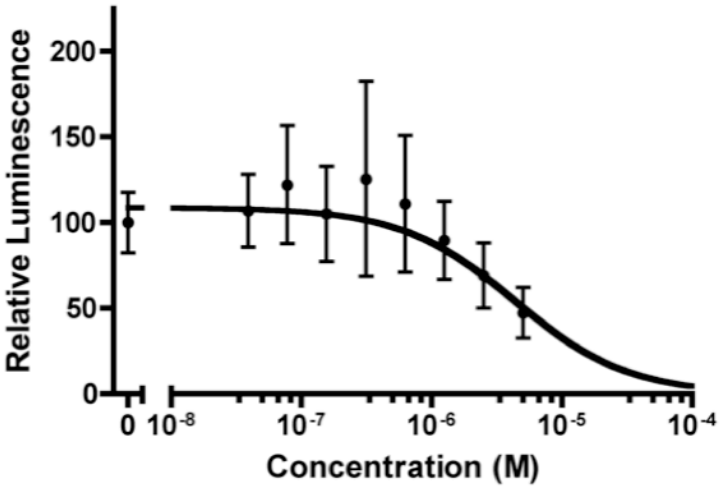

FIGURE 34: Tzm-bl assay of HIV-1 inhibition by AMD3100. Each point represents the mean ± standard deviation of 3 experiments. Tzm-bl cells were seeded to a 96 well plate at a density of $5x10^3$ cell/well. Serial dilutions of the AMD3100 were added in 100 µl of DMEM. HIV-I III_B (X4 strain) at an MOI = 0.03 was added to the wells in 100 µl of DMEM. Cells and virus were incubated for 72 h, lysed using Promega Steady-Glo reagent. HIV-1 replication dependent luciferase generated luminescence was measure using Tecan GENios Microplate reader. The IC_{50} of AMD3100 against HIV-1 X4 strain was 0.415 nM with a 95% confidence range of 0.219 to 0.785 nM.

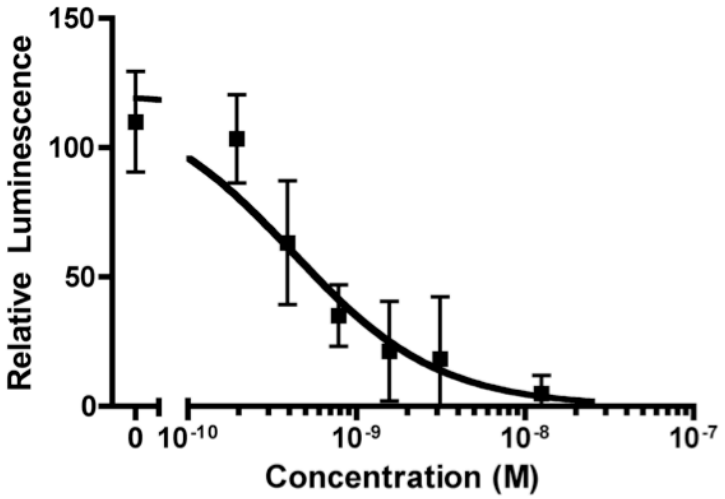

FIGURE 35: Tzm-bl assay of HIV-1 inhibition by CXCR4 mAb. Each point represents the mean ± standard deviation of 3 experiments. Tzm-bl cells were seeded to a 96 well plate at a density of $5x10^3$ cell/well. Serial dilutions of the CXCR4 mAb were added in 100 µl of DMEM. HIV-I III_B (X4 strain) at an MOI = 0.03 was added to the wells in 100 µl of DMEM. Cells and virus were incubated for 72 h, lysed using Promega Steady-Glo reagent. HIV-1 replication dependent luciferase generated luminescence was measure using Tecan GENios Microplate reader. The IC_{50} of CXCR4 mAb peptide against HIV-1 X4 strain was 106 nM with a 95% confidence range of 60 to 187 nM.

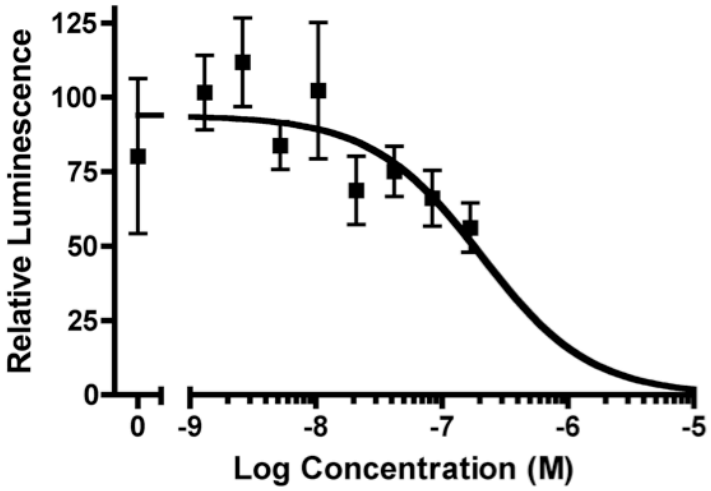

FIGURE 36: Competitive inhibition of MP401 (4DV3-Biot) binding by the small molecule CXCR4 inhibitor AMD3100. Triplicates of TZM-bl cells were plated at a density of $1.0x10^5$ cells/ml in 0.75 ml/well. Cells were incubated with HBSS, 1 μM 4DV3-Biot in HBSS, 1 μM 4DV3-Biot + 20 μM AMD3100 in HBSS, or 1 μM 4DV3-Biot + 200 μM AMD3100 in HBSS for 1 h. Cells were then washed twice with HBSS and then incubated for 30 min with 5-FAM conjugated streptavidin. Cells were then washed twice with HBSS and lysed with 75 μl of 2 N NaOH overnight. NaOH was neutralized with 75 μl 2 N HCl, the well contents transferred to an opaque plate, and then measured the fluorescence on a Tecan GENios microplate reader at excitation 485 nm emission 535 nm. Mean ± standard deviation of three experiments is reported. Significant difference determined by one-way ANOVA. Solid line denotes those groups that were significantly different to a $p< 0.001$. Dotted line denotes significant difference between groups to a $p<0.05$. All groups were normalized to the control group (cells treated with HBSS only) and the group treated with 4DV3-Biot alone.

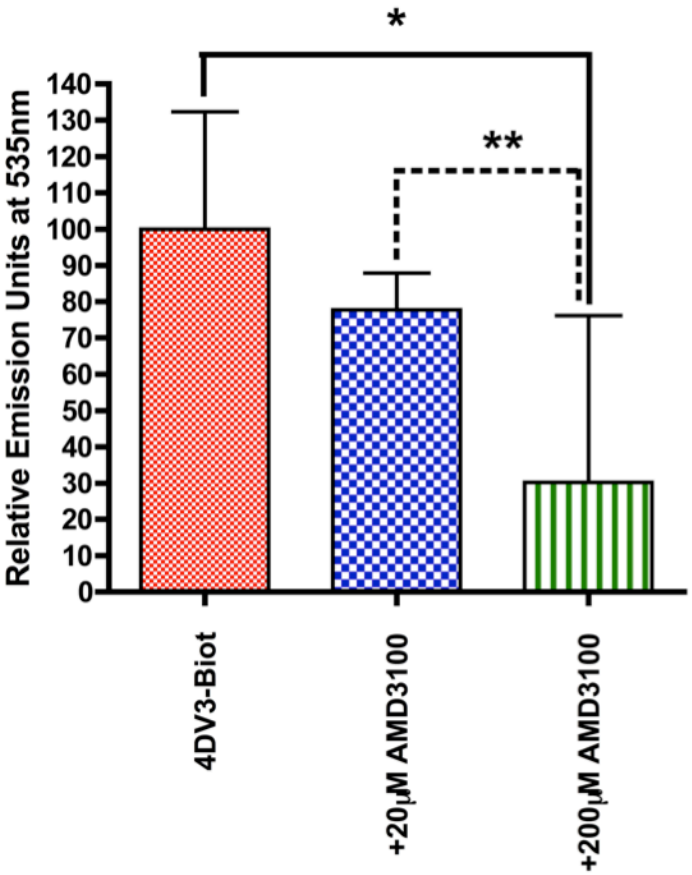

FIGURE 37: Competitive inhibition of MP401 by a CXCR4 mAb. Triplicate wells of Tzm-bl cells were fixed with 3.7% formalin in PBS (w/v). Cells were washed 3x with PBS. Then incubated with varying concentration of MP401 or AMD3100 in the presence of 1 ug/ml CXCR4 monoclonal antibody for 40 min on ice. Cells were washed 3x with TBST (tris buffered saline with tween 20). Cells were incubated with secondary antibody conjugated with horseradish peroxidase (HRP) for 1 h at room temperature. Cells were 3x with TBST then incubated wells with HRP substrate. Enzymatic conversion of the substrate was stopped with 0.1 N HCl and absorbance at 450 nm was measured. Absorbance was normalized to cells untreated with MP401 or AMD3100 and mAb (0%) and cells treated with mAb and without MP401 or AMD3100 (100%). LogIC50 was calculated from 3 separate experiments using GraphPad Prism and IC50 was determined from the antilog. Mean ± standard deviation is demonstrated on the graph with best-fit non-linear regression (dashed line). IC50 for MP401 = 398 nM with 95% CI = 101 nM to 1.57 µM. The two curves indicate that MP401 was a stronger inhibitor for the CXCR4 mAb than the small molecule drug AMD3100.

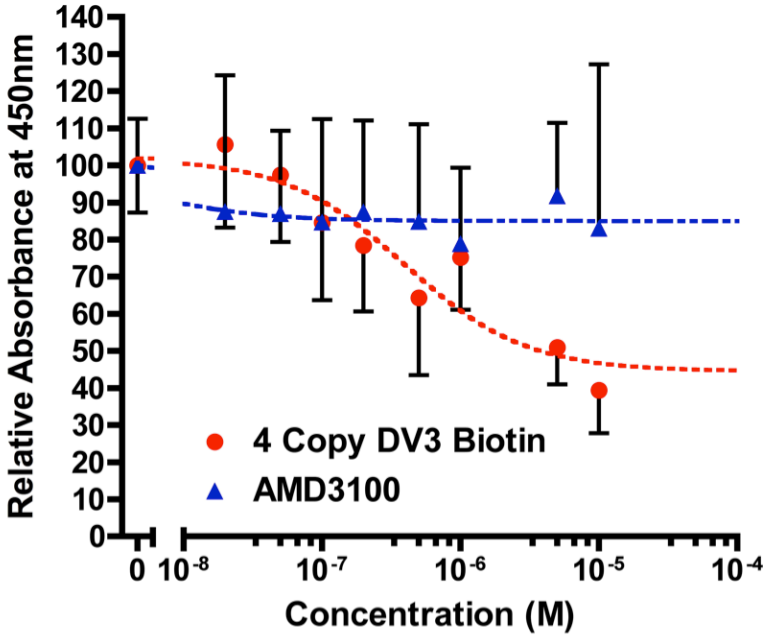

FIGURE 38: TZM-bl cells formalin fixed. Cells were seeded to 6 wells of a 24 well plate at a cellular density of $1.0x10^5$ cells/ml and allowed to attach overnight. Control cells were untreated with DV3. Cells treated with 4DV3 were incubated with 1 µM of biotinylated 4 copy DV3 peptide carrier (MP401). Cells treated with 4DV3 + Free DV3 were incubated with 1 µM of biotinylated 4 copy DV3 peptide carrier (MP401) and 100 µM of DV3 peptide. All cells were incubated with 1 µg/ml DAPI and 60nM Rhodamine-LysoTracker. Cells were incubated for 1 h at 37^o C. Cells were fixed 3.7% formalin for 20 minutes. Cells were then incubated with 10 µg/ml of fluorescently labeled streptavidin at room temperature for 1 h and then washed 2x with PBS. Cells were imaged using 500 µl PBS. The PBS was removed and cells were lysed with 2 N NaOH for 24 h. The lysate was neutralized with equal amount of 2 N HCl and the contents transferred to a black walled black bottomed 96 well plate and fluorescence measured using a Tecan Microplate reader.

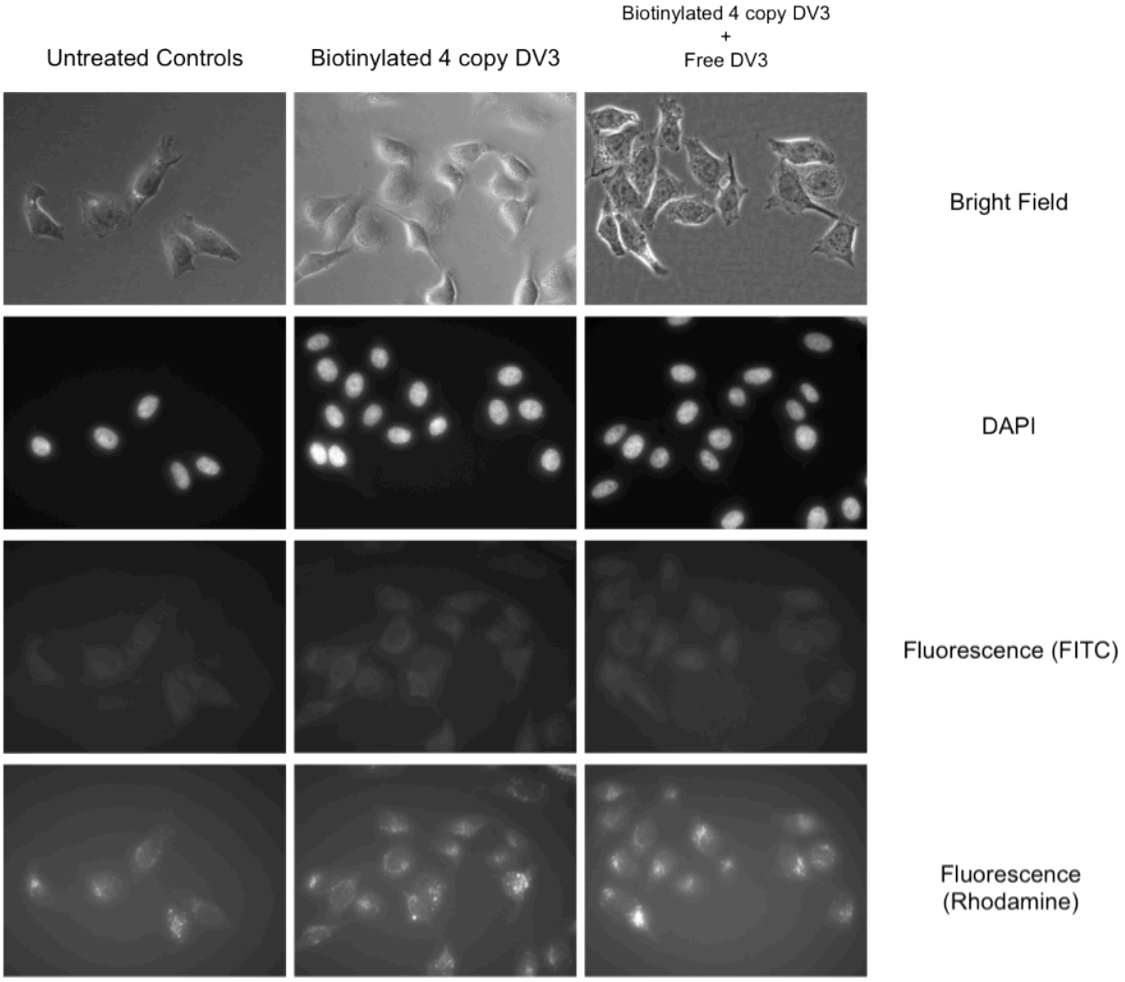

FIGURE 39: Tzm-bl cells formalin fixed and permeabilized with Triton-X 100. Cells were seeded to 6 wells of a 24 well plate at a cellular density of $1.0x10^5$ cells/ml and allowed to attach overnight. Control cells were untreated. Cells treated with 4DV3 were incubated with 1 µM of biotinylated 4 copy DV3 peptide carrier (MP401). Cells treated with 4DV3 + Free DV3 were incubated with 1 µM of biotinylated 4 copy DV3 peptide (MP401) carrier and 100 µM of DV3 peptide. All cells were incubated with 1 µg/ml DAPI and 60nM rhodamine-LysoTracker. Cells were incubated for 1 h at 37^O C. Cells were fixed 3.7% formalin for 20 minutes, washed 3x with PBS, then permeabilized with 0.2% Triton-X 100 in PBS for 5 minutes. Cells were washed again 3x with PBS. Cells were then incubated with 10 µg/ml of fluorescently labeled streptavidin at room temperature for 1 h and then washed 2x with PBS. Cells were imaged using 500 µl PBS. The PBS was removed and cells were lysed with 2 N NaOH for 24 h. The lysate was neutralized with equal amount of 2 N HCl and the contents transferred to a black walled black bottomed 96 well plate and fluorescence measured using a microplate reader.

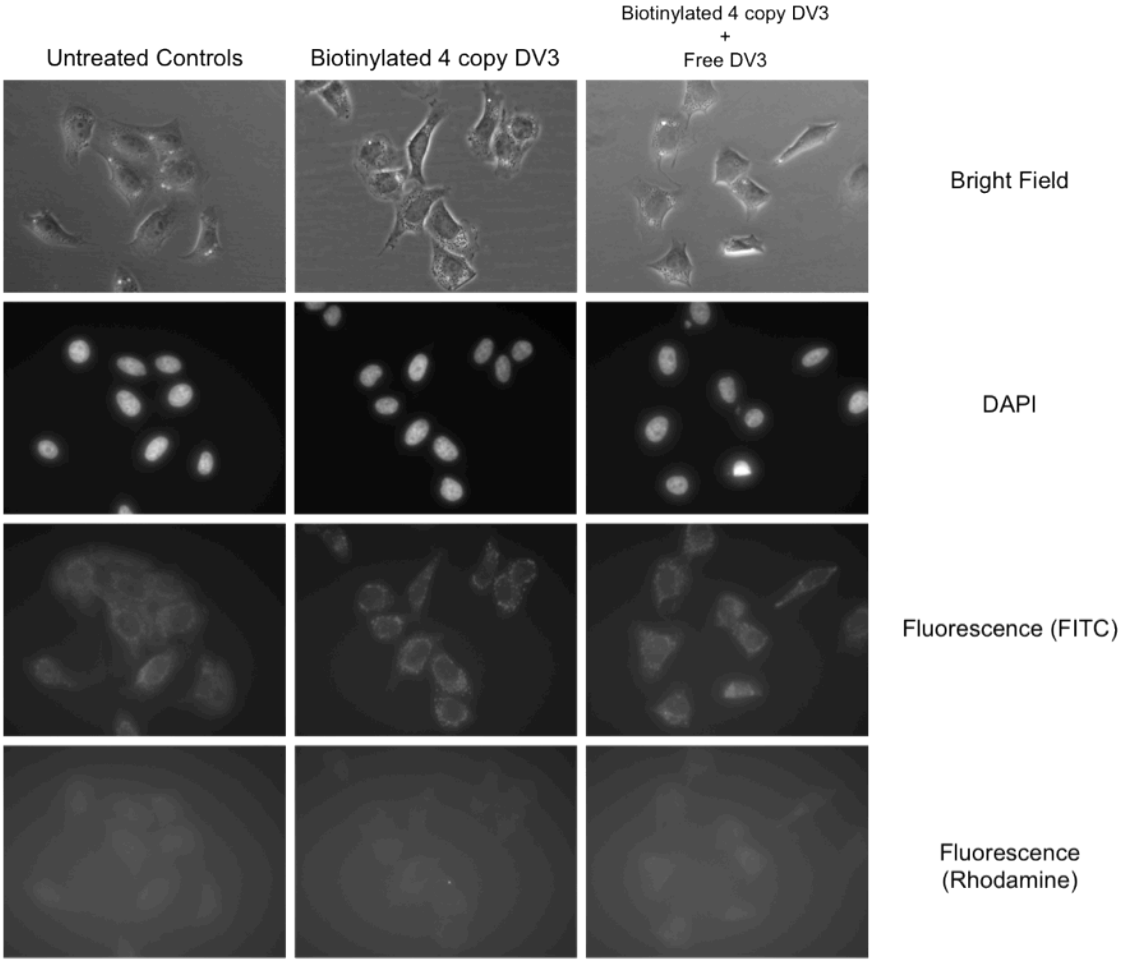

FIGURE 40: Tzm-bl cells were seeded to 6 wells of a 24 well plate at a density of $1.0x10^5$cells/ml and allowed to attach overnight. Control cells were untreated. Additional, groups of cells were treated as follows: (1 µM of biotinylated 4 copy DV3 peptide carrier (MP401, 4DV3) or 1 µM of biotinylated 4 copy DV3 peptide carrier (MP401) + 100 µM Free DV3 (4DV3 + DV3). Duplicates of each group were made from the 6 wells of cells. All cells were incubated with 1 µg/ml DAPI and 60nM Rhodamine-LysoTracker. Cells were incubated for 1 h at 37^O C. To one set of the duplicate wells, cells were fixed 3.7% formalin for 20 minutes, washed 3x with PBS. To the other set of duplicate wells, cells were formalin fixed, then permeabilized with 0.2% Triton X 100 in PBS for 5 minutes. Cells were washed again 3x with PBS. All cells were then incubated with 10 µg/ml of fluorescently labeled streptavidin at room temperature for 1 h and then washed 2x with PBS. Cells were imaged using 500 µl PBS (FIGURES 37 and 38). The PBS was removed and cells were lysed with 2 N NaOH for 24 h. The lysate was neutralized with equal amount of 2 N HCl and the contents transferred to a black walled black bottomed 96 well plate and fluorescence measured using a microplate reader. The ratio between the formalin fixed cells and fixed and permeabilized cells were calculated from 3 separate experiments and reported as the mean. No statistical significance was determined between the groups, however a 65% reduction in the mean association of biotinylated 4 copy DV3 peptide carrier was observed when inhibiting with free DV3 peptide.

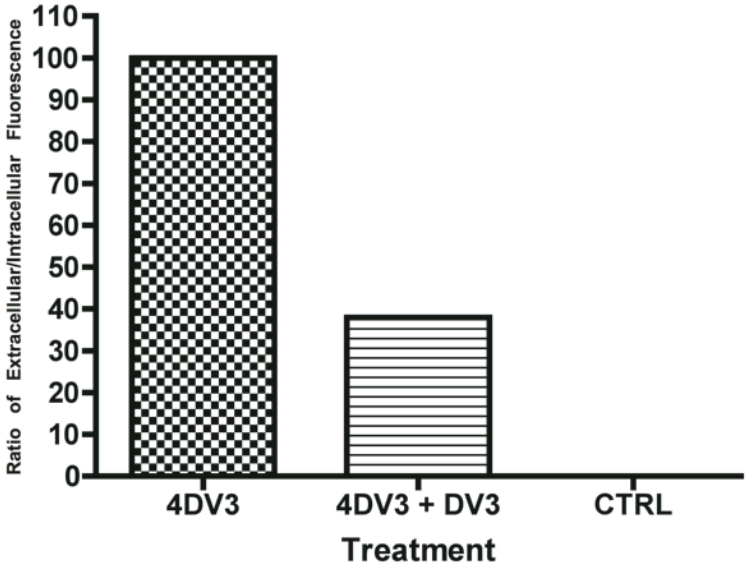

FIGURE 41: Molecular modeling of 4 copy DV3 peptide carrier interactions with CXCR4. 4 copy DV3 peptide carrier was predocked to tetrameric representation of CXCR4 (2 sets of the CXCR4 dimer crystal structure PDB 3ODU). Interactions between receptor residues and DV3 chain residues are outlined in Table 5. Each of the DV3 sequences of the 4 copy DV3 peptide carrier interacts with a receptor molecul of CXCR4 and demonstrating the possibility of a capping effect of the receptors bound to the cell surface and thereby inhibiting the interaction of HIV-1 gp120, AMD3100, or access to the epitopes of CXCR4 mAb.

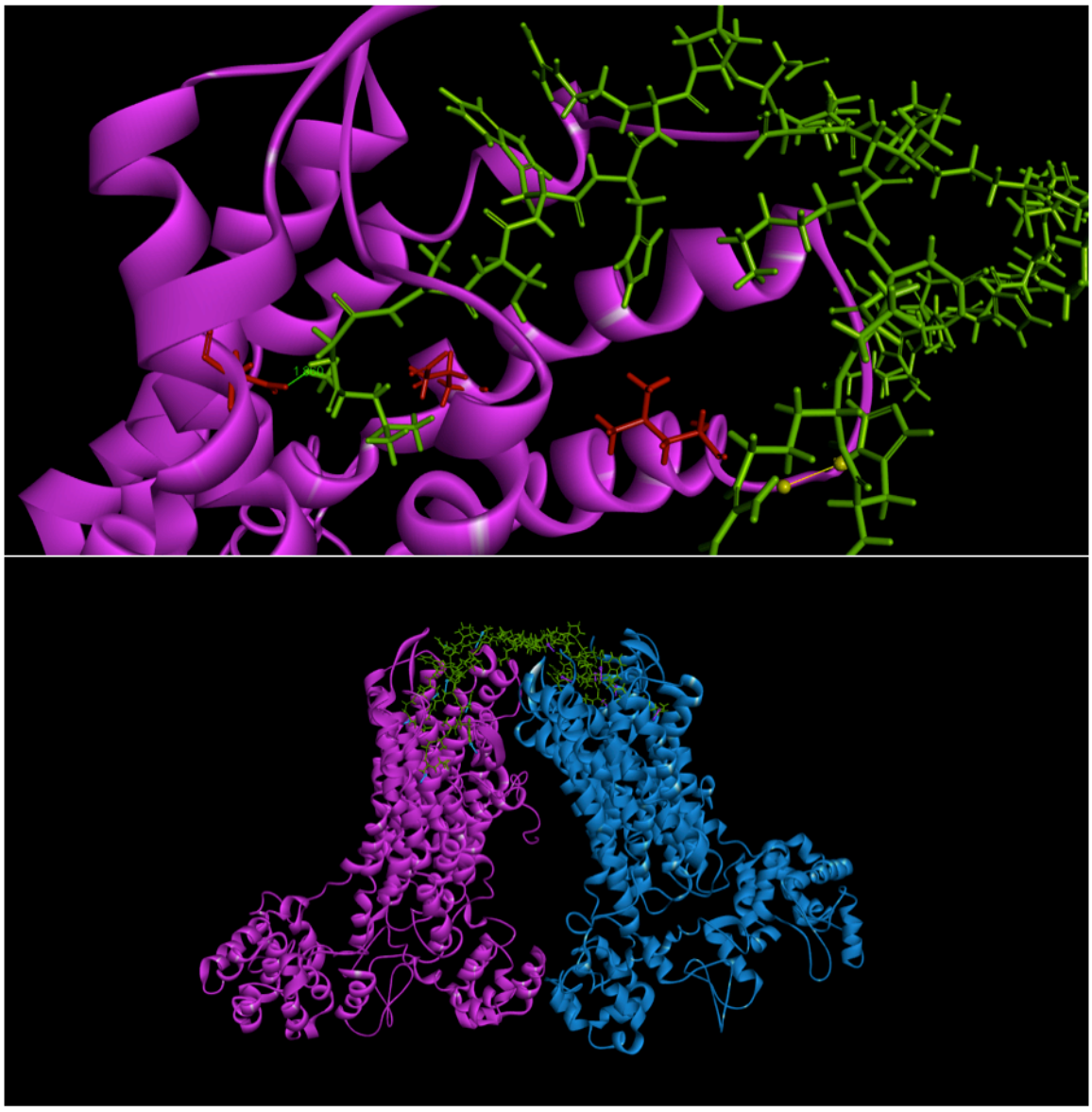

FIGURE 42: Characterization of Boc-Ala-AZT ester. (TOP) Analytical HPLC of purified Boc-Ala-AZT. The compound had a retention time of 4.224 minutes. (BOTTOM) ESI-MS of purified Boc-Ala-AZT. The major peak represents the expected molecular mass of 438 Da in negative mode seen as 437.1 Da.

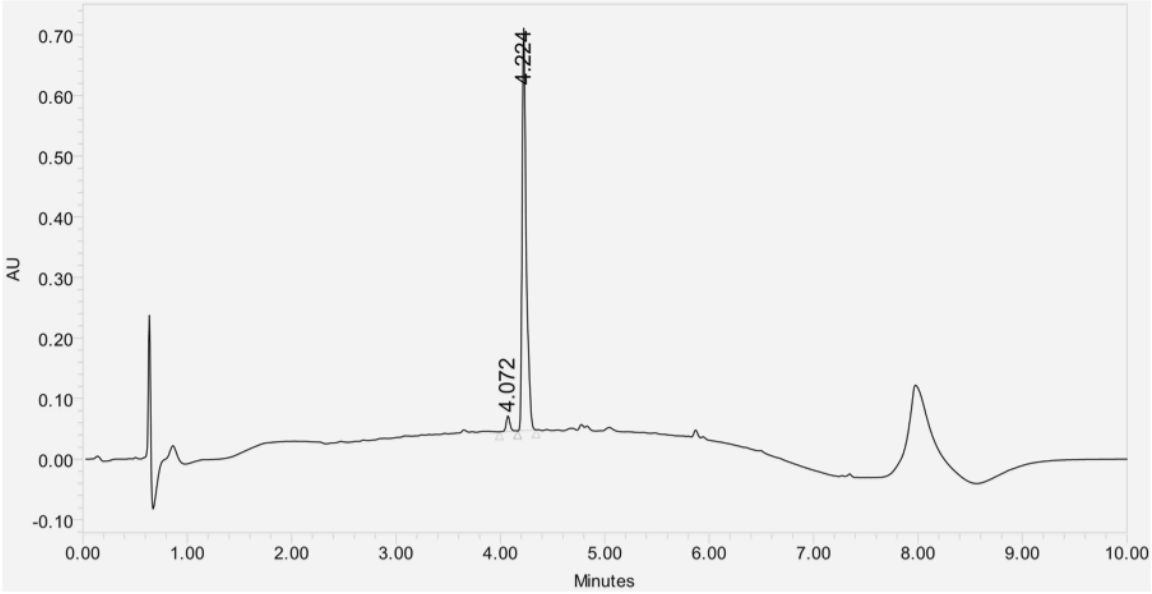

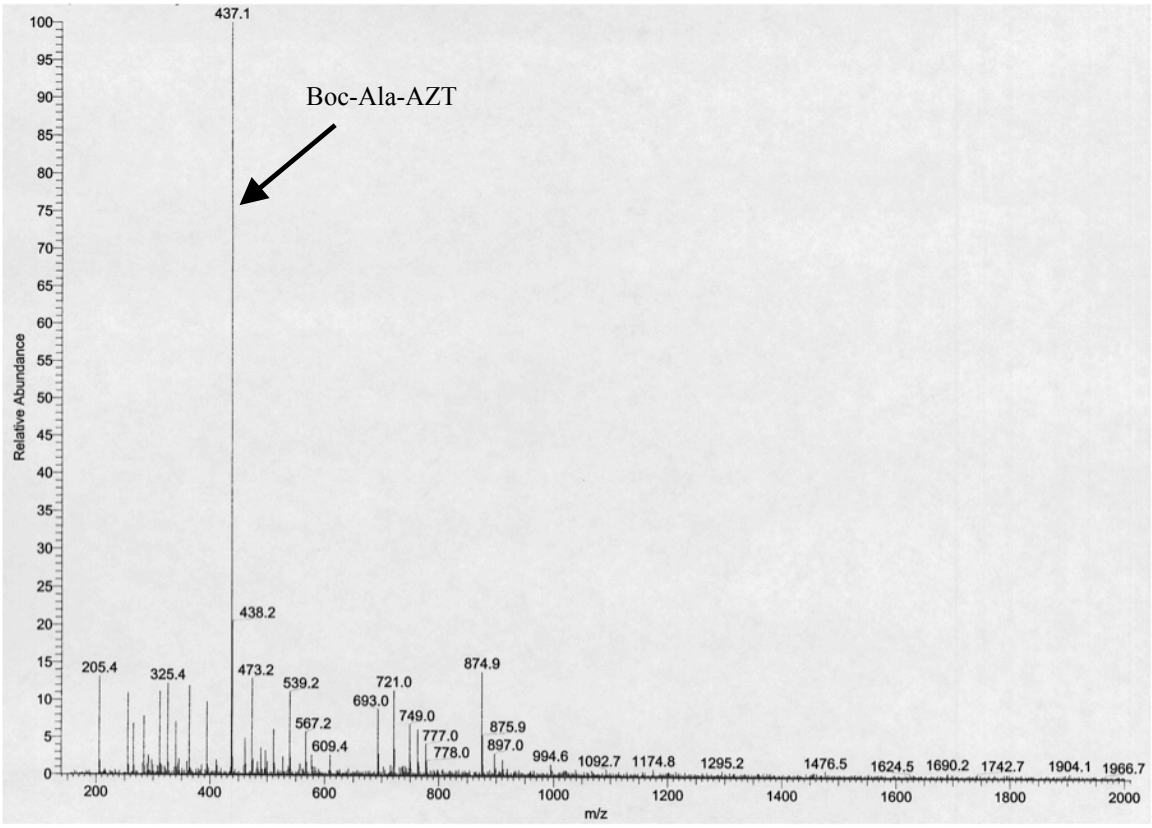

FIGURE 43: Characterization of Boc-Ala-RTV ester. (TOP) Analytical HPLC of purified Boc-Ala-RTV. The compound had a retention time of 5.895 minutes. (BOTTOM) ESI-MS of purified Boc-Ala-RTV. The major peak represents the expected molecular mass of 892 Da and a second peak of [m+Na^+] = 914 Da.

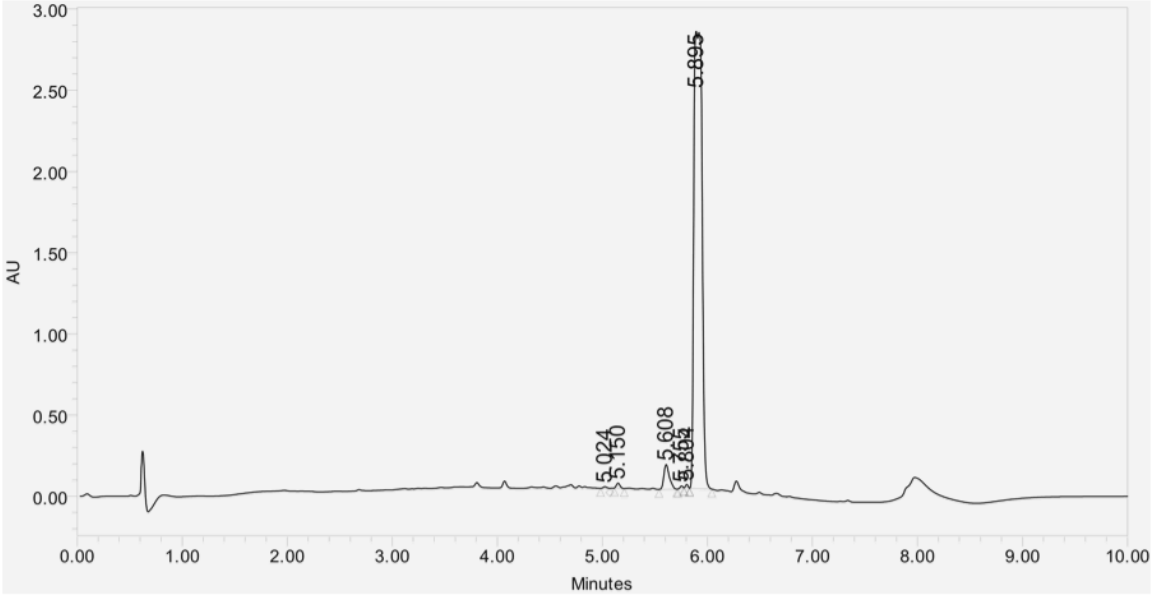

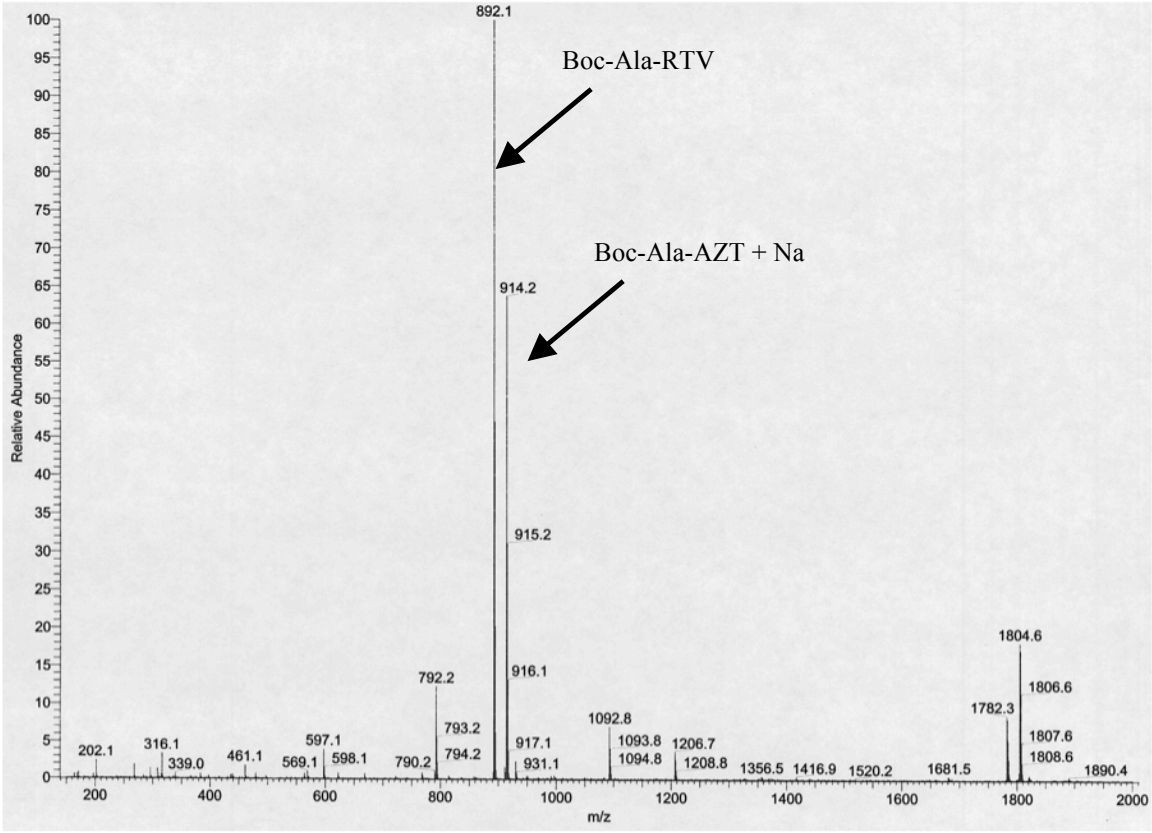

FIGURE 44: HPLC (Top) and MALDI-TOF of purified MP402 (4 copy DV3 peptide carrier). MP402 has a rention time = 2.522 minutes. Purity was determined by AUC of the chromatogram as 100%. MALDI-TOF demonstrated 2 major peaks of importance. 5179 corresponds to MP402 and 2591 corresponds to [MP402+2]/2.

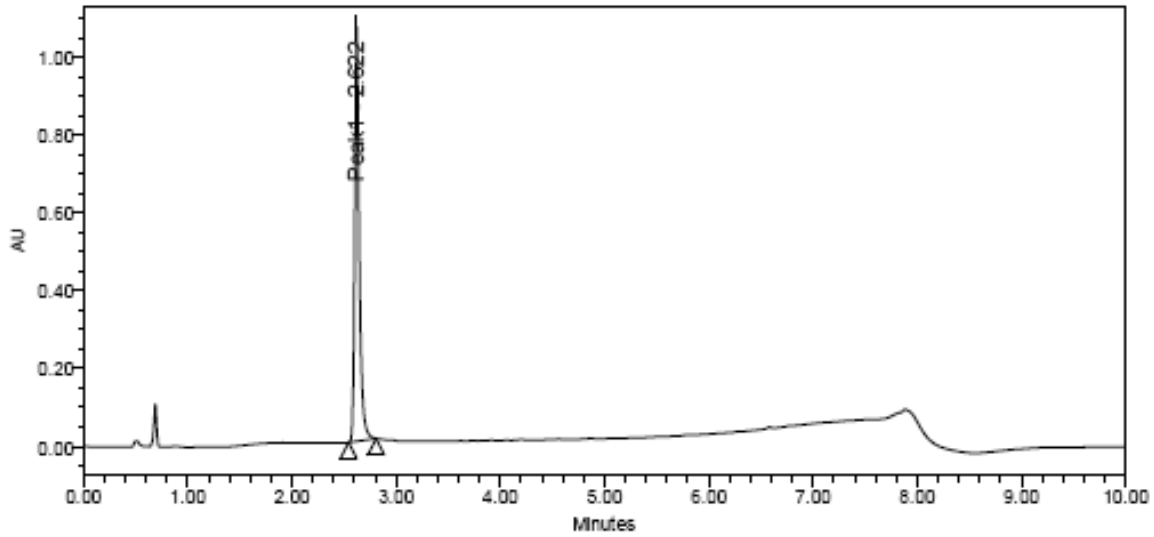

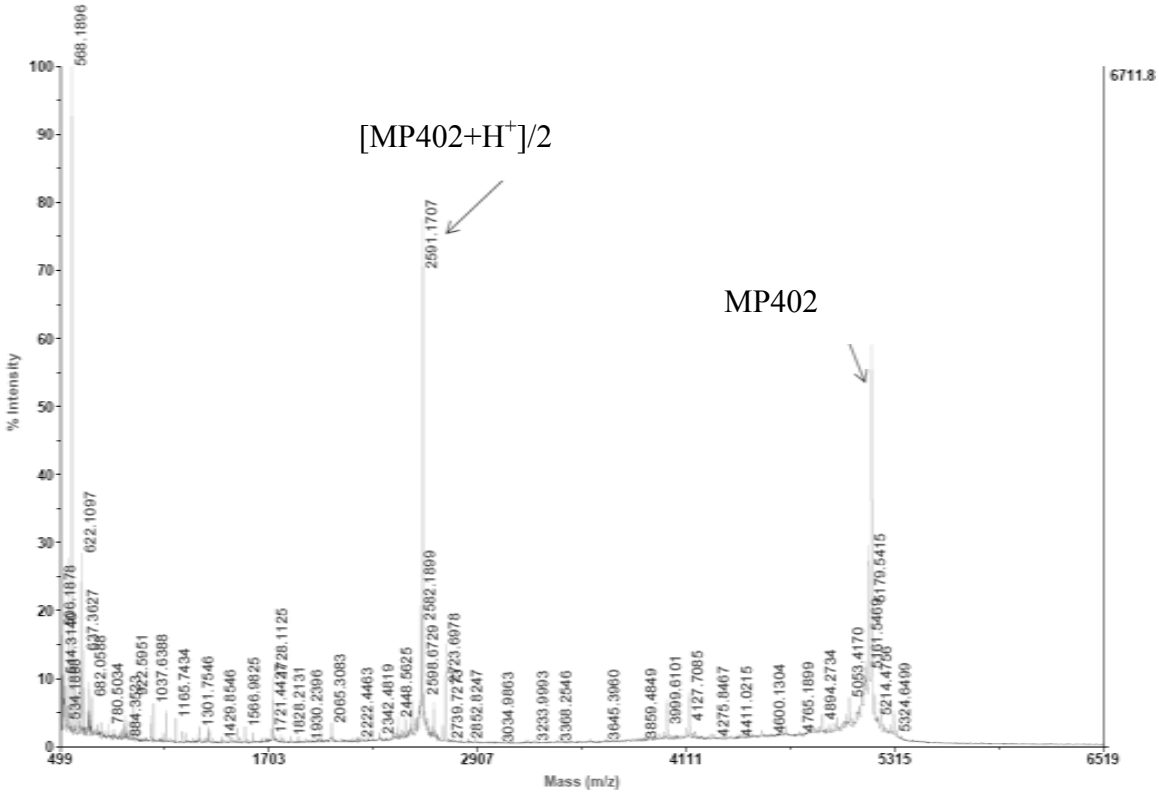

FIGURE 45: HPLC (Top) and MALDI-TOF of purified 4DV3 AZT drug conjugate (MP403). MP403 has a retention time = 2.696 minutes. MALDI-TOF demonstrated 2 major peaks of importance. 5604 corresponds to MP403 and 2801 corresponds to [MP403+2H$^+$]/2.

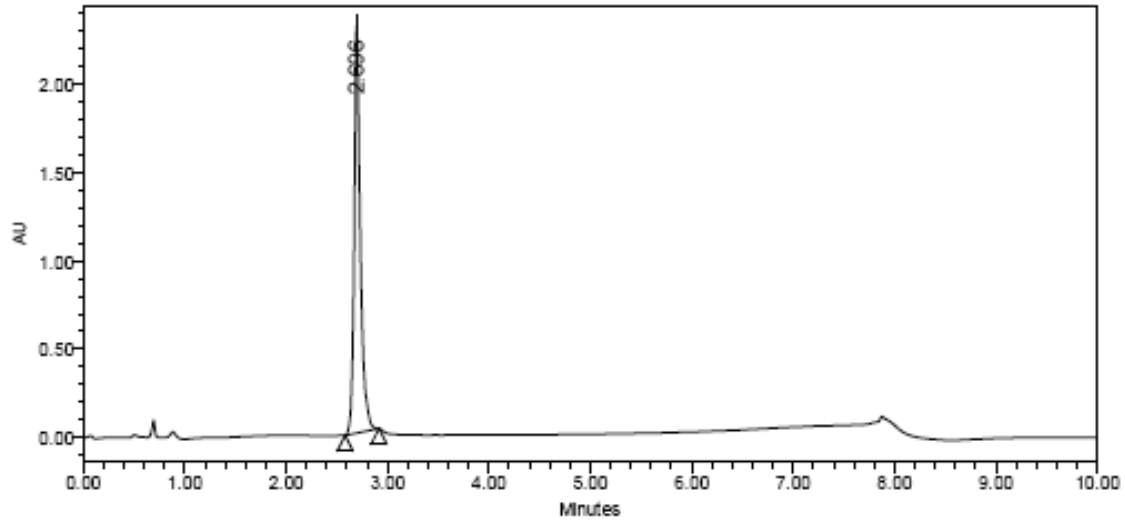

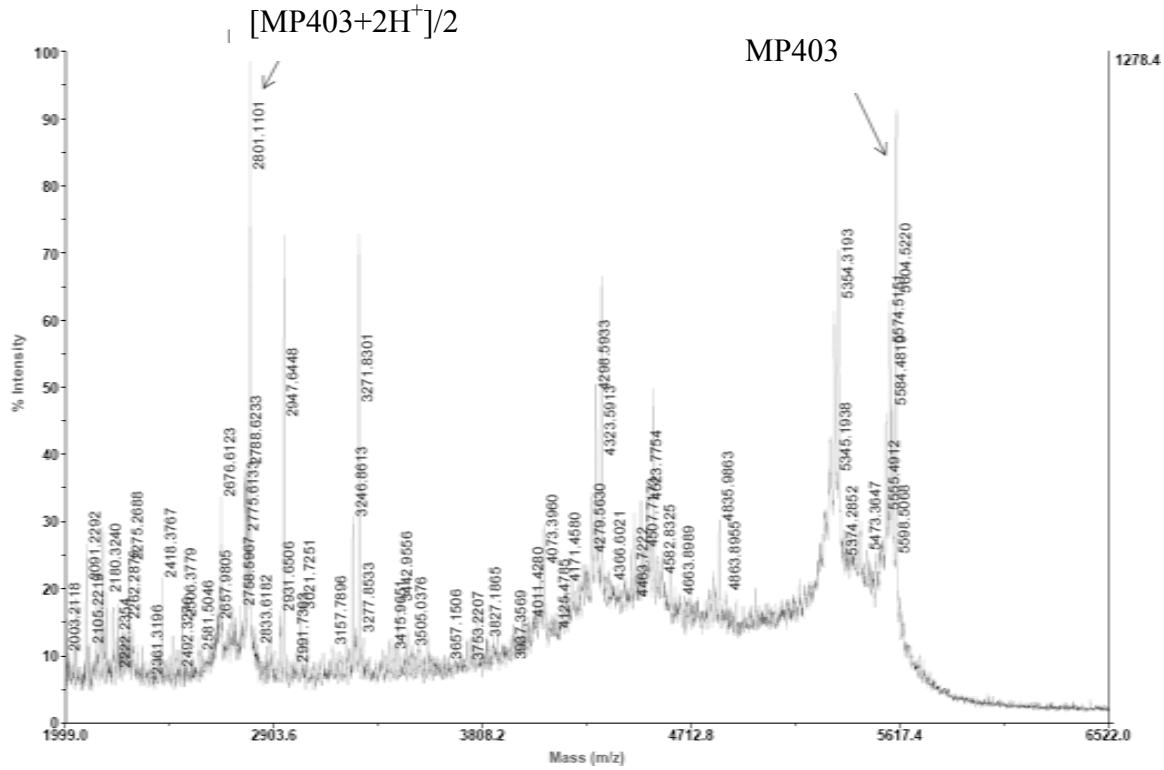

FIGURE 46: HPLC (Top) and MALDI-TOF (Bottom) of purified 4DV3 RTV drug conjugate (MP404). MP404 has a retention time = 3.186 minutes. MALDI-TOF demonstrated 2 major peaks of importance. 6057 corresponds to MP404 and 3027 corresponds to [MP404+2H$^+$]/2.

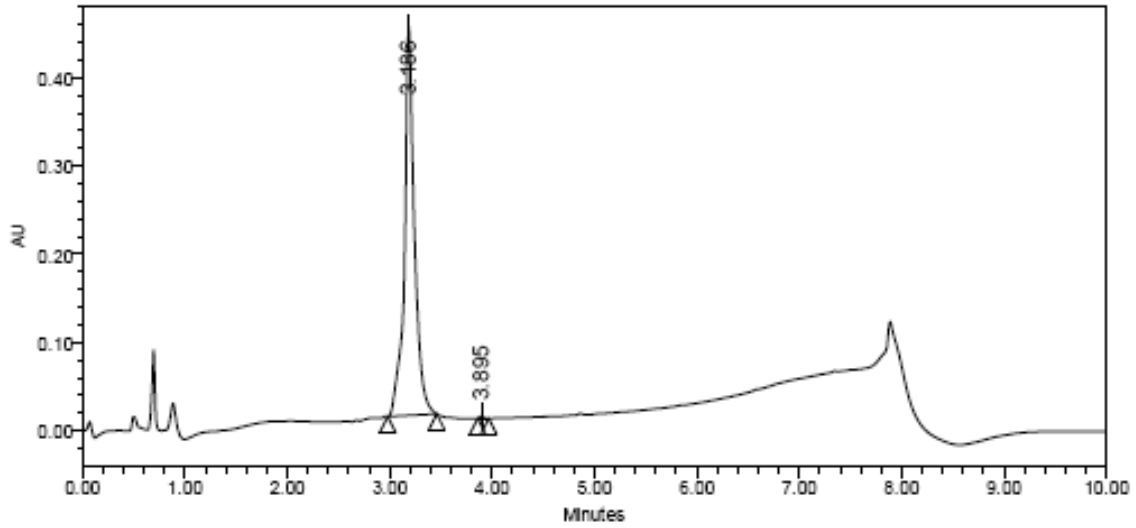

[MP404+2H$^+$]/2

MP404

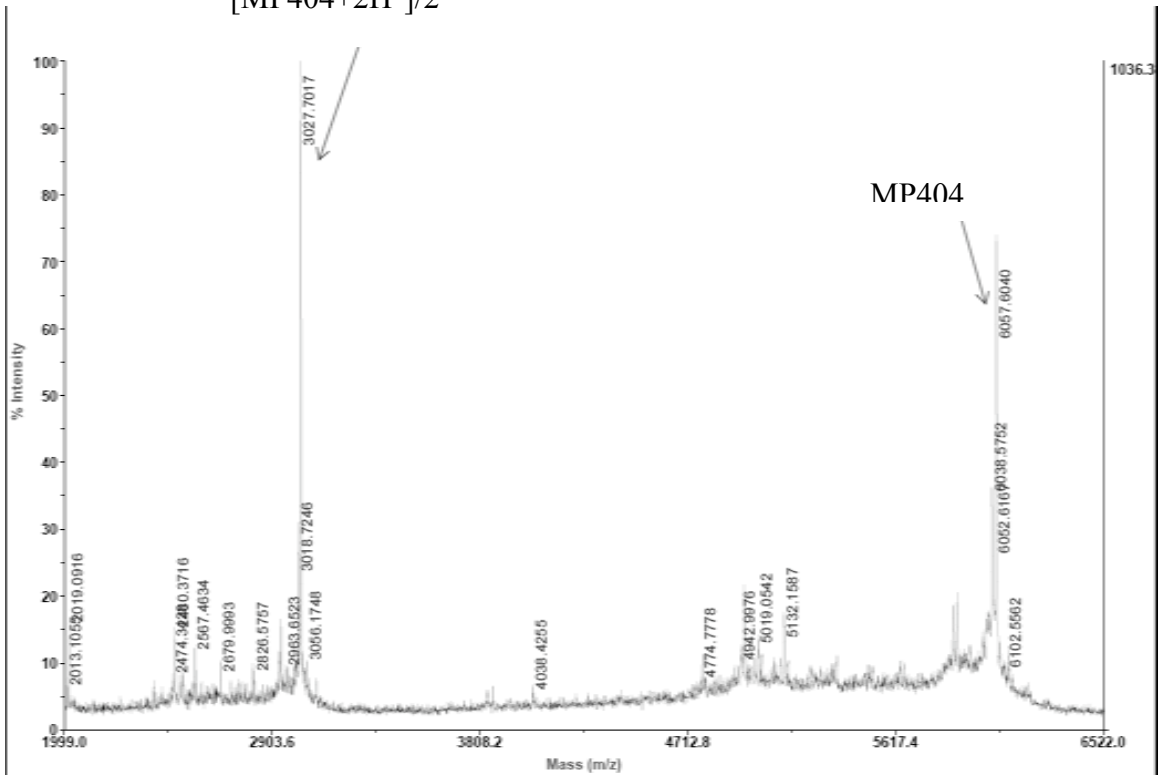

FIGURE 47: Calcium mobilization due to activation of CXCR4 by antagonists or agonists was measured using the Fluo-4 Direct Calcium Assay Kit (Invitrogen, Carlsbad, CA). Following the kit instructions, MT2 cells were suspended in the calcium assay buffer at a density of $2.5x10^6$ cells/ml. MT2 cells were added to triplicate wells of a 96 well plate ($1.25x10^5$ cells/well) and incubated at 37^o C for 1h. Added Fluo-4 direct reagent and incubated for an additional hour. To the designated triplicates 50µl of the following were added: 200nM SDF-1α, 200µM 4DV3 (MP402); 200µM DV3; and PBS. Fluorescence was measured on microplate reader and the mean ± standard deviation from three separate experiments was reported. Statistical analysis by ANOVA was unable to detect statistical significance between the groups.

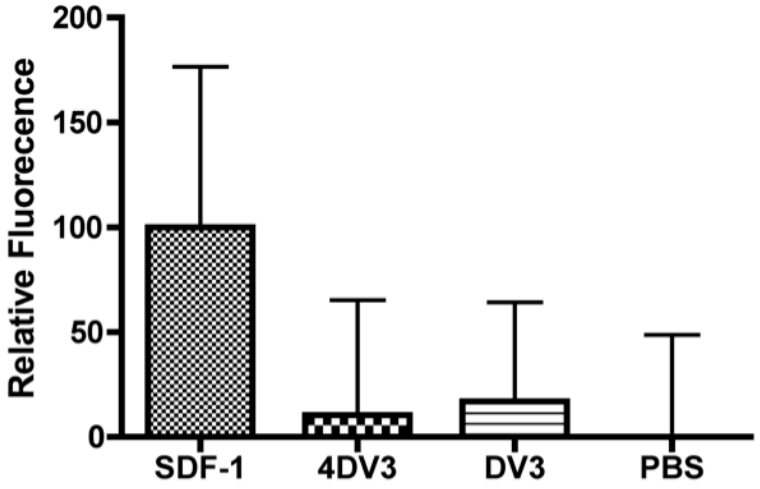

FIGURE 48: Representative standard curves of the anti-HIV-1 drugs, AZT (TOP) and RTV (BOTTOM) in human plasma. The standard curves were generated by the detected peak area by HPLC at UV_{ABS} = 210nm.

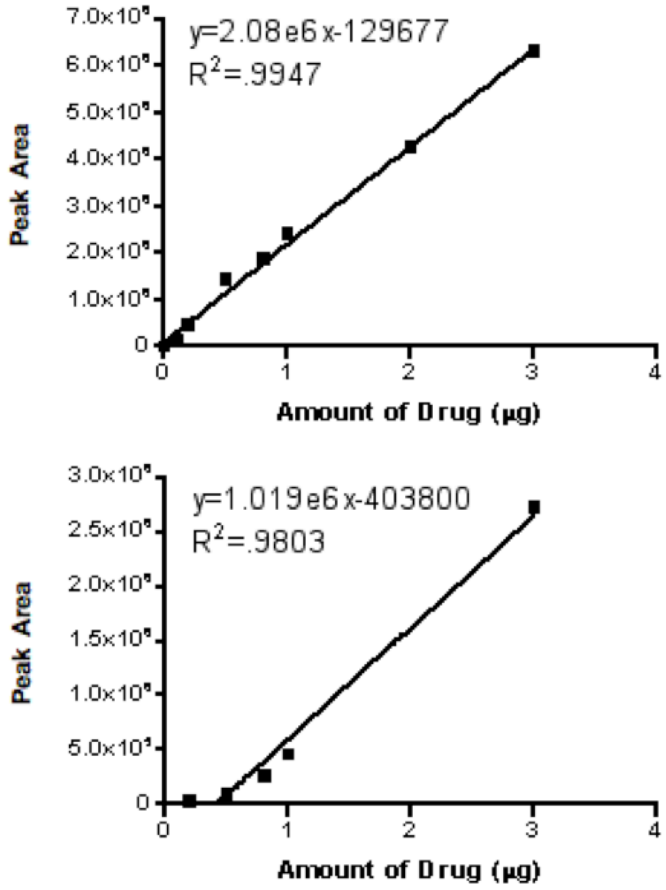

Figure 49: Representative standard curves of the anti-HIV-1 drugs, AZT (TOP) and RTV (BOTTOM) in rat plasma. The standard curves were generated by the detected peak area by HPLC at UV_{ABS} = 210nm.

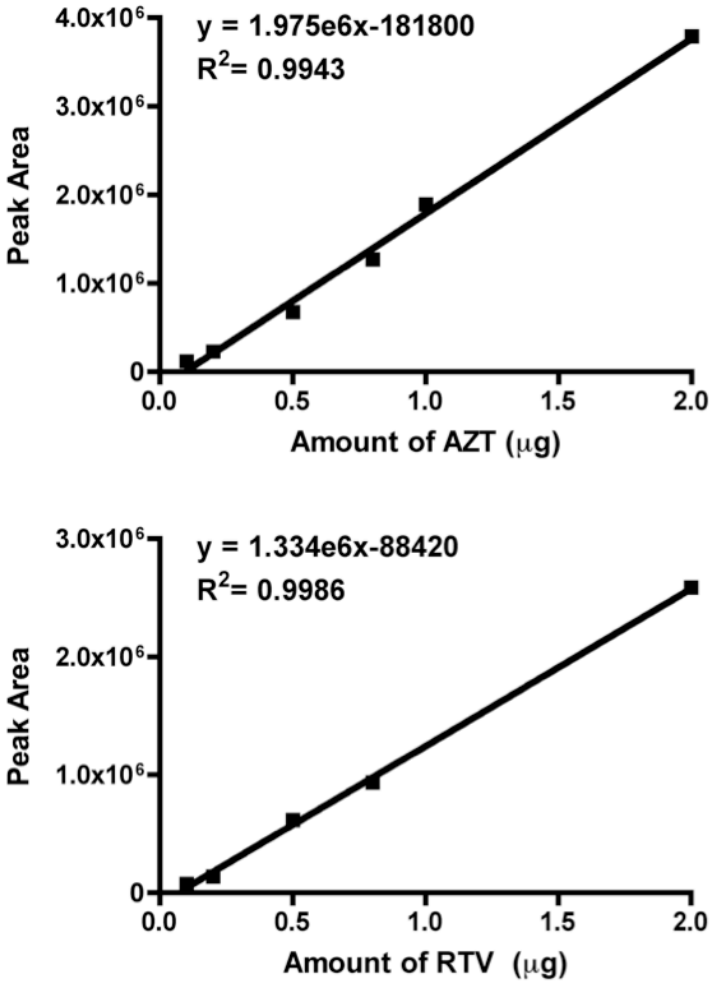

FIGURE 50: Drug release from 4 copy DV3 drug conjugates in human plasma, 4DV3-AZT (MP403) and 4DV3-RTV (MP404). Drug release from the 4DV3 conjugate was observed over a 24h period for the AZT conjugate, whereas no release was measured for the RTV conjugate. The amount of drug detected was normalized to the theoretical equivalent amount of the parent drug (0.4 μg). The $t_{1/2}$ of the 4DV3-AZT conjugate as determined by a one phase exponential equation was 3.26h. Each data point represents the mean ± standard deviation from 3 separate experiments.

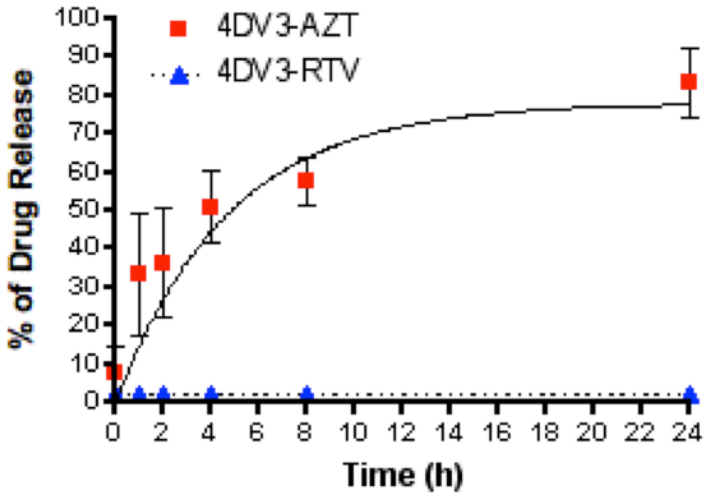

FIGURE 51: Drug release from 4 copy DV3 drug conjugates in rat plasma, 4DV3-AZT (MP403) and 4DV3-RTV (MP404). Drug release from the 4DV3 conjugate was observed over a 24h period for the AZT conjugate, whereas no release was measured for the RTV conjugate. The amount of drug detected was normalized to the theoretical equivalent amount of the parent drug (0.4 μg). The $t_{1/2}$ of the 4DV3-AZT conjugate as determined by a one phase exponential equation was 2.78 h. The $t_{1/2}$ of the 4DV3-AZT conjugate as determined by a one phase exponential equation was 117 h Each data point represents the mean $\pm$ standard deviation from 3 separate experiments..

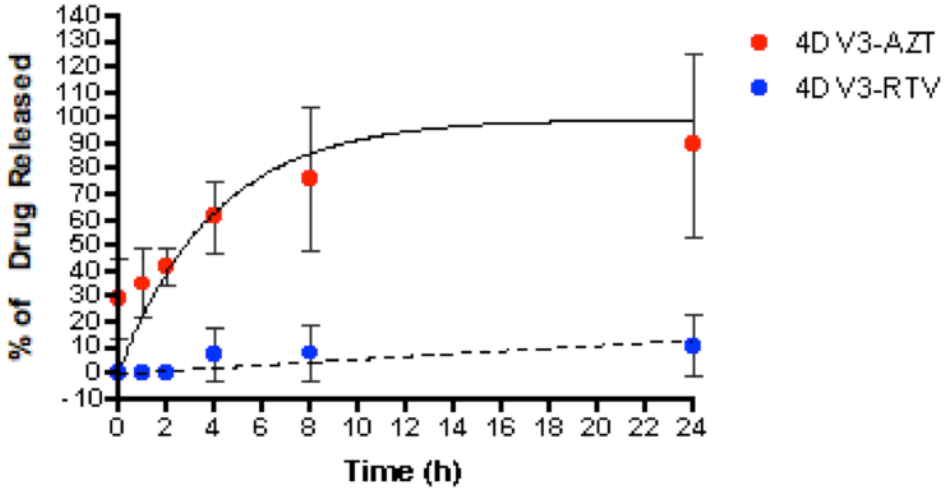

FIGURE 52: Prevention of HIV-1 replication by 4 copy DV3 peptide carriers. MP402 (2μM) was added to $5.0x10^4$ cells/ml of MT2 cells in RPMI (+DV3) and 100μl of cells was plated to triplicate wells of a 96 well plate. Untreated controls were $5.0x10^4$ cells/ml of MT2 cells in RPMI (-DV3) and 100 μl of cells were plated to triplicate wells. HIV-1 IIIB at an MOI = 0.03 was added in an equal volume to the wells and incubated for 0.5, 1, or 2 hours. The plate was centrifuged, supernatant removed, and replaced with 200 μl of 1 μM MP402 (+DV3) or RPMI (-DV3). MT2 cells were incubated for 5 days and HIV-1 replication dependent p24 protein was measure by ELISA. Two way ANOVA was used to determine significant difference between untreated and treated groups. Graph represents mean ± standard deviation from 3 separate experiments.

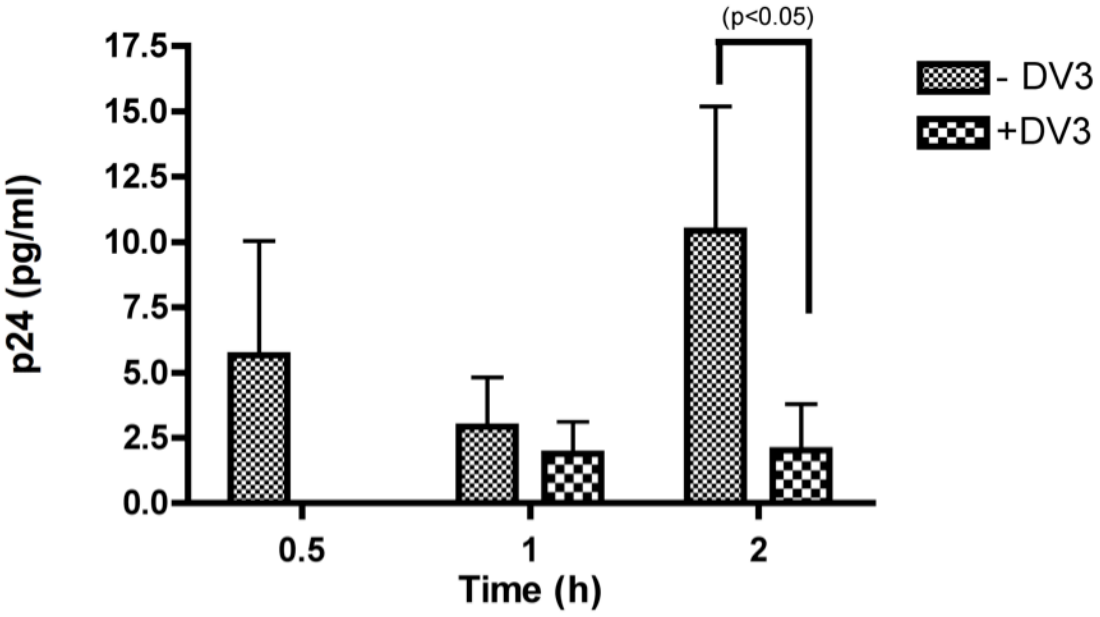

FIGURE 53: 4 copy DV3 peptide carriers inhibition of HIV-1 replication. Serial dilutions of MP402 were prepared in RPMI and added to 96 well plate. MT2 cells were prepared at a cellular density of $5.0x10^4$ cells/ml in RPMI. Cells were then infected with HIV-1 IIIB at a multiplicity of infection of 0.03. Cells plus virus were then added to the microplate of MP402 and incubated for 5 days at 37^oC with 5% CO_2. Positive control was MT2 cells exposed to HIV-1 with no MP402 and negative controls were cells without exposure to virus of MP402. p24 from HIV-1 replication was measured using ELISA kit. Syncytia formation was observed and counted using a light microscope. Nonlinear regression analysis was conducted using GraphPad Prism Software after normalizing data to positive and negative controls. IC50 was calculated from the antilog of regression analysis from three separate experiments with each data point representative of mean $\pm$ standard error (Top) and mean $\pm$ standard deviation (Bottom). IC_{50} calculated from p24 was 16.98 μM and from syncytia count was 23.6 μM.

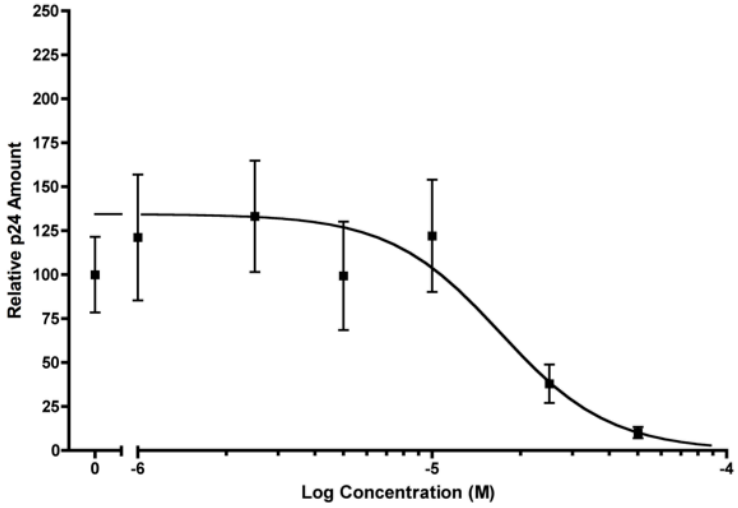

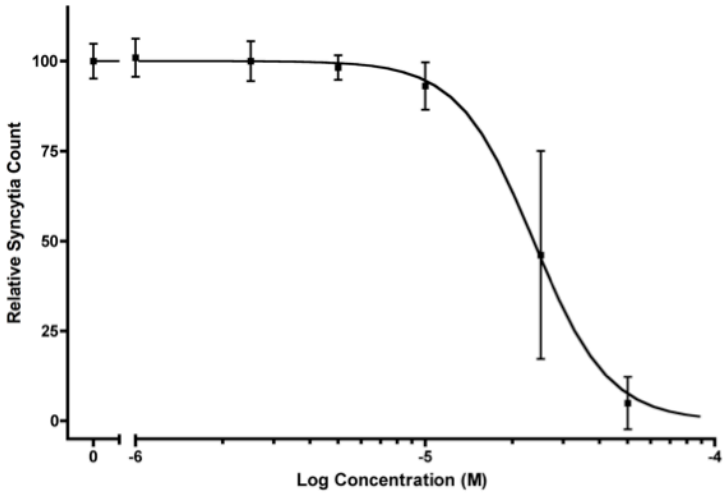

FIGURE 54: Inhibition of HIV-1 replication by 4DV3-AZT drug conjugates. Serial dilutions of 4DV3-AZT (MP403), 4DV3 (MP402) + AZT, and AZT were prepared in RPMI and added to 96 well plate. MT2 cells were prepared at a cellular density of $5.0x10^4$cells/ml in RPMI. Cells were then infected with HIV-1 III_B at a multiplicity of infection of 0.03. Cells plus virus were then added to the microplate and incubated for 5 days at 37°C with 5% CO_2. Positive control was MT2 cells exposed to HIV-1 with no treatment and negative controls were cells without exposure to virus. p24 from HIV-1 replication was measured using ELISA kit. Syncytia formation was observed and counted using a light microscope. Nonlinear regression analysis was conducted using GraphPad Prism Software after normalizing data to positive and negative controls. IC_{50} was calculated from the antilog of regression analysis from three separate experiments with each data point representative of mean ± standard deviation. IC_{50} values were calculated as follows for the p24 amount: AZT = 9 nM; 4DV3 + AZT = 11 nM; 4DV3-AZT = 32 nM. IC_{50} values were calculated as follows for the syncytia: AZT = 33 nM; 4DV3 + AZT = 26 nM; 4DV3-AZT = 80 nM.

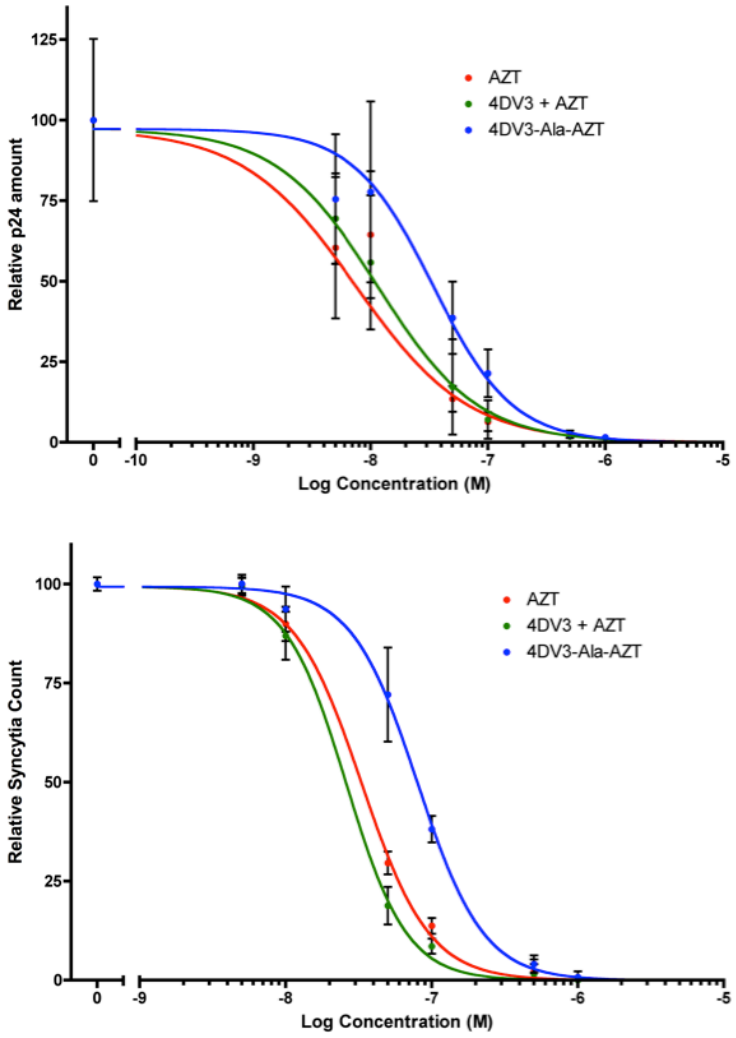

FIGURE 55: Inhibition of HIV-1 replication by 4DV3-RTV drug conjugates. Serial dilutions of 4DV3-RTV (MP404), 4DV3 (MP402) + RTV, and RTV were prepared in RPMI and added to 96 well plate. MT2 cells were prepared at a cellular density of $5.0x10^4$cells/ml in RPMI. Cells were then infected with HIV-1 III_B at a multiplicity of infection of 0.03. Cells plus virus were then added to the microplate and incubated for 5 days at 37°C with 5% CO_2. Positive control was MT2 cells exposed to HIV-1 with no treatment and negative controls were cells without exposure to virus. p24 from HIV-1 replication was measured using ELISA kit. Syncytia formation was observed and counted using a light microscope. Nonlinear regression analysis was conducted using GraphPad Prism Software after normalizing data to positive and negative controls. IC_{50} was calculated from the antilog of regression analysis from three separate experiments with each data point representative of mean ± standard deviation. IC_{50} values were calculated as follows for the p24 amount: RTV = 12 nM; 4DV3 + RTV = 10 nM; 4DV3-RTV = 598 nM. IC_{50} values were calculated as follows for the syncytia: RTV = 27 nM; 4DV3 + RTV = 24 nM; 4DV3-RTV = 713 nM.

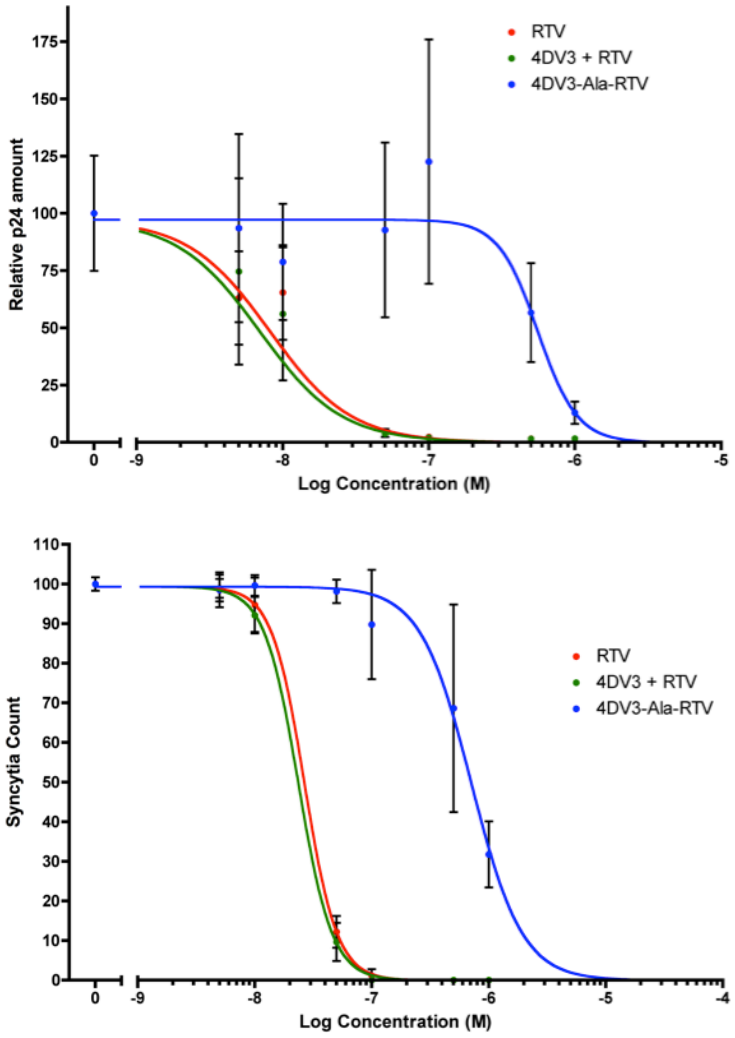

FIGURE 56: Characterization of 4 copy DV3 PEG_{12} azide (MP410). (Top) HPLC chromatogram of purified MP410. Retention time of compound was measured at 2.025minutes. (Bottom) MALDI-TOF spectra of MP410, observed peak at 5806 correlates to MP410 and peak at 2903 correlates to [M+2H]/2.

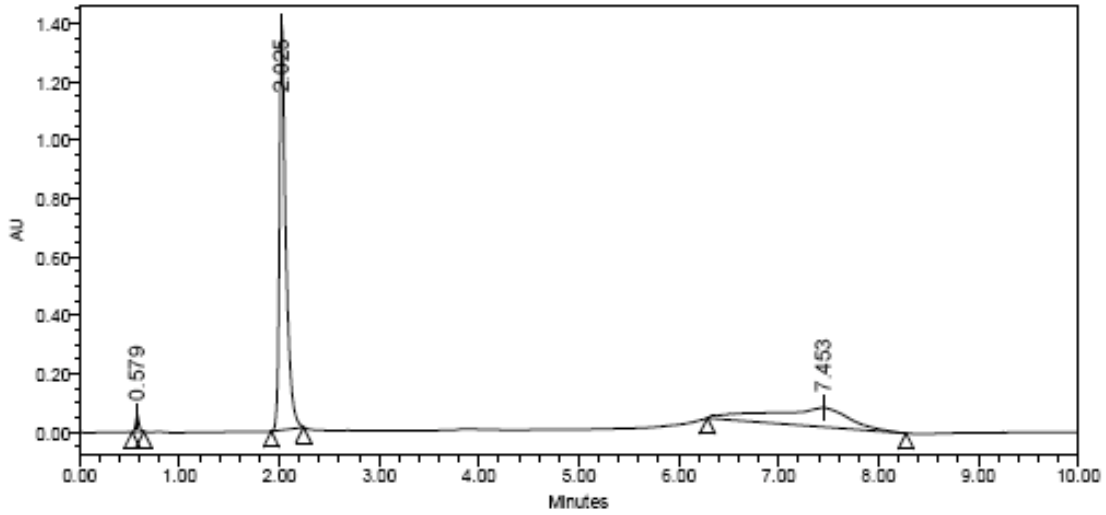

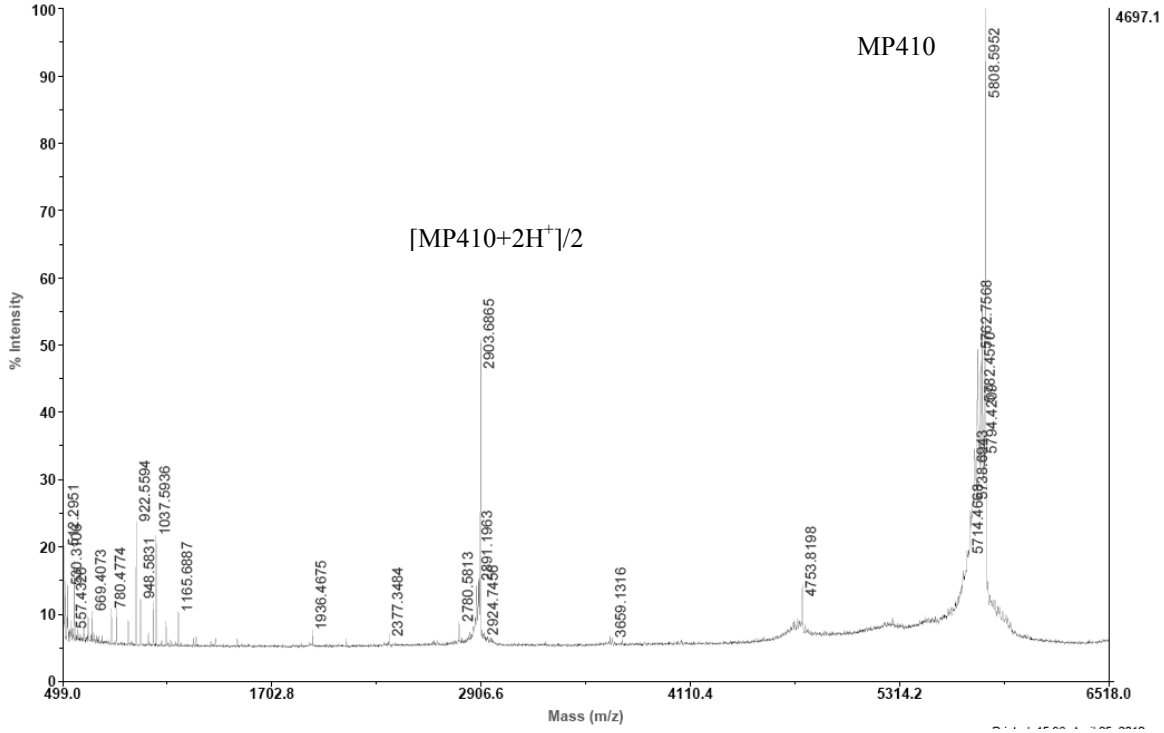

FIGURE 57: Characterization of 4 copy DV3 PEG_{12} azide after DBCO-PEG_4-DBCO addition (MP411). (Top) HPLC chromatogram of purified MP411. Retention time of compound was measured at 3.257 min. (Bottom) MALDI-TOF spectra of MP411, the observed peak at 6616 corresponds to the molecular weight of MP411.

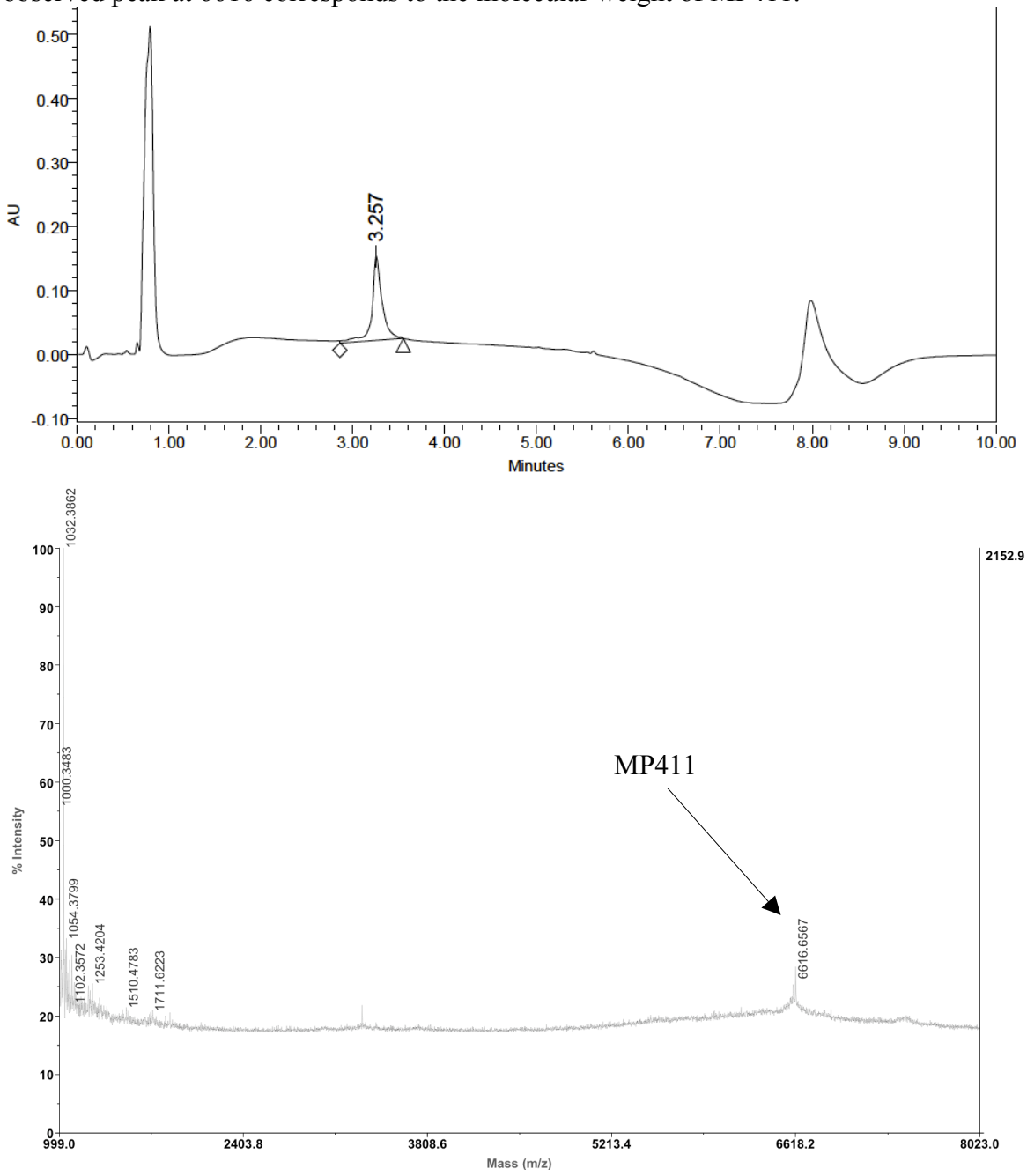

APPENDIX

ANALYSIS OF $CD4^+$ JURKAT CELLS FOR HIV-1 REPLICATION CELL MODEL

7.1 MATERIALS AND METHODS

7.1.1 Reagents: hCXCR4-Phycoerythrin mAb (clone 12G5) was purchased from R&D Systems (Minneapolis, MN). hCD4-FITC mAb (clone RPA-T4) and FACS Staining Buffer were purchased from BD Sciences (San Jose, CA). Jurkat T-cells and $CD4^+$ Jurkat T-cells were kindly received from our collaborator, Dr. Yong-Jiu Jin, from Mount Sinai School of Medicine (*252*).

7.1.2 Expression of CD4 and CXCR4 by Jurkat cells: Jurkat and $CD4^+$ Jurkat-$CD4^+$ were cultured in supplemented DMEM, centrifuged, washed, and resuspended in blocking buffer (FACS staining buffer + 10% human serum). Cells were incubated in blocking buffer for 20 min at 4^o C to block Fc receptors. Cells were counted, $2.5x10^6$ cells were transferred to 50 ml tube, washed with ice cold FACS staining buffer, then resuspended in 500 µl FACS staining buffer. For CD4 and CXCR4 staining the respective antibodies (PE conjugated CXCR4 mAb and FITC conjugated CD4 mAb) were incubated with cells individually or together for 45 minutes at 4^o C, centrifuged, and washed 3 times. All cells after staining were stored on ice until analysis. Flow cytometry analysis was conducted on a Coulter Cytomics FC500 Flow Cytometer (Beckman Coulter, Fullerton, CA) at the Analytical Cytometry/Image Analysis Core Facility (EOHSI, Rutgers, The State University of New Jersey, Piscataway, NJ).

7.1.3 Replication of HIV-1 by $CD4^+$ Jurkat cells: $CD4^+$ Jurkat cells were prepared at a cellular density of $5.0x10^4$ cells/ml and seeded to quadruplicate wells of a 96 well plate in RPMI. HIV-1 viral strains IIIB (X4 strain) or BaL (R5 strain) were added to sets of wells at either an MOI of 0.038 or 0.38 in RPMI. Cells and virus were incubated at 37^o C for 5 d. The amount of extracellular p24 was measured using an ELISA following the manufactures' instructions.

7.2 RESULTS

7.2.1 Expression of CD4 and CXCR4 by Jurkat cells: Jurkat cells are a T-cell line that have been shown to express both CXCR4 and CCR5, but undetectable amounts of CD4 (*6*). Comparative flow cytometry analysis was conducted on Jurkat cells and Jurkat cells stably transfected with CD4 supplied to our lab by Dr. Y. Jin. Jurkat cells were confirmed to have nearly undetectable expression of CD4 (Figure 58), however the stably transfected $CD4^+$ Jurkat cells represented 69% of the cell population tested indicating. Furthermore, the $CD4^+$ Jurkat cells tested were 61.96% positive for coexpression of CD4 and the HIV-1 coreceptor CXCR4 indicating that these cells may be capable to replicate HIV-1 if infected (Figure 58).

7.2.2 Replication of HIV-1 by $CD4^+$ Jurkat cells: MT2 cells were used as the propagating cells for the HIV-1 X4 strain IIIB. However MT2 cells do not express a detectable amount of the other HIV-1 coreceptor, CCR5 (*6*). Additionally, MT2 do not support the replication of R5 strains of the virus (data not shown). Therefore an

alternative cell line was necessary for testing inhibition of R5 viral strain replication. $CD4^+$ Jurkat cells were shown to coexpress CXCR4 and $CD4^+$ and are known to express CCR5 endogenously, but not previously shown for their capacity to produce new HIV-1 viral particles. Replication of both the X4 strain IIIB and the R5 strain BaL was measured by the p24 ELISA at two different multiplicities of infection (MOI). Viral replication as indicated by the extracellular p24 amount for the X4 strain was 45.63 $\pm$ 2.30 pg/ml and 315.48 $\pm$ 8.55 pg/ml for MOIs of 0.038 and 0.38 respectively. For the R5 strain BaL, considerably less replication occurred at an MOI = 0.038, 10.7 pg/ml of p24 were measured and at an MOI = 0.38 the p24 concentration was 113.41 $\pm$ 5.52 pg/ml (Figure 59).

FIGURE 58:
(TOP) Flow cytometry histogram of Jurkat cells and (BOTTOM) $CD4^+$ Jurkat cells. (A, D) Two dimensional scatter plot of Jurkat cells positive for CXCR4 (y-axis, PE conjugated CXCR4 mAb) and CD4 (x-axis, FITC conjugated CD4 mAb). (B, E) Histogram plot of Jurkat cells positive for expression of CXCR4. (C, F) Histogram plot of Jurkat cells positive for expression of CD4. There is a dramatic difference in the number of $CD4^+$ cells when comparing the wild type Jurkat cells with those stably transfected CD4 ($CD4^+$ Jurkat cells). $CD4^+$ Jurkat cells that coexpress CXCR4 account for 61.96 % of the cell population analyzed by flow cytometry. Indicating that these cells may be capable of supporting HIV-1 replication.

Jurkat Cells

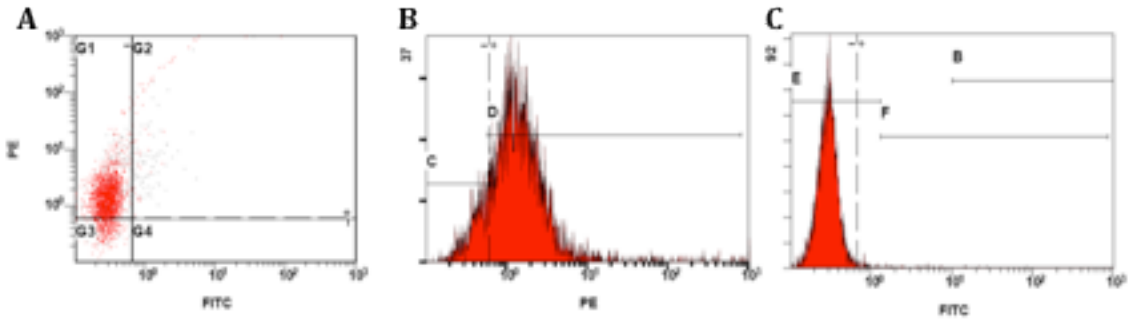

$CD4^+$ Jurkat Cells

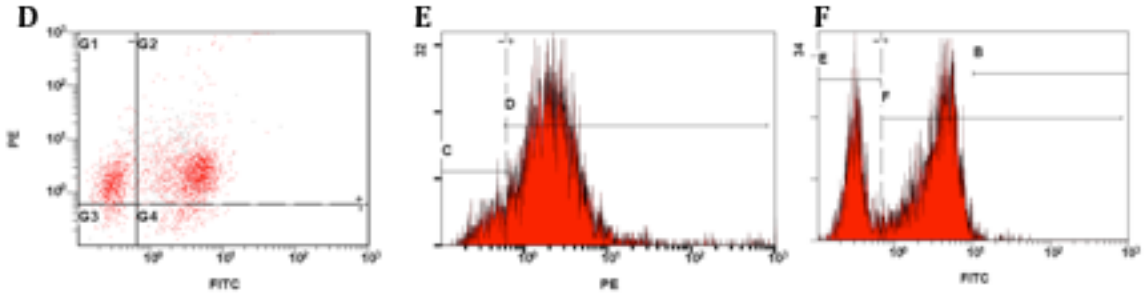

FIGURE 59: $CD4^+$ Jurkat cells were prepared at a cellular density of $5.0x10^4$cells/ml in RPMI. Cells were then infected with either the X4 strain IIIB or the R5 strain BaL at a multiplicity of infection of 0.38 (TOP) or 0.038 (BOTTOM). Cells plus virus were then added to the microplate and incubated for 5 days at 37^oC with 5% CO_2. Positive control was $CD4^+$ Jurkat cells exposed to HIV-1 with no treatment and negative controls were cells without exposure to virus. p24 from HIV-1 replication was measured using ELISA kit. Each bar represents the mean $\pm$ standard deviation from quadruplicate wells. Replication of both X4 and R5 strains were possible with the $CD4^+$ Jurkat cells and dependent upon the MOI used.

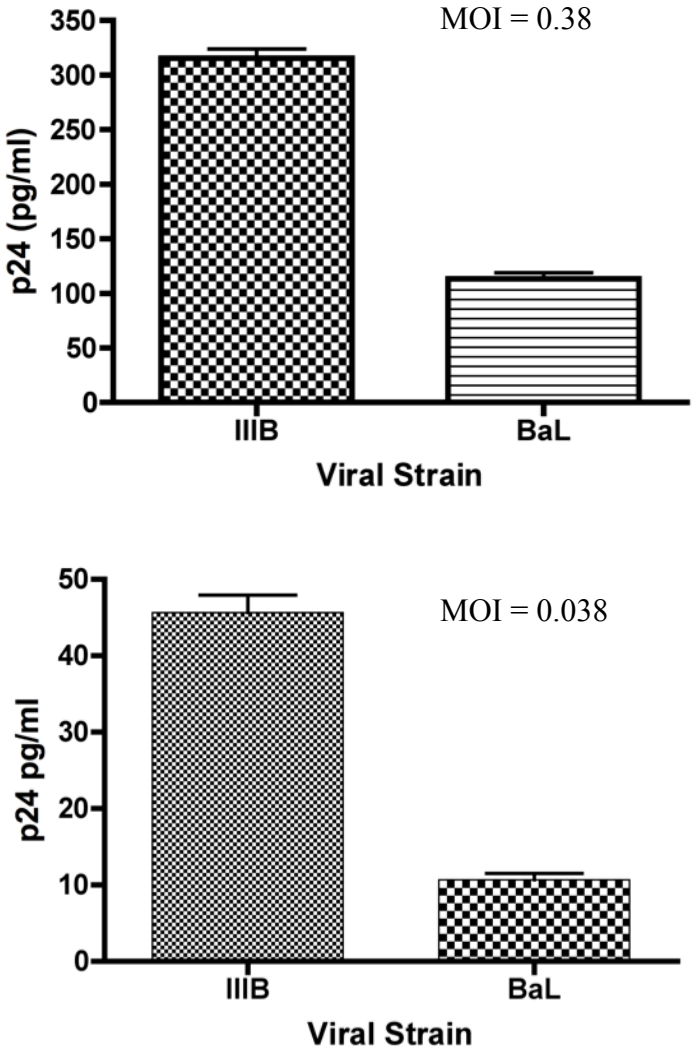

A METHOD TO CIRCUMVENT ARTIFICIAL UPTAKE OF CELL PENETRATING PEPTIDES IN MECHANISTIC STUDIES

8.1 INTRODUCTION:

A retro inverso form of a Tat CPP (R.I.Tat9) was synthesized as described before (*253*)]. TZMbl [10], a derivative of HeLa cell line obtained from Dr. John C. Kappes, Dr. Xiaoyun Wu and Tranzyme Inc., as well as the pTat plasmid encoding HIV-1 Tat protein (full name: pdDNA3.1+/Tat101-flag(pEV280)) were acquired through the NIH AIDS Research and Reference Reagent Program, Division of AIDS, NIAID, NIH. ATPLite assay kit was purchased from PerkinElmer (Waltham, MA), Bradford Protein Assay reagent from Bio-Rad (Hercules, CA), Steady-Glo Luminescence Assay Kit from Promega (Madison, WI). Tissue culture media and reagents, G418, and Lipofectamine 2000 were obtained from Invitrogen (Carlsbad, CA, USA). TZMbl and its derivative TZMbl/pTat cells were cultured in a humidified incubator supplied with 5 % of CO_2 in DMEM medium supplemented with 10 % fetal bovine serum, 1% non-essential amino acids and 200 units of penicillin/streptomycin.

TZMbl cells were transfected with pTat using Lipofectamine 2000 and selected with 800 μg/ml of G418. After screening more than 100 selected stable transfectants, one clone with the highest luciferase (Luc) activity was selected and designated as TZMbl/pTat. TZMbl/pTat cells in duplicate wells in four independent experiments (n=4) were either twice transfected with a mechanistically irrelevant BCRP siRNA as a control of the CME RNAi (-Tat/-RNAi) or chc-2 siRNA for CME RNAi (+Tat/+RNAi) according to a

published protocol [9] that was modified to fit the 24-well format and to use INTERFERin at 10 pmole of siRNA/well.

In each experiment, the efficacy of CME RNAi was verified by the disappearance of endocytosed rhodamine-labeled CME marker transferrin as well as by the massive cell death due to the suppression of the essential CME cellular function. At 72 h post the first transfection, R.I.Tat9 was added to the two groups (+Tat/-RNAi and +Tat/+RNAi) at 2.5 μM. At 96 h, the cells were detached using trypsin, and a portion of the cell suspension was used to determine Luc activity using Steady-Glo Luminescence Assay Kit and recorded on a GENios microplate reader (Tecan, Durham, NC). The remainder was used to determine MTT activity [12], total cellular protein, and total cellular ATP, respectively, using the assays mentioned above. Student t-test was used to assess the statistical difference between different groups in R.I.Tat9 uptake.

8.2 RESULTS AND DISCUSSION:

As previously mentioned, transfection commonly used in mechanistic studies is hardly compatible with arginine-rich CPPs. Specifically RNAi confers severe cell damage, therefore we present a new method that is compatible with both tranfection and quantitative analysis of arginine-rich CPP uptake. We reasoned that the crux is to quantify the uptake into only the viable cells, entirely avoiding the artificial uptake into dead and dying cells. To achieve this, we did not label the the arginine-rich Tat CPP, R.I.Tat9. We also made a new reporter cell line TZMbl/pTat, in which the Tat protein expressed from the integrated pTat constitutively turns on the expression of firefly

luciferase (Luc) from the luciferase gene (*luc*) that is under the control of HIV-1 long terminal repeat (LTR). Being derived from Tat protein, R.I.Tat9, competes in the nucleus of TZMbl/pTat cells with the Tat protein for access to the TAR binding region of a nascent HIV-1 primary transcript thereby inhibiting LTR activation and diminishing Luc expression (Figure 60). Therefore, R.I.Tat9 entry into the reporter cell line registers a reduction in Luc activity at 96h of the CME RNAi. The Luc activity in dead and dying TZMbl/pTat cells was expected to be negligible, since firefly luciferase has a short half-life of 95 minutes (*254*). Consequently, a reduction in Luc activity should be normalized to the live cell mass and not the total cell mass, since the latter includes both live and dead/dying cells. As presented below in normalizing the Luc activity, we compared the performance of two commonly used live cell mass assays, the MTT and ATP assays. We found that the MTT assay gave acceptable results while the ATP assay specified above did not. Finally, to reduce cytotoxicity while maintaining high siRNA transfection efficiency, we compared four siRNA transfection reagents specified above and found INTERFERin was more effective than the other three in this regard (data not shown).

It is well known that high concentrations of arginine-rich CPPs can be cytotoxic. In the current study, the concentration-dependence of growth inhibition was compared to the concentration-dependent reduction in Luc activity. This study revealed that 2.5μM R.I.Tat9 was minimally toxic as determined using the MTT assay (*255*) (data not shown). At this concentration, Tat CPP quantitatively reduced Luc activity (+Tat/-RNAi) to ~ 70% of the control levels (-Tat/-RNAi) (p values < 0.05) (Figure 61A-C).

Previously, it was shown that the CME RNAi almost completely suppressed CME (*256*) resulting in insignificant uptake of R.I.Tat9 into live cells (*253, 256*). Therefore, under the CME RNAi/2.5 μM R.I.Tat9 condition, the R.I.Tat9 induced reduction of Luc activity was expected to revert to the control level and occur only in live cells. As hypothesized, when the MTT assay that represents live cell mass was used to normalize the Luc activity, it returned to control levels (Figure 61A**)**. In contrast when Luc activity is normalized to total cell mass that represents both the live and dead cell masses, the normalized Luc activity (Figure 61B) did not return to the control level. This clearly shows the bias introduced by the loss of luciferase activity in dead or dying cells. Thus through a combination of relying on the functional reporting, not the fluorescence of a labeled tag, and the Luc/MTT normalization method, CME RNAi was quantitatively shown to prevent R.I.Tat9 entry into HeLa cells. When this method was not used, only qualitative conclusions could be reached (*253*).

Cellular ATP levels were determined, in parallel to the MTT assay, since ATP represents another commonly used viable cellular mass indicator. The ATP-normalized uptake of R.I.Tat9 showed wide variation and was inconclusive, most likely due to the challenge of controlling the multiple and poorly understood cellular parameters that regulate intracellular ATP concentrations (*257*). The current method emphasizes the importance of the normalization of viable cellular uptake to viable cell mass and therefore the MTT assay was superior to the ATP assay.

The principle of indicating entry only into viable cells reported in the current study could be adopted for other mechanistic CPP studies as well. A comparison of uptake values of a fluorescently labeled CPP between normalization on live and total cellular masses would reveal the extent of artificial uptake into dead/dying cells. When the difference is too large, the use of such a reporter cargo would be desirable. Fusion genes, or conjugates, then could readily be fabricated in which the reporter cargo manifests itself in the cytosol/nucleus compartment. Therefore, the method could benefit general CPP mechanistic studies and expand the usage of a number of methods developed for CPP mechanistic studies, such as the real-time reporter cell system (*258*). The current results independently support the previous conclusion that CME is required for the entry of a Tat CPP (*259*). To our knowledge, this is the first report that (a) demonstrates self-reporting of CPP cellular entry without changing the CPP's physicochemical properties through the addition of a fluorescent or radioactive tag and (b) validates the use of fluorescent tags in CPP studies since R.I.Tat9 without a tag still requires CME for entry.

8.3 CONCLUSIONS:

We present a new method that circumvents the artificial uptake of arginine-rich CPP associated with the use of transfection. If neccessary, the principle of using a reporting cargo in conjunction with indicating entry only into viable cells reported in the current study is expected to be applicable to other mechanistic CPP studies.

FIGURE 60: TZM-bl pTat cells were incubated with varying concentrations of R.I. Tat9 CPP. Bars represent mean ± std dev from duplicate experiments. The results demonstrate a concentration dependent reduction in luminescence through the inhibition of the Tat/TAR interaction by the R.I. Tat9 CPP. (*, $p<0.01$, and **, $p<0.001$ compared to 0μM concentration).

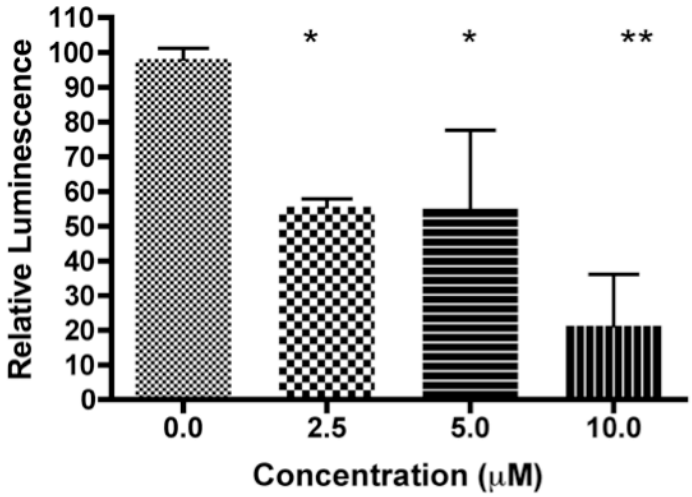

FIGURE 61: Entry of R.I.Tat9 CPP into TZM-bl/pTAT cells is reported as a reduction in Luc activity relative to the control (-Tat/-RNAi), the effect of CME RNAi is shown as the reversal of the reduction in relative Luc activity, and a proper normalization of the entry to live cell mass is important. **A** - **C** are all derived from the same cells of the same experiments but yielded different CME RNAi effects, dependent on which normalization techniques was used.

TZMbl/pTat cells in four independent experiments (n=4) were either twice transfected with a mechanistically irrelevant BCRP siRNA as a control of the CME RNAi (-Tat/-RNAi and +Tat/-RNAi) or chc-2 siRNA for CME RNAi (+Tat/+RNAi). At 72 h post the first transfection, R.I.Tat9 was added to the two groups (+Tat/-RNAi and +Tat/+RNAi). At 96 h, the cells were harvested to determine Luc and MTT activities, total cellular protein and total cellular ATP.

(A) The common MTT assay (*255*)] was used as a proxy of live cell mass to normalize the relative Luc activity. As expected from a previous study [8], with this normalization the Luc activity for the CME RNAi (+Tat/+RNAi) statistically ($p < 0.05$, as indicated by the * symbol) reversed the Luc activity from the reduced level (+Tat/-RNAi) to the control level (-Tat/-RNAi) (*253*)]. (B) When total cellular protein representing both the live and the dead cell mass was used to normalize the relative Luc activity, the data erroneously showed no reversal by CME RNAi ($p < 0.95$). (C) Cellular ATP amount was used to normalize the relative Luc activity. However, this method produced overly variable readings and hence no statistical difference between +Tat/-RNAi and +Tat/+RNAi ($p < 0.60$).

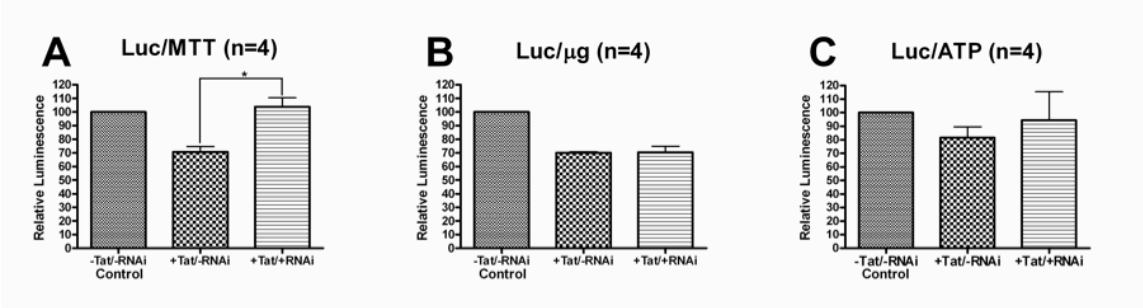

References

1. UNAIDS, *2010 Report on the global AIDS epidemic*. (World Health Organization, 2010).

2. J. A. Este, T. Cihlar, *Antiviral Research* **85**, 25 (2010).

3. D. D. Richman *et al.*, *Science* **323**, 1304 (Mar 6, 2009).

4. C. C. Bleul *et al.*, *Nature* **382**, 829 (Aug 29, 1996).

5. E. Oberlin *et al.*, *Nature* **382**, 833 (Aug 29, 1996).

6. B. Lee, M. Sharron, L. J. Montaner, D. Weissman, R. W. Doms, *Proc Natl Acad Sci U S A* **96**, 5215 (Apr 27, 1999).

7. M. Baggiolini, B. Dewald, B. Moser, *Adv Immunol* **55**, 97 (1994).

8. M. Baggiolini, *Nature* **392**, 565 (Apr 9, 1998).

9. B. Federsppiel *et al.*, *Genomics* **16**, 707 (Jun, 1993).

10. B. A. Premack, T. J. Schall, *Nat Med* **2**, 1174 (Nov, 1996).

11. M. Baggiolini, B. Dewald, B. Moser, *Annu Rev Immunol* **15**, 675 (1997).

12. A. D. Luster, *N Engl J Med* **338**, 436 (Feb 12, 1998).

13. S. Hatse *et al.*, *Mol Pharmacol* **60**, 164 (Jul, 2001).

14. L. O. Gerlach, R. T. Skerlj, G. J. Bridger, T. W. Schwartz, *J Biol Chem* **276**, 14153 (Apr 27, 2001).

15. P. M. Murphy *et al.*, *Pharmacol Rev* **52**, 145 (Mar, 2000).

16. F. Balkwill, *Nat Rev Cancer* **4**, 540 (Jul, 2004).

17. M. J. Orsini, J.-L. Parent, S. J. Mundell, J. L. Benovic, *J Biol Chem* **274**, 31076 (October 22, 1999, 1999).

18. C. Murdoch, *Immunol Rev* **177**, 175 (Oct, 2000).

19. M. Rosu-Myles *et al.*, *Proc Natl Acad Sci U S A* **97**, 14626 (Dec 19, 2000).

20. I. Petit, D. Jin, S. Rafii, *Trends Immunol* **28**, 299 (Jul, 2007).

21. Y. R. Zou, A. H. Kottmann, M. Kuroda, I. Taniuchi, D. R. Littman, *Nature* **393**, 595 (Jun 11, 1998).

22. A. Bagri *et al.*, *Development* **129**, 4249 (Sep, 2002).

23. M. Lu, E. A. Grove, R. J. Miller, *Proc Natl Acad Sci U S A* **99**, 7090 (May 14, 2002).

24. A. Segret *et al.*, *J Histochem Cytochem* **55**, 141 (Feb, 2007).

25. C. Hernandez-Lopez *et al.*, *Blood* **99**, 546 (Jan 15, 2002).

26. Q. Ma *et al.*, *Proc Natl Acad Sci U S A* **95**, 9448 (Aug 4, 1998).

27. Y. Le, Y. Zhou, P. Iribarren, J. Wang, *Cell Mol Immunol* **1**, 95 (Apr, 2004).

28. M. Baggiolini, P. Loetscher, *Immunol Today* **21**, 418 (Sep, 2000).

29. P. Loetscher, B. Moser, M. Baggiolini, *Adv Immunol* **74**, 127 (2000).

30. F. Balkwill, *Semin Cancer Biol* **14**, 171 (Jun, 2004).

31. Y. Feng, C. C. Broder, P. E. Kennedy, E. A. Berger, *Science* **272**, 872 (May 10, 1996).

32. M. P. Crump *et al.*, *EMBO J* **16**, 6996 (Dec 1, 1997).

33. M. D'Apuzzo *et al.*, *Eur J Immunol* **27**, 1788 (Jul, 1997).

34. R. K. Ganju *et al.*, *J Biol Chem* **273**, 23169 (Sep 4, 1998).

35. J. Hesselgesser *et al.*, *Journal of Immunology* **160**, 877 (Jan 15, 1998).

36. C. C. Bleul, R. C. Fuhlbrigge, J. M. Casasnovas, A. Aiuti, T. A. Springer, *J Exp Med* **184**, 1101 (Sep 1, 1996).

37. M. Shirozu *et al.*, *Genomics* **28**, 495 (Aug 10, 1995).

38. B. Moepps, R. Frodl, H. R. Rodewald, M. Baggiolini, P. Gierschik, *Eur J Immunol* **27**, 2102 (Aug, 1997).

39. K. Tashiro *et al.*, *Science* **261**, 600 (Jul 30, 1993).

40. B. J. Doranz *et al.*, *J Virol* **73**, 2752 (Apr, 1999).

41. N. Zhou *et al.*, *J Biol Chem* **277**, 17476 (May 17, 2002, 2002).

42. S. K. Gupta, K. Pillarisetti, R. A. Thomas, N. Aiyar, *Immunology Letters* **78**, 29 (2001).

43. S. p. Gravel *et al.*, *J Biol Chem* **285**, 37939 (December 3, 2010, 2010).

44. W.-b. Zhang *et al.*, *J Biol Chem* **277**, 24515 (July 5, 2002, 2002).

45. Y. Ohnishi *et al.*, *J Interferon Cytokine Res* **20**, 691 (Aug, 2000).

46. C. T. Veldkamp *et al.*, *Sci. Signal.* **1**, ra4 (September 16, 2008, 2008).

47. C. T. Veldkamp, C. Seibert, F. C. Peterson, T. P. Sakmar, B. F. Volkman, *J Mol Biol* **359**, 1400 (Jun 23, 2006).

48. M. Farzan *et al.*, *J Biol Chem* **277**, 29484 (Aug 16, 2002).

49. B. Wu *et al.*, *Science* **330**, 1066 (Nov 19, 2010).

50. S. Tian *et al.*, *J Virol* **79**, 12667 (Oct, 2005).

51. W. T. Choi, J. An, *Exp Biol Med (Maywood)* **236**, 637 (Jun 1, 2011).

52. L. Chen, G. Pei, W. Zhang, *Curr Pharm Des* **10**, 1045 (2004).

53. B. Haribabu *et al.*, *J Biol Chem* **272**, 28726 (Nov 7, 1997).

54. Y. Kuang, Y. Wu, H. Jiang, D. Wu, *J Biol Chem* **271**, 3975 (Feb 23, 1996).

55. A. Bajetto *et al.*, *J Neurochem* **77**, 1226 (Jun, 2001).

56. Y. Sun, Z. Cheng, L. Ma, G. Pei, *J Biol Chem* **277**, 49212 (Dec 20, 2002).

57. A. J. Vila-Coro *et al.*, *FASEB J* **13**, 1699 (Oct, 1999).

58. G. J. Babcock, M. Farzan, J. Sodroski, *J Biol Chem* **278**, 3378 (Jan 31, 2003).

59. Y. Percherancier *et al.*, *J Biol Chem* **280**, 9895 (Mar 18, 2005).

60. K. E. Luker, M. Gupta, G. D. Luker, *Biotechniques* **47**, 625 (Jul, 2009).

61. J. H. Wang, M. Norcross, *Drug Discov Today* **13**, 625 (Jul, 2008).

62. R. Bonecchi *et al.*, *J Exp Med* **187**, 129 (Jan 5, 1998).

63. F. Sallusto, D. Lenig, C. R. Mackay, A. Lanzavecchia, *J Exp Med* **187**, 875 (Mar 16, 1998).

64. C. C. Bleul, L. Wu, J. A. Hoxie, T. A. Springer, C. R. Mackay, *Proc Natl Acad Sci U S A* **94**, 1925 (Mar 4, 1997).

65. L. Wu *et al.*, *J Exp Med* **185**, 1681 (May 5, 1997).

66. C. R. Mackay, *Adv Immunol* **53**, 217 (1993).

67. C. R. Mackay, W. L. Marston, L. Dudler, *J Exp Med* **171**, 801 (Mar 1, 1990).

68. M. Lewis, J. F. Tarlton, S. Cose, *Immunol Cell Biol* **86**, 226 (Mar-Apr, 2008).

69. L. M. Ebert, P. Schaerli, B. Moser, *Mol Immunol* **42**, 799 (May, 2005).

70. T. A. Springer, *Cell* **76**, 301 (Jan 28, 1994).

71. R. Phillips, A. Ager, *Eur J Immunol* **32**, 837 (Mar, 2002).

72. E. R. Fedyk, D. H. Ryyan, I. Ritterman, T. A. Springer, *J Leukoc Biol* **66**, 667 (Oct, 1999).

73. M. Honczarenko *et al.*, *Blood* **94**, 2990 (Nov 1, 1999).

74. R. Forster *et al.*, *J Immunol* **160**, 1522 (Feb 1, 1998).

75. E. Delgado *et al.*, *Immunobiology* **198**, 490 (Mar, 1998).

76. T. Hori *et al.*, *J Immunol* **160**, 180 (Jan 1, 1998).

77. R. Horuk, *Nat Rev Drug Discov* **8**, 23 (Jan, 2009).

78. J. Hesselgesser *et al.*, *Curr Biol* **7**, 112 (Feb 1, 1997).

79. E. E. Jazin, S. Soderstrom, T. Ebendal, D. Larhammar, *J Neuroimmunol* **79**, 148 (Nov, 1997).

80. C. M. Coughlan *et al.*, *Neuroscience* **97**, 591 (2000).

81. S. H. Chalasani *et al.*, *J Neurosci* **23**, 4601 (Jun 1, 2003).

82. K. E. McGrath, A. D. Koniski, K. M. Maltby, J. K. McGann, J. Palis, *Dev Biol* **213**, 442 (Sep 15, 1999).

83. E. Lavi *et al.*, *Am J Pathol* **151**, 1035 (Oct, 1997).

84. A. Bajetto, R. Bonavia, S. Barbero, T. Florio, G. Schettini, *Front Neuroendocrinol* **22**, 147 (Jul, 2001).

85. A. Bajetto *et al.*, *Ann N Y Acad Sci* **876**, 201 (Jun 22, 1999).

86. A. Bajetto *et al.*, *J Neurochem* **73**, 2348 (Dec, 1999).

87. S. K. Gupta, P. G. Lysko, K. Pillarisetti, E. Ohlstein, J. M. Stadel, *J Biol Chem* **273**, 4282 (Feb 13, 1998).

88. A. T. Askari *et al.*, *Lancet* **362**, 697 (Aug 30, 2003).

89. W. Wojakowski *et al.*, *Circulation* **110**, 3213 (Nov 16, 2004).

90. J. Yamaguchi *et al.*, *Circulation* **107**, 1322 (Mar 11, 2003).

91. M. Cheng *et al.*, *Circ Res* **107**, 1083 (Oct 29, 2010).

92. E. L. Snyder *et al.*, *Cancer Res* **65**, 10646 (Dec 1, 2005).

93. C. Murdoch, P. N. Monk, A. Finn, *Cytokine* **11**, 704 (Sep, 1999).

94. H. Kulbe, N. R. Levinson, F. Balkwill, J. L. Wilson, *Int J Dev Biol* **48**, 489 (2004).

95. Y. X. Sun *et al.*, *J Cell Biochem* **89**, 462 (Jun 1, 2003).

96. A. Muller *et al.*, *Nature* **410**, 50 (Mar 1, 2001).

97. A. J. Sloane *et al.*, *Immunol Cell Biol* **83**, 129 (Apr, 2005).

98. M. Baggiolini, B. Moser, *J Exp Med* **186**, 1189 (Oct 20, 1997).

99. G. Borkow, A. Lapidot, *Curr Drug Targets Infect Disord* **5**, 3 (Mar, 2005).

100. J. M. Daoudi, J. Greiner, A. M. Aubertin, P. Vierling, *Bioorg Med Chem Lett* **14**, 495 (Jan 19, 2004).

101. E. De Clercq, *International journal of antimicrobial agents* **33**, 307 (2009).

102. E. De Clercq, *Nature Reviews Drug Discovery* **6**, 1001 (2007).

103. E. De Clercq, *Nature Reviews Drug Discovery* **1**, 13 (2002).

104. J. A. Este, A. Telenti, *Lancet* **370**, 81 (Jul 7, 2007).

105. F. Grande, A. Garofalo, N. Neamati, *Curr Pharm Des* **14**, 385 (2008).

106. X. Liang, *Chem Biol Drug Des* **72**, 97 (Aug, 2008).

107. P. Lusso, *Vaccine* **20**, 1964 (May 6, 2002).

108. J. E. Pease, R. Horuk, *Expert Opin Ther Pat* **19**, 199 (Feb, 2009).

109. J. E. Pease, R. Horuk, *Expert Opin Ther Pat* **19**, 39 (Jan, 2009).

110. F. Shaheen, R. G. Collman, *Curr Opin Infect Dis* **17**, 7 (Feb, 2004).

111. H. Tamamura, H. Tsutsumi, *Chem Biol* **13**, 8 (Jan, 2006).

112. H. Tamamura, H. Tsutsumi, N. Fujii, *Mini Rev Med Chem* **6**, 989 (Sep, 2006).

113. S. M. Philpott, *Curr HIV Res* **1**, 217 (Apr, 2003).

114. L. D. Starr-Spires, R. G. Collman, *Clin Lab Med* **22**, 681 (Sep, 2002).

115. A. Brelot, N. Heveker, M. Montes, M. Alizon, *J Biol Chem* **275**, 23736 (August 4, 2000, 2000).

116. P. Lusso, *EMBO J* **25**, 447 (Feb 8, 2006).

117. J. Weber, H. Piontkivska, M. E. Quinones-Mateu, *AIDS Rev* **8**, 60 (Apr-Jun, 2006).

118. D. Wong, W. Korz, *Clin Cancer Res* **14**, 7975 (Dec 15, 2008).

119. C. D. Rizzuto *et al.*, *Science* **280**, 1949 (Jun 19, 1998).

120. M. Sharon *et al.*, *Structure* **11**, 225 (Feb, 2003).

121. C.-c. Huang *et al.*, *Science* **310**, 1025 (2005).

122. C. L. Kuiken *et al.*, *J Virol* **66**, 4622 (Jul, 1992).

123. E. A. Berger *et al.*, *Nature* **391**, 240 (Jan 15, 1998).

124. J. P. Moore, A. Trkola, T. Dragic, *Curr Opin Immunol* **9**, 551 (Aug, 1997).

125. E. T. Brower, A. Schon, J. C. Klein, E. Freire, *Biochemistry* **48**, 779 (Feb 3, 2009).

126. I. Thordsen, S. Polzer, M. Schreiber, *BMC Infect Dis* **2**, 31 (Dec 19, 2002).

127. X. Yang, S. Kurteva, X. Ren, S. Lee, J. Sodroski, *J Virol* **80**, 4388 (May, 2006).

128. W. M. Kazmierski, T. P. Kenakin, K. S. Gudmundsson, *Chem Biol Drug Des* **67**, 13 (Jan, 2006).

129. M. Li *et al.*, *J Virol* **79**, 10108 (Aug, 2005).

130. W. Resch, N. Hoffman, R. Swanstrom, *Virology* **288**, 51 (Sep 15, 2001).

131. J. J. De Jong, A. De Ronde, W. Keulen, M. Tersmette, J. Goudsmit, *J Virol* **66**, 6777 (Nov, 1992).

132. L. Ratner *et al.*, (1985).

133. P. Lusso, *Structure* **11**, 129 (Feb, 2003).

134. N. Zhou *et al.*, *J Biol Chem* **276**, 42826 (Nov 16, 2001).

135. D. J. Chabot, C. C. Broder, *J Biol Chem* **275**, 23774 (Aug 4, 2000).

136. A. Brelot, N. Heveker, O. Pleskoff, N. Sol, M. Alizon, *J Virol* **71**, 4744 (Jun, 1997).

137. S. Ugolini *et al.*, *J Immunol* **159**, 3000 (Sep 15, 1997).

138. F. Kajumo, D. A. Thompson, Y. Guo, T. Dragic, *Virology* **271**, 240 (Jun 5, 2000).

139. M. Zaitseva, K. Peden, H. Golding, *Bba-Biomembranes* **1614**, 51 (Jul 11, 2003).

140. R. A. Fouchier *et al.*, *J Virol* **66**, 3183 (May, 1992).

141. A. Verani, P. Lusso, *Curr Mol Med* **2**, 691 (Dec, 2002).

142. J. D. Altenburg, Q. Jin, B. Alkhatib, G. Alkhatib, *J Virol* **84**, 2563 (Mar, 2010).

143. S. M. Brandt, R. Mariani, A. U. Holland, T. J. Hope, N. R. Landau, *J Biol Chem* **277**, 17291 (May 10, 2002).

144. A. Trkola *et al.*, *J Virol* **72**, 396 (Jan, 1998).

145. T. Zhou *et al.*, *Science* **329**, 811 (Aug 13, 2010).

146. X. Wu *et al.*, *Science* **329**, 856 (Aug 13, 2010).

147. T. Zhou *et al.*, *Nature* **445**, 732 (Feb 15, 2007).

148. P. D. Kwong *et al.*, *Nature* **393**, 648 (Jun 18, 1998).

149. Z.-x. Wang *et al.*, *J Biol Chem* **273**, 15007 (June 12, 1998, 1998).

150. C. W. Dieffenbach, A. S. Fauci, *Annals of Internal Medicine* **154**, 766 (2011).

151. M. S. Palombo, Y. Singh, P. J. Sinko, *J Drug Deliv Sci Technol* **19**, 3 (2009).

152. F. Titti *et al.*, *Expert Opin Emerg Drugs* **12**, 23 (Mar, 2007).

153. T. J. Wilkin, B. Taylor, S. Olender, S. M. Hammer, *Top HIV Med* **16**, 31 (Apr-May, 2008).

154. C. Flexner, *Nat Rev Drug Discov* **6**, 959 (Dec, 2007).

155. E. De Clercq, *Nature Reviews Microbiology* **2**, 704 (2004).

156. A. Sosnik, D. A. Chiappetta, A. M. Carcaboso, *J Control Release* **138**, 2 (Aug 19, 2009).

157. C. Shah, *Indian Journal of Pediatrics* **74**, 55 (2007).

158. B. Dau, M. Holodniy, *Drugs* **69**, 31 (2009).

159. M. Shehu-Xhilaga, G. Tachedjian, S. M. Crowe, K. Kedzierska, *Curr Med Chem* **12**, 1705 (2005).

160. A. R. Sedaghat, R. F. Siliciano, C. O. Wilke, *BMC Infect Dis* **8**, 2 (2008).

161. L. Shen, R. F. Siliciano, *J Allergy Clin Immunol* **122**, 22 (Jul, 2008).

162. K. Das, P. J. Lewi, S. H. Hughes, E. Arnold, *Prog Biophys Mol Biol* **88**, 209 (Jun, 2005).

163. D. D. Ho *et al.*, *Nature* **373**, 123 (Jan 12, 1995).

164. M.-N. Rousseau *et al.*, *JAIDS Journal of Acquired Immune Deficiency Syndromes* **26**, 36 (2001).

165. R. J. Pomerantz, *Clin Infect Dis* **34**, 91 (Jan 1, 2002).

166. S. Aquaro *et al.*, *J Med Virol* **68**, 479 (Dec, 2002).

167. S. Aquaro *et al.*, *Antiviral Res* **55**, 209 (Aug, 2002).

168. A. R. Sedaghat, J. B. Dinoso, L. Shen, C. O. Wilke, R. F. Siliciano, *Proc Natl Acad Sci U S A* **105**, 4832 (Mar 25, 2008).

169. L. Shen *et al.*, *Nat Med* **14**, 762 (Jul, 2008).

170. H. C. Yang, L. Shen, R. F. Siliciano, J. L. Pomerantz, *Proc Natl Acad Sci U S A* **106**, 6321 (Apr 14, 2009).

171. S. Palmer *et al.*, *Proc Natl Acad Sci U S A* **105**, 3879 (Mar 11, 2008).

172. A. J. Chase *et al.*, *J Virol* **81**, 12748 (Dec, 2007).

173. M. A. Poles, J. Elliott, P. Taing, P. A. Anton, I. S. Chen, *J Virol* **75**, 8390 (Sep, 2001).

174. R. M. Dunham *et al.*, *J Immunol* **180**, 5582 (Apr 15, 2008).

175. Y. Su, P. J. Sinko, (2006).

176. G. C. Williams, P. J. Sinko, *Adv Drug Deliv Rev* **39**, 211 (Oct 18, 1999).

177. R. B. Kim *et al.*, *Journal of Clinical Investigation* **101**, 289 (1998).

178. S. Park, P. J. Sinko, *J Pharmacol Exp Ther* **312**, 1249 (Mar, 2005).

179. D. Wu, J. G. Clement, W. M. Pardridge, *Brain Res* **791**, 313 (Apr 27, 1998).

180. H. H. Usansky, P. J. Sinko, *Pharm Res* **20**, 390 (Mar, 2003).

181. T. D'Aversa, E. Eugenin, J. Berman, *Journal of neuroscience research* **81**, 436 (2005).

182. M. Shehu-Xhilaga, D. De Kretser, N. Dejucq-Rainsford, M. Hedger, *Current HIV Research* **3**, 345 (2005).

183. X. Wei *et al.*, *Antimicrob Agents Chemother* **46**, 1896 (Jun, 2002).

184. C. A. Derdeyn *et al.*, *J Virol* **74**, 8358 (Sep, 2000).

185. Y. Singh, M. Palombo, P. J. Sinko, *Curr Med Chem* **15**, 1802 (2008).

186. S. Gunaseelan, K. Gunaseelan, M. Deshmukh, X. Zhang, P. J. Sinko, *Adv Drug Deliv Rev* **62**, 518 (Mar 18, 2010).

187. T. Mamo *et al.*, *Nanomedicine (Lond)* **5**, 269 (Feb, 2010).

188. E. De Clercq, *Biochemical pharmacology* **77**, 1655 (2009).

189. A. Marchese, J. L. Benovic, *J Biol Chem* **276**, 45509 (Dec 7, 2001).

190. N. Heveker *et al.*, *Curr Biol* **8**, 369 (Mar 26, 1998).

191. N. Heveker *et al.*, *Molecular Pharmacology* **59**, 1418 (2001).

192. M. P. Crump, E. Elisseeva, J. Gong, I. Clark-Lewis, B. D. Sykes, *FEBS Lett* **489**, 171 (Feb 2, 2001).

193. T. N. Kledal *et al.*, *Science* **277**, 1656 (Sep 12, 1997).

194. C. Boshoff *et al.*, *Science* **278**, 290 (Oct 10, 1997).

195. Z. Luo *et al.*, *Biochemistry* **39**, 13545 (Nov 7, 2000).

196. N. Zhou, Z. Luo, J. Luo, J. W. Hall, Z. Huang, *Biochemistry* **39**, 3782 (Apr 4, 2000).

197. Z. Zeng *et al.*, *Mol Cancer Ther* **5**, 3113 (Dec, 2006).

198. S. Kumar *et al.*, *Chem Biol* **13**, 69 (Jan, 2006).

199. N. M. Zhou *et al.*, *J Biol Chem* **277**, 17476 (May 17, 2002).

200. M. Mori, D. Liu, S. Kumar, Z. Huang, *Biochem Biophys Res Commun* **335**, 651 (Sep 30, 2005).

201. Y. Liu *et al.*, *Molecular Therapy* **17**, 1509 (2009).

202. A. Isidro-Llobet, M. Alvarez, F. Albericio, *Chemical reviews* **109**, 2455 (2009).

203. D. Li, D. Elbert, *The Journal of peptide research* **60**, 300 (2002).

204. D. Kadereit, P. Deck, I. Heinemann, H. Waldmann, *ChemistryñA European Journal* **7**, 1184 (2001).

205. S. Flemer, A. Wurthmann, A. Mamai, J. S. Madalengoitia, *The Journal of Organic Chemistry* **73**, 7593 (2008).

206. L. Bourel, O. Carion, H. Gras Masse, O. Melnyk, *Journal of Peptide Science* **6**, 264 (2000).

207. J. Yang, L. B. Alemany, J. Driver, J. D. Hartgerink, A. R. Barron, *Chemistry* **13**, 2530 (2007).

208. M. Jullian *et al.*, *Tetrahedron Lett* **50**, 260 (Jan 21, 2009).

209. S. Achilefu *et al.*, *Journal of medicinal chemistry* **45**, 2003 (2002).

210. A. Karlstrom, A. UndÈn, *Tetrahedron Lett* **37**, 4243 (1996).

211. M. Mergler, F. Dick, *Journal of Peptide Science* **11**, 650 (2005).

212. M. Mergler, F. Dick, B. Sax, C. St‰helin, T. Vorherr, *Journal of Peptide Science* **9**, 518 (2003).

213. M. Mergler, F. Dick, B. Sax, P. Weiler, T. Vorherr, *Journal of Peptide Science* **9**, 36 (2003).

214. M. Popovic, E. Read-Connole, R. C. Gallo, *Lancet* **2**, 1472 (Dec 22, 1984).

215. M. Popovic, M. G. Sarngadharan, E. Read, R. C. Gallo, *Science* **224**, 497 (May 4, 1984).

216. M. J. Endres *et al.*, *Cell* **87**, 745 (Nov 15, 1996).

217. C. W. Hendrix *et al.*, *Antimicrob Agents Chemother* **44**, 1667 (Jun, 2000).

218. E. De Clercq *et al.*, *Antimicrob Agents Chemother* **38**, 668 (Apr, 1994).

219. G. J. Bridger *et al.*, *J Med Chem* **38**, 366 (Jan 20, 1995).

220. A. McKnight *et al.*, *J Virol* **71**, 1692 (Feb, 1997).

221. I. Mondor, S. Ugolini, Q. J. Sattentau, *J Virol* **72**, 3623 (May, 1998).

222. T. Haertle *et al.*, *Journal of Biological Chemistry* **263**, 5870 (Apr 25, 1988).

223. W.-T. Choi *et al.*, *Biochemistry* **51**, 7078 (2012/09/11, 2012).

224. W. T. Choi *et al.*, *Biochemistry* **51**, 7078 (Sep 11, 2012).

225. W. T. Choi *et al.*, *J Virol* **79**, 15398 (Dec, 2005).

226. L. Wan *et al.*, *Bioconjug Chem* **19**, 28 (Jan, 2008).

227. S. Pooyan *et al.*, *Bioconjug Chem* **13**, 216 (Mar-Apr, 2002).

228. M. M. Wong, E. N. Fish, *Semin Immunol* **15**, 5 (Feb, 2003).

229. M. M. Rosenkilde *et al.*, *J Biol Chem* **282**, 27354 (September 14, 2007, 2007).

230. X. Carnec, L. Quan, W. C. Olson, U. Hazan, T. Dragic, *J Virol* **79**, 1930 (Feb, 2005).

231. S. Hatse *et al.*, *FEBS Letters* **546**, 300 (2003).

232. A. Amara *et al.*, *J Exp Med* **186**, 139 (Jul 7, 1997).

233. J. Nielsen, L. O. Lyngso, *Tetrahedron Lett* **37**, 8439 (Nov 11, 1996).

234. B. Li *et al.*, *Biochem Pharmacol* **70**, 1673 (Nov 25, 2005).

235. T. Le Saux *et al.*, *Journal of Chromatography B* **865**, 81 (2008).

236. A. Dunge, N. Sharda, B. Singh, S. Singh, *Journal of pharmaceutical and biomedical analysis* **37**, 1109 (2005).

237. K. C. Marsh, E. Eiden, E. McDonald, *Journal of Chromatography B: Biomedical Sciences and Applications* **704**, 307 (1997).

238. R. M. W. Hoetelmans *et al.*, *Journal of Chromatography B: Biomedical Sciences and Applications* **705**, 119 (1998).

239. E. J. J. R. P. Hammer Sm, et al., *JAMA: The Journal of the American Medical Association* **300**, 555 (2008).

240. F. M. Veronese, *Biomaterials* **22**, 405 (Mar, 2001).

241. J. M. Harris, R. B. Chess, *Nature Reviews Drug Discovery* **2**, 214 (Mar, 2003).

242. J. M. Harris, N. E. Martin, M. Modi, *Clinical Pharmacokinetics* **40**, 539 (2001).

243. E. Kaiser, R. L. Colescott, C. D. Bossinger, P. I. Cook, *Anal Biochem* **34**, 595 (Apr, 1970).

244. D. Yu, N. Vladimirov, J. M. J. Fr√©chet, *Macromolecules* **32**, 5186 (1999/08/01, 1999).

245. L. Wan *et al.*, *Pharm Res* **24**, 2110 (Nov, 2007).

246. P. J. Sinko *et al.* (US Patent App. 13/255,635, 2010).

247. P. SINKO *et al.* (WO Patent 2,010,107,831, 2010).

248. E. Fernandez-Megia, J. Correa, R. Riguera, *Biomacromolecules* **7**, 3104 (2006).

249. M. E. Fox, F. C. Szoka, J. M. J. FreÃÅchet, *Accounts of Chemical Research* **42**, 1141 (2009/08/18, 2009).

250. D. Liu *et al.*, *J Virol* **81**, 11489 (Oct, 2007).

251. B. Labrosse *et al.*, *J Virol* **72**, 6381 (Aug, 1998).

252. R. Fragoso *et al.*, *The Journal of Immunology* **170**, 913 (January 15, 2003, 2003).

253. X. Zhang *et al.*, *Mol Pharm* **(in press)**, (2009).

254. S. D. Goodman, Q. Gao, *Plasmid* **42**, 154 (Sep, 1999).

255. T. Mosmann, *J Immunol Methods* **65**, 55 (Dec 16, 1983).

256. A. Motley, N. A. Bright, M. N. Seaman, M. S. Robinson, *J Cell Biol* **162**, 909 (Sep 1, 2003).

257. F. I. Ataullakhanov, V. M. Vitvitsky, *Biosci Rep* **22**, 501 (Oct-Dec, 2002).

258. L. R. Jones *et al.*, *J Am Chem Soc* **128**, 6526 (May 24, 2006).

259. X. Zhang *et al.*, *Mol Pharm* **6**, 836 (May-Jun, 2009).